COMBUSTION INSTABILITIES IN SOLID PROPELLANT ROCKET MOTORS

F.E.C. Culick
California Institute of Technology
1200 E. California Blvd., MC 205-45
Pasadena, CA 91125, U.S.A.

Notes for Two Lectures given as part of the Special Course
"Internal Aerodynamcis in Solid Rocket Propulsion"

von Kármán Institute
27–31 May 2002

This work was supported in part by the California Institute of Technology; partly by the Caltech Multidisciplinary University Research Initiative under Grant No. N00014-95-1-1338 (Dr. Judah Goldwasser, Program Manager); partly by the Department of Energy Advanced Gas Turbine Systems Research (AGTSR) Program under Subcontract No. 98-02-SR072 (Dr. Daniel Fant & Dr. Larry Golan, Program Managers); partly by ENEL, Pisa, Italy (Dr. Giancarlo Benelli, Program Manager); and partly by the Air Force Office of Scientific Research (AFOSR) under Grant No. F49620-99-1-0118 (Dr. Mitat Birkan, Program Manager).

Paper presented at the RTO/VKI Special Course on "Internal Aerodynamics in Solid Rocket Propulsion", held in Rhode-Saint-Genèse, Belgium, 27-31 May 2002, and published in RTO-EN-023.

Report Documentation Page

Form Approved
OMB No. 0704-0188

1. REPORT DATE	2. REPORT TYPE	3. DATES COVERED
00 JAN 2004	**N/A**	**-**

4. TITLE AND SUBTITLE	5a. CONTRACT NUMBER
Combustion Instabilities In Solid Propellant Rocket Motors	5b. GRANT NUMBER
	5c. PROGRAM ELEMENT NUMBER
6. AUTHOR(S)	5d. PROJECT NUMBER
	5e. TASK NUMBER
	5f. WORK UNIT NUMBER
7. PERFORMING ORGANIZATION NAME(S) AND ADDRESS(ES) **California Institute of Technology 1200 E. California Blvd., MC 205-45 Pasadena, CA 91125, U.S.A.**	8. PERFORMING ORGANIZATION REPORT NUMBER
9. SPONSORING/MONITORING AGENCY NAME(S) AND ADDRESS(ES)	10. SPONSOR/MONITOR'S ACRONYM(S)
	11. SPONSOR/MONITOR'S REPORT NUMBER(S)

12. DISTRIBUTION/AVAILABILITY STATEMENT
Approved for public release, distribution unlimited

13. SUPPLEMENTARY NOTES
See also ADM001656., The original document contains color images.

14. ABSTRACT

15. SUBJECT TERMS

16. SECURITY CLASSIFICATION OF:			17. LIMITATION OF ABSTRACT	18. NUMBER OF PAGES	19a. NAME OF RESPONSIBLE PERSON
a. REPORT	b. ABSTRACT	c. THIS PAGE			
unclassified	**unclassified**	**unclassified**	**UU**	**178**	

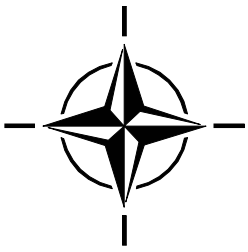

Contents

ABSTRACT 1

1. A BRIEF SURVEY OF COMBUSTION INSTABILITIES IN SOLID ROCKETS 1

1.1. Introduction 2

1.2. Historical Background 5

1.3. Solid Propellant Rocket Motors 6

1.4. Mechanisms of Combustion Instabilities 8

1.5. Physical Characteristics of Combustion Instabilities 9

1.6. Linear Behavior 12

1.6.1. Gains and Losses of Acoustic Energy; Linear Stability 14

1.7. Nonlinear Behavior 18

1.7.1. Linear Behavior Interpreted as the Motion of a Simple Oscillator 19

1.7.2. Nonlinear Behavior Interpreted as the Motion of a Nonlinear Oscillator 21

1.8. Analysis and Numerical Simulations of Combustion Instabilities 24

2. MECHANISMS OF COMBUSTION INSTABILITIES IN SOLID PROPELLANT ROCKETS 27

2.1. Qualitative Interpretation of the Basic Mechanism 27

2.2. Analysis of the QSHOD Model 31

2.3. Measurements of the Response Function; Comparison of Experimental Results and the QSHOD Model 39

2.4. The Zel'dovich-Novozhilov (Z-N) Model 40

2.5. Revisions and Extensions of the QSHOD Model 42

2.5.1. Additional Dynamics in the Condensed Phase 42

2.5.2. Additional Dynamics in the Gas Phase 42

2.6. Modeling the Effects of Velocity Coupling on the Global Dynamics of Combustion Chambers 42

2.6.1. The Model Framework 43

2.6.2. Models of the Surface Layer 44

CONTENTS

2.6.3. Models of the Gas Phase 45

2.6.4. Some Results for the Combustion Response Function 45

2.7. Velocity Coupling, the Combustion Response, and Global Dynamics 46

2.8. Generation of Vorticity and Vortex Shedding 53

2.8.1. Generation of Vorticity 54

2.8.2. Shedding of Large Scale Vortices 54

2.9. Distributed Combustion 57

3. EQUATIONS FOR UNSTEADY MOTIONS IN COMBUSTION CHAMBERS 59

3.1. Modes of Wave Motion in a Compressible Medium 59

3.2. Equations of Motion for a Reacting Flow 59

3.3. Two-Parameter Expansion of the Equations of Motion 61

3.3.1. Expansion in Mean and Fluctuating Values 62

3.3.2. Equations for the Mean Flow 64

3.3.3. Systems of Equations for the Fluctuations 65

3.4. Nonlinear Wave Equations for the Pressure Field 67

4. MODAL EXPANSION AND SPATIAL AVERAGING; AN ITERATIVE METHOD OF SOLUTION 71

4.1. Application of a Green's Function for Steady Waves 71

4.1.1. Approximate Solution by Iteration 75

4.2. An Alternative Derivation of the First Order Formula 76

4.3. Approximate Solution for Unsteady Nonlinear Motions 76

4.4. Application of Time-Averaging 79

4.5. The Procedure for Iterative Solution 82

4.5.1. Linear Energy Transfer Between the Mean and Fluctuating Motions 83

4.5.2. Energy Transfer Between Modes; Nonlinear Mode Coupling 86

4.5.3. Zeroth and First Order Solutions to the Oscillator Equation 86

5. SOME FUNDAMENTALS OF ACOUSTICS 89

5.1. The Linearized Equations of Motion; The Velocity Potential 89

5.1.1. The Velocity Potential 91

5.2. Energy and Intensity Associated with Acoustic Waves 92

5.3. The Growth or Decay Constant 93

CONTENTS

5.4. Boundary Conditions: Reflections from a Surface 94
5.4.1. Reflections of Plane Waves at a Surface 95
5.5. Wave Propagation in Tubes; Normal Modes 97
5.5.1. Waves in Tubes 97
5.5.2. Normal Modes for Tubes Having Discontinuities of Cross-Sectional Area 99
5.6. Normal Acoustic Modes and Frequencies for a Chamber 100
5.6.1. Normal Modes for Rectangular Chambers 101
5.6.2. Normal Modes for a Circular Cylindrical Chamber 102
6. LINEAR STABILITY OF COMBUSTOR DYNAMICS 105
6.1. Solution for the Problem of Linear Stability 105
6.2. An Alternative Calculation of Linear Stability 106
6.3. An Example: Linear Stability with Distributed Sources of Heat and Motion of the Boundary 107
6.4. Rayleigh's Criterion and Linear Stability 109
6.5. Explicit Formulas For Linear Stability 111
6.5.1. Linear Stability in Three Dimensions 111
7. NONLINEAR BEHAVIOR 117
7.1. The Two-Mode Approximation 117
7.2. Application of a Continuation Method 122
7.3. Hysteresis and Control of Combustion Instabilities 124
7.4. Representing Noise in Analysis of Combustor Dynamics 126
7.5. System Identification for Combustor Dynamics with Noise 128
8. PASSIVE CONTROL OF COMBUSTION INSTABILITIES 133
A. EQUATIONS OF MOTION 135
A.1. General Equations of Motion 135
A.2. Expansions in Mean and Fluctuating Variables 137
B. THE EQUATIONS FOR ONE-DIMENSIONAL UNSTEADY MOTIONS 139
B.1. Equations for Unsteady One-Dimensional Motions 140

REFERENCES 141

ATTACHMENT — AIAA-2002-3592
N. Ananthkrishnan, Shardul Deo, F.E.C. Culick 157

CONTENTS

Abstract 1

1. Introduction 1

2. Coupled Oscillator Equations 3

2.1. Energy Transfer 4

2.2. Modal Truncation 5

3. Triggered Limit Cycles 6

4. Velocity Coupling Models 8

5. Conclusions 11

6. Acknowledgments 11

Bibliography 13

COMBUSTION INSTABILITIES IN SOLID PROPELLANT ROCKET MOTORS

F.E.C. Culick
California Institute of Technology
1200 E. California Blvd., MC 205-45
Pasadena, CA 91125, U.S.A.

ABSTRACT

These notes for two lectures are intended to provide the basic ideas for understanding and interpreting coherent oscillations is solid propellant rocket motors. The discussion is concerned mainly with the dynamics of a system consisting of two coupled sub-systems: the chamber containing combustion products; and the combustion processes confined almost entirely to a thin region adjacent to the surface of burning propellant. Coupling between the sub-systems is always present due to the sensitivity of the ocmbustion processes to local values of pressure and velocity. Thus the primary mechanisms for instabilities in solid rockets are related to those interactions. A second mechanism involves vortex shedding, a cause of instabilities mainly in large motors, notably the Space Shuttle and Ariene V boost motors. Following a brief review of the history of combustion instabilities in solid rockets, the mechanisms and their quantitative representations are discussed. The remainder of the lectures is devoted to an approximate analysis providing a general framework convenient for understanding, predicting and interpreting combustion instabilities.

1. A BRIEF SURVEY OF COMBUSTION INSTABILITIES IN SOLID ROCKETS

Chemical propulsion systems depend fundamentally on the conversion of energy stored in molecular bonds to mechanical energy of a vehicle in motion. The first stage of the process, combustion of oxidizer and fuel, takes place in a vessel open only to admit reactants and to exhaust the hot products. Higher performance is achieved by increasing the rate of energy release per unit volume. For example, the power density in the Atlas engine (1950s) was 146.4 gigawatts/m^3. The power densities in solid rockets are much less. For a cylindrical bore, the values are approximately $0.25(r/D)$ gigawatts/m^3, where r is the linear burning rate, typically a few centimeters per second, and D is the diameter. Thus the power densities rarely exceed one gigawatt/m^3. These are indeed very large power densities. We cannot be surprised that such enormous power densities should be accompanied by relatively small fluctuations whose amplitudes may be merely annoying or possibly unacceptable in the worst cases.

We are concerned in these lectures with the dynamics of combustion systems using solid propellants. The motivation for addressing the subject arises from particular problems of combustion instabilities observed in all types of solid rockets. Typically the instabilities are observed as pressure oscillations growing spontaneously out of the noise during a firing. As a practical matter, combustion instabilities are more likely encountered during development of new combustion systems intended to possess considerable increases of performance in some sense. The present state of theory and experiment has not provided a sufficiently strong foundation to provide a complete basis for prediction. Hence there are only a few guidelines available to help designers avoid combustion instabilities. In that respect, more is known about the dynamical behavior of solid rockets than about corresponding problems in other propulsion systems.

Under such conditions, it is extremely important to pay attention to the experience gained in the laboratory as well as in full-scale tests of devices: theory alone is quite helpless because of the impossibility of obtaining quantitative results solely from first principles. Moreover, because of the many properties of the behavior common to the various systems, much is to be gained from understanding the characteristics of systems other than the one that may be of immediate concern. It is therefore proper to begin with a survey of some typical examples drawn from many years' experience. Theory is an indispensable aid to making sense of observational results. Conversely, discussion of various experimental observations is a natural place to introduce many of the basic ideas contained in the theory.

From the beginning of this subject, the central practical question has been: What must be done to eliminate combustion instabilities? Traditionally, the approach taken has been based on passive measures, largely *ad hoc* design changes or notably for solid propellant rockets, favorable changes of propellant composition. During the past few years, considerable effort has been expended on the problem of applying active feedback control to combustion systems. It's an attractive proposition to control or eliminate instabilities with feedback control, particularly because one implication, often made explicit, is that the use of feedback will somehow allow one to get around the difficult problems of understanding the details of the system's behavior. Many laboratory, and several full-scale demonstrations with gas turbines support that point of view. Proposals have been made for active control of solid rockets but there seem to be no successful demonstrations. In any case, for at least two reasons, serious application of feedback control must be based on understanding the dynamics of the system to be controlled:

(i) all experience in the field of feedback control generally has demonstrated that the better the controlled plant is understood, the more effective is the control;
(ii) without understanding, development of a control system for a full-scale device is an *ad hoc* matter, likely to involve expensive development with neither guarantee of success nor assurance that the best possible system has been designed.

Consequently, whatever one's motivation for investigating combustion instabilities, it is essential to have a good understanding of experiences with as many systems as possible. Therefore we begin this book with a lengthy survey of combustion instabilities observed in various systems. The theoretical framework is constructed to accommodate these observations, but later emerges also as a perfect vehicle for investigating the use of active feedback control.

1.1. Introduction. For the kinds of propulsion systems normally used, combustion chambers are intended to operate under conditions that are steady or vary little. The central questions addressed in the monograph concern the stability and behavior subsequent to instability of steady states in combustors. If a state is unstable to small disturbances, then an oscillatory motion usually ensues. Such combustion instabilities commonly exhibit well-defined frequencies ranging from 15 hz or less to many kilohertz. Even at the highest amplitudes observed in practice, the instabilities consume only a small fraction of the available chemical energy. Thus, except in extremely severe instances, the oscillations do not normally affect the mean thrust or steady power produced by the systems. Serious problems may nevertheless arise due to structural vibrations generated by oscillatory pressures within the chamber or by fluctuations of the thrust. In extreme cases, internal surface heat transfer rates may be amplified ten-fold or more, causing excessive erosion of the chamber walls.

An observer perceives an unstable motion in a combustion chamber as "self-excited," a consequence of the internal coupling between combustion processes and unsteady motion. Except in cases of large disturbances (e.g. due to passage of a finite mass of solid material through the nozzle), the amplitude of the motion normally seems to grow out of the noise without the intrusion of an external influence. Two fundamental reasons explain the prevalence of instabilities in combustion systems:

(i) an exceedingly small part of the available energy is sufficient to produce unacceptably large unsteady motions;
(ii) the processes tending to attenuate unsteady motions are weak, chiefly because combustion chambers are nearly closed.

These two characteristics are common to all combustion chambers and imply that the possibility of instabilities occurring during development of a new device must always be recognized and anticipated. Treating combustion instabilities is part of the price to be paid for high-performance chemical propulsion systems. It is a corollary of that condition that the problem will never be totally eliminated. Advances in research will strengthen the methods for solution in practical applications, and will provide guidelines to help in the design process.

The fact that only a small part of the total power produced in a combustor is involved in combustion instabilities suggests that their existence and severity may be sensitive to apparently minor changes in the system. That

conclusion is confirmed by experience. Moreover, the complicated chemical and flow processes block construction of a complete theory from first principles. It is therefore essential that theoretical work always be closely allied with experimental results, and vice versa. No single analysis will encompass all possible instabilities in the various practical systems. There are nevertheless many features common to all combustion chambers. Indeed, it is one theme of this book that the characteristics shared by propulsion systems in many respects dominate the differences. While it is not possible to predict *accurately* the occurrence or details of instabilities, a framework does exist for understanding their general behavior, and for formulating statements summarizing their chief characteristics. For practical purposes, the theory often serves most successfully when used to analyze, understand, and predict *trends* of behavior, thereby also providing the basis for desirable changes in design. Experimental data are always required to produce quantitative results and their accuracy in turn is limited by uncertainties in the data.

Special problems may be caused by combustion instabilities interacting with the vehicle. Because the frequencies are usually well-defined in broad ranges, resonances with structural modes of the vehicle or with motions of components are common. Perhaps the best known form of this sort of oscillation is the POGO instability in liquid rockets. Strong couplings between chamber pressure oscillations, low-frequency structural vibrations, and the propellant feed system sustain oscillations. The amplitudes may grow to unacceptable limits unless measures are taken to introduce additional damping. A striking example occurred in the Apollo vehicle. The central engine of the cluster of five in the first stage was routinely shut off earlier than the others in order to prevent growth of POGO oscillations to amplitudes such that the astronauts would be unable to read instruments. Comments on the vibrations and the early shut off may be heard in communications recorded during the launch phase of several Apollo missions.

In the U.S., and possibly in other countries, notably Germany and Russia before and during World War II, combustion instabilities were first observed in solid and liquid propellant rocket engines. Subsequent to the war, considerable effort was expanded in Russia and in the U.S. to solve the problem, particularly in large liquid systems. Probably the most expensive program was carried out during development of the F-1 engine for the Apollo vehicle (Ofelein and Yang, 1993).

Liquid-fueled, air-breathing propulsion systems also commonly suffer combustion instabilities. Axial oscillations in ramjet engines are troublesome because their influence on the shock system in the inlet diffuser can reduce the inlet stability margin. Owing to their high power densities and light construction, thrust augmenters or afterburners are particularly susceptible to structural failures.

For any afterburner, conditions can be found under which steady operation is not possible. As a result, the operating envelope is restricted by the requirement that combustion instabilities cannot be tolerated. Due to structural constraints placed on the hardware, combustion instabilities in afterburners are particularly undesirable and are therefore expensive to treat.

In recent years combustion instabilities in the main combustor of gas turbines have become increasingly troublesome. The chief reason is ultimately due to requirements that emission of pollutants, notably oxides of nitrogen, be reduced. A necessary strategy, particularly for applications to flight, is reduction of the average temperature at which combustion takes place. Generation of NO by the thermal or 'Zel'dovich' mechanism is then reduced. Lower combustion temperature may be achieved by operating under lean conditions, when the flame stabilization processes tend to be unstable. Fluctuations of the flame cause fluctuations of energy release, which in turn may produce fluctuations of pressure, exciting acoustical motions in the chamber and affecting the generation of nitrogen oxides.

Finally, almost all solid rockets exhibit instabilities, at least during development, and occasionally motors are approved even with low levels of oscillations. Actual failure of a motor itself is rare in operations, but vibrations of the supporting structure and of the payload must always be considered. To accept the presence of weak instabilities in an operational system one must have sufficient understanding and confidence that the amplitudes will not unexpectedly grow to unacceptable levels. One purpose of these lectures is to provide an introduction to the foundation for gaining the necessary understanding.

In the most general sense, a combustion instability may be regarded as an unsteady motion of a dynamical system capable of sustaining oscillations over a broad range of frequencies. The source of energy associated

with the motions is ultimately related to the combustion processes, but the term 'combustion instability,' while descriptive, is misleading. In most instances, and always for the practical problems we discuss in this book, the combustion processes themselves are stable: uncontrolled explosions and other intrinsic chemical instabilities are not an issue. Observations of the gas pressure or of accelerations of the enclosure establish the presence of an instability in a combustion chamber. Excitation and sustenance of oscillations occur because coupling exists between the combustion processes and the gasdynamical motions, both of which may be stable. What is unstable is the entire system comprising the propellants, the propellant supply system, the combustion products that form the medium supporting the unsteady motions, and the containing structure.

If the amplitude of the motions is small, the vibrations within the chamber are usually related to classical acoustic behavior possible in the absence of combustion and mean flow. The geometry of the chamber is therefore a dominant influence. Corresponding to classical results, traveling and standing waves are found at frequencies approximated quite well by familiar formulas depending only on the speed of sound and the dimensions of the chamber. If we ignore any particular influences of geometry, we may describe the situation generally in the following way, a view valid for any combustion instability irrespective of the geometry or the type of reactants.

Combustion processes are generally sensitive to fluctuations of pressure, density, and temperature of the environment. A fluctuation of burning produces local changes in the properties of the flow. Those fluctuations propagate in the medium and join with the global unsteady field in the chamber. Under favorable conditions, the field develops to a state observable as a combustion instability. As illustrated schematically in Figure 1.1, we may view the process abstractly in analogy to a feedback amplifier in which addition of feedback to a stable oscillator can produce oscillations. Here the oscillator is the combustion chamber, or more precisely, the medium within the chamber that supports the unsteady wave motions. Feedback is associated with the influences of the unsteady motions on the combustion processes or on the supply system, which in turn generate fluctuations of the field variables. The dynamical response of the medium converts the local fluctuations to global behavior. In the language of control theory, the field in the chamber is the 'plant,' described by the general equations of motion.

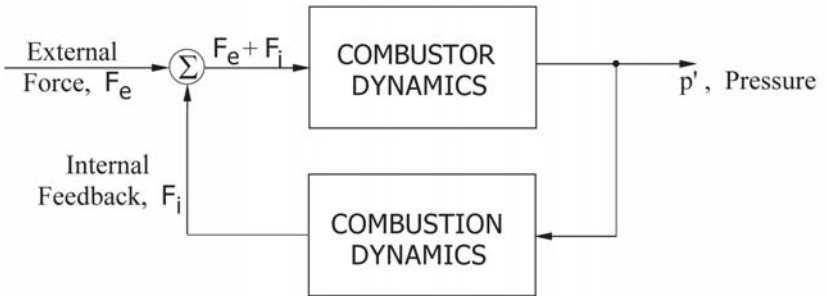

FIGURE 1.1. Schematic Diagram of a Combustion System as a Feedback Amplifier

The diagram in Figure 1.1 illustrates the global point of view taken here. Broadly, the subjects covered divide into two categories: those associated with the plant—the fluid mechanics and other physical processes comprising the *combustor dynamics;* and those connected primarily with the feedback path, chiefly combustion processes and their sensitivity to time-dependent changes in the environment, the *combustion dynamics.* Splitting is particularly clear for solid rockets because practically all of the combustion processes are completed in a thin region adjacent to the burning propellant. The theory we will describe encompasses all types of combustion instabilities in a general framework having the organization suggested by the sketch. External forcing functions are accommodated as shown in the sketch, but the causes associated with the feedback path are far more significant in practice.

Figure 1.1 is motivated by more than a convenient analogy. For practical purposes in combustion systems, we generally wish to eliminate instabilities. Traditionally that has meant designing systems so that small disturbances are stable, or adding some form of energy dissipation to compensate the energy gained from the combustion processes, that is, *passive control.* However, in the past few years interest has grown in the possibility of *active control* of instabilities. If that idea is to be realized successfully, it will be necessary to combine modern control theory with the sort of theory described here. It is advantageous to think from the beginning in terms that encourage this merger of traditionally distinct disciplines.

We will return to the subject of passive control for solid rockets at the end of these lectures. Any method of control is rendered more effective the more firmly it rests on understanding the problem to be solved. Understanding a problem of combustion instabilities always requires a combination of experiment and theory. For many reasons, including intrinsic complexities and inevitable uncertainties in basic information (e.g., material properties, chemical dynamics, turbulent behavior of the flow field, ...), it is impossible to predict from first principles the stability and nonlinear behavior of combustion systems. Hence the purpose of theory is to provide a framework for interpreting observations, both in the laboratory and full-scale devices; to suggest experiments to produce required ancillary data or to improve the empirical base for understanding; to formulate guidelines for designing full-scale systems; and globally to serve, like any good theory, as the vehicle for understanding the fundamental principles governing the physical behavior, thereby having predictive value as well.

All theoretical work in this field has been carried out in response to observational and experimental results. We therefore spend much of the remainder of this introductory chapter on a survey of the characteristics of combustion instabilities observed, and occasionally idealized, for combustion systems generally to be analyzed in later chapters. The general point of view taken throughout the book will then be formulated in heuristic fashion, based on experimental results.

1.2. Historical Background. Some of the consequences and symptoms of combustion instabilities were first observed in the late 1930s and early 1940s, roughly at the same time for liquid and solid propellant rockets, and apparently somewhat earlier in the Soviet Union than in the U.S. With the later development of turbojet engines, high-frequency instabilities were found in thrust augmenters or afterburners in the late 1940s and early 1950s. Although the problem had been encountered in ramjet engines in the 1950s, it became a matter of greater concern in the late 1970s and 1980s. The introduction of compact dump combustors led to the appearance of longitudinal or axial oscillations that interfered with the inlet shock system, causing loss of pressure margin and 'unstart' in the most severe cases. Owing to availability, almost all of the data cited here as examples will be derived from liquid rockets, solid rockets and laboratory devices. Figure 1.2 is a qualitative representation of the chronology of combustion instabilities. Due to the accessibility of documentation and the experiences of the author, particular cases cited are mainly those reported in the U.S.

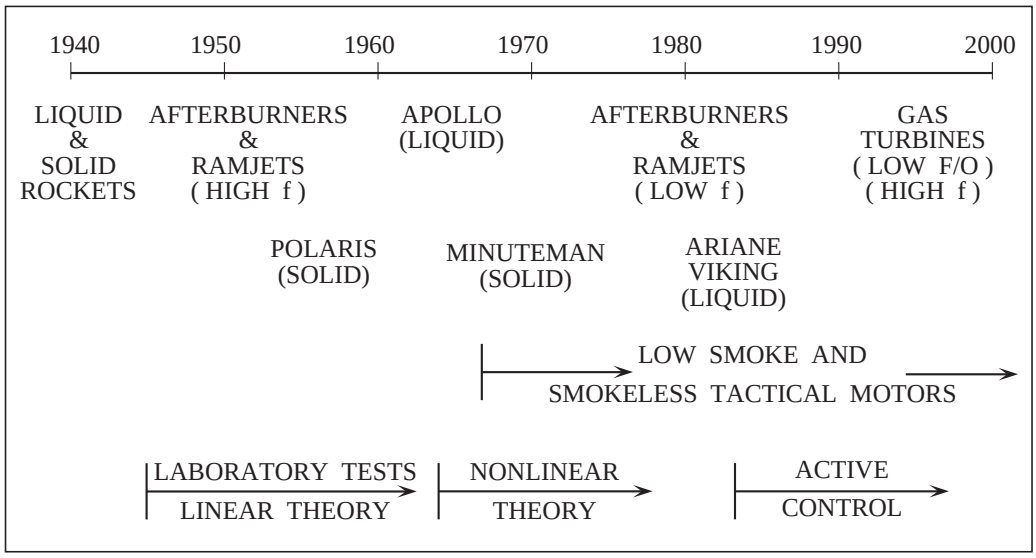

FIGURE 1.2. A Chronology of Combustion Instabilities

Several reviews of early experiences with combustion instabilities have been prepared for liquid rockets (Ross and Datner 1954) and for solid rockets (Wimpress 1950; Price 1968; Price and Flandro 1992). The details are not important here, but the lessons learned certainly are. Often forgotten is the most important requirement of good high-frequency instrumentation to identify and understand combustion instabilities in full-scale as well as in laboratory systems. Until the early 1940s, transducers and instrumentation for measuring pressure had inadequate dynamic response to give accurate results for unsteady motions. Ross and Datner note that "Prior to 1943,

the resolution of Bourdon gauges, photographed at 64 and 128 fps, constituted the principal instrumentation." Recording oscillographs were introduced sometime in 1943, but not until the late 1940s were transducers available with sufficient bandwidth to identify instabilities at higher frequencies (hundreds of hertz and higher).

The situation was even more difficult with solid rockets because of the practical difficulties of installing and cooling pressure transducers. Probably the experience with cooling chamber and nozzle walls helps explain why quantitative results were obtained for instabilities in liquid rockets earlier than for solid rockets (E. W. Price, private communication). Prior to the appearance of high-frequency instrumentation, the existence of oscillations was inferred from such averaged symptoms as excessive erosion of inert surfaces or propellant grains due to increased heat transfer rates; erratic burning appearing as unexpected shifts in the mean pressure; structural vibrations; visible fluctuations in the exhaust plume; and, on some occasions, audible changes in the noise produced during a firing.

Experimental work progressed for several years before various unexplained anomalies in test firings were unambiguously associated with oscillations. By the late 1940s, there was apparently general agreement among researchers in the U.S. and Europe that combustion instabilities were commonly present in rocket motors and that they were somehow related to waves in the gaseous combustion products. In addition to measurements with accelerometers, strain gauges, and pressure transducers, methods for flow visualization soon demonstrated their value, mainly for studies of liquid propellant rockets (Altseimer 1950; Berman and Logan 1952; and Berman and Scharres 1953). Characteristics of the instabilities as acoustic vibrations, or weak shock waves, were revealed.

It is much more difficult to observe the flow field in a solid rocket motor and during the early years of development, the only results comparable to those for liquid rockets were obtained when excessive chamber pressures caused structural failures. Partially burned grains often showed evidence of increased local burning rates, suggesting (possibly) some sort of influence of the gas flow. The same events also produced indications of unusual heating of the unburned solid propellant, attributed to dissipation of mechanical vibrational energy (Price and Flandro, 1992). Subsequently that interpretation was confirmed by direct measurements (Shuey, 1987).

High-frequency or 'screech' oscillations were also first encountered in afterburners in the late 1940s; as a result of the experience with rockets and the availability of suitable instrumentation, the vibrations were quickly identified as combustion instabilities. The staff of the Lewis Laboratory (1954) compiled most of the existing data and performed tests to provide a basis for guidelines for design.

Thus by the early 1950s most of the basic characteristics of combustion instabilities had been discovered in both liquid-fueled and solid-fueled systems. Many of the connections with acoustical properties of the systems, including possible generation of shock waves, were recognized qualitatively. Although the frequencies of oscillations found in tests could sometimes be estimated fairly closely with results of classical acoustics, no real theory having useful predictive value existed. During the 1950s and the 1960s the use of sub-scale and laboratory tests grew and became increasingly important as an aid to solving problems of combustion instabilities occurring in the development of new combustion systems.

1.3. Solid Propellant Rocket Motors. Since the late 1950s, serious concern with instabilities in solid propellant motors has been sustained by problems arising in both small (tactical) and large (strategic and large launch systems) rockets. The volume of collected papers compiled and edited by Berle (1960) provides a good view of the state of the field at the end of the 1950's in the Western countries. The level of activity remained high and roughly unchanged through the 1960's, due entirely to the demands of the Cold War: the use of solid rocket boosters in systems for launching spacecraft, and for changing trajectories, came later. During the 1950's and 1960's strong emphasis was already placed on sub-scale and laboratory tests, a strategy dictated at least partly by the large costs of full-scale tests. As a result, more is understood about combustion instabilities in solid rockets than in other systems. Moreover, methods and viewpoints developed by the solid rocket community have strongly influenced the approaches to treating combustion instabilities in other systems. The theory developed in this book is an example of that trend.

A problem with the third stage of the Minuteman II launch vehicle in the late 1960's (Joint Prop. Mtg 1972) initially motivated considerable research activity during the following decade, sponsored largely by the Air Force Rocket Propulsion Laboratory. The causes of three failures in test flights had been traced to the presence of

combustion instabilities. Thorough investigation showed that although oscillations had been present throughout the history of the motor, a significant change occurred during production, apparently associated with propellant Lot 10. Figure 1.3 shows the main observable features.

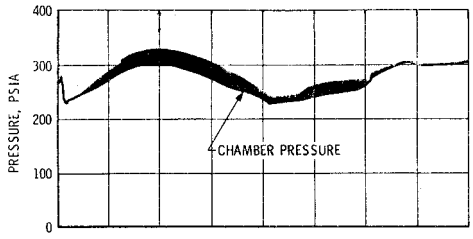

(a)

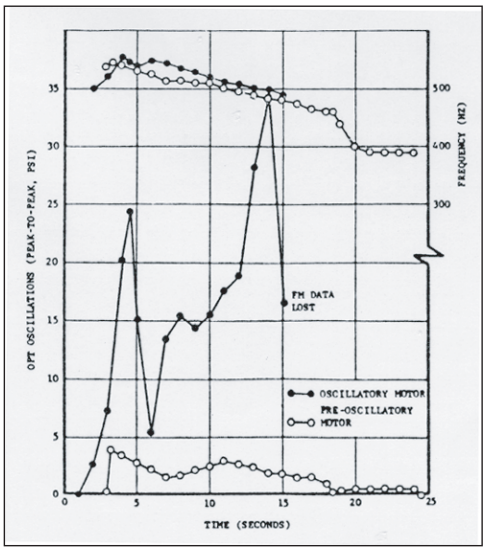

(b)

FIGURE 1.3. Frequencies and Amplitudes of Combustion Instabilities in the Minuteman II, Stage 3 Motor: (a) A Pressure Record from a Flight Test; (b) Frequencies and Amplitudes Measured During Static Tests.

The oscillations existed during the first fifteen seconds of every firing and always had frequency around 500 Hertz. Whatever occurred with production Lot 10 caused the maximum amplitudes of oscillations to be unpredictably larger in motors containing propellant from that and subsequent lots. The associated structural vibrations caused failures of a component in the thrust control system.

This example exhibits several characteristics common to many instances of combustion instabilities in solid rockets. In test-to-test comparisons, frequencies are reproducible and amplitudes show only slight variations unless some change occurs in the motor. Any changes must be of two sorts: either geometrical, i.e. the internal shape of the grain, or chemical, consequences of variations in the propellant. Chemical changes, i.e. small variations in the propellant composition, are most likely to affect the dynamics of the combustion processes and indirectly other physical processes in the motor. That is apparently what happened in the Minuteman.

Between production of propellant Lots 9 and 10, the supplier of aluminum particles was changed, because the original production facility was accidentally destroyed. The new aluminum differed in two respects: shapes of the particles, and the proportion of oxide coating. Testing during investigation of the instability led to the conclusion that consequent changes in the processes responsible for the production of aluminum oxide products of combustion generated smaller particle sizes of Al_2O_3. The smaller sizes less effectively attenuated acoustic waves; the net tendency to excite waves therefore increased. As a result, the motors were evidently more unstable and also supported larger amplitudes of oscillation. The second conclusion was purely speculative at the time of

the investigation, but can now be demonstrated with the theory covered in this book. Nevertheless, the details explaining why the change in the aluminum supplied led eventually to the significant changes in the combustion products remain unknown.

Subsequent to the Minuteman problem, the Air Force Rocket Propulsion Laboratory supported a substantial program of research on many of the most important problems related to combustion instabilities in solid rockets. Broadly, the intellectual centroid of that program lay closer to the areas of combustor dynamics and combustion dynamics than to the detailed behavior of propellants. The synthesis, chemistry and kinetics of known and new materials belonged to programs funded by other agencies in the U.S. and in Europe, notably ONERA in France. By far most of the related work in Russia has always been concerned with the characteristics and combustion of propellants, with relatively little attention to the dynamics of combustors.

As the research activities related specifically to solid rockets decreased during the 1980s and new programs began for liquid-fueled systems, the communities, previously quite separate, grew closer together. For example, prompted by contemporary concern with problems in ramjets, a workshop sponsored by JANNAF (Culick 1980) was organized partly with the specific intention to bring together people experienced in the various propulsion systems. During the 1980s there was considerable interchange between the various research communities and since that time, a significant number of people have worked on both solid and liquid-fueled systems. That shift in the sociology of the field has provided the possibility and much of the justification for this book. Events of the past decade have confirmed that the field of combustion instabilities is very usefully approached as a unification of the problems arising in all systems.

In Europe during the 1990's, work on combustion instabilities in solid propellant rockets has been motivated largely by low frequency oscillations in the booster motors for the Ariane 5. The most intensive and comprehensive recent work in the U.S. has been carried out in two Multiuniversity Research Initiators (MURI) involving 15 different universities. An unusual characteristic of those programs, active for five years beginning in 1995, was the inclusion of coordinated research on all aspects of problems of combustion instabilities in solid propellant rockets, from fundamental chemistry to the internal dynamics of motors. Results of recent works will be covered here in the appropriate places.

1.4. Mechanisms of Combustion Instabilities. Just as for steady operation, the chief distinctions among combustion instabilities in different combustors must ultimately be traceable to differences in geometry and the states of the reactants. The root causes, or 'mechanisms', of instabilities are imbedded in that context and are often very difficult to identify with certainty. Possibly the most difficult problem in this subject is to quantify the mechanism. Solving that problem requires finding an accurate representation of the relevant dynamics.

The simplest and most convenient characterization of an unstable oscillation is expressed in terms of the mechanical energy of the motion. Linear theory produces the result that the rate of growth of the amplitude is proportional to the fractional rate of change of energy, the sum of kinetic and potential energies. The idea is discussed further in the following section. What matters at this point is that the term 'mechanism' refers to a process that causes transfer of energy to the unsteady motion from some other source. Thus, mechanisms form the substance of the feedback path in Figure 1.1. Generally there are only three sorts of energy sources for unsteady motions in a combustor: the combustion processes; the mean flow, which of course itself is caused by combustion; and a combination of combustion and mean flow simultaneously acting. The distinction is important because the physical explanations of the energy transfer are very different in the three cases.

Combustion processes are sensitive to the macroscopic flow variables, particularly pressure, temperature and velocity. Even slow changes of those quantities affect the energy released according to rules that can be deduced from the behavior for steady combustion. In general, however, representations of that sort, based on assuming quasi-steady behavior, are inadequate. Combustion instabilities normally occur in frequency ranges such that genuine dynamical behavior is significant. That is, the transient changes of energy release do not follow precisely in phase with imposed changes of a flow variable such as pressure.

The next simplest assumption is that the combustion processes behave as a first order dynamical system characterized by a single time delay or relaxation time. That idea was apparently first suggested by Karman as a basis for interpreting instabilities discovered in early experiments with liquid propellant rockets at Caltech

(Summerfield, 1941). That representation, which came to be called the '$n - \tau$ model' was developed most extensively by Crocco and his students at Princeton during the 1950s and 1960s. Time delays may be due, for example, to processes associated with ignition of reactants. Subsequent to injection as the reactants flow downstream, finite times may be required for vaporization, mixing, and for the kinetics mechanism to reach completions. Both effects may be interpreted as a convective time delay. Under unsteady conditions, the initial state of the reactants, their concentrations, pressure, and velocity, also fluctuate, causing the delay time to be both nonuniform in space and in time. As a result, rate of energy release downstream in the chamber is also space- and time-dependent, and acts as a source of waves in the combustor.

The approximation of first order behavior fails entirely for the dynamics of burning solid propellants (Culick 1968). Although in good first approximation dominated by unsteady heat transfer in the condensed phase, a diffusive process, the combustion dynamics in this case exhibits behavior closer to that of a second order system. The frequency response of that burning rate tends normally to have a large broad peak centered at a frequency falling well within the range of the frequencies characteristic of the chamber dynamics. Hence there is a clear possibility for a resonance and instability suggested by the diagram in Figure 1.1. The chief mechanisms for instabilities in solid rockets are discussed in the following chapter.

Generation of oscillations by the average flow is due to causes roughly like those active in wind musical instruments. In all such cases, flow separation is involved, followed by instability of a shear layer and formation of vortices. Direct coupling between the vortices and a local velocity fluctuation associated with an acoustic field is relatively weak; that is, the rate of energy exchange is in some sense small. However, the interaction between the velocity (or pressure) fluctuation and the initial portion of the shear layer is normally a basic reason that feedback exists between the unsteady field in the volume of the combustor and vortex shedding.

It has long been known experimentally that vortices shed in a chamber more effectively generate acoustic waves if they impinge in an obstacle downstream of their origin (Flandro and Jacobs, 1975; Magiawala and Culick, 1979; Flandro, 1986). The first example of this phenomenon was the solid rocket booster for the Shuttle launch system in the 1970s. It was that problem that motivated the works just cited, but since then vortex shedding has been recognized as a mechanism for generating acoustic oscillations in other systems as well, notably the booster motors on the Space Shuttle and on the Ariane 5.

1.5. Physical Characteristics of Combustion Instabilities. Owing to the difficulty of making direct measurements of the flow field within a combustion chamber, virtually all that is known about combustion instabilities rests on close coordination of experiment and theory. The subject is intrinsically semi-empirical, theoretical work being founded on observational data both from full-scale machines and laboratory devices. Conversely, the theoretical and analytical framework occupies a central position as the vehicle for planning experimental work and for interpreting the results. The chief purpose of this section are to summarize briefly the most important basic characteristics of observed instabilities; and to introduce the way in which those observations motivate the formulation of the theoretical framework.

In tests of full-scale propulsion systems, only three types of data are normally available; obtained from pressure transducers, accelerometers, and strain gauges. Measurements of pressure are most direct but are always limited, and often not possible when the necessary penetration of the enclosure to install instruments is not allowed. Hence the unsteady internal pressure field is often inferred from data taken with accelerometers and strain gauges. In any case, because it is the fundamental variable of the motions, the pressure will serve here as the focus of our discussion.

Figure 1.4a and 1.4b is an example of a fully developed instability, shown with its power spectral densities. The well-defined peaks reflect the clear presence of several frequencies in the waves, the larger amplitudes occurring at the lower frequencies, as commonly happens. A substantial background of broad-band noise is of course always present due to turbulent fluctuations of the flow, noise emission by combustion processes, and possibly other unsteady motions such as flow separation. Some recent laboratory tests have shown that the level of noise depends on the presence and amplitude of combustion instabilities, but the cause is unknown and no such observations exist for full-scale combustors.

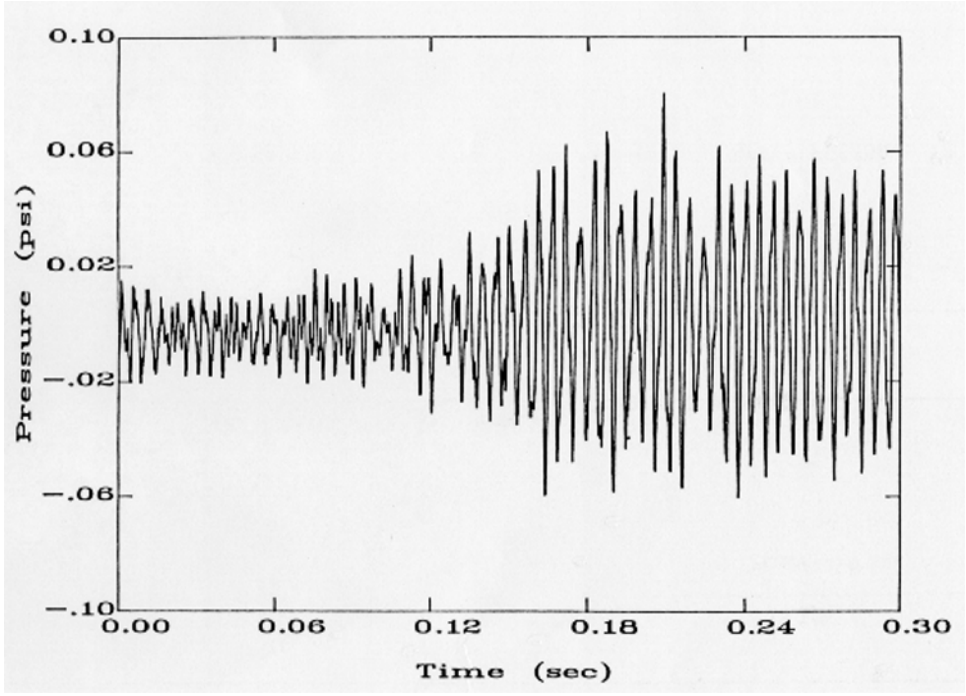

(a)

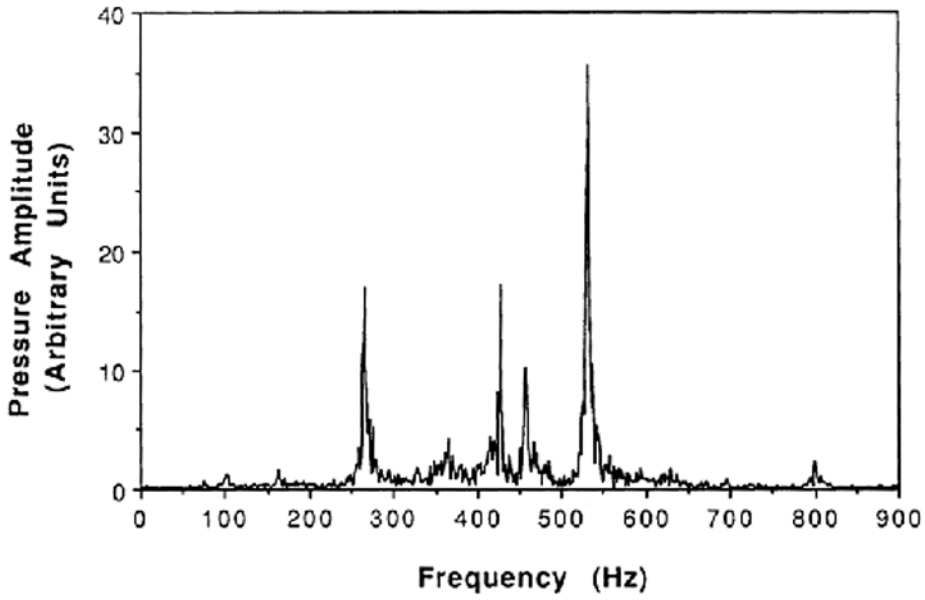

(b)

FIGURE 1.4. Waveform and Spectrum for an Instability in the Caltech Dump Combustor

Much of these lectures is devoted to understanding the origins of the behavior illustrated by the examples in Figures 1.3 and 1.4. The classical theory of acoustics has provided the basis for under standing combustion instabilities since early recognition that some unexpected observations could be traced to pressure oscillations. Many basic results of classical acoustics have been applied directly and with remarkable success to problems of instabilities. It is often taken for granted that well-known acoustics formulas should be applicable—their use can in fact be justified on fundamental grounds. However, in the first instance, it is surprising that they work so well,

because the medium is far from the ideal uniform quiescent gas assumed in the classical acoustics of resonating chambers.

A combustion chamber contains a non-uniform flow of chemically reacting species, often present in condensed as well as gaseous phases, exhausting through a nozzle that is choked in rockets, ramjets, and afterburners. Moreover, the flow is normally turbulent and may include regions of separation. Yet estimates of the frequencies of oscillations computed with acoustics formulas for the natural modes of a closed chamber containing a uniform gas at rest commonly lie within 10–15 percent or less of the frequencies observed for combustion instabilities, if the speed of sound is correctly chosen.

There are three main reasons that the classical view of acoustics is a good first approximation to wave propagation in combustion chamber: (1) the Mach number of the average flow is commonly small, so convective and refractive effects are small; (2) if the exhaust nozzle is choked, incident waves are efficiently reflected, so for small Mach numbers the exit plane appears to be nearly a rigid surface; and (3) in the limit of small amplitude disturbances, it is a fundamental result for compressible flows that any unsteady motion can be decomposed into three independent modes of propagation, of which one is acoustic (Chu and Kovazsnay 1956). The other two modes of motion are vortical disturbances, the dominant component of turbulence, and entropy (or temperature) waves. Hence even in the highly turbulent non-uniform flow usually present in a combustion chamber, acoustic waves behave in good first approximation according to their own simple classical laws. That conclusion has simplified enormously the task of gaining qualitative understanding of instabilities arising in full-scale systems as well as in laboratory devices.

Of course, it is precisely the departures from classical acoustics that define the class of problems we call combustion instabilities. In that sense, this book is concerned chiefly with perturbations of a very old problem, standing waves in an enclosure. That point of view has significant consequences; perhaps the most important is that many of the physical characteristics of combustion instabilities can be described and understood quite well in a familiar context. The remainder of this chapter is an elaboration of that conclusion.

The most obvious evidence that combustion instabilities are related to classical acoustic resonances is the common observation that frequencies measured in tests agree fairly well with those computed with classical formulas. Generally, the frequency f of a wave equals its speed of propagation, a, divided by the wavelength, λ:

$$f = \frac{a}{\lambda} \tag{1.1}$$

On dimensional grounds, or by recalling classical results, we know that the wavelength of a resonance or normal mode of a chamber is proportional to a length, the unobstructed distance characterizing the particular mode in question. Thus the wavelengths of the organ-pipe modes are proportional to the length, L, of the pipe, those of modes of motion in transverse planes of a circular cylindrical chamber are proportional to the diameter, D, and so forth. Hence (1.1) implies

$$f \sim \frac{a}{L} \quad \text{longitudinal modes}$$

$$f \sim \frac{a}{D} \quad \text{transverse modes} \tag{1.2 a, b}$$

There are two basic implications of the conclusion that the formulas (1.2 a, b), with suitable multiplying constants, seem to predict observed frequencies fairly well: evidently the geometry is a dominant influence on the special structure of the instabilities; and we can reasonably define some sort of average speed of sound in the chamber, based on an approximation to the temperature distribution. In practice, estimates of a use the classical formula $a = \sqrt{\gamma RT}$ with T the adiabatic flame temperature for the chemical system in question, and with the properties γ and R calculated according to the composition of the mixture in the chamber. Usually, mass-averaged values, accounting for condensed species, seem to be close to the truth. If large differences of temperature exist in the chamber, as in a flow containing flame fronts, nonuniformities in the speed of sound must be accounted for to obtain good estimates of the frequencies.

Even for more complicated geometries, notably those often used in solid rockets, when the simple formulas (1.2 a, b) are not directly applicable, numerical calculations of the classical acoustic motions normally give good

approximations to the natural frequencies and pressure distributions. Thus quite generally we can adopt the point of view that combustion instabilities are acoustical motions excited and sustained in the first instance by interactions with combustion processes. That the classical theory works so well for estimating frequencies and distributions of the unsteady motions means that computation of those quantities is not a serious test of a more comprehensive theory. What is required first of a theory of combustion instabilities is a basis for understanding how and why combustion instabilities differ from classical acoustics.

In particular, two global aspects of minor importance in most of classical acoustics, are fundamental to understanding combustion instabilities: transient characteristics and nonlinear behavior. Both are associated with the property that with respect to combustion instabilities, a combustion chamber appears to an observer to be a *self-excited system*: the oscillating appear without the action of externally imposed forces. Combustion processes are the sources of energy which ultimately appear as the thermal and mechanical energy of the fluid motions. If the processes tending to dissipate the energy of a fluctuation in the flow are weaker than those adding energy, then the disturbance is unstable.

1.6. Linear Behavior. When the amplitude of a disturbance is small, the rates of energy gains and losses are usually proportional to the energy itself which in turn is proportional to the square of the amplitude of the disturbance; the responsible processes are said to be linear because the governing equations are linear in the flow variables. An unstable disturbance then grows exponentially in time, without limit if all processes remain linear. Exponential growth of the form $A_0 e^{\alpha t}$, where A_0 is the amplitude of the initial small disturbance, is characteristic of the initial stage of an instability in a self-excited system, sketched in Figure 1.5(a). In contrast, the initial transient in a linear system forced by an invariant external agent grows according to the form $1 - e^{-\beta t}$, shown in Figure 1.5(b). The curve $e^{\alpha t}$ is concave upward and evolves into a constant limiting value for a physical system only if nonlinear processes are active. However, the plot of $1 - e^{-\beta t}$ is concave downward and approaches a limiting value for a linear system because the driving agent supplies only finite power.

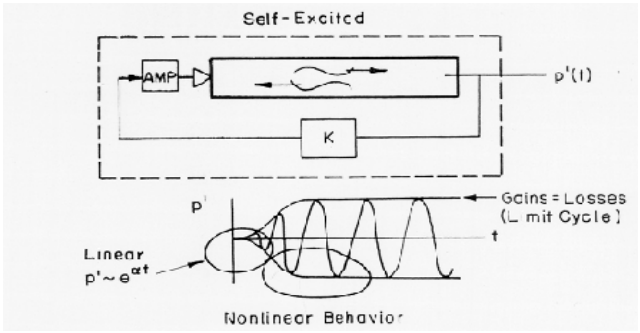

(a)

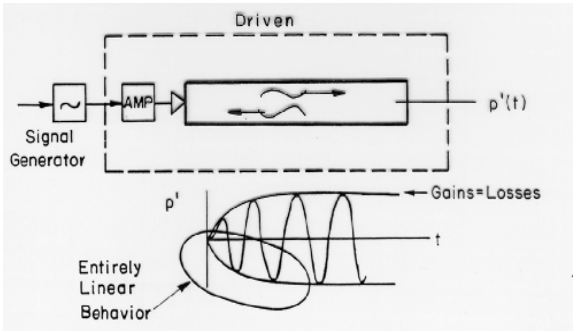

(b)

FIGURE 1.5. Transient behavior of (a) Self Excited Linearly Unstable Motions; (b) Forced Motions.

Data of the sort reproduced in Figure 1.4 leave no doubt that the unstable motions in combustion chambers are self-excited, having the characteristics shown in Figure 1.5(a). The physical origin of this behavior is the dependence of the energy gains and losses on the motions themselves. For combustion instabilities, the 'system' is the dynamical system whose behavior is measured by the instrument sensing the pressure oscillations. Thus, in view of earlier remarks, the dynamical system is in some sense the system of acoustical motions in the chamber coupled to the mean flow and combustion processes (recall Figure 1.1).

It is a fundamental and extremely important conclusion that by far most combustion instabilities are motions of a self-excited dynamical system. Probably the most significant implication is that in order to understand fully the observed behavior, and how to affect it and control it, one must understand the behavior of a nonlinear system. When the motion in a combustion chamber is unstable, except in unusual cases of growth to destruction, the amplitude typically settles down to a finite value: the system then executes a limiting motion, usually a periodic limit cycle. For practical applications, it is desirable to know how the amplitude of the limit cycle depends on the parameters characterizing the system. That information may serve as the basis for changing the characteristics to reduce the amplitude, the goal in practice being zero. In any case, good understanding of the properties of the

limit cycle will also provide some appreciation for those variables which dominate the behavior and to which the motions may be most sensitive, a practical matter indeed.

Our global view, then, is that a combustion instability is an oscillatory motion of the gases in the chamber, which can in first approximation be synthesized of one or more modes related to classical acoustic modes. The mode having lowest frequency is a 'bulk' mode in which the pressure is nearly uniform in space but fluctuating in time. Because the pressure gradient is everywhere small, the velocity fluctuations are nearly zero. This mode corresponds to the vibration of a Helmholtz resonator obtained, for example, by blowing over the open end of a bottle. The cause in a combustion chamber may be the burning process itself, or it may be associated with oscillations in the supply of reactants, caused in turn by the variations of pressure in the chamber.

Structural vibrations of a solid rocket are not normally influential, but an instability of the bulk mode (there is only one bulk mode for a given geometry) has often been a problem in motors designed for use in space vehicles. In those cases, the term L*-instability has been used because the stability of the mode is predominantly a function of the L* of the motor and the mean pressure (Sehgal and Strand 1964). The instability is associated with the time lag between fluctuations of the burning rate and of mass flux through the nozzles: that time lag is proportional to the residence time, and hence L*, for flow in the chamber. L*-instabilities occur in motors qualified for space flight because they arise in the lower ranges of pressure at which such rockets operate.

Whatever the system, most combustion instabilities involve excitation of the acoustic modes, of which there are an infinite number for any chamber. The values of the frequencies are functions primarily of the geometry and of the speed of sound, the simplest examples being the longitudinal and transverse modes of a circular cylinder, with frequencies behaving according to 1.2 a, b. Which modes are unstable depends on the balance of energy supplied by the exciting mechanisms and extracted by the dissipating processes. We consider here only linear behavior to illustrate the point.

In general the losses and gains of energy are strongly dependent on frequency. For example, the attenuation due to viscous effects typically increases with the square root of the frequency. Other sources of energy loss associated with interactions between the oscillations and the mean flow tend to be weaker functions of frequency. That is the case, for example for reflections of waves by a choked exhaust nozzle. The gains of energy usually depend in a more complicated way on frequency.

The sources of energy for combustion instabilities i.e. the mechanisms responsible for their existence, present the most difficult problems in this field. For the present we confine our attention to qualitative features of energy exchange between combustion to unsteady motions. For example, the magnitude of the energy addition due to coupling between acoustic waves and combustion processes for a solid propellant normally rises from some relatively small quasi-steady value at low frequencies, passes through a broad peak, and then decreases to zero at high frequencies. Recent experimental results suggest that flames may exhibit similar behavior (Pun 2001). Energy is transferred to a pressure oscillation having a particular frequency at a rate proportional to the part of the coupling that is in phase with the pressure at that frequency.[1] Figure 1.6 is a schematic illustration of this sort of behavior.

In Figure 1.6, the gains exceed the losses in the frequency range $f_1 < f < f_2$. Modes having frequencies in that range will therefore be linearly unstable. An important characteristic, typical of combustion chambers generally, is that in the lower ranges of frequency, from zero to somewhat above the maximum frequency of instability, the net energy transfer is a small difference between relatively larger gains and losses. That implies the difficulty, confirmed by many years' experience, of determining the net energy flow accurately. Unavoidable uncertainties in the gains and losses themselves become much more significant when their difference is formed. That is the main reason for the statement made earlier that analysis of combustion instabilities has been useful in practice chiefly for predicting and understanding trends of behavior rather than accurate calculations of the conditions under which a given system is unstable. The ultimate source of all of these difficulties is the fact, cited in Section 1.1, is the property that the motions in question consume and contain only small portions of the total energy available within the system. Hence in both laboratory tests and in operational systems one is confronted with determining the characteristics of essentially small disturbances imbedded in a complicated dynamic environment.

[1]It is possible, due to the behavior of the phase angle, that in a range of high frequencies the combustion processes may in fact extract energy from the acoustic waves and hence contribute to the losses of energy.

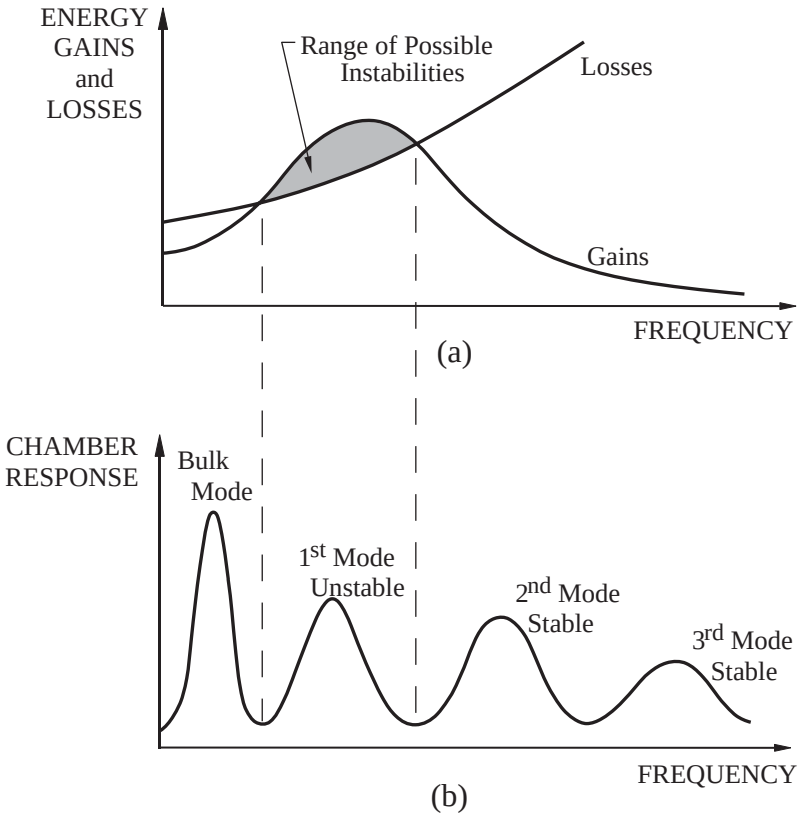

FIGURE 1.6. Qualitative Dependence of (a) Energy Gains and Losses; and (b) the Frequency Response of a Combustor.

The best and most complete data illustrating the preceding remarks have been obtained with solid propellant rockets. There are several reasons for that circumstance. First, the ignition period — the time to cause all of the exposed propellant surface to begin burning — is relatively short and the average conditions in the chamber quickly reach their intended values. Unless oscillations are severely unstable, and growing rapidly during the ignition transient, there is a good opportunity to observe the exponential growth characteristic of a linear instability. The measurements shown in Figures 1.4(a) and (b) are good examples.

Secondly, it is probably true that more effort has been spent on refining the measurements and predictions of linear stability for solid rockets than for other systems because of the expense and difficulty of carrying out replicated tests. There is no practical, routine way of interrupting and resuming firings and it is the nature of the system that an individual motor can be fired only once. Particularly for large motors used in space launch vehicles, successive firings involve great expense. Development by empirical trial-and-error is costly and there is considerable motivation to work out methods of analysis and design applicable to individual tests.

1.6.1. *Gains and Losses of Acoustic Energy; Linear Stability.* It is a general result of the theory of linear systems that if a system is unstable, a small disturbance of an initial state will grow exponentially in time:

$$\text{amplitude of disturbance } \sim e^{\alpha_g t} \tag{1.3}$$

where $\alpha_g > 0$ is called the *growth constant.* If a disturbance is linearly stable, then its amplitude decays exponentially in time, being proportional to $e^{-\alpha_d t}$ and $\alpha_d > 0$ is the *decay constant.* The definition (1.3) implies that for a variable of the motion, say the pressure, having maximum amplitude $\hat{p}_0$ in one cycle of a linear oscillation:

$$p'(t) = \hat{p}_0 e^{\alpha_g (t-t_0)} \tag{1.4}$$

where $\hat{p}_0$ is the amplitude at time $t = t_0$. Then if p'_1, p'_2 are the peak amplitudes at time t_1, t_2 as indicated in Figure 1.7,

$$\frac{\hat{p}_2}{\hat{p}_1} = \frac{p'(t=t_2)}{p'(t=t_1)} = \frac{e^{\alpha_g(t_2-t_0)}}{e^{\alpha_g(t_1-t_0)}} = e^{\alpha_g(t_2-t_1)} \tag{1.5}$$

The logarithm of (1.5) is

$$\log \frac{\hat{p}_2}{\hat{p}_1} = \alpha_g(t_2 - t_1) \tag{1.6}$$

In practice, $t_2 - t_1$ is taken equal to the period τ, the time between successive positive (or negative) peaks. Then the logarithm of the ratio $\hat{p}_2/\hat{p}_1$ for a number of pairs of successive peaks is plotted versus the time t_1 or t_2 at which the first or second peak occurs. The line is straight, having slope α_g.

Whatever the system, the analytical treatment of linear stability is essentially the same. There is really only one problem to solve: find the growth and decay constants and the frequencies of the modes. Determining the actual mode shapes is part of the general problem, but is often not essential for practical purposes. Typically, both the frequency and the mode shape for small-amplitude motions in a combustion chamber are so little different from their values computed classically as to be indistinguishable by measurement in operating combustors. By "classical" we mean here a computation according to the equations of classical acoustics for the geometry at hand, and with account taken of large gradients in the temperature, which affect the speed of sound. The presence of combustion processes and a mean flow field are not accounted for explicitly, but it may be necessary for satisfactory results, to include a good approximation to the boundary condition applied at the exhaust nozzle, particularly if the average Mach number is not small.

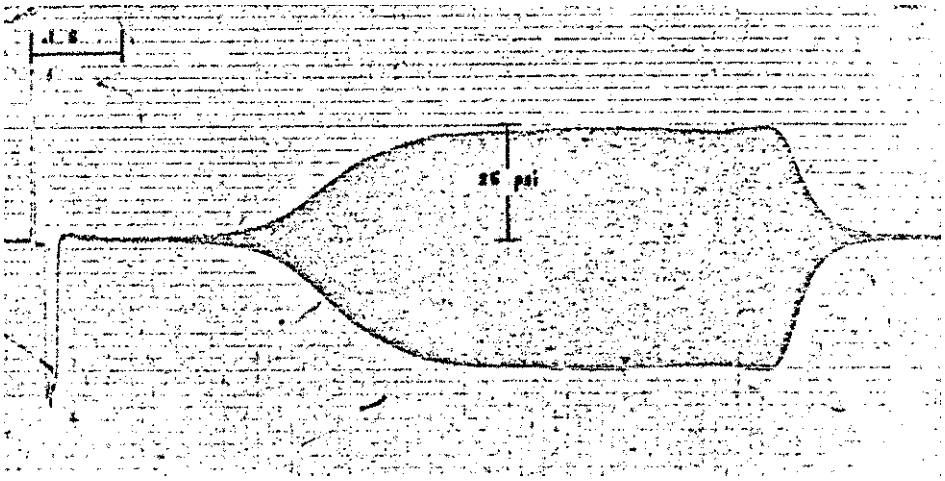

FIGURE 1.7. Exponential Growth of a Linearly Unstable Motion (Perry 1968)

Hence the linear stability problem is really concerned with calculations of the growth and decay constants for the modes corresponding to the classical acoustic resonances. An arbitrary small amplitude motion can, in principle, be synthesized with the results, but that calculation is rarely required for practical applications. Results for the net growth or decay constant have been the central issue in both theoretical and practical work. In combustors, processes causing growth of disturbances and those causing decay act simultaneously. Hence an unstable disturbance is characterized by a net growth constant that can be written $\alpha = \alpha_g - \alpha_d$. Because the problem is linear, the growth constants can quite generally be expressed as a sum of the contributions due to processes accounted for in the formulation, as for example:

$$\alpha := \alpha_g - \alpha_d = (\alpha)_{\text{combustion}} + (\alpha)_{\text{nozzle}} + (\alpha)_{\text{mean flow}} + (\alpha)_{\text{condensed}} + (\alpha)_{\text{structure}} + \cdots \tag{1.7}$$

The labels refer to processes of interaction between the acoustic field and combustion, the nozzle, the mean flow, condensed species, the containing structure,.... Structural interactions comprise not only the vibrations mentioned earlier as a necessary part of the POGO instability, but also quite generally any motions of mechanical components, including propellant. For example, in large, solid propellant rockets, motions of the viscoelastic

material of the grain may be a significant source of energy losses through internal dissipation (McClure, Hart, and Bird 1960).

The stability boundary—the locus of parameters marking the boundary between unstable ($\alpha > 0$) and stable ($\alpha < 0$) oscillations—is defined by $\alpha = 0$ in (1.7). That statement is a formal rendition of the physical condition that the energy gained per cycle should equal the energy lost per cycle:

$$\alpha_g = \alpha_d \tag{1.8}$$

Usually the main source of energy is combustion and in terms of the contributions shown in (1.7), this relation becomes

$$(\alpha)_{\text{combustion}} = -(\alpha)_{\text{nozzle}} - (\alpha)_{\text{mean flow}} - (\alpha)_{\text{condensed}} - (\alpha)_{\text{structure}} \tag{1.9}$$

There are situations in which the acoustic/mean flow interactions may provide a gain of energy. That is, energy is transferred from the average flow to the unsteady motions (as happens, for example, in wind instruments and sirens), but there is no need to consider the matter at this point.

As simple as it appears, equation (1.7) defining α, and its special form (1.8) defining the stability boundary, are basic and extremely important results. There is no evidence, for any propulsion system, contradicting the view that these results are correct representations of actual linear behavior. Difficulties in practice arise either because not all significant processes are accounted for, or, more commonly, insufficient information is available to assign accurately the values of the various individual growth or decay constants.

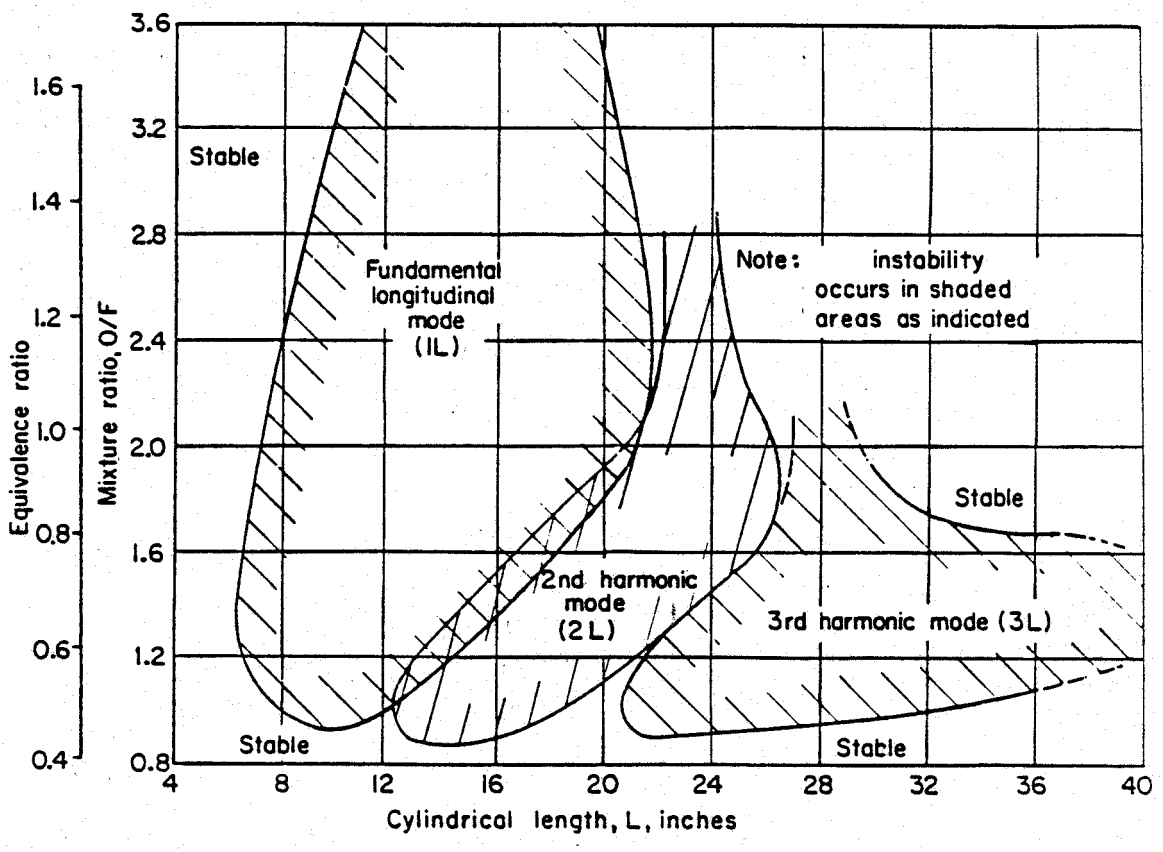

FIGURE 1.8. Stability Boundary for a Laboratory Gas-Fueled Rocket (Crocco, Grey, and Harrje)

As examples, Figure 1.8 shows stability boundaries computed for longitudinal oscillations in a gas-fueled laboratory rocket motor (Crocco, Grey, and Harrje 1960) and Figure 1.9 shows the results of calculations for a large, solid propellant rocket (Beckstead 1974). Those results illustrate the two uses mentioned above for the

formula (1.9). In the case of the gas-fired rocket, the calculations contained two parameters not known from first principles, namely n and τ arising in the time-delay model of the interactions between combustion and the acoustic field. All other parameters defining the geometry and the average flow field were known. The purpose of the work was to compare the calculations with measurements of the stability boundary to infer values of n and τ.

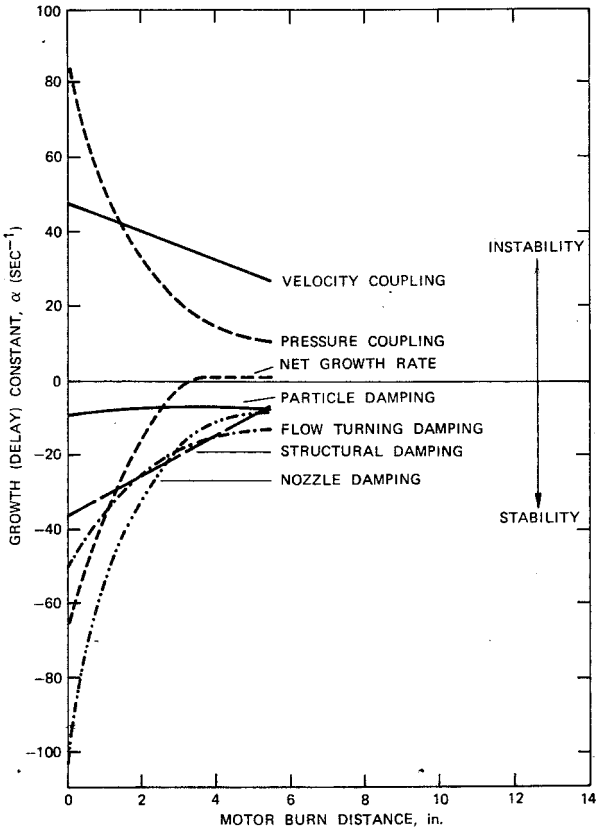

FIGURE 1.9. Predicted Stability Boundary for a Large Solid Propellant Rocket Motor, and the Separate Contributions to α_d and α_g. (Beckstead 1974)

The purpose of the results reproduced in Figure 1.9 was to predict the stability of a full-scale motor prior to test firing. In that case, all of the parameters appearing in (1.7) must be known. Usually some of the information is available only from ancillary laboratory tests, notably those required to characterize the coupling between propellant combustion and the acoustic field.

Indeed, an important application of the formulas (1.11) and (1.12) is to do exactly that for a laboratory device called the "T-burner". It is not necessary to restrict attention to the stability boundary if good measurements of the growth constant can be made. Then if all the losses can be computed, one can find the value of the growth constant due to combustion (or, more generally all energy gains) as the difference

$$\alpha_{\text{combustion}} = \alpha - \alpha_{\text{losses}} \tag{1.10}$$

Results for $\alpha_{\text{combustion}}$ can either be adapted for use directly in computing the stability of a motor; or they can be interpreted with models of the combustion processes to obtain better understanding of unsteady combustion. That procedure has been used extensively to assess the combustion dynamics of solid propellants and to investigate trends of behavior with operating conditions and changes of composition.

The growth constant has a simple interpretation beyond that given by 1.10 as the slope of a semi-logarithmic plot of the peak amplitudes versus time: twice α is the fractional rate of change of time-averaged energy in the classical acoustic field. We will prove the result more rigorously in Chapter 3 but this interpretation is so central to all problems of linear stability that it is useful to have it in hand from the beginning. By the definition of α,

both the pressure and velocity oscillations have the time dependence

$$p' \sim e^{\alpha t}\cos\omega t; \quad u' \sim e^{\alpha t}\sin\omega t$$

multiplied by their spatial distributions. The acoustic energy density is the sum of the local kinetic energy, proportional to ${u'}^2$, and potential energy, proportional to ${p'}^2$:

$$\text{K.E.} \sim e^{2\alpha t}\cos^2\omega t; \quad \text{P.E.} \sim e^{2\alpha t}\sin^2\omega t$$

If we assume that the period of oscillation, $\tau = 2\pi/\omega$, is much smaller then the decay rate, $1/\alpha$, then the values of these functions averaged over a cycle of the oscillation are proportional to $e^{2\alpha t}$. Hence the acoustic energy density is itself proportional to $e^{2\alpha t}$. Integrating over the total volume of the chamber we find that the total averaged energy $\langle\mathcal{E}\rangle$ in the acoustic field has the form

$$\langle\mathcal{E}\rangle = \langle\mathcal{E}_0\rangle e^{2\alpha t} \tag{1.11}$$

where $\langle\mathcal{E}_0\rangle$ is a constant depending on the average flow properties and the geometry. We then find directly from (1.11) the result claimed:

$$2\alpha = \frac{1}{\langle\mathcal{E}\rangle}\frac{d\langle\mathcal{E}\rangle}{dt} \tag{1.12}$$

Another elementary property worth noting is that $1/\alpha$ is the time required for the amplitude of oscillation to decay to $1/e$ of some chosen initial value. Also, the fractional change of the peak value in one cycle of oscillation ($t_2 - t_l = \tau = 2\pi/\omega$) is

$$|p'_2| - |p'_1| = \delta|p'|_m \sim e^{\alpha t_1} - e^{\alpha t_2} = e^{\alpha t_2}\left[e^{\alpha(t_1-t_2)} - 1\right]$$

where $|\quad|_m$ denotes the magnitude of the peak amplitude. We assume as above that the fractional change in one period τ is small so

$$e^{\alpha(t_1-t_2)} \approx 1 + \alpha(t_1 - t_2) = 1 + \alpha\tau$$

The amplitude itself is approximately proportional to $e^{\alpha t_2}$ or $e^{\alpha t_1}$ and we can write the fractional change as

$$\frac{\delta|p'|_m}{|p'|_m} \approx \alpha\tau = \frac{\alpha}{f} \tag{1.13}$$

where f is the frequency in cycles per second, $f = 1/\tau$. The dimensionless ratio f/α is a convenient measure of the growth or decay of an oscillation. According to the interpretation of $1/\alpha$ noted above, $(1/\alpha)/\tau = f/\alpha$ is the number of cycles required for the maximum amplitudes of oscillation to decay to $1/e$ or grow to e times an initial value.

The ratio α/f must be small for the view taken here to be valid. Intuitively, α must in some sense be proportional to the magnitude of the perturbations of the classical acoustics problem. We will find that the most important measure of the perturbations is a Mach number, $\bar{M}_r$, chacterizing the mean flow; for many significant processes, α/f equals $\bar{M}_r$ times a constant of order unity. Roughly speaking, then, the measured value of α/f is an initial indication of the validity of the view that a combustion instability can be regarded as a motion existing because of relatively weak perturbations of classical acoustics.

1.7. Nonlinear Behavior. It is a fundamental and extremely important conclusion that combustion instabilities are motions of a self-excited nonlinear dynamical system. Probably the most significant implication is that in order to understand fully the observed behavior, and how to affect or control it, one must ultimately understand the behavior of a nonlinear system. When the motion in a combustion chamber is unstable, except in unusual cases of growth to destruction, the amplitude typically settles down to a finite value: the system then executes a limiting motion, usually a periodic limit cycle. For practical applications, it is desirable to know how the amplitude of the limit cycle depends on the parameters characterizing the system. That information may serve as the basis for changing the characteristics to reduce the amplitude, the goal in practice being zero. In any case, good understanding of the properties of the limit cycle will also provide some appreciation for those variables which determine the behavior and to which the motions may be most sensitive, a practical matter indeed.

Rarely do the motions in a combustion chamber exhibit clear limit oscillations of the sort commonly encountered with simpler mechanical systems. Figure 1.3 and 1.4illustrate the point. It appears that combustion devices

are subject to influences, probably not easily identified, that prevent constant frequencies and amplitudes in the limit motions. The motions seem not to be limit cycles in the strict sense. However, experience gained in the past few years suggests that the deviations from the well-defined behavior of simpler systems are normally due to secondary influences. There are several possibilities, although not enough is known about the matter to make definite statements. Recent analysis (Burnley, 1996; Burnley and Culick, 1999) has demonstrated that noise, and interactions between random and acoustical motions can cause departures from purely periodic limit cycles appearing very similar to those found in pressure records for operating combustors. The random or stochastic motions are likely associated with flow separation, turbulence, and combustion noise.

Probably other causes of departures from strictly periodic limit cycles are associated with the parameters characterizing steady operation of a combustor; and with 'noise' or random fluctuation of flow variables. As we have already emphasized, the unsteady motions require only a negligibly small part of the energy supplied by the combustion processes. Relatively minor variations in the combustion field, due, for example, to small fluctuations in the supplies of reactants, may alter the rates of energy transfer to instabilities and hence affect features of a limit cycle. Similarly, adjustments in the mean flow, notably the velocity field and surface heat transfer rates, will directly influence the unsteady field. Laboratory experiments clearly show such phenomena and considerable care is required to achieve reproducible results. In solid propellant rockets, the internal geometry necessarily changes during a firing. That happens on a time scale much longer than periods of unsteady motions, but one obvious result is the decrease of frequencies normally observed in tests. Because there is ample reason to believe that the phenomena just mentioned are not essential to the global nonlinear behavior of combustion instabilities, we ignore them in the following discussion.

1.7.1. *Linear Behavior Interpreted as the Motion of a Simple Oscillator.* Intuitively we may anticipate that nonlinear behavior may be regarded in first approximation as an extension of the view of linear behavior described in the preceding section, made more precise in the following way. Measurement of a transient pressure oscillation often gives results similar to those shown in Figures 1.5(a). The frequency in each case varies little, remaining close to a value computed classically for a natural resonance of the chamber, and the growth of the peak amplitude during the initial transient period is quite well approximated by the rule for a linear instability, $e^{\alpha t}$. Thus the behavior is scarcely distinguishable from that of a classical linear oscillator with damping, and having a single degree of freedom. The governing equation for a simple mass (m)/ spring (k)/ dashpot (r) system is

$$m\frac{d^2x}{dt^2} + r\frac{dx}{dt} + kx = 0 \tag{1.14}$$

It is surely tempting to model a linear combustion instability by identifying the pressure fluctuation, p', with the displacement x of the mass. Then upon dividing (1.14) by m and tentatively replacing x by p', we have

$$\frac{d^2p'}{dt^2} + 2\alpha\frac{dp'}{dt} + \omega_0^2 p' = 0 \tag{1.15}$$

where $2\alpha = r/m$ and the undamped natural frequency is $\omega_0 = \sqrt{k/m}$. The familiar solution to (1.15) has the form of the records shown in Figures 1.5(a), $p' = \hat{p}_0 e^{\alpha t}\cos\Omega t$ where $\Omega = \omega_0\sqrt{1-(\alpha/\omega_0)^2}$ and $\hat{\rho}_0$ is the value of p' at $t = 0$.

The preceding remarks suggest the course we should follow to investigate the linear behavior of combustion instabilities, and indeed is the motivation behind the general view described earlier. But this is purely descriptive heuristic reasoning. No basis is given for determining the quantities 'mass,' 'damping coefficient,' and 'spring constant' for the pressure oscillation. The procedure for doing so is developed in Chapter 4; the gist of the matter is the following, a brief description of the method used later to analyze combustion instabilities.

According to the theory of classical acoustics for a sound wave, we may identify both kinetic energy per unit mass, proportional to the square of the acoustic velocity u', and potential energy per unit mass, proportional to the square of the acoustic pressure p'. The acoustic energy per unit volume is

$$\frac{1}{2}\left(\bar{\rho}u'^2 + \frac{p'^2}{\bar{\rho}\bar{a}^2}\right) \tag{1.16}$$

where $\bar{\rho}$ and $\bar{a}$ are the average density and speed of sound. This expression corresponds to the formula for the energy of a simple oscillator,

$$\frac{1}{2}(m\dot{x}^2 + kx^2) \tag{1.17}$$

Now consider a stationary wave in a closed chamber. Both the velocity and pressure fluctuations have spatial distributions such that the boundary condition of no velocity normal to a rigid wall is satisfied. Hence the local pressure p' in equation (1.15) must depend on position as well as time. However, the frequency ω_0 depends on the geometry of the entire chamber and according to equation (1.12), we should be able to interpret 2α in equation (1.15) as the fractional rate of change of averaged energy in the entire volume. Therefore, we expect that the parameters m, k, and r implied by the definitions $\alpha = r/2m$ and $\omega_0 = k/m$ must be related to properties of the entire chamber. The approximate analysis used in most of this book is based partly on spatial averaging defined so that the properties ascribed to a particular mode are local values weighted by the spatial distribution of the mode in question, and averaged over the chamber volume.

Locally in the medium, the 'spring constant' is supplied by the compressibility of the gas, and the mass participating in the motion is proportional to the density of the undisturbed medium. When the procedure of spatial averaging is applied, both the compressibility and the density are weighted by the appropriate spatial structure of the acoustical motion. As a result, the damping constant and the natural frequency are expressed in terms of global quantities characterizing the fluctuating motion throughout the chamber. We will find rigorously that in the linear limit, an equation of the form (1.15) does apply, but instead of p' itself, the variable is $\eta_n(t)$, the time dependent amplitude of an acoustic mode represented by

$$p'_n = \bar{p}\eta_n(t)\psi_n(\vec{r}) \tag{1.18}$$

where $\bar{p}$ is the mean pressure and $\psi_n(\vec{r})$ is the spatial structure of the classical acoustic mode identified by the index $(\quad)_n$. Hence the typical equation of motion is

$$\frac{d^2\eta_n}{dt^2} + 2\alpha_n\frac{d\eta_n}{dt} + \omega_n^2\eta_n = 0 \tag{1.19}$$

The constants α_n and ω_n contain the influences of all linear processes distinguishing the oscillation in a combustion chamber from the corresponding unperturbed classical motion governed by the equation

$$\frac{d^2\eta_n}{dt^2} + \omega_{n0}^2\eta_n = 0 \tag{1.20}$$

if dissipation of energy is ignored. Because damping in a mechanical system causes a frequency shift, and the actual frequency is not equal tot he unperturbed value, ω_{n0}.

For technical reasons not apparent at this point, it is convenient to regard the linear perturbing process as a force $F_n(\eta_n, \dot{\eta}_n)$ is acting on the 'oscillator' and equation (1.19) is written

$$\frac{d^2\eta_n}{dt^2} + \omega_{n0}^2\eta_n = F_n^L(\eta_n, \dot{\eta}_n) \tag{1.21}$$

The superscript $(\quad)^L$identifies the 'force' as linear, and for simplicity ω_{n0}^2 is written ω_n^2. We will consistently use the symbol ω_n for the unperturbed classical acoustic frequency. If there is no linear coupling between the modes (typically linear coupling is small), the force F_n^L consists of two terms, one representing the damping of the mode and one the frequency shift:

$$F_n^L = -\Delta\omega_n^2\eta_n + 2\alpha_n\dot{\eta}_n \tag{1.22}$$

Equations (1.21) and (1.22) produce (1.19) with ω_n^2 replaced by $\omega_n^2 + \Delta\omega_n^2$.

With the above reasoning we have heuristically constructed equation (1.21) as the fundamental equation for a linear combustion instability corresponding to a classical acoustic mode of the chamber. Its simplicity masks the fact that a great amount of effort is required to determine realistic functions $F_n^L(\eta_n, \dot{\eta}_n)$ applicable to the motions in a combustion chamber. The approximate analysis developed later provides a framework for accommodating all linear processes but does not contain explicit formulas for all of them. Most importantly, there are terms

representing interactions between combustion processes and the unsteady motions, but their computation requires modeling the mechanisms that cause combustion instabilities. Some of the purely gasdynamical processes, arising with coupling between mean and fluctuating motions, are given explicitly.

According to classical acoustic theory, a closed chamber of gas at rest has an infinite number of normal or resonant modes. The spatial structures (mode shapes) and resonant frequencies are found as solutions to an eigenvalue problem. A general motion in the chamber, having any spatial structure, can then be represented as a linear superposition of the normal modes. The process of spatial averaging, leading to equation (1.20), amounts to representing any motion as an infinite collection of simple oscillators, one associated with each of the normal modes. That interpretation holds as well for equation (1.21) except that now each mode may suffer attenuation ($\alpha_n < 0$) or excitation ($\alpha_n > 0$). It is this point of view that allows natural extension of the analysis to nonlinear behavior.

1.7.2. *Nonlinear Behavior Interpreted as the Motion of a Nonlinear Oscillator.* In view of the observation that measurements often show development of limit cycles like those shown in Figure **??**, it is tempting simply to add a nonlinear term to the oscillator equation (1.21) and assume that a combustion instability involves only a single mode. Thus, for example, we could add to the right-hand side a force $F_n^{nL} = c_1\eta_n^2 + c_2\dot{\eta}_n^2 + c_3\eta_n\dot{\eta}_n + c_4|\eta_n| + \cdots$ where the constants c_1,... may be chosen by fitting the solution to data. Culick (1971) showed that quite good results could be obtained with this approach applied to limited data. Figure 1.10 shows one example. Of course this is a purely *ad hoc* approach and provides no means of computing the coefficients from first principles.

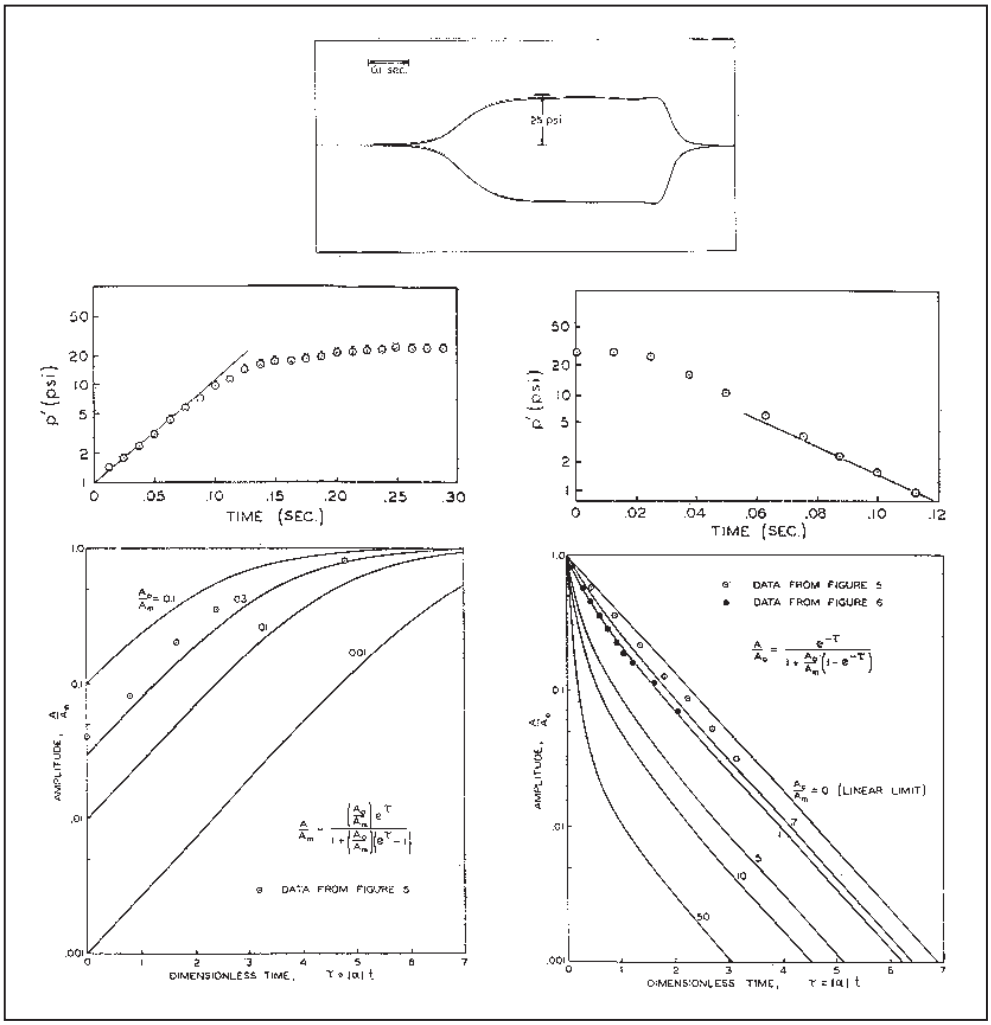

FIGURE 1.10. An Example of Fitting T-Burner Data with the Model of a Simple Nonlinear Oscillator (Culick 1971).

Subsequently, Jensen and Beckstead (1973) applied that procedure to extensive data taken in laboratory devices intended for measuring the characteristics of unsteady burning of solid propellants. The chief result was that the data could be matched equally well with rather broad ranges of the constants, and no particular kind of nonlinearity seemed to dominate the motions. Consequently, representation with a single mode was not successful. Even though analysis of pressure records for limit cycles often showed relatively small (it seemed) amounts of harmonics of the principle mode, it appeared necessary to account for two modes at least, with coupling due to nonlinear processes.

In other contexts, that conclusion is surely not surprising. The development of a small amplitude compressive disturbance into a shock wave is the oldest and most familiar example in gasdynamics. Steepening of a smooth wave arises primarily from two nonlinear influences: convection of the disturbance by its own motion, and dependence of the speed of sound on the local temperature, itself dependent on the wave motion. A good approximation to the phenomenon is obtained if viscous stresses and heat conduction are ignored. If the disturbance is regarded as a combination of various modes, the flow of energy from modes in the low frequency range to those having higher frequencies is favored by the nonlinear gasdynamic coupling. The rapid growth of the higher-frequency modes having shorter wavelengths produces the steepening, eventually limited, in real flows, by the actions of various effects. In a combustion chamber possible consequences of nonlinear combustion processes cannot be ignored.

In extreme cases of combustion instabilities, particularly in liquid and solid rockets, the approximately sinusoidal motions, substantially systems of stationary waves, may be absent or evolve into a different form. The motions then appear to be weak shock waves, or pulses having measurable width, propagating in the chamber. Instabilities of that type are commonly produced subsequent to excitation by finite pulses. Examples were observed early in tests of liquid rockets, typically involving motions mainly transverse to the axis, identified as 'spinning' transverse modes. Their presence is particularly harmful due to the greatly increased surface heat transfer rates causing unacceptable scouring of the chamber walls.

The corresponding cases in solid rockets usually are longitudinal motions. They rarely occur in large motors and seem to have been first observed in pulse testing of laboratory motors (Dickenson 1962; Brownlee 1964). An example is reproduced in Figure 1.11 (Brownlee, 1964). Often this sort of instability is accompanied by a substantial increase of the mean pressure, seriously affecting the steady performance of the motors. The primary cause of the pressure rise is evidently the increased burn rate, although precisely why the rate increases is not well understood. More recently, these pulsed instabilities have been the subject of successful comparisons between laboratory test results and numerical simulations (Baum and Levine 1982; Baum, Levine, and Lovine 1988). Figure 1.12 shows an example of their results.

For combustion instabilities, the situation is very different from that for shock waves in a pure gas because the processes governing the transfer of energy from combustion to the gasdynamical motions cannot be ignored and in general depend strongly on frequency. Indeed, it may happen, as seems sometimes to be the case for combustion of solid propellants, that the coupling may cause attenuation of higher frequencies. For that reason, the tendency for steepening by the gasdynamics is partially compensated by the combustion processes, may be linear or nonlinear. As a result, in a chamber, a limit cycle may be formed having very closely the spatial structure and frequency of the unstable mode (commonly, but not always, the fundamental mode) and relatively modest amounts of higher modes. It is that behavior that seems to be important in many combustion problems, explaining in part why the approach taken in the approximate analysis has enjoyed some success.

Naturally the preceding is a greatly simplified and incomplete description of the events actually taking place in a given combustion chamber. The essential conclusion that nonlinear gasdynamical processes are partly augmented and partly compensated by combustion processes seems to be an important aspect of all combustion instabilities. It appears that the idea was first explicitly recognized in work by Levine and Culick (1972, 1974), showing that realistic limit cycles could be formed with nonlinear gasdynamics and linear combustion processes. Perhaps the most important general implication of those works is that the nonlinear behavior familiar in flows of pure nonreacting gases is not a reliable guide to understanding the nonlinear behavior in combustion chambers.

For nonlinear problems, the governing equations obtained after spatial averaging have the form

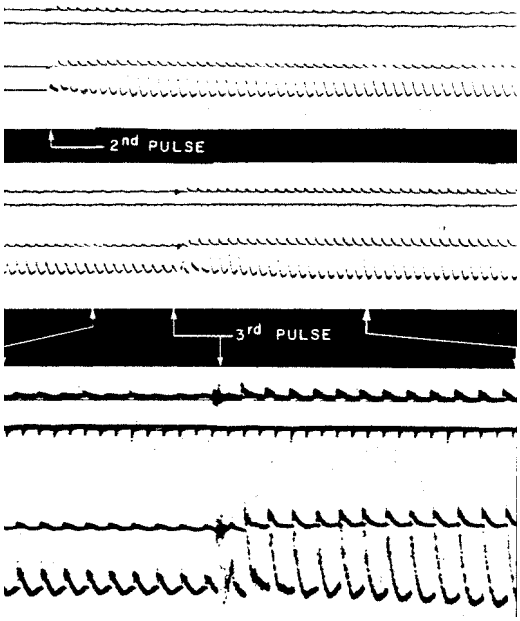

FIGURE 1.11. Steep-fronted Waves Observed in Solid Propellant Rocket Motors (Brownlee, 1964)

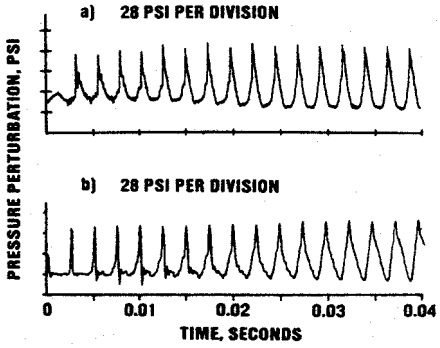

FIGURE 1.12. A Comparison of Observed and Simulated Steep-Fronted Waves in a Solid Propellant Rocket Motor. (a) Observed; (b) numerical Simulation (Baum and Levine, 1982).

$$\frac{d^2\eta_n}{dt^2} + \omega_n^2\eta_n = F_n^L(\eta_n, \dot{\eta}_n) + F_n^{NL}(\eta_i, \dot{\eta}_i) \tag{1.23}$$

where $F_n^{NL}(\eta_i, \dot{\eta}_i)$ is the nonlinear force depending on all amplitudes η_i, including η_n itself. Thus we may regard a combustion instability as the time-evolution of the motions of a collection of nonlinear oscillators, one associated with each of the classical acoustic modes for the chamber. In general the motions of the oscillators may be coupled by linear as well as nonlinear processes, although linear coupling seems rarely to be important. The analytical framework established by the dynamical system (1.23) will serve throughout this book as the primary means for analyzing, predicting, and interpreting combustion instabilities.

Representation of unsteady motions in a combustion by expansion in acoustic modes ('modal expansion') and application of spatial averaging was first accomplished by Culick (1961, 1963) using a Green's function. The work by Jensen and Berkstead cited above motivated extension to nonlinear behavior (Culick 1971 and 1975; and Zinn and Powell (1970a, 1970b) first used an extension of Galerkin's method to treat nonlinear behavior is in liquid rockets; the method was subsequently extended to solid rockets by Zinn and Lores (1972). In practice, application of a method based on modal expansion and spatial averaging is normally useful only if a small number of modes is required. Yet there are a large number of experimental results showing the presence of steep-fronted waves, often sufficiently steep to be interpreted as shock waves. Hence an analysis of the sort followed here would

seem to be quite seriously limited unless one is prepared to accommodate a large number of modes. That is, one would expect that wave motions exhibiting rapid temporal changes and large spatial gradients must contain significant amounts of higher modes. However, results have also shown that due to fortunate phase relationships, a surprisingly small number of modes serves quite well even to represent many features of waves having steep fronts. The method gives quite a good approximation to both the limiting motions and the transient development of disturbances into weak shock waves.

1.8. Analysis and Numerical Simulations of Combustion Instabilities. In these lectures, the vehicle for unification is a theoretical framework originating in the late 1960s and early 1970s with treatments of instabilities in liquid rockets (Culick 1961, 1963; Powell 1968; Zinn and Powell 1968; and Powell and Zinn 1971) and in solid rockets (Culick 1971, 1976). Those analyses differed from previous work mainly in their use of a form of spatial averaging, in some instances related to Galerkin's method, to replace the partial differential equations of conservation by a system of ordinary differential equations. The dependent variables are the time-dependent amplitudes of the acoustic modes used as the basis for series expansion of the unsteady pressure. It is the process of spatial averaging over the volume of the chamber that produces a formulation convenient for handling models of widely different geometries and physical processes. Consequently, in return for the approximate nature of the analysis (for example, the series must be truncated to a finite number of terms), one obtains both convenience and a certain generality of applications not normally possible when partial differential equations are used directly. In general form, this approach is applicable to all types of combustors. Different systems are distinguished by different geometries and the forms in which the reactants are supplied (liquid, solid, gas, slurry, ...). Those differences affect chiefly the modeling of the dominant physical processes.

Some analysis of combustion instabilities has customarily accompanied experimental work as an aid to interpreting observations. The paper by Grad (1949) treating instabilities in solid rockets is probably the first entirely theoretical work dealing with small amplitude acoustical motions in a mean flow field with combustion sources. During the 1950s and 1960s, many theoretical works were published on the subject of oscillations in solid rockets (Bird, McClure, and Hart 1963; Cheng 1954, 1962; Hart and McClure 1959, 1965; Cantrell and Hart 1964; Culick 1966) and in liquid rockets (Crocco 1952, 1956, 1965; Crocco and Cheng 1956; Reardon 1961; Culick 1961, 1963; Sirignano 1964; Sirignano and Crocco 1964; Zinn 1966, 1968, 1969; Mitchell, Crocco, and Sirignano 1969). It was during that period that the view of combustion instability as a perturbation of classical acoustics was first extensively developed.

Most of the analyses cited in the previous paragraph (those by Sirignano, Zinn and Mitchell are notable exceptions) were restricted to linear problems. Their chief purpose was to compute the stability of small amplitude motions. Indeed, since the earliest works on combustion instabilities, practical and theoretical considerations were directed mainly to the general problem of linear stability: the reasoning is that if the system is stable to small disturbances (e.g. associated with 'noise' always present in a combustion chamber) then undesirable instabilities cannot arise. There is a flaw in that reasoning: the processes in a combustion chamber are nonlinear, so a linearly stable system may in fact be unstable to sufficiently large disturbances. In any case, oscillations in combustors reach limiting amplitudes due to the action of nonlinear processes. Hence understanding nonlinear behavior is the necessary context in which one can determine what changes to the system may reduce the amplitudes. Ultimately, a complete theory, and therefore understanding, must include nonlinear behavior, a subject covered at considerable length in these lectures, largely within the context cited in the first paragraph.

Recognition of the practical implications of the deficiencies of a view founded on linear behavior motivated the development of the technique of "bombing" liquid rocket chambers in the 1960s by NASA in its Apollo program. The idea is to subject an operating combustion chamber to a succession of increasingly large disturbances (generated by small explosive charges) until sustained oscillations are produced. Then the size of the disturbance required to "trigger" the instability is evidently a measure of the relative stability of the chamber. Another measure is the rate of decay of oscillations subsequent to a pulse injected into a linearly stable system; the method was invented by NASA during the development of engines for the Apollo vehicle in the 1960's. What constitutes the correct 'measure' of relative stability cannot of course be determined from experiments alone, but requires deeper understanding accessible only through theoretical work. This is part of the reason that the nonlinear analyses cited above were carried out; also an extensive program of numerical calculations was supported. Owing to the limitations of computing resources at that time, those early numerical calculations involved solutions to quite restricted problems, commonly sectors or annular regions of chambers. It was not possible to compute what are

now usually called 'numerical simulations.' Moreover, the results were often plagued—and were thus sometimes rendered invalid—by noise in the computations or difficulties with stability of the numerical techniques.

While the intense activities on instabilities in liquid rockets nearly ceased in the early 1970s, work on numerical simulation of combustion instabilities in solid rockets began (Levine and Culick 1972, 1974; Kooker 1974; Baum and Levine 1982). In contrast to the case for liquid rockets, it is a good approximation to ignore chemical processes within the cavity of a solid rocket, an enormous simplification. Combustion occurs largely in a thin layer adjacent to the solid surface and its influences can be accommodated as boundary conditions. Consequently, with the growth of the capabilities of computers, it became possible to carry out more complete computations for the entire unsteady field in a motor. Also during this period appeared the first attempt to compare results of an approximate analysis with those obtained by numerical simulation for the 'same' problem (Culick and Levine 1974).

The main idea motivating that work was the following. At that time, the size and speed of available computers did not allow numerical simulations of three-dimensional problems, nor in fact even two-dimensional or axisymmetric cases. Moreover, no numerical calculations had been done of one-dimensional unsteady transient motions in a solid rocket, with realistic models of the combustion dynamics and partial damping. Approximate analysis of the sort mentioned above could be applied, in principle, to instabilities in arbitrary geometries, but owing to the approximations involved, there were no means of determining the accuracy of the results. Experimental data contain sufficiently large uncertainties that comparisons of analytical results with measurements cannot be used to assess accuracy of the analysis. Hence it appeared that the only way to assess the limitations of the approximate analysis must be based on comparison with numerical simulations. It was also important to confirm the validity of the approximate analysis because of its great value for doing theoretical work and for gaining general understanding of unsteady motions in combustion chambers.

That reasoning remains valid today. Despite the enormous advances in computing resources, it is true here as in many fields, that approximate analysis still occupies, and likely always will, a central position. A major reason is its great value in providing understanding. Numerical simulations advanced considerably during the 1980s and important work is in progress. Accomplishments for systems containing chemical processes, including combustion of liquid fuels, within the chambers far exceed those possible twenty years ago (see, for example, Liang, Fisher, and Chang 1988; Liou, Huang, and Hung 1988; Habiballah, Lourmé, and Pit 1991; Kailasanath, Gardner, Boris, and Oran 1987a, b; and Menon and Jou 1988).

Numerical simulations of flows in solid rockets have begun to incorporate current ideas and results of turbulence modeling (Dunlop *et al.* 1986; Sabnis, Gibeling, and McDonald 1985; Tseng and Yang 1991; Sabnis, Madabhushi, Gibeling, and McDonald 1989). The results have compared quite favorably with cold flow experiments carried out using chambers with porous walls. In the past five years, much progress has been made in numerical simulations (some based on the ideas of LES) of solid rockets including computations of the burning propellant. There is no reason to doubt that eventually it will be possible to produce accurate computations of the steady turbulent flow fields in virtually any configuration expected in practical applications.

Remarkable success has also been achieved with computations of unsteady one-dimensional motions in straight cylindrical chambers (e.g. Baum and Levine 1982; Baum, Lovine, and Levine 1988; Tseng and Yang 1991). Particularly notable are the results obtained by Baum, Lovine, and Levine (1988) showing very good agreement with data for highly nonlinear unsteady motions induced in the laboratory by pulses. Although parameters in the representation of the unsteady combustion processes were adjusted as required to produce the good comparison, a minimal conclusion must be that the numerical methods are already quite satisfactory.

Numerical simulation will always suffer some disadvantages already mentioned. In addition, because each simulation is only one case and the problems are nonlinear, it is difficult to generalize the results to gain fundamental understanding. However, the successes of this approach to investigating complicated reacting flows are growing rapidly and the methods are becoming increasingly important for both research and practical application. Historically, we have seen that the three aspects of the subject—experimental, analytical, and numerical simulations—began chronologically in that order. There seems to be no doubt that, as in many other fields of modern engineering, the three will coexist as more-or-less equal partners. We have therefore tried in this book to balance our discussion of methods and results of experiment, analysis, and numerical simulation with much

less emphasis on the last. The integration of those activities forms a body of knowledge within which one may understand, interpret and predict physical behavior.

It is important to realize that experimental information about unsteady motions in combustion chambers is very limited. Commonly only measurements of pressure are available. Accelerometers and strain gauges mounted in a chamber may provide data from which some characteristics of the pressure field can be inferred. Quantitative surveys of the internal flow are virtually unavailable owing to the high temperatures, although optical methods are useful in laboratory work to give qualitative information and, occasionally, useful quantitative data.

As a practical matter we are therefore justified in assuming only that the pressure is available, at most as a function of time and position on the surface of the chamber. That restriction is a fundamental guide to the way in which the theory and methods of analysis for combustion instabilities are developed. Throughout these lectures we emphasize determining and understanding the unsteady pressure field. The approximate analysis constituting the framework in which we will discuss instabilities is based on the pressure as the primary flow variable.

2. MECHANISMS OF COMBUSTION INSTABILITIES IN SOLID PROPELLANT ROCKETS

Identifying the ultimate cause, the mechanism, is probably the single most important task in understanding combustion instabilities in full-scale systems. The term "mechanism" refers to that phenomenon or collection of processes forming the chief reason that the instability exists. There may be more than one mechanism, but in any case the ultimate reason for an instability is that energy is transferred from the combustion processes, or the mean flow, to unsteady organized motions. Instabilities are commonly observed as nearly periodic oscillations having time-dependent amplitudes. As a practical matter, the chief goal is to reduce the amplitudes to acceptable levels. For that purpose it is essential first to understand the cause, and then to work out the connections with the chamber dynamics.

In the context defined by Figure 1.1, understanding the mechanism of combustion instabilities is equivalent to understanding combustion dynamics. It is essential to keep in mind always that by its very definition, combustion involves chemistry and chemical kinetics within the setting of fluid mechanics. Depending on the mechanism, one or another of those phenomena may dominate. Hence, for example, in some cases involving the dynamics of vortex formation and shedding, we may find that burning is not a central issue. Nevertheless, the presence of the flow field supporting the vortices is itself produced by combustion of reactants. We may therefore justifiably include the phenomenon under the general label 'combustion dynamics.' Hence all of the topics comprising the subject of mechanisms belong largely to the feedback path in Figure 1.1.

In some respects combustion in a solid propellant rocket chamber appears to be less complicated than those in any other type of combustor. The burning processes occur almost entirely within a thin region, normally less than one millimeter thick, adjacent to the propellant surface. Although some residual combustion normally occurs when the propellant contains aluminum or other metallic additives, there is no unambiguous evidence that combustion within the volume contribute significantly as a cause of combustion instabilities. We assume that to be the case, leaving surface combustion and purely fluid mechanical processes as origins of possible mechanisms. Of these, the dynamics of surface combustion is by far the most common and most important. The four chief mechanisms for instabilities in solid rockets are shown in Figure 2.1 surface combusiton; vortices shed from obstacles, or growing out of the shear flow at a burning surface; and residual combustion within the volume of the chamber.

Vortex shedding from obstacles—as in the Shuttle solid rocket booster—or vortices produced at the lateral surface ('parietal vortex shedding')—as in the Ariane 5 solid rocket booster—have been identified as mechanisms only in large motors. Excitation of acoustic waves by vortices is of course a well-known phenomenon in a wide variety of wind musical instruments. The idea that vortices might be responsible for oscillations in a combustion chamber seems to have been proposed first by Flandro and Jacobs (1974).

The dynamics of residual combustion far from the burning surface—mostly likely associated with aluminum or other metal fuel additives not completely burned at the surface—remains poorly understood. Although some attention has been given to the process (Beckstead *et al.* 1987), analysis of the dynamics is incomplete. No calculations exist assessing quantitatively the possible contributions of residual combustion to linear stability relative to those of surface combustion.

On the other hand, there is no disagreement that the dynamics of surface combustion is the dominant mechanism causing most combustion instabilities in all types and sizes of solid rockets. We therefore begin with examination of that subject.

2.1. Qualitative Interpretation of the Basic Mechanism. The dependence of the burning rate of a solid propellant on the pressure has long been known as a basic characteristic. Experiment and theory for the combustion of gases shows that the reaction rates vary strongly with both pressure and temperature. It is therefore not surprising that the burning rate of a solid is sensitive to the impressed temperature and pressure. What **is** surprising is that the processes in the gas and condensed phases in the vicinity of the burning conspire to produce a dynamical response that exhibits significant dependence in frequency. That dependence on frequency is particularly important because the response is noticeably greater over a rather broad frequency range. In that range the combustion processes act to amplify pressure fluctuations. That is, some of the energy released in chemical reactions is transformed to mechanical energy of motions in the combustion products. Hence the

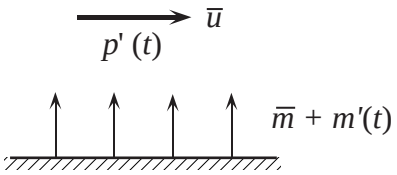

(a) Pressure Coupling

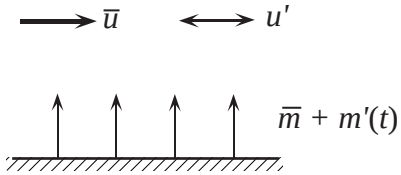

(b) Velocity Coupling

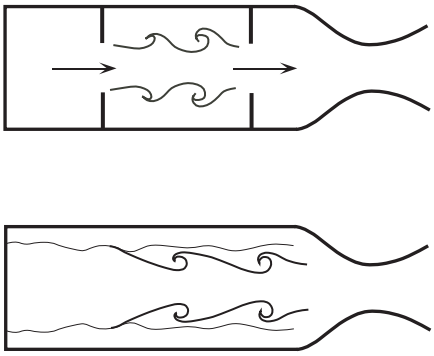

(c) Vortex Shedding

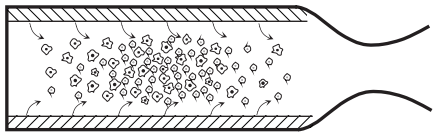

(d) Residual Combustion

FIGURE 2.1. The Four Chief Mechanisms for Combustion Instabilities in Solid Rockets

dynamics in the feedback path, Figure 1.1, not only provide feedback but as well promote an unstable situation. The burning surface exhibits a sort of resonant behavior but without possessing the inertial and spring-like (i.e. restoring) forces associated with a resonant oscillating system such as the simple mass/spring oscillator.

Since the cavity in a solid rocket possesses its own acoustic resonances, we have a system of two coupled oscillators. If it should happen that resonant frequencies of the two oscillators are close, then conditions clearly favor an instability. That is the situation commonly occurring in solid rockets and is the simplest direct explanation for the widespread occurrences of instabilities in tactical as well as strategic motors (Blomshield, 2000).

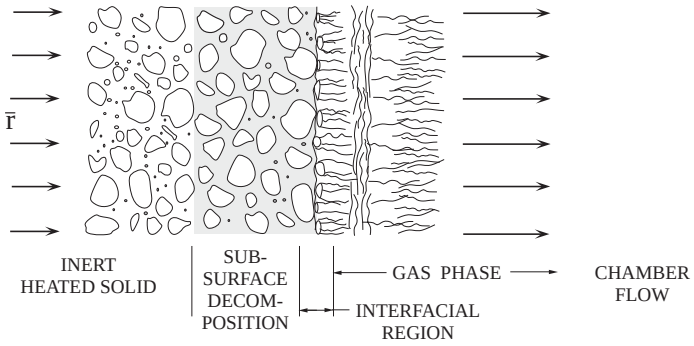

FIGURE 2.2. Sketch of Unsteady Combustion of a Solid Propellant.

The essential features of the combustion processes dominating the behavior just described have long been known. Figure 2.2 is an idealized sketch showing the main characteristics of a burning composite propellant exposed to an oscillation of the chamber pressure. Ultimately it is the fluctuation of velocity of gases leaving the

combustion zone that is the essence of the mechanism. Oscillation of the flow causes the surface to appear like an acoustic speaker, a source of acoustic waves. Formally the situation is identical to a planar array of monopoles having zero-average mass flow superposed on the mean flow due to combustion. However, the fluctuation of burning rate is a consequence of fluctuating heat transfer so we can understand the mechanism best by examining the behavior of the temperature profile. We will treat the propellant as if it were a perfectly homogeneous isotropic material in the condensed phase, and use the one-dimensional approximation throughout, from the cold condensed solid phase to the hot combustion products. Figure 2.3 is one frame from a film of a burning solid taken at the Naval Weapons Center, suggesting that any sort of one-dimensional approximation seems unrealistic. That is certainly true on the scale of the particle sizes (10s to 100s of microns).

However, the variations of velocity and pressure in the chamber occur over distances of the order of the chamber dimensions. Hence it is appealing to suppose that for interactions between the combustion zone and the motions in the chamber, the heterogeneous character propellant can be overlooked in some sense. For example, the linear burning rate of a propellant is measured without special regard for spatial variations on the small scale of compositional inhomogeneities. No instrument is available to do otherwise. That is not to say, of course, that the burn rate and the combustion dynamics do not depend on spatial variations of the condensed material and the gas phase. Rather, we suppose that dependence in such things as the size distribution of oxidizer particles is accounted for by some sort of averaging procedure. Thus, parameters appearing in the final results, such as A and B in the QSHOD model discussed here, must depend on, for example, an average particle size. No rules exist for the averaging, but recently impressive progress has been made for computed steady burning rates using a "random packing" model (Kochevets and Buckmaster, 2001). In all of the discussion here we adhere to the one-dimensional approximation with no attention paid to the possible errors incurred. In any case it seems a good assumption that if the averaging process is good, any errors are likely to be less than uncertanties arising in other parts of the problem, e.g. material properties.

The mechanism in question here is, broadly speaking, primarily a matter of combustion dynamics. It has become customary to represent the mechanism quantitatively as an admittance or response function. We use the latter here, defined generally as the fluctuation of mass flow rate of gases departing the combustion zone to the imposed fluctuation of either the pressure or the velocity. Thus the response function for pressure fluctuations (referred to as the "response to pressure coupling") is defined in dimensionless form as R_ρ,

$$R_\rho = \frac{m'/\overline{m}}{p'/\overline{p}} \tag{2.1}$$

where $(\ )'$ means fluctuation and $\overline{(\ )}$ is an average value. The average value $\overline{m}$ represents the average inflow of mass due to the propellant burning. In almost all applications, the fluctuations are steady sinusoidal oscillations, written as

$$\frac{m'}{\overline{m}} = \frac{\hat{m}}{\overline{m}} e^{-i\omega t}$$
$$\frac{p'}{\overline{p}} = \frac{\hat{p}}{\overline{p}} e^{-i\omega t} \tag{2.2a,b}$$

and

$$R_\rho = \frac{\hat{m}/\overline{m}}{\hat{p}/\overline{p}} \tag{2.3}$$

where $\hat{(\ )}$ denotes the amplitude of the oscillation, including both magnitude and phase. Because generally the oscillations of mass flux rate are not in phase with the pressure oscillations, the function R_p is complex, the real part representing that part of $m'/\overline{m}$ that is in phase with the pressure oscillation.

Although the response function for pressure coupling is most commonly used, there is a second response function, that associated with velocity coupling, which under some practical circumstances is far more important. At this point we confine our remarks to the response function for pressure coupling.

A simple interpretation of the response function explains its importance to combustion instabilities. According to the definition (2.3), a pressure oscillation having amplitude $\hat{p}/\overline{p}$ produces the oscillation $\hat{m}/\overline{m}$ of mass flow into

the chamber

$$\frac{\hat{m}}{\overline{m}} = R_\rho \frac{\hat{p}}{\overline{p}} \tag{2.4}$$

Viewed from the chamber, the boundary appears then to oscillate. The apparent motion is entirely analogous to that of a speaker or piston mounted at the boundary. Thus pressure waves are generated in a fashion similar to that of a loudspeaker in a room. Through a complicated sequence of processes whose details are not germane here, those waves coalesce and combine with the original pressure waves causing the fluctuations of mass flux. Whether or not that merging process augments or subtracts from the existing wave system in the chamber depends on the phase between $\hat{m}$ and $\hat{p}$. The part of $\hat{m}$ in-phase with $\hat{p}$ increases the amplitude of the wave system and is therefore destabilizing. For a particular motor, the tendency for combustion dynamics to drive instabilities is proportional to the integral of R_p over the entire area of burning surface. Hence it is clearly essential to know the response function for the propellant used.

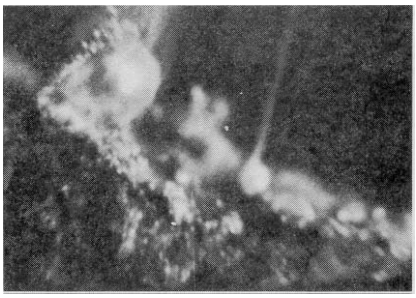

FIGURE 2.3. View of the Surface of a Burning Solid Propellant Containing Aluminum.

Traditional composite propellants using ammonium perchlorate as oxidizer, as well as advanced propellants using higher energy oxidizers and binder, burn in qualitatively similar fashion. The interface between the condensed and gas phases is fairly well defined, may be dry or wet, and may exhibit local dynamical activity owing to the presence of solid particles and responsive collections of liquid pools or drops. The dynamics of the interfacial region is particularly noticeable in microcinematography when the propellant contains aluminum. The metal collects in molten droplets, mobile and ignitable on the surface; those not fully consumed are carried away by the gaseous products of the interface. The high temperature at the surface is sustained by a balance between heat flow away from the interface, required to heat the cool propellant advancing to the surface; energy required to effect the phase changes at and near the interface; and the heat transfer supplied to the interfacial region from the combustion zone in the gas phase. It's a delicate balance, easily disturbed by changes in the chemical processes in the interfacial region, particularly within the subsurface region in the condensed phase. Figure 2.4 is a sketch of the temperature field, showing also the possible consequences of additional exothermic reactions in the sub-surface condensed phase. Note that in this figure we imagine that the temperature exists in a spatially averaged sense. Local variations on the scale of oxidizer particles are smeared out in the averaging procedure and explicit effects of inhomogeneities are absent.

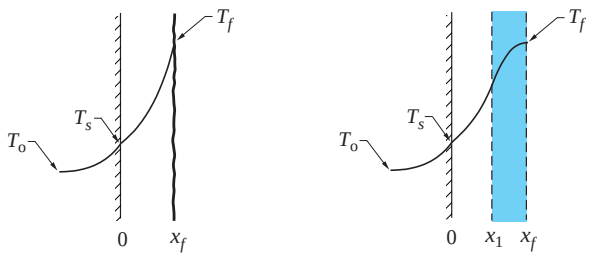

(a) Flame Front (b) Distributed Combustion

FIGURE 2.4. Representation of the Temperature Field in a Burning Solid Propellant.

The essentials of the behavior represented macroscopically by response functions can be described as a sequence of elementary steps, described here in simplified form with reference to Figure 2.4:

(i) Suppose that for some reason the rate of reactions in the combustion zone increases-perhaps due to a fluctuation of pressure, or temperature, or to increased local mixing associated with greater intensity of turbulence locally in the chamber.
(ii) Increased reaction rates produce a rise in the rate of energy release and an increase of temperature of the combustion zone.
(iii) Due both to radiation and heat conduction, the heat transfer from the combustion zone to the interfacial region increases, having at least two possible consequences: the temperature at the surface is increased; and the rate at which condensed material is converted to gas is also increased.
(iv) Because the temperature in the interfacial region rises, so also does the heat flow to the subsurface region and further into the solid, tending to cool the interface.
(v) If there are subsurface reactions, the heat flow will tend to increase their rate, with consequences depending on the associated energy release (or absorption) rate.
(vi) Exothermic subsurface reactions will act to maintain higher temperature locally, thereby encouraging the conversion of condensed material to gas at the interface, but also tending to increase the heat flow to the cooler solid.
(vii) The net result may be that if the fluctuation of heat flow, and reduction of temperature, at the interface does not happen too quickly, the enhanced reaction rate assumed in Step (i) may produce a fluctuation of mass flow leaving the surface, that is in phase with the initial perturbation. Hence in this event the entire process is destabilizing in the sense that the initial disturbance has the result that the disturbed mass flow into the chamber tends to augment that initial disturbance.

Whether or not the preceding sequence will be destabilizing depends entirely on details of the processes involved. Notably, if sub-surface reactions are endothermic, then the sequence (v)–(vii) leads to the conclusion that the reactions may cause the propellant combustion to be less sensitive to disturbances.

The model we will analyze first is the simplest possible capturing a dominant contribution to the combustion dynamics. Only unsteady heat transfer in the condensed phase causes true dynamical behavior, i.e. dependence of the response to pressure coupling. That process must in any case be present. This problem (model) is therefore the reference always used to assess the possible influences of other dynamical processes, in particular, those in the gas phase and decomposition in the condensed phase. The substance of the model is defined by the following assumptions:

(i) **q**uasi-**s**teady behavior of all processes except unsteady conductive heat transfer in the condensed phase;
(ii) **h**omogeneous and constant material properties, non-reacting condensed phase;
(iii) **o**ne-**d**imensional variations in space;
(iv) conversion of condensed material to gas phase at an infinitesimally thin interface.

The acronym QSHOD for this model derives from the five letters in assumptions (i)–(iii).

During the early years of this subject, from the mid-1950s to the mid-1960s, roughly ten analyses of the response function were published in the Western literature, giving apparently distinct results. Culick (1968) showed that, due to the fact that all of the models were based in the same set of assumptions (i)–(iv), the results were dynamically identical. That is, all had the same dependence on frequency and, with appropriate values for the various parameters involved, give coincident numerical values. Hence the term QSHOD is a useful term referring to a class of models. Differences between the models are associated with different detailed models of the steady processes, notably the flame structure in the gas phase.

A different approach to compute the combustion response was taken by Zel'dovitch (1942) in Russia and elaborated in great depth by Novozhilov (1965, 1973, 1996). The result has come to be known as the Z-N model. The Z-N representation of the response has certain distinct advantages, most importantly giving convenient connections between the parameters in the response function and quantities easily measured in steady combustion. The idea is explained in Section 2.

2.2. Analysis of the QSHOD Model. Analysis of the model sketched in Figure 2.2 amounts to quantitative representation of the sequence (i)–(iv). Even in the simplest form described here, the problem is too

complicated for a closed form solution. Apart from recent results obtained numerically for the entire region, covering the cold solid to the hot combustion products the usual procedure, familiar in many problems of this sort, is based on solutions found for the separate regions defined above, and matched the results at the interfaces. The solutions and the matching conditions are based on the one-dimensional equations of motion. In the approach taken here, the interfaces move, a feature that must be correctly incorporated in the analysis.

The following remarks are based on the review cited above, Culick (1968). Since that time much work has been done to determine the consequences of relaxing the assumptions on which the following analysis (the QSHOD model) is based. We will later examine some of those ideas. In this section we assume that the combustion proceeds as transformation of a condensed phase at a single flat interface to the gas phase, requiring that solutions be matched at only one interface. We choose a reference system with origin ($x = 0$) fixed[2] to the average position of the interface. Hence the cold unreacted solid material progresses inward from the lift. Figure 2.5 shows this definition and the matching conditions that must be satisfied at the interface. Note that the velocity $\dot{x}_s$ of the interface appears explicitly in these conditions and is to be determined as part of the solution to the complete problem.

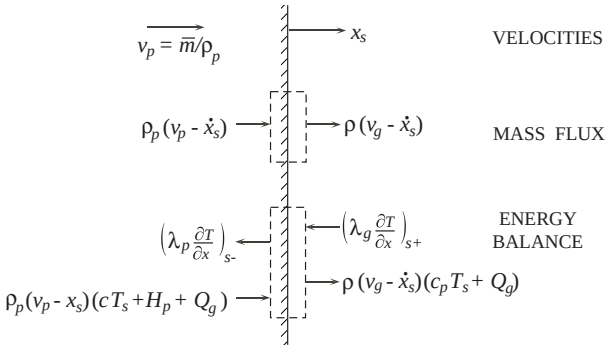

FIGURE 2.5. Reference System and Matching Conditions for the QSHOD Model.

For the simple model used here, the analysis involves only three steps: solution for the temperature field in the solid phase; solution for the temperature field in the gas phase; and matching the two solutions at the interface. Because the temperature field is central to the analysis, the final results should correctly be regarded as a thermal theory of steady and unsteady combustion of a solid propellant. No diffusive contributions are accounted for and the pressure is uniform throughout the region considered: the momentum of the flow does not enter the problem.

(a) Solid Phase

The energy equation for the temperature in the solid phase assumed to have uniform and constant properties, is

$$\lambda_p \frac{\partial^2 T}{\partial x^2} - \overline{m} c \frac{\partial T}{\partial x} - \rho_p c \frac{\partial T}{\partial t} = -\dot{Q}_d \tag{2.5}$$

where $\overline{(\ )}$ means time-averaged value; $(\ )_p$ denotes propellant; c is the specific heat of the solid; $\overline{m} = \rho_p \overline{r}$ is the average mass flux in the reference system defined in Figure 2.5; and $\dot{Q}_d$ is the rate at which energy is released per unit volume due to decomposition of the solid ($\dot{Q}_d > 0$ for exothermic decomposition). We assume $\dot{Q}_d = 0$ here an assumption to be relaxed in Section 2. It is convenient to use the dimensionless variables

$$\xi_p = \frac{\overline{r}}{\kappa_c} x \ ; \quad \tau = \frac{T}{\overline{T}_s} \tag{2.6}$$

[2]Alternatively, the reference frame may be fixed to the instantaneous position of the surface and therefore is not an inertial frame for the unsteady problem. For the linear problem, it is easy to show the equivalence of the results obtained with the two choices of reference systems. If more than three regions are treated—e.g. when an additional decomposition zone is included in the condensed phase—it may be more convenient to take $x_s = 0$ and account for the motions of the remaining interfaces.

where values at the interface are identified by subscript s and $\kappa_p = \lambda_p/\rho_p c$ is the thermal diffusivity of the propellant. Equation (2.5) becomes

$$\frac{\partial^2 \tau}{\partial \xi^2} - \frac{\partial \tau}{\partial \xi_p} - \frac{\lambda_p \rho_p}{\overline{m}^2 c}\frac{\partial \tau}{\partial t} = 0 \tag{2.7}$$

Solution to (2.7) with the time derivative dropped gives the formula for the normalized mean temperature

$$\overline{\tau} = \overline{\tau_c} + (1 - \overline{\tau_c})e^{\xi_p} \tag{2.8}$$

satisfying the conditions $\overline{\tau} = \overline{\tau_s} = 1$ at the surface and $\overline{\tau}_c = \overline{T_c}/\overline{T}_s$ far upstream ($\overline{T} = \overline{T_c}$) in the cold propellant.

For harmonic motions, with $\tau = \overline{\tau} + \tau'$ and[3] $\tau' = \hat{\tau} e^{-i\omega t}$, $\hat{\tau}$ being the amplitude, a complex function of position in the solid material. Substitution in (2.7) leads to the equation for $\hat{\tau}(\xi_p)$, easily solved to give

$$\tau' = \hat{\tau}_0 e^{\lambda \xi_p} e^{-i\omega t} \tag{2.9}$$

where λ satisfies the relation

$$\lambda(\lambda - 1) = -i\Omega \tag{2.10}$$

and Ω is the important dimensionless frequency,

$$\Omega = \frac{\lambda_p \rho_p}{\overline{m}^2 c}\omega = \frac{\kappa_p}{\overline{r}^2}\omega \tag{2.11}$$

In order that $\tau' \to 0$ for $x \to -\infty$, the solution of (2.10) with positive real part must be used; $\lambda = \lambda_r - i\lambda_r$ and

$$\begin{aligned} \lambda_r &= \frac{1}{2}\left\{1 + \frac{1}{\sqrt{2}}\left[(1 + 16\Omega^2)^{1/2} + 1\right]^{1/2}\right\} \\ \lambda_i &= \frac{1}{2\sqrt{2}}\left[(1 + 16\Omega^2)^{1/2} - 1\right] \end{aligned} \tag{2.12a,b}$$

Due to the choice of reference system, $\hat{\tau}$ in (2.9) is the fluctuation of temperature at the average position of the interface ($\xi_p = 0$). However, matching conditions at the interface requires values and derivatives of the temperature at the interface itself, having position x_s and velocity $\dot{x}_s$. Values at the interface are calculated with Taylor series expansions about $x = 0$; only the first order terms are retained for the linear problem, and on the solid side of the interface[4]:

$$\begin{aligned} \overline{T}_s(x_s) &= \overline{T}(0) + x_s\left(\frac{d\overline{T}}{dx}\right)_{0-} \quad ; \quad \left(\frac{d\overline{T}}{dx}\right)_{s-} = \left(\frac{d\overline{T}}{dx}\right)_{0-} + x_s\left(\frac{d^2\overline{T}}{dx^2}\right)_{0-} \\ T'_s(x_s) &= T'_{0-}(0) + x_s\left(\frac{\partial \overline{T}}{dx}\right)_{0-} \quad ; \quad \left(\frac{\partial T'}{\partial x}\right)_{s-} = \left(\frac{\partial T'}{\partial x}\right)_{0-} + x_s\left(\frac{\partial^2 T'}{\partial x^2}\right)_{0-} \end{aligned} \tag{2.13}$$

Hence the required results for the upstream side of the interface cannot be completed until the interfacial region is analyzed.

(b) Interfacial Region

Three relations govern the behavior at the interface: conservation of mass and energy, and the law for conversion of solid to gas. The first two are established by considering a small control volume placed about the true burning surface, as sketched in Figure 2.5. The volume is then collapsed to give "jump" conditions associated with the total unsteady mass and energy transfer in the upstream ($s-$) and downstream ($s+$) sides of the interface:

$$\begin{aligned} \frac{\rho_p \dot{x}_s}{\overline{m}} &= -\left[1 - \frac{\overline{\rho}_{gs}}{\rho_{ps}}\right]\frac{m'_s}{\overline{m}} \approx -\frac{m'_s}{\overline{m}} \\ \left[\lambda_g \frac{\partial T}{\partial x}\right]_{s+} &= \left[\lambda_p \frac{\partial T}{\partial x}\right]_{s-} + \overline{m}\left[1 - \frac{\overline{\rho}_p \dot{x}_s}{\overline{m}}\right](L_s) \end{aligned} \tag{2.14a,b}$$

[3]Note that consistently throughout these notes we use the negative exponential, $\exp(-i\omega t)$. In some of the literature the positive exponential is used, so care must be taken when making comparisons of results.

[4]The temperature is continuous at the interface, but on $x = 0$, the fluctuations T'_{0-} and T'_{0+} computed from the solutions for the solid and gas phase need not be continuous.

The mean gas density $\overline{\rho}$ near the surface is much smaller than the density of the condensed phase, for cases of current interest, so the term $\overline{\rho}/\rho_p \ll 1$ will hereafter be dropped. For an exothermic surface reaction, the change $L_s = h_{s+} - h_{s-}$ of the enthalpy is positive and may be viewed as a 'latent heat'. The heat fluxes $[\lambda_p \partial T/\partial x]_{s-}$ and $[\lambda_g \partial T/\partial x]_{s+}$ are respectively flows of heat *from* the interface to the condensed phase and *to* the interface *from* the gas phase.

An Arrhenius law has commonly been assumed for the conversion of solid to gas, giving the total surface mass flux

$$m_s = B p^{n_s} e^{-E_s/R_0 T_s} \tag{2.15}$$

To first order in small quantities, the perturbed form of (2.15) is

$$\frac{m_s'}{\overline{m}} = E e^{i\omega\tau_1} \tau_s' + n_s e^{i\omega\tau_2} \frac{p'}{\overline{p}} \tag{2.16}$$

where $E = E_s/R_0 T_s$ is the dimensionless activation energy for the surface reaction. Time delays or lags τ_1 and τ_2 are included in (2.16), but presently there is no way to compute them; hence they will largely be ignored here except for some results given in Section 2.6.

For steady combustion, the energy balance (2.14)b, with (2.8) substituted for $d\overline{T}/dx$, becomes

$$\left(\lambda_g \frac{d\overline{T}}{dx}\right)_{s+} = \overline{m}\left[c\left(\overline{T}_s - T_c\right) + L_s\right] \tag{2.17}$$

The linear unsteady part of (2.14)b is

$$\left(\lambda_g \frac{\partial T}{\partial x}\right)'_{s+} = \left(\lambda_p \frac{\partial T}{\partial x}\right)'_{s-} + m_s' \overline{L}_s + \overline{m}(c_p - c) T_s' \tag{2.18}$$

Combination of (2.8) and (2.9) and the appropriate parts of (2.13) gives the formula for the heat transfer into the condensed phase from the interface:

$$\left(\lambda_p \frac{\partial T}{\partial x}\right)'_{s-} = \overline{m} c \left[\lambda T_s' + \frac{1}{\lambda}\left(\overline{T}_s - T_c\right) \frac{m_s'}{\overline{m}}\right] \tag{2.19}$$

In this result, the approximation in (2.14)a has been used. Substitution of (2.19) in (2.18) leads to the boundary condition to be set on the unsteady temperature at the downstream side of the interface:

$$\left(\lambda_g \frac{\partial T}{\partial x}\right)'_{s+} = \overline{m} c \left[\lambda T_s' + \left(\frac{c_p}{c} - 1\right) T_s' + \left\{\frac{1}{\lambda}\left(\overline{T}_s - T_c\right) + \frac{L_s}{c}\right\} \frac{m_s'}{\overline{m}}\right] \tag{2.20}$$

This results contains two assumptions:

(i) $\overline{\rho}_g/\overline{\rho}_p \ll 1$ $(x = x_s)$
(ii) nonreacting condensed phase having constant and uniform properties

Normally, the first is reasonable. However, the second is restrictive, possibly seriously so according to some analyses; see Section 2.5. The important point is that (2.20) explicitly contains the transient behavior (the dynamics) associated with unsteady heat transfer in a benign solid material. If no further dynamics is attributed to the processes at the interface or in the gas phase, then the response function found with this analysis reflects only the dynamics of unsteady heat transfer in the condensed phase. That is the QSHOD result. Hence it is apparent that the form of the dependence of the response function in frequency *will necessarily in this case be independent of the model chosen for the quasi-static behavior of the gas phase.* The details of the model selected will affect *only* the particular values of parameters appearing in the formula for the response function.

Thus, to complete the analysis, it is best at this stage to choose the simplest possibility. We assume that the thermal conductivity is uniform in the gas phase and that the combustion processes (i.e. the rate of energy release per unit volume) are also uniform in a region beginning some distance from the interface and extending downstream, ending at a location, that is, by definition, the edge of the flame zone. This is a useful model containing two simple limits: uniform combustion beginning at the interface; and a flame sheet, obtained by

letting the thickness of the combustion zone become infinitesimally thin. Figure 2.6 is a sketch of the model. Analysis of the model for steady burning was given by Culick (1969) with the following results.

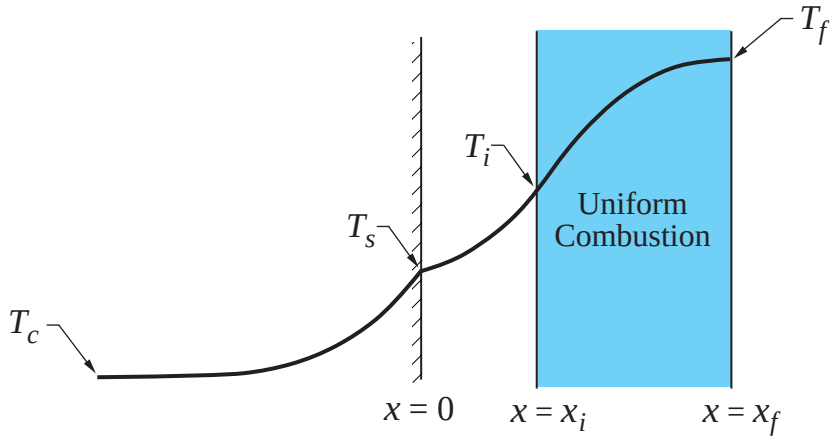

FIGURE 2.6. Sketch of the Model of a Solid Propellant Burning with Uniform Combustion in the Gas Phase.

The governing equation for this thermal theory is

$$mc_p \frac{dT}{dx} - \frac{d}{dx}\left(\lambda_g \frac{dT}{dx}\right) = \rho_g Q_f \dot{s} \tag{2.21}$$

where Q_f is the energy released per unit mass of reactant mixture (assumed to be constant), ρ_g is the local gas density and $\dot{s}$ is the local rate of reaction. At the downstream edge of the combustion zone, the boundary conditions are

$$T = T_f \; ; \quad \frac{dT}{dx} = 0 \quad (x = x_f) \tag{2.22a,b}$$

where T_f is the adiabatic flame temperature. On the interface,

$$T = T_s \tag{2.23}$$

and the energy balance at the interface gives

$$\left(\lambda_g \frac{dT}{dx}\right)_{s+} = \overline{m}\left[c\left(\overline{T}_s - T_c\right) + L_s\right] \tag{2.24}$$

For steady combustion, consideration of the energy flow across the gas phase gives

$$\left(\lambda_g \frac{dT}{dx}\right)_{s+} = \overline{m}\left[Q_f - c_p\left(T_f - T_s\right)\right] \tag{2.25}$$

On the other hand, integration of (2.21) across the combustion zone, and application of the boundary conditions (2.22)a,b and (2.23) leads to

$$\left(\lambda_g \frac{dT}{dx}\right)_{s+} = \int_0^\infty \rho_g Q_f \dot{s} dx - mc_p\left(T_f - T_s\right) \tag{2.26}$$

Because Q_f is constant, comparison of (2.25) and (2.26) leads to the requirement on the overall reaction rate

$$\int_0^\infty \rho_g \dot{s} dx = m \tag{2.27}$$

We assume λ_g constant (an assumption that is easily relaxed) and transform from x to the dimensionless variable ζ:

$$\zeta = e\frac{mc_p}{\lambda_g}x \tag{2.28}$$

The energy equation (2.21) becomes

$$-\zeta^2 \frac{d^2T}{d\zeta^2} = \Lambda^2 \tag{2.29}$$

where the eigenvalue Λ^2 is

$$\Lambda^2 = \frac{\lambda_g Q_f w}{m^2 c_p^2 T_s} \tag{2.30}$$

and

$$w = \rho_g \dot{\epsilon} \tag{2.31}$$

Generally, of course, $\dot{\epsilon}$ and hence w and therefore Λ^2 are dependent at least on temperature, so Λ^2 is implicitly a function of ζ. However, we assume Λ^2 constant, defining the condition of uniform combustion. Then with ζ_i the value of ζ at the beginning of the combustion zone (where ignition is assumed to occur) and ζ_f the value at the downstream edge of the flame, the first integral of (2.29) gives

$$\left(\frac{dT}{d\zeta}\right)_{s+} = \left(\frac{\zeta_f - \zeta_i}{\zeta_f \zeta_i}\right) \Lambda^2 \tag{2.32}$$

Thus

$$\left(\lambda_g \frac{dT}{dx}\right)_{s+} = \frac{\lambda_g Q_f}{c_p} \left(\frac{1}{\zeta_i} - \frac{1}{\zeta_f}\right) \frac{w}{m} \tag{2.33}$$

For $\zeta_f \gg \zeta_i$, and in the limit of combustion beginning at the solid/gas interface so $\zeta_i = 1$,

$$\left(\lambda_g \frac{dT}{dx}\right)_{s+} = \frac{\lambda_g Q_f}{c_p} \frac{w}{m} \tag{2.34}$$

The assumption of quasi-steady behavior implies that the fluctuation of heat transfer at the surface is given simply by the linearized form of (2.33):

$$\left(\lambda_g \frac{dT}{dx}\right)'_{s+} = \overline{m} c_p \overline{T}_s \Lambda^2 \left(\frac{w'}{\overline{w}} - \frac{m'}{\overline{m}}\right) \tag{2.35}$$

We also find as the linearized form of (2.25):

$$\left(\lambda_g \frac{dT}{dx}\right)'_{s+} = m' \left[Q_f - c_p \left(\overline{T}_f - \overline{T}_s\right)\right] - \overline{m} c_p \left(\overline{T}_f - \overline{T}_s\right) \tag{2.36}$$

This equation gives a formula for the fluctuation of flame temperature,

$$T'_f = T'_s + \frac{m'}{\overline{m}} \left[\frac{Q_f}{c_p} - \left(\overline{T}_f - \overline{T}_s\right)\right] - \frac{1}{\overline{m} c_p} \left(\lambda_g \frac{dT}{dx}\right)'_{s+} \tag{2.37}$$

Substitution of (2.35) for the last term gives the formula for computing T'_f when the combustion is uniform. In general, T'_f is not equal to the local fluctuation of temperature due to acoustical motions in the gas phase, the difference appearing the temperature fluctuation associated with an entropy wave carried by the mean flow departing the combustion zone.

By letting $\zeta_i \to \zeta_f$, the corresponding results can be obtained for a flame sheet; see Culick (1969; 2002). We will consider here only the case of finite combustion zone; the response functions found for the two cases differ only in small details.

To progress further, we must specify the form of $w = \rho_g \dot{s}$; the reaction rate per unit volume. For the quasi-steady part of the processes, we assume that the mass flow provided by the surface is well-approximated by the Arrhenius law (2.15) and its fluctuation is (2.16) with zero time delays,

$$\frac{m'}{\overline{m}} = E \frac{T'_s}{\overline{T}_s} + n_s \frac{p'}{\overline{p}} \tag{2.38}$$

Due to the assumption of quasi-steady behavior, this formula represents the fluctuation of mass flow throughout the gas phase.

Finally, we need an explicit form for w as a function of the flow variables. To construct a consistent formula for the reaction rate in the gas phase, we equate the two results for heat transfer to the interface during steady burning: (2.24), the energy balance generally valid at the interface; and (2.34) found for the special case of uniform combustion. We find the expression for w:

$$w = \frac{c_p}{\lambda_g Q_f} m^2 \left[c \left(\overline{T}_s - T_c \right) + L_s \right] \tag{2.39}$$

We assume that the right-hand side can be written as a function of pressure only by approximating the pyrolysis law $m = a(T_s)p^n$ as

$$m = ap^n = b(T_s - T_c)^s p^{n_s} \tag{2.40}$$

so

$$T_s - T_c = \left(\frac{a}{b} p^{n-n_s} \right)^{\frac{1}{s}} \tag{2.41}$$

Then (2.39) becomes

$$w = \frac{c_p}{\lambda_g Q_f} (ap^n)^2 \left[c \left(\frac{a}{b} p^{n-n_s} \right)^{\frac{1}{s}} + L_s \right] \tag{2.42}$$

The fluctuation w' of the reaction rate is then

$$\frac{w'}{\overline{w}} = \frac{\left(1 - \frac{T_c}{\overline{T}_s}\right)}{\Lambda^2} \frac{c}{c_p} w \frac{p'}{\overline{p}} \tag{2.43}$$

where Λ^2 is given by (2.30) for the steady problem,

$$\Lambda^2 = \frac{\lambda_g Q_f \overline{w}}{\overline{m}^2 c_p^2 \overline{T}_s} \tag{2.44}$$

and

$$\begin{aligned} w &= \left[2(1+H) + \frac{c_p}{c} \frac{1 - \frac{n_s}{n}}{c} \right] \\ H &= -\frac{L_s}{c(\overline{T}_s - T_c)} \end{aligned} \tag{2.45a,b}$$

Instead of the calculations leading from (2.34) to (2.43) one could as well simply assune $w' \sim p'$. The only purpose of these remarks is to give an example of relating fluctuations of the reaction rate to the pressure for a well-defined model of combustion in the gas phase.

(c) Construction of the Response Function

We find the formula for the response function in the following way:

(i) Substitute the pyrolysis law (2.38) in (2.20) which combines the interfacial conditions for energy and mass transfer:

$$\frac{1}{\overline{m} c \overline{T}_s} \left(\lambda_g \frac{\partial T}{\partial x} \right)'_{st} = \left(\lambda + \frac{A}{\lambda} \right) \frac{T'_s}{\overline{T}_s} + \left(\frac{c_p}{c} - 1 + \frac{LA}{1 - \frac{T_c}{\overline{T}_s}} \right) \frac{T'_s}{\overline{T}_s} + n_s \left(L + \frac{1 - \frac{T_c}{\overline{T}_s}}{\lambda} \right) \frac{p'}{\overline{p}} \tag{2.46}$$

where

$$\begin{aligned} L &= \frac{L_s}{c\overline{T}_s} \\ A &= (1 - \frac{T_c}{\overline{T}_s})(\alpha_s + \frac{E_s}{R_o \overline{T}_s}) \end{aligned} \tag{2.47a,b}$$

(ii) Substitute the reaction rate (2.43) into the expression (2.35) for the heat loss from the gas phase:

$$\frac{1}{\overline{m}c\overline{T}_s}\left(\lambda_g\frac{\partial T}{\partial x}\right)'_{st} = \left(1-\frac{T_c}{\overline{T}_s}\right)w\frac{p'}{\overline{p}} - \frac{c_p}{c}\Lambda^2\frac{m'}{\overline{m}} \tag{2.48}$$

(iii) Equation (2.46) and (2.48), use the pyrolysis law to eliminate $T'_s/\overline{T}_s$; this step leaves an equation which can be rearranged to give the ratio defined to be the response function for pressure coupling:

$$R_p = \frac{m'/\overline{m}}{p'/\overline{p}} = \frac{\left(AW+\frac{c_p}{c}n_s\right)+n_s(\lambda-1)}{\lambda+\frac{A}{\lambda}+\left[\frac{c_p}{c}E\Lambda^2-HA+\frac{c_p}{c}-1\right]} \tag{2.49}$$

(iv) Write (2.49) in the form

$$R_p = \frac{c_1+n_s(\lambda-1)}{\lambda+\frac{A}{\lambda}+c_2} \tag{2.50}$$

For the assumed steady burning rate law, $m = ap^n$, the fluctuation can be written

$$R_p = \frac{m'/\overline{m}}{p'/\overline{p}} = n \tag{2.51}$$

Thus in the limit of zero frequency ($\lambda = 1$), the right-hand side of (2.50) must equal n, giving the condition

$$\frac{c_1}{1+A+c_2} = n$$

Define B with

$$c_1 = nB$$

and

$$c_2 = B-(1+A)$$

Hence (2.50) becomes

$$R_p = \frac{nB+n_s(\lambda-1)}{\lambda+\frac{A}{\lambda}-(1+A)+B} \tag{2.52}$$

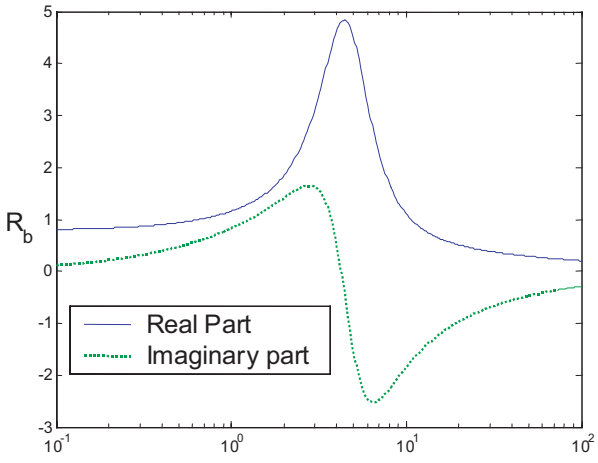

FIGURE 2.7. Real and Imaginary Parts of a QSHOD Response Function Computed with Equation 2.52.

Figure 2.7 shows typical results for the real and imaginary parts of this formulas when $n_s = 0$. Experimental results given in the following section have long established that the QSHOD model captures a major contribution to the dynamical behavior, due to unsteady heat transfer in the condensed phase. Thus it is important to inderstand the preceding analysis. However, even with the large experimental errors associated with all current

experimental methods, it seems there is little doubt that other dynamical processes cannot be ignored for many propellants, especially in the range of frequencies above that where the broad peak of the real part of R_b appears.

2.3. Measurements of the Response Function; Comparison of Experimental Results and the QSHOD Model. For more than forty years, measurement of the response function has been the most important task is research on combustion instabilities in solid rockets. Without accurate data, the truth of theoretical results cannot be assessed; predictions and interpretations of instabilities in motors are uncertain; and the ability to screen propellants for optional behavior is seriously compromised. Unfortunately no entirely satisfactory method exists for accurate measurements of the combustion response, irrespective of cost. Two recent reports of extended programs (Caltech MURI, 2002 and UIUC MURI, 2002) have led to this conclusion after five years' investigation of the five main existing methods:

(i) T-burner
(ii) ultrasonic apparatus
(iii) laser recoil method
(iv) magnetohydrodynamic method
(v) microwave technique

A sixth method based on using a burner (e.g. an L* burner) in which bulk oscillations are excited, was not investigated, partly because it is intrinsically limited to low frequencies.

It is not our purpose here to review these methods; see the two MURI reports; Couty (1999) and references contained in those works for all discussions of all but the last. The microwave technique was introduced in the 1970's and has been continually improved, but the accuracy of the data remains inadequate, particularly for metallized propellants for which the method is useless under some conditions.

The central question for modeling and theory is: how good is the agreement between predicted and measured values? It appears that the first extensive comparison for this purpose were carried out many years ago (Beckstead and Culick, 1971) soon after the recognition that all the available models/analyses were equivalent to the QSHOD (A,B) model. With only two parameters available to adjust the theoretical results to fit data, the task of comparing theory and experiment became manageable. At that time, only T-burner data were available. Figures 2.8 and 2.9 show two results.

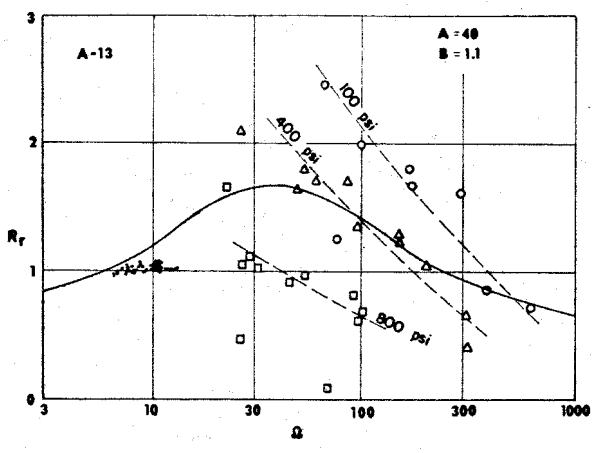

FIGURE 2.8. The real part of the response function vs. the non-dimensional frequency, $\alpha_t\omega/r^2$ for A-13 propellant: the solid curve is calculated from the QSHOD formula for the values of A and B shown; the dashed curves represent the T-burner data at the indicated pressures. (Beckstead and Culick 1969).

One purpose of the report by Beckstead and Culick was to combine the formula for the QSHOD response function with results obtained from analyses of the T-burner and the L*-burner to obtain formulas for the

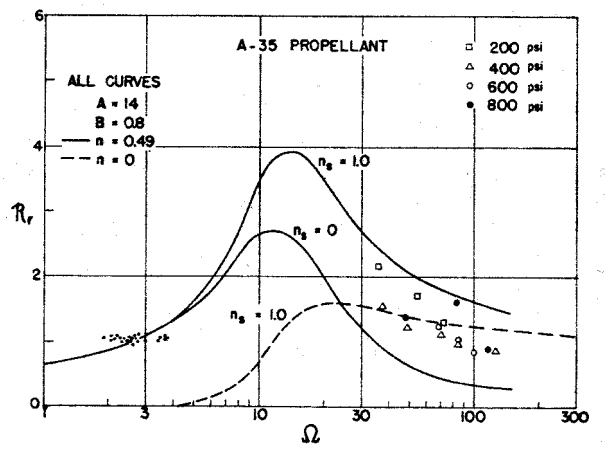

FIGURE 2.9. The real part of the response function vs. the non-dimensional frequency for A-35 propellant; the curves were calculated from the QSHOD formula. (Beckstead and Culick 1969).

parameters A and B in terms of measurable quantities. The main conclusion was that unique values of A and B could not be obtained for a given propellant tested at a chosen value of operating pressure. Consequently, large differences existed between the data and curves of the sort shown in Figure 2.7.

Since that time, many examples of using the A, B model to fit data have been given. Most, if not all, approach the matter as a two-parameter (A and B) curve fitted to data for the real part of the response function only. Strictly, that tactic is incorrect and could produce misleading results. The proper approach requires that the two-parameter representation be used to fit simultaneously the real and imaginary parts of the response function. There are also cases in which investigators have failed to respect the distinction between the response function $R_p \sim m'/p'$ and the admittance function $A_p \sim u'/p'$ defined for velocity fluctuations.

Without attention to both of those points, any comparisons between data and a model are suspect. Despite those common deficiencies, there is no doubt that the QSHOD model cannot and does not represent the dynamics of actual propellants. One would anticipate even without experimental results that the assumption of quasi-steady behavior in the gas phase must fail at high frequencies, commonly believed to be around 1000 Hertz and higher. Moreover, observations of steady combustion have shown that important decomposition processes take place in the sub-surface zone near the interface of most propellants. Hence at least two improvements of the QSHOD model should be made.

Before examining examples of more complicated models, we review the essentials of another approach to deriving the QSHOD model, the Z-N model.

2.4. The Zel'dovich-Novozhilov (Z-N) Model . Zel'dovich (1942) was first to consider true combustion dynamics for solid propellants. He was concerned with problems of transient burning—i.e. what happens to combustion of a propellant when the impressed pressure is changed rapidly—but now explicitly with the response function. Novozhilov (1965) later used Zel'dovich's basic ideas to find a formula for the response of a burning propellant to sinusoidal oscillations of pressure. The result has exactly the same dependence on frequency as the QSHOD model, i.e. it is identical with the formula obtained by Denison and Baum four years earlier.

The Z-N model incorporates quasi-steady behavior of the burning in a clever and instructive fashion. Moreover, the parameters—there are, of course two corresponding to A and B in the QSHOD model—are so defined as to be assigned values from measurements of steady combustion of the propellant in question. Hence there is no need to become enmeshed in the details of modeling the combustion processes in the gas phase. If the measurements could be done accurately, it would be possible to obtain good predictions of the combustion response for propellants, subject of course to all the assumptions built into the QSHOD model. Unfortunately, the required quantities are difficult to measure accurately. Confirmation of the results still requires measurements of both the real and imaginary parts of the response function.

The condensed phase and interfacial region are treated as described in Section 2.2 for the QSHOD model. Instead of detailed analysis of the gas phase, that is, construction of a "flame model", the assumption of quasi-steady behavior is applied by using relations among the properties of steady combustion, the burning rate and the surface temperature as functions of the initial temperature of the cold propellant and the operating pressure:

$$m = m(T_c, p) \qquad T_s = T_s(T_c, p) \tag{2.53a,b}$$

The assumption is also made that these functions are known sufficiently accurately that their derivatives can also be formed, introducing the four parameters

$$\nu = \left(\frac{\partial \ln \overline{m}}{\partial \ln \overline{p}}\right)_{T_c} \qquad \mu = \frac{1}{\overline{T}_s - T_c}\left(\frac{\partial \overline{T}_s}{\partial \ln \overline{p}}\right)_{T_c}$$
$$k = (\overline{T}_s - T_c)\left(\frac{\partial \ln \overline{m}}{\partial T_c}\right)_{\overline{p}} \qquad r_{ZN} = \left(\frac{\partial \overline{T}_s}{\partial T_c}\right)_{\overline{p}} \tag{2.54a,b,c,d}$$

Subscript ZN is attached to r to distinguish it from the linear burning rate. It is not apparent from the remarks here why the four parameters (2.54)a,b are significant in this theory.

Recall from Section 2.2 that the sole reason for analyzing a model of combustion in the gas phase was to produce a formula for the heat feedback, $\lambda_g(\partial T/\partial x)_{s+}$, to the interface. That is the central problem here as well: to find the heat feedback from considerations of steady combustion and assume (the quasi-steady approximation) that the form of the result holds under unsteady conditions. The trick is to work out the relation between the feedback and the properties of steady combustion. It is in that process that the parameters (2.54)a–d appear.

The formula for the response function corresponding to (2.52) is usually written (e.g. Cozzi, DeLuca and Novozhilov 1999)

$$R_p = \frac{\nu + \delta(\lambda - 1)}{r_{ZN}(\lambda - 1) + k\left(\frac{1}{\lambda} - 1\right) + 1} \tag{2.55}$$

where

$$\delta = \nu r_{ZN} - \mu k \tag{2.56}$$

Comparison of (2.52) and (2.55) gives the formulas connecting the parameters in the two formulations:

$$A = \frac{k}{r_{ZN}}\ , \quad B = \frac{1}{k}\ , \quad n = \nu\ , \quad n_s = \frac{\delta}{r_{ZN}} \tag{2.57}$$

Much emphasis has been placed in the Russian literature on the "boundary of intrinsic stability", the locus of values of (A,B), or (k, r_{ZN}) for which the denominator of (2.55) vanishes. Under those conditions, the propellant burn rate suffers a finite perturbation in the limit of a vanishingly small change of pressure. Hence, from measured values of ν and r_{ZN}, one can infer how close an actual propellant is to that stability boundary.

With these models, the opportunity exists to use experimental results to determine how accurately the QSHOD approximations capture the combustion dynamics of solid propellants:

(1) measure ν, μ, k, r_{ZN} from tests of steady combustion;
(2) measure the real and imaginary parts of R_p;
(3) compute R_p from (2.52) or (2.55) and compare with (2)

There seem to be no published reports of results for this procedure.

2.5. Revisions and Extensions of the QSHOD Model. As we have already noted in Section 2.3, even with the large uncertainties accompanying the experimental results obtained with current methods, it is clear that the QSHOD model does not capture some important dynamical processes. Considerable effort has been devoted to improving the model, with a certain amount of success, but unfortunately the deficiencies in the experimental procedures still prevent definitive identification of the most significant contributions.

Attention has been given to all three of the regions sketched in Figure 2.2. It is important to recognize that simply changing the model for steady combustion—for example including a finite zone of decomposition in the solid phase—will not change the form of the QSHOD result. Any additional spatial zones or processes must also contain new dynamics, a lesson the author learned the hard way (Culick 1969).

Here we will only cite a few of the recent works without giving details of the analyses. To be possibly unseemly parochial, Section 2.6 contains a more extensive, but brief description of recent work at Caltech.

2.5.1. *Additional Dynamics in the Condensed Phase.* It seems that three types of processes have been considered:

1) temperature-dependent thermal properties;
2) phase transitions; and
3) decomposition zones.

Louwers and Gadiot (1999) have reported results for numerical calculations based on a model of HNF. Melting at some interface within the condensed phase is accounted for, as well as energy released by sub-surface reactions. Combustion in the gas phase is also treated numerically. The computed response functions also show that the new processes may increase the values of $R_p^{(r)}$ by as much as 10–30% and more in the frequency range above the peak. The peak value is unchanged.

Brewster and his students at the University of Illinois have produced a number of interesting works treating additional dynamics related to chemical processes in the condensed phase and at the interface (Zebrowski and Brewster, 1996; Brewster and Son, 1995).

Gusachenko, Zarko and Rychkov (1999) have investigated the effects of melting in the response function, finding quite significant consequences. Lower melting temperatures and larger energy absorption in the melt layer increase the magnitude of the response function.

Cozzi, DeLuca and Novozhilov (1999) worked out an extension of the Z-N method to account for phase transition at an infinitesimally thin interface in the condensed phase. The analysis includes new dynamics by allowing different properties of the thermal waves on the two sides of the interface. Additional heat release is allowed only at the interface of the transition and with conversion of condensed material to gaseous products. They found that the response function is increased by exothermic reaction at the internal interface and by reduced temperature of the phase transition.

2.5.2. *Additional Dynamics in the Gas Phase.* DeLuca (1990; 1992) has given thorough reviews of the various models used for the dynamics of the gas phase. Most, however, involve no dynamics, so there are no effects on the dependence of the response function on frequency. Truly dynamical effects are covered in the next section.

2.6. Modeling the Effects of Velocity Coupling on the Global Dynamics of Combustion Chambers. The research summarized in this section has been reported in a Ph.D. Thesis (Isella, 2001) and in three publications (Culick, Isella and Seywert, 1998; Isella and Culick, 2000a; 2000b). Chiefly two general problems have been addressed:

1) develop a simple general analysis of the combustion dynamics of a solid propellant that will conveniently accommodate models of the relevant chemical and physical processes, especially those in the interfaced region; and
2) investigate the influences of changes in the combustion response function on observable features of the combustor dynamics, particularly properties of limit cycles.

Both of these problems were chosen to try to determine answers to the question: what properties of a solid propellant are responsible for the often observed sensitivity of the dynamics of a solid rocket to apparently small (sometimes not well-known) changes in the composition of the propellant. The main conclusions are:

(i) small changes in the composition and thermodynamic properties of a propellant have significant consequences for dynamical behavior due to pressure coupling only if the propellant is burning near its intrinsic instability boundary; and
(ii) on the contrary the dynamics due to velocity coupling is evidently significantly sensitive to small compositional changes.

If these conclusions are true, then future work in the area of combustion instabilities must include intensive attention to modeling and measuring the combustion dynamics-i.e. the response function-associated with velocity coupling.

2.6.1. *The Model Framework.* One important purpose of the work cited above was to construct a framework within which it should be possible easily to investigate the consequences of various processes participating in the combustion of a solid. Representation of the combustion dynamics must be in a form required for analyzing the global dynamics (Section 3.2). The simplest approach is an extension of the well-known one-dimensional analysis producing the QSHOD response function for pressure coupling (Culick, 1968; Beckstead *et al.*, 1969; T'ien, 1972; among many works). Others have followed a similar tack (e.g. Louwers and Gadiot, 1999); the main novel aspect of this work is inclusion simultaneously of surface physical dynamics (e.g. due to mobility of liquid or solid particles); dynamics, rather than quasi-steady behavior, of the gas phase; and an elementary representation of velocity coupling.

On the submillimeter scale, a burning solid is heterogeneous both in the region adjacent to the interface and in the gas phase where much of the conversion to products takes place. The flow field in the chamber, in particular the unsteady acoustic field, has spatial variations normally the order of centimeters and larger. The dynamics of the combustion processes at the surface are formally accommodated as a boundary condition, a response function of some sort, in the analytical framework for the global dynamics. Hence the vast difference in characteristic scales is accommodated, in principle, by spatially averaging the combustion dynamics. The averaging is done over a surface in some sense far from the interface so far as the propellant combustion is concerned, but practically at the interface so far as the field within the chamber is concerned. In that way, the results of solution to the "inner" problem of combustion dynamics in the surface region are used as the boundary conditions for solution to the "outer" problem of the unsteady flow field in the chamber.

We are not concerned here with the matter of spatial averaging: we assume it can be done, not necessarily an easy or obvious process. It's an important part of the general problem. Therefore we proceed from the beginning with a one-dimensional analysis. The spatial framework for the model shown in Figure 2.10.

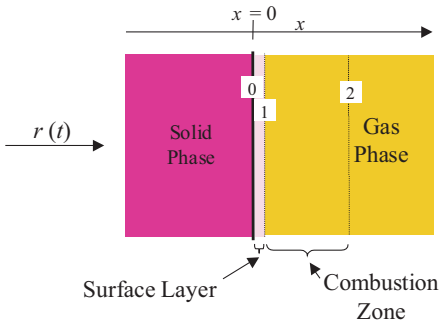

FIGURE 2.10. Spatial Definition of the Model

The strategy of the analysis is not novel and has been used in many previous works: solve the relevant equations, or postulate a model, governing the behavior in each of the three regions: solid phase; surface layer; and gas phase, including the region called 'combustion zone' in Figure 2.10. A major purpose of the analysis

has been to determine the quantitative effects of the dynamics in the surface layer and gas phase in the response function found from the QSHOD model. Hence throughout the work we assume the same model for the solid phase: the dynamics is due to unsteady heat transfer in a homogeneous material having uniform and constant properties.

Separate solutions or representations are obtained for each of the three regions. Unspecified constants or functions are then eliminated by satisfying boundary conditions and applying matching conditions at the two interfaces. Initially we intended, or hoped, to find such a form for the general behavior that different models for the surface layer and gas phase could easily be substituted and their consequences assessed. That goal has not been realized and probably is unattainable. Results require detailed numerical calculations before interesting information is obtained.

2.6.2. *Models of the Surface Layer.* From the beginning of this work we anticipated, because the dynamics of the gas phase are fast (owing to the relatively low material density), that the dynamics of the surface region should have greater effect on the combustion response function. We investigated two models of the region:

(i) first order dynamics represented by a constant time lag; and
(ii) unsteady heat transfer, with material properties different from those in the solid phase.

The idea of using a time lag is of course an old one, having been used by Grad (1949) in the first analysis of combustion instabilities, and later by Cheng (1982) as part of the Princeton group's extensive investigations (nearly a technical love affair) of time lag representations of unsteady combustion. The result in the present work, for the fluctuation of mass flux is

$$\frac{m'/\overline{m}}{p'/\overline{p}} = R_p \frac{e^{-i\Omega t}}{\sqrt{1+(\Omega t)^2}}$$

where R_p (sometimes written as R_b) is the response function found in the QSHOD theory. Thus R_p has the familiar two-parameter (A,B) representation. The dimensionless frequency is $\Omega = \omega\kappa/F^2\kappa$ is the thermal diffusivity and $\overline{r}$ is the linear burning rate and τ is the dimensionless time lag, equal to the physical time lag divided by $\kappa/\overline{r}^2$. Figure 2.11 shows a typical result (A = 14; B = 0.85; τ = 1.5). The graphs illustrate clearly a basic problem with a time lag theory: if the time lag is assumed constant (i.e. independent of frequency) the response (in this case the real part) possesses an oscillatory behavior with period increasing with frequency. Such behavior has never been observed.

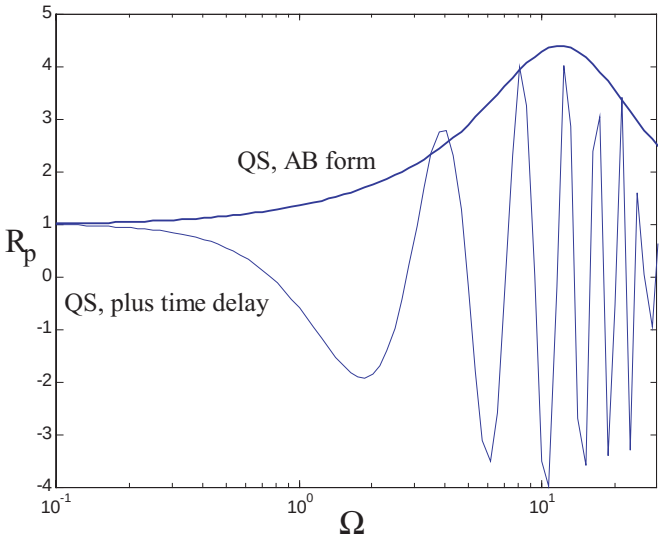

FIGURE 2.11. QSHOD Response Function with a Time lag: Thick Line, QSHOD Theory; Thin Line, QSHOD Model Including a Surface Layer Having First Order (time lag) Dynamics.

It is true that any response function can be written in a form showing a time lag behavior, but in general the time lag varies with frequency (Culick, 1968). If the physical model is sufficiently detailed, the dependence of t on frequency is found as part of the solution. In particular, the QSHOD theory gives $\tau(\Omega)$ such that the amplitude of the response function decays smoothly for frequencies higher than that at which the single peak occurs.

The second model for the surface is the only one considered for the following results. It is a simple representation of the dynamical behavior making use of the same solution as that for the homogeneous solid phase, with two differences:

(i) the uniform and constant properties are different from those of the condensed solid material;
(ii) the solution is forced to satisfy matching conditions of continuous temperature and heat transfer at the interfaces with the condensed phase and the gas phase.

2.6.3. *Models of the Gas Phase.* In this analysis, all combustion processes are assumed to occur in the gas phase; upstream only phase changes are accounted for, assumed to take place at the interfaces. We assume distributed combustion of a simplified form, a single one-step reaction as previous treatments have used (T'ien, 1972; Huang and Micci, 1990; Lazmi and Clavin, 1992). Solutions must then be found numerically for the steady and linear unsteady temperature distributions, and subsequently matched to the solution for the surface layer.

2.6.4. *Some Results for the Combustion Response Function.* Many experimental results exist suggesting that the responses of actual propellants tend often to be higher than that predicted by the QSHOD model for high frequencies. Initially the strongest motivation for this work on the response function was to determine in simple and relatively crude fashion what processes might have greatest effect on the values of the pressure-coupled response at frequencies greater than that at which the peak magnitude occurs. Roughly what that means, is finding one or more processes having 'resonant behavior' or characteristic times in the appropriate range. Unfortunately the analysis is sufficiently complicated that it has not been possible yet to deduce any explicit 'rules of thumb.' Therefore we present here a few plots of computed results to illustrate the behavior.

Figure 2.12 shows the basic or reference response function computed from the simple QSHOD model. The influences of dynamics in the surface layer and gas phase will be shown relative to that reference.

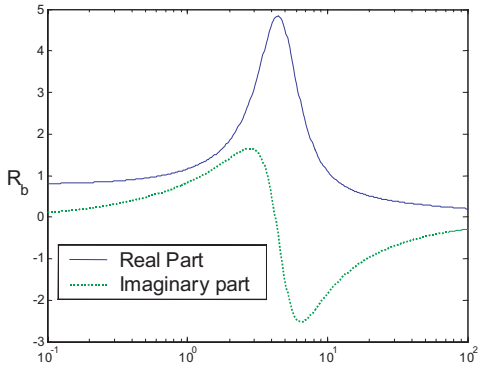

FIGURE 2.12. Reference Case: QSHOD Result with A = 6.0, B = 0.60.

(i) Influence of Gas Phase Dynamics.

Figure 2.13 is the result when only the dynamics in the gas phase is added to the QSHOD model. The results are similar to those found by T'ien (1972) and Lazmi and Clavin (1992), not a surprising conclusion. As expected, the dynamics of the gas phase introduce a single additional peak at a frequency higher than that of the peak caused by unsteady heat transfer in the condensed phase.

(ii) Combined Influences of the Dynamics of the Surface Layer and the Gas Phase.

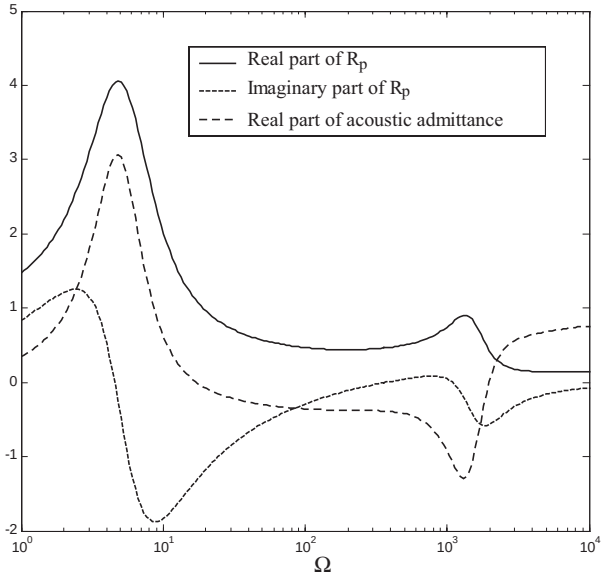

FIGURE 2.13. Combustion Response, QSHOD Model with Gas Phase Dynamics

The dynamics of the surface layer itself is the same as those of the condensed phase, but with different values of the defining parameters Figure 2.14 illustrates the effects of changing the surface activation energy and the material density on a function characterizing the response of heat transfer in the layer. The shape of this function differs from that (Figure 2.12) of the basic response function because it depends on the dependence of several flow variables on frequency.

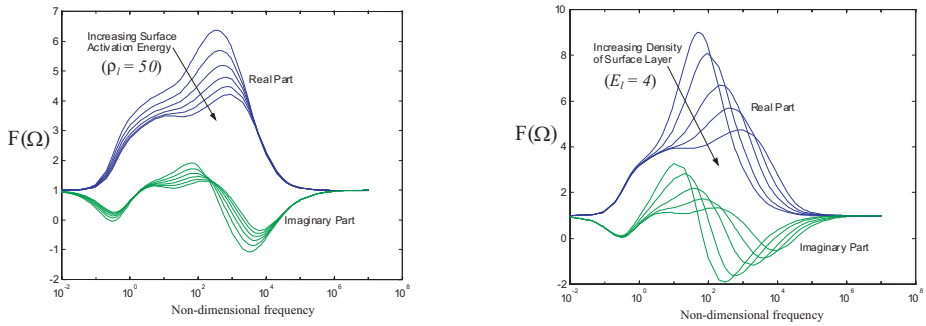

FIGURE 2.14. Effects of Activation Energy and Density on the Dynamics of the Surface Layer.

Finally, Figure 2.15 shows the result for one example of the response function with the dynamics of both the surface layer and the gas phase accounted for. Evidently for the conditions examined here the dynamics of the gas phase has more obvious influence on the response, in the higher frequency range, than does the surface layer.

One way of summarizing the results is shown in Figure 2.16, showing the contributions to the response function by the solid (condensed) phase, the surface layer and the gas phase. The overall response function for the propellant is the product of the three contributions.

2.7. Velocity Coupling, the Combustion Response, and Global Dynamics. The research summarized in this section amounts to using some characteristics of the global combustor dynamics—the amplitudes and harmonic context of limit cycles—to draw some inferences about qualitative features of the combustion dynamics.

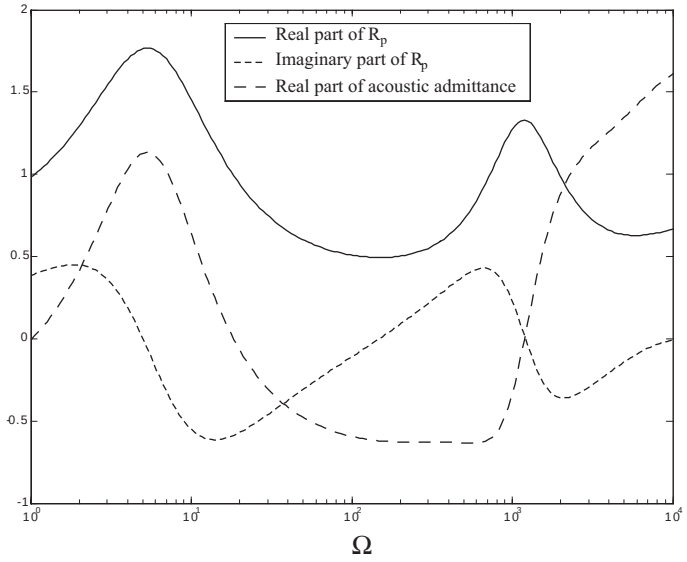

FIGURE 2.15. Combustion Response Function Including the Dynamics of the Surface Layer and the Gas Phase.

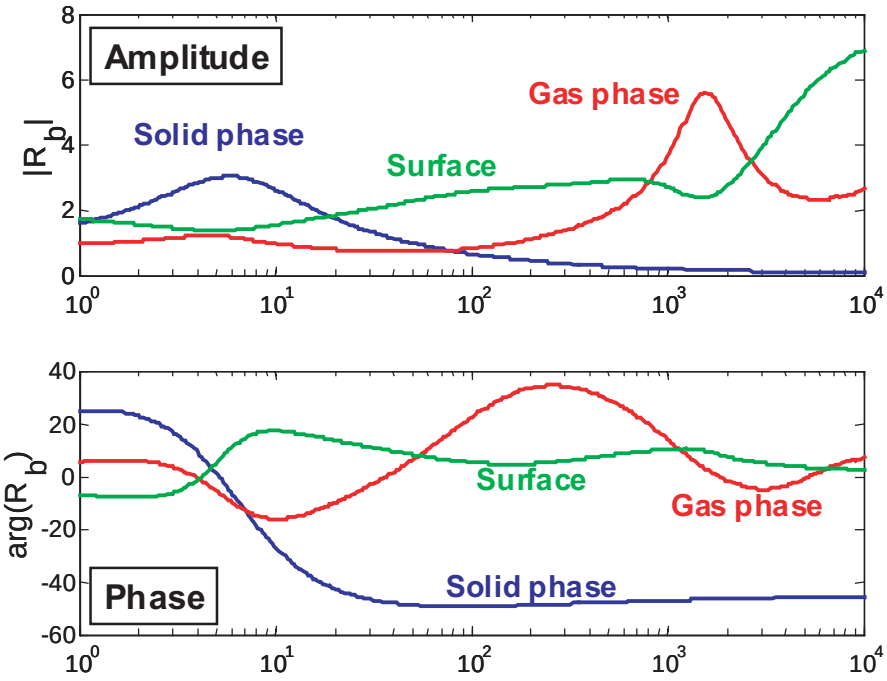

FIGURE 2.16. The Combustion Response Function Represented as Magnitudes and Phases of Individual Contributions.

At the beginning of the MURI program, during completion of his dissertation, Burnley (1996) showed that rectification associated with a velocity-coupled response function having also a threshold velocity, could be responsible for nonlinear or pulsed instabilities in a solid rocket motor. This result confirmed a conclusion reached several years previously by Levine and Baum (1983). That was the first example of using the behavior of the global dynamics as essentially a diagnostic tool to learn about the influences of the combustion dynamics on observable phenomena.

In the current work, the main questions at hand have to do with the apparent sensitivity of the global dynamics to small changes of propellant composition (see remarks (i) and (ii) in the introductory part of the section). We assume that small changes of composition likely have relatively small effects on the magnitude and phase of the response function. Therefore, we are really investigating the effects of small changes in the response function on the observable global dynamics. Our main conclusion is that the sensitivity of the dynamics to changes in the response associated with velocity coupling is significantly greater than that for the response due to pressure coupling. The implications for directions in future research are substantial.

Isella (2001) and Isella and Culick (2000) have reported the main results. Here we will only cite a couple of examples. The idea is to use the framework described in Section 3.2 below to compute the growth and limiting amplitudes for limit cycles. Essentially a modest parameter study has been done, the response function itself (i.e. the combustion dynamics) being the parameter. Following the tactic first introduced by Culick, Isella and Seywert (1998), it is helpful to display the response function, as a function of frequency, and the amplitudes of the modes forming a limit cycle, as two parts of the same figure, such as Figure 2.17 prepared for a typical case for the QSHOD response function. The chamber is cylindrical, 0.6 m long, 0.025 m in diameter, operated at a chamber mean pressure equal to 1.06×10^7 Pa. It is the same motor considered by Culick and Yang (1992).

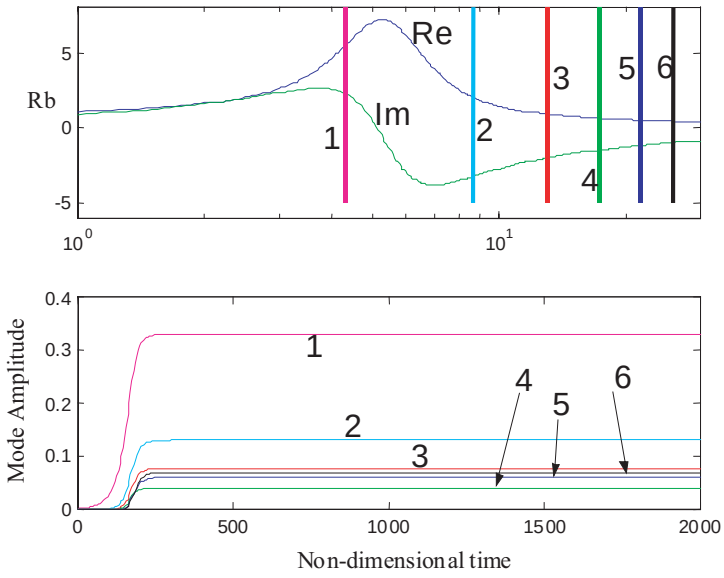

FIGURE 2.17. Results of a Simulation with a QSHOD Combustion Response (Pressure Coupling: A= 8.0, B = 0.6, n = 0.8).

Figures 2.18–2.20 show results obtained for the same motor and basic combustion response but including, respectively, a time delay; surface layer dynamics; and dynamics of both a surface layer and gas phase, all according to the analysis described above.

Owing to the significantly different dynamics added to the basic QSHOD model, the three examples illustrated in Figures 2.18–2.20 show quite different response functions—all, it must be emphasized-representing responses due to pressure coupling. The question here concerns the sensitivity of the response function to changes of composition (not the qualitative dynamics) and consequently the sensitivity of the global chamber dynamics.

For the examples chosen, the waveforms in the limit cycles are similar whether or not dynamics of the surface layer and gas phase are accounted for. This result is due mainly to the substantial attenuation of higher harmonics due to particle damping (Culick and Yang, 1992). If the damping is reduced, the amplitudes and amounts of higher harmonics are substantially affected, as Figures 2.21 and 2.22 show.

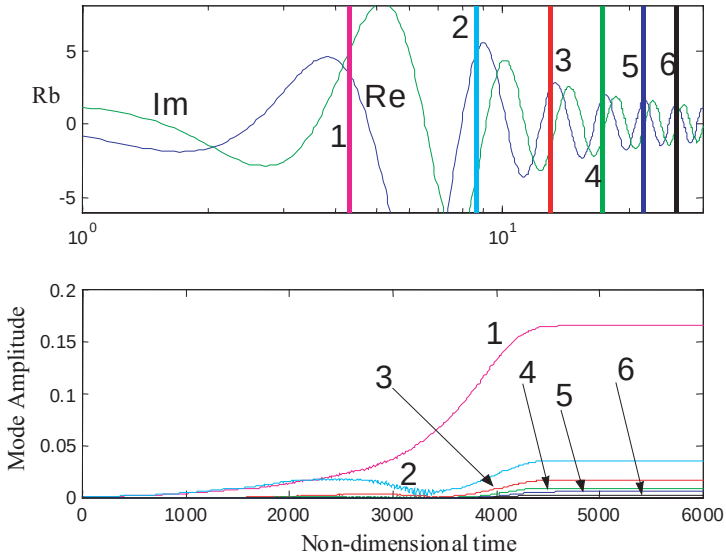

FIGURE 2.18. Results of a Simulation Including a Time Delay ($\tau = 1.5$)

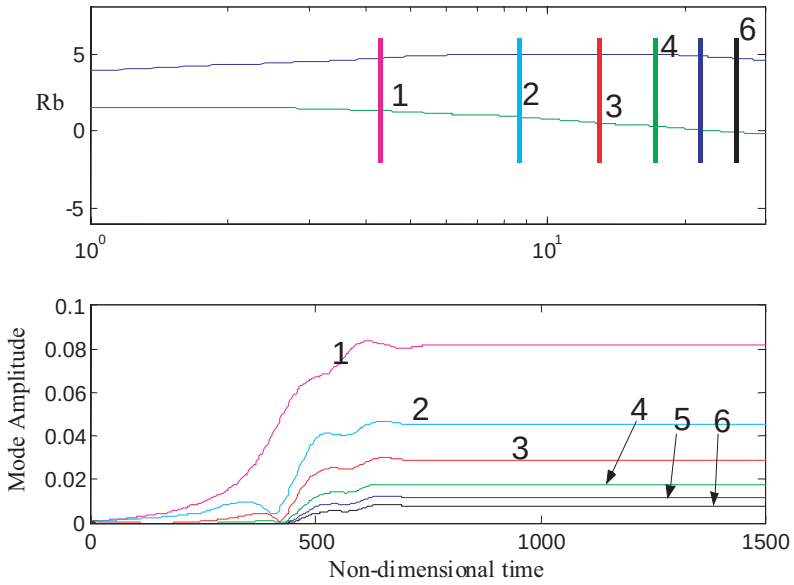

FIGURE 2.19. Results of a Simulation Including Dynamics of a Surface Layer

In general, models based on pressure coupling do not show dramatic sensitivity of the combustor dynamics to small changes of composition. Hence we investigated similar problems with a simple model of the response due to velocity coupling. The idea is based on the model introduced by Levine and Baum (1988).

Some recent work done on the dynamics resulting from functional form of the equations used in the analysis by Ananthkrishnan (2002) (See attachment to these notes.) seems to prove that the absolute value function in itself, as it appears in a simple model of velocity coupling, is sufficient to produce a subcritical bifurcation (pitchfork) followed by a fold (saddle-node bifurcation).

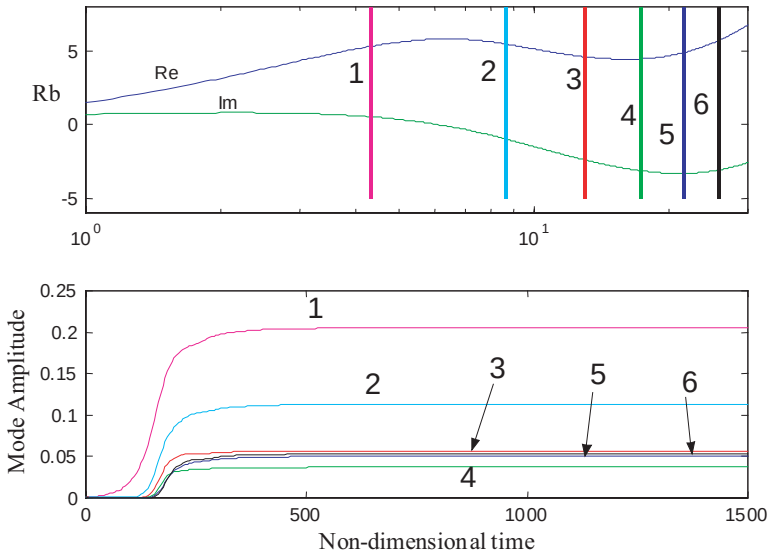

FIGURE 2.20. Results of a Simulation Including Dynamics of a Surface Layer and the Gas Phase

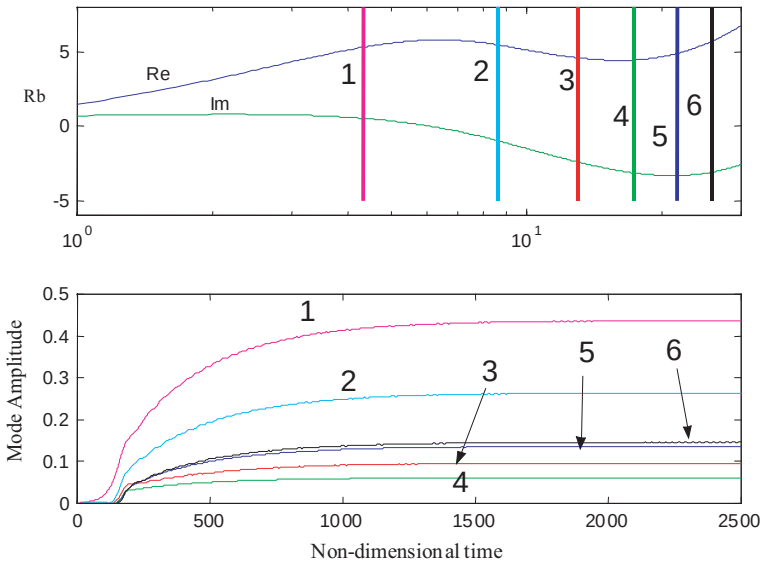

FIGURE 2.21. Simulations with Dynamics of the Surface Layer and Gas Phase Included, but with Reduced Particle Damping (10% Reduction Over the Entire Frequency Range)

In order to analyze the effect of velocity coupling on the overall dynamics, the following two relative sensitivities are defined:

$$S_{\tilde{R}_{vc}}^{A_{LC}} = \frac{1}{A_{LC}} \frac{\partial A_{LC}}{\partial \tilde{R}_{vc}} \tag{2.58}$$

$$S_{\tilde{R}_{vc}}^{\alpha_{BP}} = \frac{1}{\alpha_{BP}} \frac{\partial \alpha_{BP}}{\partial \tilde{R}_{vc}} \tag{2.59}$$

where A_{LC} is the amplitude of the limit cycle (defined at a fixed value of α), and α_{BP} is the value of the growth rate at which the unstable fold turns to a stable fold. Equation (2.58) defines the relative sensitivity of

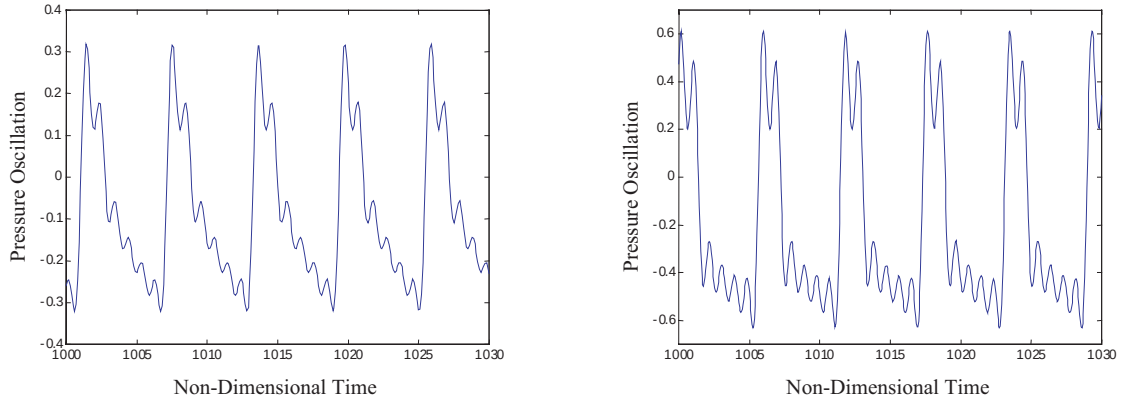

(a) (b)

FIGURE 2.22. Waveforms for the Limit Cycles (a) Figure 2.20; (b) Figure 2.21.

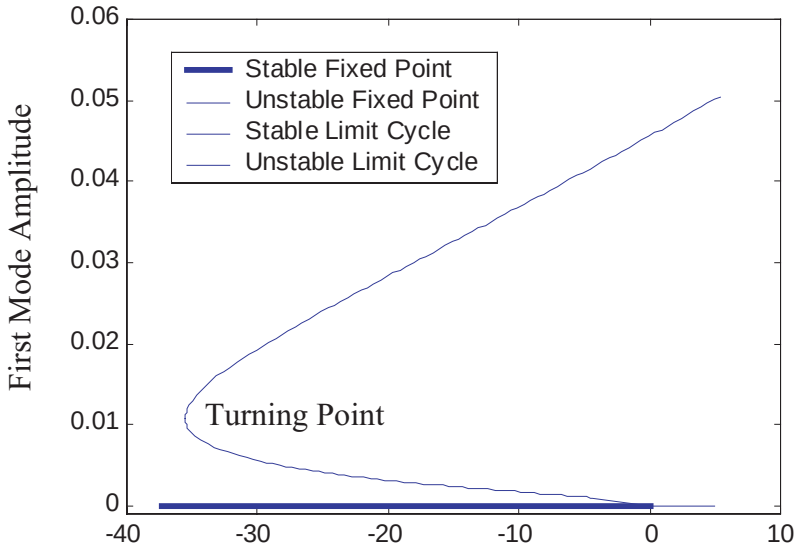

FIGURE 2.23. Bifurcation Diagram

the amplitude of the limit cycle to variations in the velocity coupling coefficient; equation (2.59) refers to the sensitivity of the turning point to the same coefficient.

Figure 2.24 shows a plot of the sensitivities, calculated for the combustion chamber used in the examples of the previous section, and using a six mode approximation of the system. Note that the sensitivity of the turning point is very high, and also the sensitivity of the amplitude of the limit cycle is quite large in the range 0.15 to 0.25 of the coupling coefficient.

We now analyze the same combustor described in Section 2.6 with the introduction of the extra terms due to velocity coupling. For reference, Figure 2.25 presents the results of the simulation for the system with a combustion response based on the quasi-steady theory. The top section presents the combustion response function; the vertical lines mark the non-dimensional frequencies of the acoustic modes of the combustion chamber considered in the simulations. The bottom half shows the time evolution of the amplitude of each mode. The values of the parameters are: A = 6.0, B = 0.55, n = 0.50.

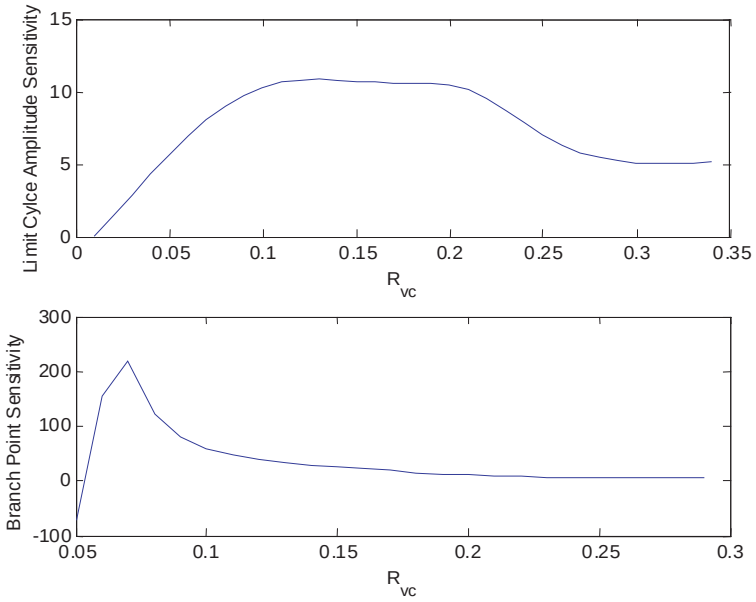

FIGURE 2.24. Sensitivity of Global Dynamics to Variations of the Coupling Coefficient

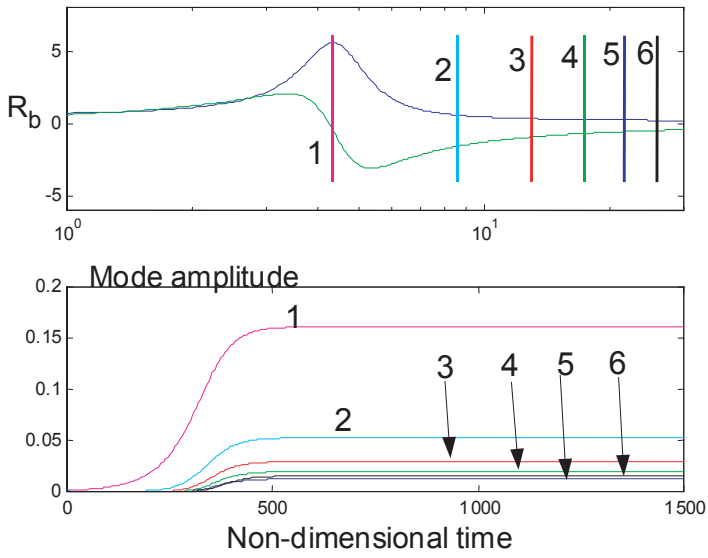

FIGURE 2.25. Simulation Results for QSHOD Combustion Response

The first mode is unstable and rapidly grows to a limit amplitude, while the other modes are all stable, and draw energy from the first mode (allowing the system to enter a limit cycle).

Figure 2.24 shows that there is a region of high sensitivity of the amplitude of the limit cycle for variations in the velocity-coupling coefficient. Figure 2.26 presents the global response for a small variation of the velocity coupling coefficient ($\tilde{R}_{\nu c} = 0.15$ and $\tilde{R}_{\nu c} = 0.165$).

The simulation uses the same coefficients for the pressure coupling as in the results of Figure 2.25, with the addition of the velocity coupling terms. Figure 2.27 and 2.28 show the pressure trace and the harmonic content for the same two cases.

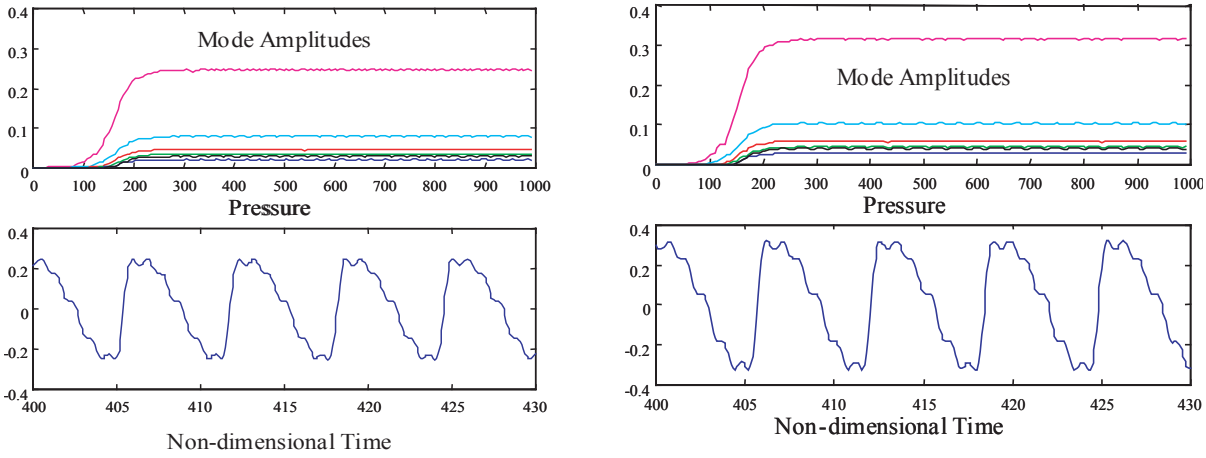

(a) (b)

FIGURE 2.26. Simulations with Velocity Coupling for: (a) $\tilde{R}_{\nu c} = 0.15$, (b) $\tilde{R}_{\nu c} = 0.165$.

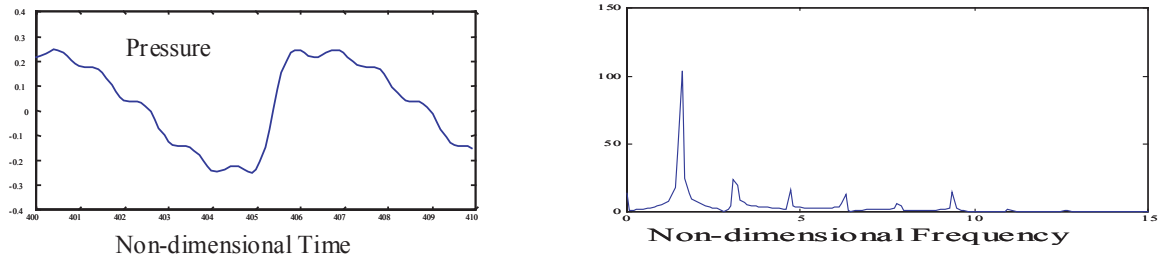

FIGURE 2.27. Pressure Trace and Harmonic Content for the Case $\tilde{R}_{\nu c} = 0.15$

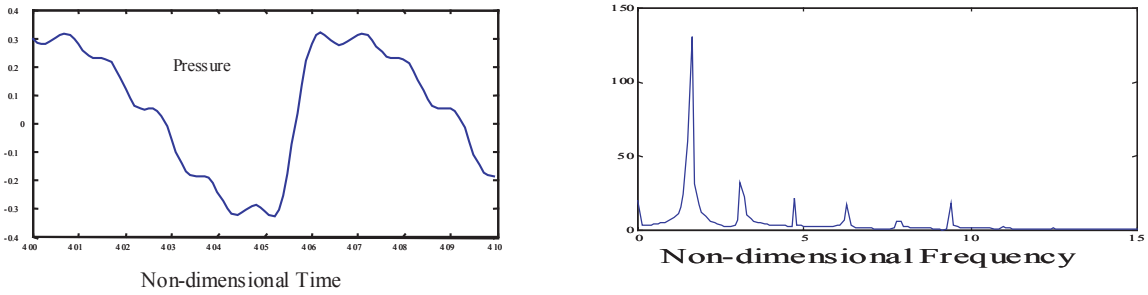

FIGURE 2.28. Pressure Trace and Harmonic Content for the Case $\tilde{R}_{\nu c} = 0.165$

In summary, we have shown with these calculations that the global dynamics of a solid propellant motor seem to be affected more significantly by small changes in the combustion response to velocity coupling then in the combustion response to pressure coupling. We cannot claim at this time that this is a universal result but the possible implications are important. It appears in any case that to determine why small changes of propellant composition seem on a number of occasions to have relatively large effects in the chamber dynamics, one must investigate the phenomenon of velocity coupling. The most serious need is experimental. Attention must be paid to developing a method for measuring the combustion dynamics associated with velocity coupling.

2.8. Generation of Vorticity and Vortex Shedding. There are two principal connections between vorticity and combustion instabilities in solid rockets:

1) generation of unsteady vorticity at burning surfaces; and
2) coupling between acoustical motions and large vortices shed at obstacles or growing out of the region adjacent to the lateral burning surface.

Both of these phenomena have motivated much interesting work—analytical, numerical and experimental. And although both sorts of behavior fundamentally involve production of vorticity, their characters and the positions they occupy in the area of oscillatory behavior are very different.

2.8.1. *Generation of Vorticity.* The generation of vorticity at a burning surface is special to solid rockets. It occurs whenever there is a variation of pressure fluctuation in the direction tangential to a surface from which there is average mass flow normal to surface into the chamber. The vorticity is created because the velocity inward is perpendicular to the surface—the 'no-slip' boundary condition. Imposition of a tangential velocity fluctuation, due to the non-uniform pressure along the surface, on the average inward flow constitutes an inviscid mechanism of vorticity generation. Moreover, conservation of mass in the region close to the surface causes a periodic pumping action normal to the surface. Both the vorticity generation and the pumping exist at the expense of work done by the impressed acoustic field and therefore ultimately appear as losses to the acoustic field in the chamber.

An oversimplified and incomplete interpretation of the phenomenon is that the incoming average flow normal to the surface gains some kinetic energy because it must acquire the oscillatory motion parallel to the surface. Thus there is effectively a "turning" of the flow. The inelastic acceleration of the mass flow causes a loss that is the unsteady counterpart of the loss accompanying mass injection into a duct flow. This "flow-turning loss" was, not surprisingly, discovered in an analysis of unsteady one-dimensional flow with mass injection at the lateral surface (Culick 1970). However, the connection with vorticity generation was not pointed out. It was Flandro (1995) who clarified the phenomenon in terms of the unsteady production of vorticity, emphasizing the central importance of the no-slip boundary condition. Flandro carried out the first rigorous formal analysis of the problem, work that has since prompted a stream of calculations on the basic problem at hand, as well as variations (e.g. Majdalani, 1999; Kassoy, 1999; Majdalani, Flandro and Roh, 2000; and many others).

Generation of vorticity can provide a significant contribution to the loss of acoustic energy and hence to stability. That is why it has become the subject of some controversy in the community of researchers concerned with combustion instabilities. There is not presently uniform agreement on the true effects of vorticity generation on linear stability (unfortunately). The situation in the analyses is more complicated than that described superficially above. Besides the dissipation of vorticity in the chamber—due both to laminar viscous effects and interactions between the vorticity and turbulence, there are one or two effects not mentioned above. Hence depending on interpretation of the basic phenomenon, and also on the particular configuration of motor considered, the next effect of vorticity generation may be stabilizing or de-stabilizing. The matter remains unresolved and deserves resolution, but not in these notes.

We should note that there are also many experimental results related to this problem, some obtained in university laboratories, and some gained in subscale practical configurations (e.g. Dunlap *et al.* 1990).

2.8.2. *Shedding of Large Scale Vortices.* So far as practical consequences are concerned, the production of large vortices in motors has been far more significant than has the generation of vorticity discussed above. The latter is present in all solid rockets, and contributes always to linear stability, although the true quantitative value remains controversial. On the other hand, while the prediction and influences of vortex shedding may contain uncertainties, it is fair to say that the general characteristics are well-known and settled. Moreover, vortex shedding has been identified unambiguously as the mechanism for oscillation observed in several large motors including the Space Shullte SRM, the Titan IV SRMV and the Ariane 5 SRM. Note that the mechanism is apparently active only in large motors.

The main reason for that conclusion seems to be the required special near-coincidence between the frequency of sheding and the frequency of an acoustic mode. Simple laboratory tests demonstrate that basic feature (Magiawala and Culick 1979; Nomoto and Culick 1982; Aaron and Culick 1984): satisfaction of the condition requires suitable combinations of geometry, mean flow speed, thichness of shear layer at the origin of the vortex shedding and acoustic frequency which depends mainly on the speed of sound and length of chamber.

Vortex shedding in large motors has appeared in two forms: shedding from obstacles or sharp edges; and growth out of the region of reletively high shear near the lateral burning surface. Motivated by some experimental results (Price *et al.* 1972) involving vortex shedding, Flandro and Jacobs (1974) first proposed the excitation of acoustic modes in a chamber due to coupling with vortices shed from an obstacle. Within a couple of years that process was discovered[5] as the mechanism for potentially serious pressure oscillations in the Space Shuttle SRM (Mathes 1980).

The appearance of vortex shedding in the Titan motors caused formation of a very useful program of extensive tests of a subscale cold-flow model of the motor (Dunlap and Brown 1981; Brown *et al.* 1981). Those tests produced extensive date for the internal flow fields, eventually including results that formed part of the basis for the theoretical work on unsteady vorticity cited in the preceeding section.

In 1986, Flandro reported his collaboration and extension of the analysis he had carried out with Jacobs twelve years earlier. The work brought together previous ideas of instability of a shear layer as the initiation of a shear wave; growth and roll-up of the wave into a vortex; propagation of the vortex at a speed something less than that of the average flow; and impingement of the vortices on a solid surface, producing a pulse of pressure that can excite and sustain acoustic waves in the chamber. An acoustic pulse will propagate upstream to the region of the shear instability, possibly to initiate another disturbance to be amplified within the layer, later to develop into another vortex... The process will continue, becoming periodic when the frequency of the vortex shedding is nearly equal to the acoustic frequency.

When that behavior occurs in a rocket, toroidal vortices are shed from the inner edge of an annular obstruction, as in the Shuttle and Titan motors, or at the transition from slots to primary cylindrical chamber (Figure 2.29). The acoustic frequency is determined mainly by the length of the chamber, while the vortex shedding frequency

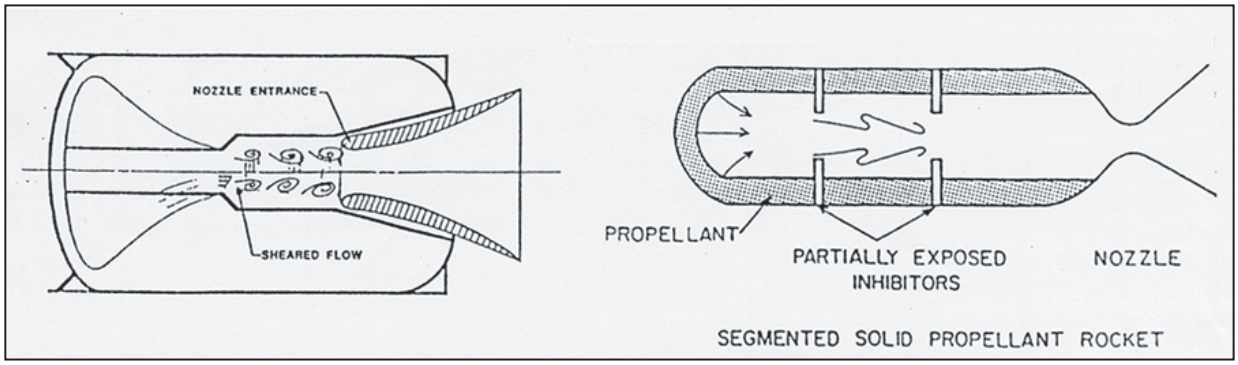

FIGURE 2.29. Vortex Shedding from (a) a transition zone in a rocket chamber; and (b) a residual annulus of inhibitor material (Flandro 1986).

is influenced by the local geometry and average flow. The local geometry determines the growth of the shear layer and in particular its momentum thickness, a fundamental parameter defining the conditions for instability. Flandro's analysis—an adaptation of earlier work by Michalle—and experimental results have confirmed that the vortex shedding is characterized by the value of the Strouhal number S at which the growth rate of an unstable disturbance is maximum. The Strouhal number is defined as the product of shedding frequency f_s times a characteristic length δ divided by a characteristic speed U so the shedding frequency is given by the formula

$$f_s = S\frac{U}{\delta} \tag{2.60}$$

where S has some value roughly constant and set by the geometry. The frequencies of the acoustic modes are only weakly dependent on the mean flow of the Mach number so small but do depend strongly on the geometry. For a chamber having length L and closed at both ends[6], the longitudinal modes have frequencies given by

$$f_a = \ell\pi\frac{a}{L} \tag{2.61}$$

[5]The initial report of those oscillations prompted the laboratory demonstration reported by Culick and Magiawala (1979).

[6]A rocket physically closed at one end and exhausting through a choked nozzle appears to acoustic waves as if it is approximately closed at both ends.

where a is the speed of sound and $\ell = 1, 2, \ldots$ identifies the mode.

Some interesting results reported by Nomoto and Culick (1982) confirm the truth of the preceding ideas for a simple laboratory apparatus consisting of two annuli fitted in a tube, separated by some distance ℓ and having a mean flow in the axial direction. Figure 2.30 shows lines drawn according to (2.60) and (2.61) and data points indicating the occurences of oscillations without regard to amplitude. For the conditions of the experiment, significant oscillations were excited only in regions in which (2.60) and (2.61) are simultaneously satisfied. Note that the separate diagonal lines for shedding frequency given by (2.60) represent cases in which there are $1, 2, 3, \ldots$ vortices existing between the annuli at any given time.

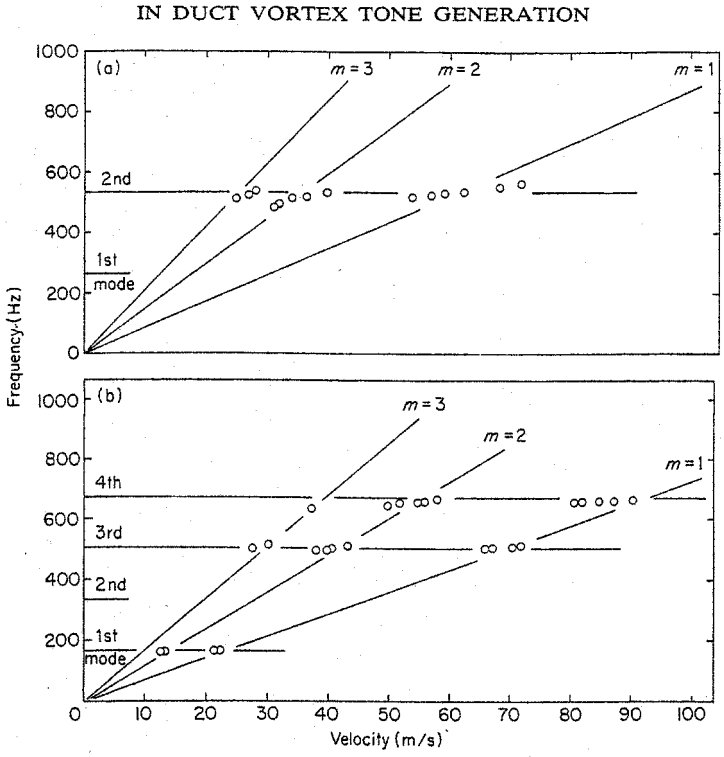

FIGURE 2.30. Experimental Results for the Excitation of Acoustic Modes by Vortex Shedding (Nomoto and Culick 1982).

An important implication of Figure 2.30 is that the dependence of the observed frequency of oscillation may not have a simple—or obvious—dependence on the length and mean flow speed during the firing of a solid rocket. In fact, as several researchers have noted (see, e.g., Vuillot 1995) the shift of frequency with time is a good basis for distinguishing vortex shedding as the mechanism for oscillations.

Instabilities sustained by feedback involving combustion dynamics almost always show dependence on geometry closely given vy the formulas of classical acoustics: $f_a \sim 1/L$. Thus, if there is little or no propellant cast at the head end, the longitudinal frequency is nearly constant in time. Or, if, as usually is the case for large motors, there are slots and fins at the head end, the effective length of the chamber tends to increase during a firing and hence the frequency of oscillation decreases.

However, according to the results given in Figure 2.30, because the mean velocity may increase during a burn as more propellant is exposed, the frequency may increase. It is possible (and has been observed) that the frequency suffers discrete changes, corresponding to transition between groups of data points shown in Figure **??**, that is the state of the oscillating system shifts because the number of shed vortices present between the shedding and impingement points changes.

An important and very interesting second cause of vortex shedding was discovered several years ago by Vuillot and his colleagues at ONERA while investigating the mechanism for unstable oscillations observed in teh Ariane

5 solid rocket boosters. Subscale firings of motors showed that large vortices were initiated, grew, and were shed from the region near the burning surface. (Vuillot *et al.* 1993; Traineau *et al.* 1997). Hence the phenomenon was called "parietal vortex shedding" by Lupuglazoff and Vuillot (1996).

In an exemplary systematic research program, the group at ONERA have established most of the characteristics of parietal vortex shedding relevant to practical applications. Some issues of scale apparently remain, but very good agreement has been found between subscale hot firings; subscale tests with flow visualization (Avalon *et al.* 2000); and numerical analyses of stability and vortex shedding. LeBreton *et al.* (1999) have given a good review of the subject, including some results for the effects of resudual combustion.

Possibly the most important aspect of this subject is weak understanding of nonlinear behavior. No simple explanation exists for the amplitudes of oscillations that can be generated by coupling with the shedding of large vortices. According to LeBreton *et al.* (1999) parietal vortex shedding produces, in their examples, larger amplitudes of oscillation than shedding from an annulus (inhibitor ring in a segmented rocket). It would clearly be a significant aid to design and development if a rule of thumb could be constructed to place an upper limit to the amplitudes of oscillation caused by vortex shedding. Because the mechanism involves conversion of mechanical energy of the near flow to acoustic energy, it is likely that the maximum possible amplitudes must be much smaller than those that can be generated by coupling between acoustics and combustion dynamics.

2.9. Distributed Combustion. Combustion of the major components of a solid propellant—the primary oxidizer and the binder in the case of composite solids—normally takes place to completion near the burning surface. Thus the term 'distributed combustion' refers to combustion of particles as they are carried into the volume of the chamber. Almost all attention has been directed to residual combustion of aluminum for which there is much photographic evidence. Steady combustion of aluminum particles has long been and continues to be a subject of research owing to its vital importance to the efficiency and performance of motors, and in the formation of slag.

Relatively little notice has been taken of the possible influences of residual combustion on the stability of motors. Probably the main reason for this lack of interest is the general view that generally the existence of combustion instabilities in motors can be satisfactorily explained by other mechanisms, notably the dynamics of surface combustion and vortex shedding. It appears that the dynamics of aluminum combustion within the volume of the chamber must provide at most a small contribution to stability. There are at least two reasons for this conclusion: the available data contain uncertainties too large to allow identification of the influences of unsteady aluminum combustion; and any destabilizing tendencies of the particles are roughly compensated by the attenuation of unsteady motions due to the presence of particles. The second is known to be significant if the particles are inert and have suitable sizes for the frequencies of the instability in question.

Several works (Marble and Wooten (1970); Dupays and Vuillot 1998) have treated the effects of condensation and vaporization of non-burning particles, on attenuation of acoustic waves. Whether the attenuation is increased or decreased depends on many factors, including the sizes of particles and the rates at which the particles gain or lose mass. When, for example, a particle is vaporizing, it seems that in the presence of an acoustic wave, the phenomenon of 'flow turning' discussed in the preceding section should cause increased attenuation for a given particle size and frequency. However, while the analysis by Wooten (1966) supports that conclusion, recent work by Dupays (1999) suggests that the result is not always true. Moreover, suggestions have been made by investigators of combustion instabilities in ramjets (Sirignano) and in liquid rockets (Merkl) that the process of vaporization of liquid drops is destabilizing. Those conclusions may be misleading because due to implied direct connections between the vaporization and burning rates. It may in fact be the case that the destabilization found is due to combustion rather than vaporization *per se.*

Owing to the necessary connection between vaporization and combustion of particles, the problem of residual combustion presents certain difficulties of distinguishing what process is really responsible for attenuation or driving of waves. The most extensive work is the problem has been done by Beckstead and his students (Brooks and Beckstead, 1995; Raun and Beckstead, 1993; Beckstead, Richards and Brewster, 1984). Probably the most compelling reason for investigating the manner was the discover of anomalous (and still not completely understood) results obtained with a device called the 'velocity-coupled T-burner'. In this configuration, large areas of propellant

are mounted in the lateral boundary to emphasize the interactions between surface combustion and velocity fluctuations parallel to the surface.

For reasons not discussed here, Beckstead concluded that residual combustion was possibly a reason that unusually large values of the response function were found. The idea was based partly on the suspicion that the tangential velocity disturbances can strip incompletely burned aluminum from the surface. Subsequently, with both calculations and further experiments (Raun and Beckstead, 1993). Beckstead has strengthened his case that the effects of unsteady residual combustion should not be dismissed out-of-hand. However, there is presently no analysis accommodating the process in computations of combustion instabilities in solid rockets. It is worth noting the conclusion by Brooks and Beckstead (1995) that the greatest effect of residual combustion (of aluminum) on stability was indirect, due to its effect on the mean temperature profile.

3. EQUATIONS FOR UNSTEADY MOTIONS IN COMBUSTION CHAMBERS

The examples described in Section 1, and many others, establish a firm basis for interpreting unsteady motions in a combustor in terms of acoustic modes of the chamber. That view has been formalized during the past fifty years and has led to the most widely used methods for analyzing combustor dynamics. In this section, we present the foundations of a particularly successful version of methods based on expansion in normal modes and spatial averaging. We assume familiarity with most of the required background in classical fluid dynamics and acoustics. Section 5 covers the principles and chief results of classical acoustics required as part of the foundation for understanding combustion instabilities. The discussions in this and the following sections are quite formal, intended to serve as the basis for a general framework within which unsteady motions, especially combustion instabilities, in all types of combustors may be treated. Analyses using *ad hoc* models will be covered when particular systems are considered, as in Section 2.

3.1. Modes of Wave Motion in a Compressible Medium. In this section, the term 'modes' refers not to natural motions or resonances of a chamber but rather to a *type* or class of motions in compressible flows generally. The brief discussion here is intended to address the question: how is it possible that apparently coherent nearly-classic acoustic waves exist in chambers containing highly turbulent non-uniform flow? It's a fundamentally important observation that such is the case. The explanation has been most thoroughly clarified by Chu and Kovasznay (1957), who elaborated and combined some results known for nearly a century. Their conclusions most significant for present purposes may be summarized as follows:

(1) Any small amplitude (linear) disturbance may be synthesized of three modes of propagation: *entropy waves* or 'spots', small regions having temperatures slightly different from the ambient temperature of the flow; *vortical* or *shear waves* characterized by nonuniform vorticity; and *acoustic waves.*

(2) In the linear approximation, *if the flow is uniform,* the three types of waves propagate independently, but may be coupled at boundaries (e.g. nozzles) or in combustion zones.

Entropy and vortical waves propagate with the mean flow speed ('convected') but acoustic waves propagate with their own speeds of sound. Moreover, in this linear limit, only acoustic waves carry disturbances of pressure. All three types of waves are accompanied by velocity fluctuations. If the flow is non-uniform or at finite amplitudes, the three modes become coupled. As a result, each of the waves then carries pressure, temperature and velocity fluctuations. Extension of the fundamental theory has not been accomplished completely (see Chu and Kovasznay). Some of the consequences of these types of modal coupling arise in the theory developed here, but much remains to be investigated. In particular, interactions between turbulence and an acoustic field is an important process represented by coupling of the basic linear modes of propagation.

3.2. Equations of Motion for a Reacting Flow. Combustion systems commonly contain condensed phases: liquid fuel or oxidizer, and combustion products including soot and condensed metal oxides. Hence the equations of motion must be written for two phases consisting of at least one species each. For investigating the dynamics of combustors, it is entirely adequate to represent each phase as its mass average over all member species. For a medium consisting of a multicomponent mixture of reacting gases and, for simplicity, a single liquid phase, it is a straightforward matter to construct a system of equations representing a single fluid. The procedure is summarized in Appendix A. As a result we can treat combustor dynamics under broad conditions as unsteady motions of a fluid having the mass-averaged properties of the actual medium.[7] The dimensional governing equations are (A.9)–(A.14)

[7]We now use $C_v, \gamma, R, \cdots$ to stand for the mass-averaged properties represented by bold-face symbols in Appendix A.

Conservation of Mass

$$\frac{\partial \rho}{\partial t} + \mathbf{u} \cdot \nabla \rho = -\rho \nabla \cdot \mathbf{u} + \mathcal{W} \tag{3.1}$$

Conservation of Momentum

$$\rho \left[\frac{\partial \mathbf{u}}{\partial t} + \mathbf{u} \cdot \nabla \mathbf{u} \right] = -\nabla p + \boldsymbol{\mathcal{F}} \tag{3.2}$$

Conservation of Energy

$$\rho C_v \left[\frac{\partial \mathbf{T}}{\partial t} + \mathbf{u} \cdot \nabla T \right] = -p \nabla \cdot \mathbf{u} + \mathcal{Q} \tag{3.3}$$

Equation for the Pressure

$$\frac{\partial p}{\partial t} + \mathbf{u} \cdot \nabla p = -\gamma p \nabla \cdot \mathbf{u} + \mathcal{P} \tag{3.4}$$

Equation for the Entropy

$$\rho \left[\frac{\partial s}{\partial t} + u \cdot \nabla s \right] = \frac{1}{T} \mathcal{S} \tag{3.5}$$

Equation of State

$$p = R \rho T \tag{3.6}$$

All definitions are given in Appendix A.

It is particularly important to realize that the source functions $\mathcal{W}$, $\boldsymbol{\mathcal{F}}$, $\mathcal{Q}$ and $\mathcal{P}$ contain all relevant processes in the systems to be analyzed here. They include, for example, the modeling and representations of the actions of actuation mechanisms used for active control. Eventually, the most difficult problems arising in this field are associated with modeling the physical processes dominant in the problems addressed.

Both for theoretical and computational purposes it is best to express the equations in dimensionless variables using the reference values:

L : reference length

ρ_r, p_r, T_r, a_r : reference density, pressure, temperature and speed of sound

C_{vr}, C_{pr}, R_r : reference values of C_v, C_p, R

Then define the dimensionless variables represented by $\mathbf{M}$ and the same symbols used for dimensional variables:

$$\mathbf{M} = \frac{\mathbf{u}}{a_r}; \quad \frac{\rho}{\rho_r} \to \rho; \quad \frac{p}{\rho_r a_r^2} \to p; \quad \frac{T}{T_r} \to T; \quad \frac{C_v}{C_{vr}} \to C_v, \text{ etc.}; \quad \frac{s}{C_{vr}} \to s$$

The dimensionless source functions are

$$\frac{L}{\rho_r a_r} \mathcal{W} \to \mathcal{W}; \quad \frac{L}{\rho_r a_r^2} \boldsymbol{\mathcal{F}} \to \boldsymbol{\mathcal{F}}; \quad \frac{L}{\rho_r a_r^3} \mathcal{Q} \to \mathcal{Q}; \quad \frac{L}{\rho_r a_r} \mathcal{P} \to \mathcal{P}; \quad \frac{\mathcal{S}}{\rho_r a_r C_{vr}} \to \mathcal{S}$$

Substitution of these definitions in equations (3.1)–(3.6) leads to the set of dimensionless equations for the single fluid model:

$$Mass: \quad \frac{D\rho}{Dt} = -\rho\nabla\cdot\mathbf{M} + \mathcal{W} \tag{3.7}$$

$$Momentum: \quad \rho\frac{D\mathbf{M}}{Dt} = -\nabla p + \boldsymbol{\mathcal{F}} \tag{3.8}$$

$$Energy: \quad \rho C_v\frac{DT}{Dt} = -p\nabla\cdot\mathbf{M} + \mathcal{Q} \tag{3.9}$$

$$Pressure: \quad \frac{Dp}{Dt} = -\gamma p\nabla\cdot\mathbf{M} + \mathcal{P} \tag{3.10}$$

$$Entropy: \quad \rho\frac{Ds}{Dt} = \frac{1}{T}\mathcal{S} \tag{3.11}$$

$$State: \quad p = \rho RT \tag{3.12}$$

and

$$\frac{D}{Dt} = \frac{\partial}{\partial t} + \mathbf{M}\cdot\nabla \tag{3.13}$$

We emphasize again that the source terms accommodate all relevant physical processes and can be interpreted to include the influences of actuation used in active control.

3.3. Two-Parameter Expansion of the Equations of Motion. The general equations (3.7)–(3.13) are written in the form suggestive of problems that are dominated by fluid mechanical processes, a tactic dictated by the observations described earlier. This point of view is the basis for the approach taken here to construct a general framework within which both practical and theoretical results can be obtained by following systematic procedures.

We are not concerned at this point with simulations or other methods relying essentially on some sort of numerical anaylsis and large scale computations. The nature of the problems we face suggests perturbation methods. If the source terms $\mathcal{W}$, ... were absent from (3.7)–(3.11), the homogeneous equations then represent nonlinear inviscid motions in a compressible fluid: Nonlinear acoustics in a medium without losses. One useful method for investigating such problems is based on expansion of the equations in a small parameter, ε, measuring the amplitude of the motion. Specifically, ε can be taken equal to M_r', a Mach number characteristic of the fluctuating flow, $\varepsilon := M_r'$.

The problems we are concerned with here are defined essentially by the non-zero functions $\mathcal{W}$, ... Because observed behavior seems to be dominated by features recognizable as 'acoustical', those sources which excite and sustain the actual motions must in some sense be small. They should therefore be characterized by at least one additional small parameter. It has become customary to select only one such parameter, $\mu := \bar{M}_r$, a Mach number $\bar{M}_r$ characterizing the mean flow, for the following reasons.[8]

Any operating combustion chamber contains an average steady flow produced by combustion of the fuel and oxidizer to generate products. The intensity of the flow, partly measurable by the Mach number, is therefore related to the intensity of combustion and both processes can in some sense be characterized by the same quantity, namely the Mach number of the average flow. Thus many of the processes represented in the source functions may be characterized by μ, in the sense that their influences become vanishingly small as $\mu \to 0$ and are absent when $\mu = 0$.

[8]We use the symbols ε and μ rather than M_r' and $\bar{M}_r$ to simplify writing.

It is important to understand that the two small parameters ε and μ have different physical origins. Consequently, they also participate differently in the formal perturbation procedures. Familiar nonlinear gas dynamical behavior is, in the present context, governed by the parameter ε; steepening of compressive waves is a notable example. In the expansion procedure worked out here, the term 'nonlinear behavior' refers to the consequences of terms higher order in ε.

On the other hand, the parameter μ characterizes perturbations of the gasdynamics due in the first instance to combustion processes and the mean flow. Terms of higher order in μ, but linear in ε, represent linear processes in this scheme. Failure to recognize this basic distinction between ε and μ can lead to incorrect applications of formal procedures such as the method of time-averaging. Instances of this point will arise as the analysis is developed.

3.3.1. *Expansion in Mean and Fluctuating Values.* There is no unique procedure for carrying out a two-parameter expansion. We begin here by writing all dependent variables as sums of mean $\bar{(\ )}$ and fluctuating $(\ )'$ parts without regard to ordering

$$p = \bar{p} + p', \quad \mathbf{M} = \bar{\mathbf{M}} + \mathbf{M}', \ldots, \quad \mathcal{W} = \bar{\mathcal{W}} = \mathcal{W}', \quad \boldsymbol{\mathcal{F}} = \bar{\boldsymbol{\mathcal{F}}} + \boldsymbol{\mathcal{F}}', \ldots \tag{3.14}$$

We take the fluctuations of the primary flow variables (p', $\mathbf{M}'$, ρ', T', s') to be all of the same order in the amplitude ε of the unsteady motion. Generally, the source terms are complicated functions of the flow variables and therefore their fluctuations will contain terms of many orders in ε. For example, suppose $\mathcal{W} = kp^3$. Then setting $p = \bar{p} + p'$ and expanding, we have

$$\mathcal{W} = k(\bar{p} + p')^3 = k\left[\bar{p}^3 + 3\bar{p}^2 p' + 3\bar{p}p'^2 + p'^3\right]$$

Hence we define orders of the fluctuations of the source $\mathcal{W}$ and write

$$\mathcal{W} = \bar{\mathcal{W}} + \mathcal{W}'_1 + \mathcal{W}'_2 + \mathcal{W}'_3 + \mathcal{W}'_4 + \ldots$$

where the subscript denotes the order with respect to the amplitude: Here, for the example $\mathcal{W} = kp^3$, $\mathcal{W}'_2 = (2k\bar{p})p'^2$. All source functions are written symbolically in the general form shown for ω, but modeling is required to give explicit formulas.

Most combustors contain flows of relatively low Mach number, say $\bar{\mathbf{M}} \lesssim 0.3$ or so. Thus we can assume that for a broad range of circumstances, processes depending on the square of $\bar{\mathbf{M}}$, i.e. of order μ^2, probably have small influences on the unsteady motions. We therefore neglect all terms of order μ^2 and higher in the equations. As a practical matter, the equations are greatly simplified with this assumption.

After substituting all variables split into sums of mean and fluctuating values, and collection of terms by orders, we can rewrite (3.7)–(3.13) as[9]

$$\left[\frac{D\bar{\rho}}{Dt} + \bar{\rho}\nabla\cdot\bar{\mathbf{M}} - \bar{\mathcal{W}}\right] + \left[\frac{\partial\rho'}{\partial t} + \bar{\rho}\nabla\cdot\mathbf{M}'\right] + \left[\bar{\mathbf{M}}\cdot\nabla\rho' + \rho'\nabla\cdot\bar{\mathbf{M}} + \mathbf{M}'\cdot\nabla\bar{\rho} + \nabla\cdot(\rho'\mathbf{M}')\right] - \mathcal{W}' = 0 \tag{3.15}$$

$$\begin{aligned}\left[\bar{\rho}\frac{D\bar{\mathbf{M}}}{Dt} + \nabla\bar{p} - \bar{\boldsymbol{\mathcal{F}}}\right] + \left[\bar{\rho}\frac{\partial\bar{\mathbf{M}}}{\partial t} + \nabla p'\right] + \left[\bar{\rho}\left(\bar{\mathbf{M}}\cdot\nabla\mathbf{M}' + \mathbf{M}'\cdot\nabla\bar{\mathbf{M}}\right) + \bar{\rho}\frac{\bar{D}\bar{\mathbf{M}}}{Dt}\right] \\ + \left[\rho'\frac{\partial\mathbf{M}'}{\partial t} + \bar{\rho}\mathbf{M}'\cdot\nabla\mathbf{M}' + \rho'\left(\bar{\mathbf{M}}\cdot\nabla\mathbf{M}' + \mathbf{M}'\cdot\nabla\bar{\mathbf{M}}\right)\right] + \left[\rho'\mathbf{M}'\cdot\nabla\mathbf{M}'\right] - \boldsymbol{\mathcal{F}}' = 0\end{aligned} \tag{3.16}$$

[9]We do not include here terms $O(\bar{M}_r M'^2_r)$, i.e. first order in the mean flow and second order in fluctuations.

$$\left[\bar{\rho}C_v\frac{D\bar{T}}{Dt}+\bar{p}\nabla\cdot\bar{\mathbf{M}}-\bar{\mathcal{Q}}\right]+C_v\left[\bar{\rho}\frac{\partial T'}{\partial t}+\bar{p}\nabla\cdot\mathbf{M}'\right]+\left[\bar{\rho}C_v\left(\bar{\mathbf{M}}\cdot\nabla T'+\mathbf{M}'\cdot\nabla\bar{T}\right)+C_v\rho'\frac{\bar{D}\bar{T}}{Dt}+p'\nabla\cdot\bar{\mathbf{M}}\right]$$
$$+\left[C_v\bar{\rho}\frac{\partial T'}{\partial t}+C_v\rho'\left(\bar{\mathbf{M}}\cdot\nabla T'+\mathbf{M}'\cdot\nabla\bar{T}\right)+C_v\rho'\mathbf{M}'\cdot\nabla T'+p'\nabla\cdot\mathbf{M}'\right]+\left[C_v\bar{\rho}\mathbf{M}'\cdot\nabla T'\right]-\mathcal{Q}'=0 \tag{3.17}$$

$$\left[\frac{\partial\bar{p}}{\partial t}+\bar{\mathbf{M}}\cdot\nabla\bar{p}+\gamma\bar{p}\nabla\cdot\bar{\mathbf{M}}-\bar{\mathcal{P}}\right]+\left[\frac{\partial p'}{\partial t}+\gamma\bar{p}\nabla\cdot\mathbf{M}'\right]+\left[\bar{\mathbf{M}}\cdot\nabla p'+\mathbf{M}'\cdot\nabla\bar{p}+\gamma p'\nabla\cdot\bar{M}\right]$$
$$+\left[\mathbf{M}'\cdot\nabla p'+\gamma p'\nabla\cdot\mathbf{M}'\right]-\mathcal{P}'=0 \tag{3.18}$$

$$\left[\bar{\rho}\bar{T}\frac{\bar{D}\bar{s}}{Dt}-\bar{\mathcal{S}}\right]+\left[\bar{\rho}\bar{T}\frac{\partial s'}{\partial t}\right]+\left[\bar{\rho}\bar{\mathbf{M}}\cdot\nabla s'+\rho'\bar{T}\frac{\bar{D}\bar{s}}{Dt}+\bar{\rho}\bar{T}\mathbf{M}'\cdot\nabla\bar{s}+\bar{\rho}T'\bar{\mathbf{M}}\cdot\nabla\bar{s}\right]$$
$$+\left[\rho'\bar{T}\frac{\bar{D}s'}{Dt}+\rho'T'\frac{\bar{D}\bar{s}}{Dt}+\rho'\bar{T}\mathbf{M}'\cdot\nabla\bar{s}+\bar{\rho}T'\mathbf{M}'\cdot\nabla\bar{s}+\bar{\rho}T'\frac{\partial s'}{\partial t}\right] \tag{3.19}$$
$$+\left[\left(\bar{\rho}T'+\rho'\bar{T}\right)\mathbf{M}'\cdot\nabla s'+\rho'T'\left(\mathbf{M}'\cdot\nabla\bar{s}+\bar{\mathbf{M}}\cdot\nabla s'\right)\right]$$
$$+\left[\rho'T'\mathbf{M}'\cdot\nabla s'\right]-\mathcal{S}'=0$$

$$\left[\bar{p}-R\bar{\rho}\bar{T}\right]+\left[p'-R\left(\bar{\rho}T'+\rho'\bar{T}\right)\right]+\left[-R\rho'T'\right]=0 \tag{3.20}$$

where the convective derivative following the mean flow is

$$\frac{\bar{D}}{Dt}=\frac{\partial}{\partial t}+\bar{\mathbf{M}}\cdot\nabla \tag{3.21}$$

As a convenience in writing, it is useful to introduce some symbols defining groups of ordered terms. The set of equations (3.15)–(3.21) then become:

$$\left[\frac{\bar{D}\bar{\rho}}{Dt}+\bar{\rho}\nabla\cdot\bar{\mathbf{M}}-\bar{\mathcal{W}}\right]+\left(\frac{\partial\rho'}{\partial t}+\bar{\rho}\nabla\cdot M'\right)+\{[\rho]\}_1+\{\rho\}_2-\mathcal{W}'=0 \tag{3.22}$$

$$\left[\bar{\rho}\frac{\bar{D}\bar{\mathbf{M}}}{Dt}+\nabla\bar{p}-\bar{\boldsymbol{\mathcal{F}}}\right]+\left(\bar{\rho}\frac{\partial\mathbf{M}'}{\partial t}+\nabla p'\right)+\{[\mathbf{M}]\}_1+\{\mathbf{M}\}_2+\{\mathbf{M}\}_3-\boldsymbol{\mathcal{F}}'=0 \tag{3.23}$$

$$\left[\bar{\rho}C_v\frac{\bar{D}\bar{T}}{Dt}+\bar{p}\nabla\cdot\bar{\mathbf{M}}-\bar{\mathcal{Q}}\right]+\left(\bar{\rho}C_v\frac{\partial T'}{\partial t}+\bar{p}\nabla\cdot M'\right)+\{[T]\}_1+\{T\}_2+\{T\}_3-\mathcal{Q}'=0 \tag{3.24}$$

$$\left[\frac{\bar{D}\bar{p}}{Dt}+\gamma\bar{p}\nabla\cdot\bar{\mathbf{M}}-\bar{\mathcal{P}}\right]+\left(\bar{\rho}C_v\frac{\partial P'}{\partial t}+\bar{p}\nabla\cdot M'\right)+\{[p]\}_1+\{p\}_2-\mathcal{P}'=0 \tag{3.25}$$

$$\left[\bar{\rho}\frac{\bar{D}\bar{s}}{Dt}-\bar{\mathcal{S}}\right]+\left(\bar{\rho}\bar{T}\frac{\partial s'}{\partial t}\right)+\{[s]\}_1+\{s\}_2+\{s\}_3+\{s\}_4=0 \tag{3.26}$$

$$\left[\bar{p}-R\bar{\rho}\bar{T}\right]+\{p-R\rho T\}_1+\{R\rho'T\}_2=0 \tag{3.27}$$

The definitions of the bracketted terms $\{\rho\}_1$, $\cdots$ etc. are given in Appendix A, Section A.2; the subscript $\{\quad\}_n$ on the brackets identifies the orders of terms with respect to the fluctuations of flow variables, and the square brackets $[\quad]$ indicate that the terms are first order in the average Mach number. We have shown here

in each equation terms of the highest order fluctuations generated by the purely fluid mechanical contributions plus sources that must be expanded to orders appropriate to particular applications. Only the entropy equation produces terms of fourth order.

Time derivatives of quantities identified with the mean flow are retained to accommodate variations on a time scale long relative to the scale of the fluctuations. This generality is not normally required for treating combustion instabilities and unless otherwise stated, we will assume that all averaged quantities are independent of time.

3.3.2. *Equations for the Mean Flow.* At this point we have two choices. Commonly the assumption is made that the equations for the mean flow 'satisfy their own equations'. That implies that the square brackets [ ] in (3.22)–(3.27) vanish identically. With the time derivatives absent, the equations for the mean flow are:

$$\bar{\mathbf{M}} \cdot \nabla \bar{\rho} + \bar{\rho} \nabla \cdot \bar{\mathbf{M}} = \bar{\mathcal{W}} \tag{3.28}$$

$$\bar{\rho} \bar{\mathbf{M}} \cdot \nabla \bar{\mathbf{M}} + \nabla \bar{p} = \bar{\boldsymbol{\mathcal{F}}} \tag{3.29}$$

$$\bar{\rho} C_v \bar{\mathbf{M}} \cdot \nabla \bar{T} + \bar{p} \nabla \cdot \bar{\mathbf{M}} = \bar{\mathcal{Q}} \tag{3.30}$$

$$\bar{\mathbf{M}} \cdot \nabla \bar{p} + \gamma \bar{p} \nabla \cdot \bar{\mathbf{M}} = \bar{\mathcal{P}} \tag{3.31}$$

$$\bar{\rho} \bar{T} \bar{\mathbf{M}} \cdot \nabla \bar{s} = \bar{\mathcal{S}} \tag{3.32}$$

$$\bar{p} = R \bar{\rho} \bar{T} \tag{3.33}$$

This set of equations certainly applies when the average flow is strictly independent of time and there are no fluctuations. The time derivatives cannot be ignored when the flow variables change so slowly that the motion may be considered as 'quasi-steady' and fluctuations are still ignorable.

It is possible that when fluctuations are present, interactions among the flow variables cause transfer of mass, momentum and energy between the fluctuating and mean flows, generating time variations of the averaged variables. Then the appropriate equations are obtained by time-averaging (3.22)–(3.27) to give[10]

$$\frac{\bar{D}\bar{\rho}}{Dt} + \bar{\rho} \nabla \cdot \bar{\mathbf{M}} = \bar{\mathcal{W}} - \overline{\{[\rho]\}_1} - \overline{\{\rho\}_2} + \overline{\mathcal{W}'} \tag{3.34}$$

$$\bar{\rho} \frac{\bar{D}\bar{\mathbf{M}}}{Dt} + \nabla \bar{p} = \bar{\boldsymbol{\mathcal{F}}} - \overline{\{[\mathbf{M}]\}_1} - \overline{\{\mathbf{M}\}_2} - \overline{\{\mathbf{M}\}_3} + \overline{\boldsymbol{\mathcal{F}}'} \tag{3.35}$$

$$\bar{\rho} C_v \frac{\bar{D}\bar{T}}{Dt} + \bar{p} \nabla \cdot \bar{\mathbf{M}} = \bar{\mathcal{Q}} - \overline{\{[T]\}_1} - \overline{\{T\}_2} - \overline{\{T\}_3} + \bar{\mathcal{Q}}' \tag{3.36}$$

$$\frac{\bar{D}\bar{p}}{Dt} + \gamma \bar{p} \nabla \cdot \bar{\mathbf{M}} = \bar{\mathcal{P}} - \overline{\{p\}_1} - \overline{\{p\}_2} + \overline{\{p\}_3} \tag{3.37}$$

$$\bar{\rho} \bar{T} \frac{\bar{D}\bar{s}}{Dt} = \bar{\mathcal{S}} - \overline{\{s\}_1} - \overline{\{s\}_2} - \overline{\{s\}_3} - \overline{\{s\}_4} \tag{3.38}$$

$$\bar{p} = \mathbf{R} \bar{\rho} \bar{T} - \overline{\{\rho T\}_1} - \overline{\{\rho T\}_2} \tag{3.39}$$

[10] Note that the fluctuations of the source terms, $\mathcal{W}' \cdots$ etc., actually contain squares and higher order products of the dependent variables; hence their time averages will generally be non-zero.

If the mean flow is strictly independent of time, then time averages of all first-order brackets, $\overline{\{\quad\}}_1$, must vanish. For generality we allow them to be nonzero. There seem to be no analyses in which their variations have been taken into account.

The two sets of equations governing the mean flow in the presence of unsteady motion define two distinct formulations of the general problem. In the first, equations (3.28)–(3.33), computation of the mean flow is uncoupled from that of the unsteady flow. Hence formally we are concerned with the stability and time evolution of disturbances superposed on a given, presumed known, mean flow unaffected by the unsteady motions. That is the setting for all investigations of combustion instabilities founded on the splitting of small flow variables into sums of mean and fluctuating values. This approach excludes, for example, possible influences of oscillations on the mean pressure in the chamber (often called 'DC shift'), not an unusual occurrence in solid propellant rockets. When they occur, DC shifts of this sort are almost always unacceptable in operational motors; they may or may not be significantly and directly affected by the fluctuations.

In contrast, the set (3.34)–(3.39) is strongly coupled to the fluctuating field. The situation is formally that producing the problem of 'closure' in the theory of turbulent flows (see, for example, Tennekes and Lumley, 1972). We will not explore the matter here, but we note only that the process of time averaging terms on the right-hand sides of the equations introduces functions of the fluctuations that are additional unknowns. Formal analysis then requires that those functions be modeled; perhaps the most familiar example in the theory of turbulence is the introduction of a 'mixing length' as part of the representation of stresses associated with turbulent motions.

Numerical simulations of combustion instabilities do not exhibit the problem of closure if the complete equations are used, avoiding the consequences of the assumption (3.14). Thus, for example, the results obtained by Baum and Levine (1982, 1988) do show time-dependence of the average pressure in examples of instabilities in solid rockets. Another possible cause of that behavior, probably more important in many cases, is nonlinear dependence of the burning rate on the pressure or velocity near the surface of a solid propellant rocket. Within the structure given here, that behavior may arise from time-averaged functions of p', $\mathbf{M}'$, ... contained in the boundary conditions, or from some nonlinear dependence such as $|\mathbf{M}'|$.

We use in these lectures the formulation assuming complete knowledge of the mean flow, given either by suitable modeling or by solution to the governing equations (3.28)–(3.33) or (3.34)–(3.39).

3.3.3. *Systems of Equations for the Fluctuations.* The general equations of motion (3.22)–(3.27) and those for the mean flow written in Section 3.3.1 contain a restriction only on the magnitude of the average Mach number. Such generality blocks progress with the analysis and for many applications is unnecessary. The set of equations (3.22)–(3.27) must be simplified to forms that can be solved to give useful results. Many possibilities exist. We follow here a course that previous experience has shown to be particularly fruitful for investigations of combustor dynamics. The choices of approximations and tactics are usually motivated by eventual applications and the type of analysis used.

First we assume that the mean flow is determined by its own system of equations; that is, we avoid the problem of closure and use the first formulation, equations (3.28)–(3.33), discussed in Section 3.3.1. Consequently, the mean flow is taken to be independent of time and the combinations in square brackets [ ], equations (3.22)–(3.27), vanish identically. Using the definitions of the remaining brackets,

$$\frac{\partial \rho'}{\partial t} + \bar{\rho}\nabla \cdot \mathbf{M}' = -\{[\rho]\}_1 - \{\rho\}_2 + \mathcal{W}' \tag{3.40}$$

$$\bar{\rho}\frac{\partial \mathbf{M}'}{\partial t} + \nabla p' = -\{[\mathbf{M}]\}_1 - \{\mathbf{M}\}_2 - \{\mathbf{M}\}_3 + \boldsymbol{\mathfrak{F}}' \tag{3.41}$$

$$\bar{\rho}C_v\frac{\partial T'}{\partial t} + \bar{p}\nabla \cdot \mathbf{M}' = -\{[T]\}_1 - \{T\}_2 - \{T\}_3 + \mathcal{Q}' \tag{3.42}$$

$$\frac{\partial p'}{\partial t} + \gamma\bar{p}\nabla\cdot\mathbf{M}' = -\{[p]\}_1 - \{p\}_2 + \mathcal{P}' \tag{3.43}$$

$$\bar{\rho}\bar{T}\frac{\partial s'}{\partial t} = -\{[s]\}_1 - \{s\}_2 - \{s\}_3 - \{s\}_4 + \mathcal{S}' \tag{3.44}$$

The various brackets are defined in Section A.2 of Appendix A. They are formed to contain terms ordered with respect to both the mean Mach number and the amplitude of the fluctuations:

$$\begin{aligned}
[\quad] &: 1^{st} \text{ order in } \bar{\mathbf{M}};\ 1^{st} \text{ order in } \mathbf{M}',\ O(\varepsilon)\\
\{\quad\}_2 &: 0^{th} \text{ order in } \bar{\mathbf{M}};\ 2^{nd} \text{ order in } \mathbf{M}',\ O(\varepsilon^2)\\
\{\quad\}_3 &: 0^{th} \text{ order in } \bar{\mathbf{M}};\ 3^{rd} \text{ order in } \mathbf{M}',\ O(\varepsilon^3)\\
\{\quad\}_4 &: 0^{th} \text{ order in } \bar{\mathbf{M}};\ 4^{th} \text{ order in } \mathbf{M}',\ O(\varepsilon^4)
\end{aligned} \tag{3.45}$$

No terms have been dropped in passage from the set (3.22–(3.27) to the set (3.40)–(3.44), but fluctuations of the sources $\mathcal{W}', \cdots, \mathcal{S}'$ are not now classified into the various types defined by the brackets (3.45).

We have put the equations in the forms (3.40)–(3.44) to emphasize the point of view that we are considering classes of problems closely related to motions in classical acoustics. If the right-hand sides are ignored, (3.40)–(3.44) become the equations for linear acoustics of a uniform non-reacting medium at rest. The perturbations of that limiting class arise from three types of processes:

(i) interactions of the linear acoustic field with the mean flow, represented by the terms contained in the square brackets, $\{[\quad]\}$;
(ii) nonlinear interactions between the fluctuations, represented by the curly brackets conveniently referred to as: $\{\quad\}_2$, second order acoustics; $\{\quad\}_3$, third order acoustics; and $\{\quad\}_4$, fourth order acoustics;
(iii) sources associated with combustion processes, represented by the source terms $\mathcal{W}', \boldsymbol{\mathcal{F}}', \mathcal{Q}', \mathcal{P}'$ and $\mathcal{S}'$.

By selectively retaining one or more of these types of perturbations we define a hierarchy of problems of unsteady motions in combustors. We label these classes of problems O, I, II, III, IV according to the orders of terms retained in the right-hand side when the left-hand side comprise only the terms of order $\varepsilon := \mathbf{M}'_r$ defining clssical linear acoustics.

O. **Classical Acoustics**, $(\mu = 0, \varepsilon \to 0)$

Perturbations to first order in ε are retained in (3.40)–(3.44):

$$\begin{aligned}
\frac{\partial \rho'}{\partial t} + \bar{\rho}\nabla\cdot\mathbf{M}' &= \mathcal{W}'\\
\bar{\rho}\frac{\partial \mathbf{M}'}{\partial t} + \nabla p' &= \boldsymbol{\mathcal{F}}'\\
\bar{\rho}C_v\frac{\partial T'}{\partial t} + \bar{p}\nabla\cdot\mathbf{M}' &= \mathcal{Q}'\\
\frac{\partial p'}{\partial t} + \gamma\bar{p}\nabla\cdot\mathbf{M}' &= \mathcal{P}'\\
\bar{\rho}\bar{T}\frac{\partial s'}{\partial t} &= \mathcal{S}'
\end{aligned} \tag{3.46 a-e}$$

I. **Linear Stability**, $O(\varepsilon, \mu\varepsilon)$

Retain interactions linear in the average Mach number and in the fluctuations:

$$\begin{aligned}
\frac{\partial \rho'}{\partial t} + \bar{\rho}\nabla\cdot\mathbf{M}' &= -\{[\rho]\}_1 + \mathcal{W}' \\
\bar{\rho}\frac{\partial \mathbf{M}'}{\partial t} + \nabla p' &= -\{[\mathbf{M}]\}_1 + \boldsymbol{\mathcal{F}}' \\
\bar{\rho}C_v\frac{\partial T'}{\partial t} + \bar{p}\nabla\cdot\mathbf{M}' &= -\{[T]\}_1 + \mathcal{Q}' \\
\frac{\partial p'}{\partial t} + \gamma\bar{p}\nabla\cdot\mathbf{M}' &= -\{[p]\}_1 + \mathcal{P}' \\
\bar{\rho}\bar{T}\frac{\partial s'}{\partial t} &= -\{[s]\}_1 + \mathcal{S}'
\end{aligned} \tag{3.47 a-e}$$

II. **Second Order Acoustics**, $O(\varepsilon, \mu\varepsilon, \varepsilon^2)$

Retain the linear interactions and the nonlinear second order acoustics:

$$\begin{aligned}
\frac{\partial \rho'}{\partial t} + \bar{\rho}\nabla\cdot\mathbf{M}' &= -[\{[\rho]\}_1 + \{\rho\}_2] + \mathcal{W}' \\
\bar{\rho}\frac{\partial \mathbf{M}'}{\partial t} + \nabla p' &= -[\{[\mathbf{M}]\}_1 + \{\mathbf{M}\}_2] + \boldsymbol{\mathcal{F}}' \\
\bar{\rho}C_v\frac{\partial T'}{\partial t} + \bar{p}\nabla\cdot\mathbf{M}' &= -[\{[T]\}_1 + \{T\}_2] + \mathcal{Q}' \\
\frac{\partial p'}{\partial t} + \gamma\bar{p}\nabla\cdot\mathbf{M}' &= -[\{[p]\}_1 + \{p\}_2] + \mathcal{P}' \\
\bar{\rho}\bar{T}\frac{\partial s'}{\partial t} &= -[\{[s]\}_1 + \{s\}_2] + \mathcal{S}'
\end{aligned} \tag{3.48 a-e}$$

III. **Third Order Acoustics**, $O(\varepsilon, \mu\varepsilon, \varepsilon^2, \varepsilon^3)$

Retain the linear interactions and the nonlinear acoustics up to third order:

$$\begin{aligned}
\frac{\partial \rho'}{\partial t} + \bar{\rho}\nabla\cdot\mathbf{M}' &= -[\{[\rho]\}_1 + \{\rho\}_2] + \mathcal{W}' \\
\bar{\rho}\frac{\partial \mathbf{M}'}{\partial t} + \nabla p' &= -[\{[\mathbf{M}]\}_1 + \{\mathbf{M}\}_2 + \{\mathbf{M}\}_3] + \boldsymbol{\mathcal{F}}' \\
\bar{\rho}C_v\frac{\partial T'}{\partial t} + \bar{p}\nabla\cdot\mathbf{M}' &= -[\{[T]\}_1 + \{T\}_2 + \{T\}_3] + \mathcal{Q}' \\
\frac{\partial p'}{\partial t} + \gamma\bar{p}\nabla\cdot\mathbf{M}' &= -[\{[p]\}_1 + \{p\}_2] + \mathcal{P}' \\
\bar{\rho}\bar{T}\frac{\partial s'}{\partial t} &= -[\{[s]\}_1 + \{s\}_2 + \{s\}_3] + \mathcal{S}'
\end{aligned} \tag{3.49 a-e}$$

Four other classes of problems possible to define in this context will not be considered here since no results have been reported: second order acoustics with mean flow interactions; fourth order acoustics; and third and fourth order acoustics with nonlinear acoustics/mean flow interactions.

In problems I–III, the source terms $\mathcal{W}', \cdots$ must be expanded to order consistent with the orders of the fluid-mechanical perturbations retained.

3.4. Nonlinear Wave Equations for the Pressure Field. Practically all of the subsequent material in this book will be either directly concerned with pressure waves, or with interpretations of behavior related pressure waves. The presence of unsteady vorticity causes important revisions of such a restricted point of view, as we have already mentioned in Section 3.1, but the basic ideas remain in any event. Hence the wave equation

for pressure fluctuations occupies a meaningful position in all five classes of problems defined in the preceding section. Its formation follows the same procedure used in classical acoustics.

Define $\boldsymbol{\mathcal{M}}$ and $\mathcal{R}$ to contain all possible terms arising in the sets of equations constructed for the problems O–III:

$$\bar{\rho}\frac{\partial \mathbf{M}'}{\partial t} + \nabla p' = -\boldsymbol{\mathcal{M}} + \boldsymbol{\mathcal{F}}' \tag{3.50}$$

$$\frac{\partial p'}{\partial t} + \gamma \bar{p}\nabla \cdot \mathbf{M}' = -\mathcal{R} + \mathcal{P}' \tag{3.51}$$

where

$$\boldsymbol{\mathcal{M}} = \{[\mathbf{M}]\}_1 + \{\mathbf{M}\}_2 + +\{\mathbf{M}\}_3 \tag{3.52}$$

$$\mathcal{R} = \{[p]\}_1 + \{p\}_2 \tag{3.53}$$

Differentiate 3.50 with respect to time and substitute 3.50 for $\partial \mathbf{M}'/\partial t$:

$$\frac{\partial^2 p'}{\partial t^2} - \gamma \bar{p}\nabla \cdot \left[-\frac{1}{\bar{\rho}}\nabla p' - \frac{1}{\bar{\rho}}\left(\boldsymbol{\mathcal{M}} - \boldsymbol{\mathcal{F}}'\right)\right] = -\frac{\partial \mathcal{R}}{\partial t} + \frac{\partial \mathcal{P}'}{\partial t}$$

Rearrange the equation to find

$$\nabla^2 p' - \frac{1}{\bar{a}^2}\frac{\partial^2 p'}{\partial t^2} = h \tag{3.54}$$

with

$$h = -\bar{\rho}\nabla \cdot \left[\frac{1}{\bar{\rho}}\left(\boldsymbol{\mathcal{M}} - \boldsymbol{\mathcal{F}}'\right)\right] + \frac{1}{\bar{a}^2}\frac{\partial}{\partial t}(\mathcal{R} - \mathcal{P}') + \frac{1}{\bar{\rho}}\nabla\bar{\rho} \cdot \nabla p' \tag{3.55}$$

The boundary condition for the pressure field is found by taking the scalar product of the outward normal, at the chamber boundary, with:

$$\hat{\mathbf{n}} \cdot \nabla p' = -f \tag{3.56}$$

$$f = -\bar{\rho}\frac{\partial \mathbf{M}'}{\partial t} \cdot \hat{\mathbf{n}} + (\boldsymbol{\mathcal{M}} - \boldsymbol{\mathcal{F}}') \cdot \hat{\mathbf{n}} \tag{3.57}$$

Replacing $\boldsymbol{\mathcal{M}}$ and $\mathcal{R}$ by their definitions (3.52), we have the formulation based on the inhomogeneous nonlinear wave equation and its boundary condition:

$$\begin{aligned} \nabla^2 p' - \frac{1}{\bar{a}^2}\frac{\partial^2 p'}{\partial t^2} &= h \\ \hat{\mathbf{n}} \cdot \nabla p' &= -f \end{aligned} \tag{3.57 a,b}$$

with

$$\begin{aligned} h = &-\left[\bar{\rho}\nabla \cdot \frac{1}{\bar{\rho}}\{[\mathbf{M}]\}_1 - \frac{1}{\bar{a}^2}\frac{\partial\{[p]\}_1}{\partial t}\right] - \left\{\bar{\rho}\nabla \cdot \frac{1}{\bar{\rho}}\{\mathbf{M}\}_2 - \frac{1}{\bar{a}^2}\frac{\partial\{p\}_2}{\partial t}\right\} - \bar{\rho}\nabla \cdot \frac{1}{\bar{\rho}}\{\mathbf{M}\}_3 \\ &+ \frac{1}{\bar{\rho}}\nabla\bar{\rho} \cdot \nabla p' + \bar{\rho}\nabla \cdot \frac{1}{\bar{\rho}}\boldsymbol{\mathcal{F}}' - \frac{1}{\bar{a}^2}\frac{\partial \mathcal{P}'}{\partial t} \end{aligned} \tag{3.58}$$

$$f = \bar{\rho}\frac{\partial \mathbf{M}'}{\partial t} \cdot \hat{\mathbf{n}} + \hat{\mathbf{n}} \cdot [\{[\mathbf{M}]\}_1 + \{\mathbf{M}\}_2 + \{\mathbf{M}\}_3] - \boldsymbol{\mathcal{F}}' \cdot \hat{\mathbf{n}} \tag{3.59}$$

With this formulation, the wave equations and boundary conditions for the classes of problems defined in Section 3.3 are distinguished by the following functions h and f:

O. **Classical Acoustics**

$$h_O = \bar{\rho}\nabla\cdot\frac{1}{\bar{\rho}}\boldsymbol{\mathcal{F}}' - \frac{1}{\bar{a}^2}\frac{\partial \mathcal{P}'}{\partial t}$$
$$f_O = \bar{\rho}\frac{\partial \mathbf{M}'}{\partial \mathbf{t}}\cdot\hat{\mathbf{n}} - \boldsymbol{\mathcal{F}}'\cdot\hat{\mathbf{n}} \qquad (3.60)\ \text{a,b}$$

I. **Linear Stability**

$$h_I = -\left[\bar{\rho}\nabla\cdot\frac{1}{\bar{\rho}}\{[\mathbf{M}]\}_1 - \frac{1}{\bar{a}^2}\frac{\partial\{[p]\}_1}{\partial t}\right] + \frac{1}{\bar{\rho}}\nabla\bar{\rho}\cdot\nabla p' + \bar{\rho}\nabla\cdot\frac{1}{\bar{\rho}}\boldsymbol{\mathcal{F}}' - \frac{1}{\bar{a}^2}\frac{\partial \mathcal{P}'}{\partial t}$$
$$f_I = \bar{\rho}\frac{\partial \mathbf{M}'}{\partial t}\cdot\hat{\mathbf{n}} + \hat{\mathbf{n}}\cdot\{[\mathbf{M}]\}_1 - \boldsymbol{\mathcal{F}}'\cdot\hat{\mathbf{n}} \qquad (3.61)\ \text{a,b}$$

Allowing $\boldsymbol{\mathcal{F}}'$ and $\mathcal{P}'$ to be non-zero gives the opportunity for representing sources of mass, momentum, and energy both within the volume and at the boundary. The first term in f_0 accounts for motion of the boundary.

II. **Second Order Acoustics**

$$h_{II} = -\left[\bar{\rho}\nabla\cdot\frac{1}{\bar{\rho}}\{[\mathbf{M}]\}_1 - \frac{1}{\bar{a}^2}\frac{\partial\{[p]\}_1}{\partial t}\right] - \left\{\bar{\rho}\nabla\cdot\frac{1}{\bar{\rho}}\{\mathbf{M}\}_2 - \frac{1}{\bar{a}^2}\frac{\partial\{p\}}{\partial t}\right\}$$
$$+\frac{1}{\bar{\rho}}\nabla\rho'\cdot\nabla p' + \bar{\rho}\nabla\cdot\frac{1}{\bar{\rho}}\boldsymbol{\mathcal{F}}' - \frac{1}{\bar{a}^2}\frac{\partial \mathcal{P}'}{\partial t} \qquad (3.62)\ \text{a,b}$$
$$f_{II} = \bar{\rho}\frac{\partial \mathbf{M}'}{\partial t}\cdot\hat{\mathbf{n}} + \hat{\mathbf{n}}\cdot[\{[\mathbf{M}]\}_1 + \{\mathbf{M}\}_2] - \boldsymbol{\mathcal{F}}'\cdot\hat{\mathbf{n}}$$

III. **Third Order Acoustics**

$$h_{III} = -\left[\bar{\rho}\nabla\cdot\frac{1}{\bar{\rho}}\{[\mathbf{M}]\}_1 - \frac{1}{\bar{a}^2}\frac{\partial\{[p]\}_1}{\partial t}\right] - \left\{\bar{\rho}\nabla\cdot\frac{1}{\bar{\rho}}\{\mathbf{M}\}_2 - \frac{1}{\bar{a}^2}\frac{\partial\{p\}_2}{\partial t}\right\}$$
$$-\bar{\rho}\nabla\cdot\frac{1}{\bar{\rho}}\{\mathbf{M}\}_3 + \frac{1}{\bar{\rho}}\nabla\bar{\rho}\cdot\nabla p' + \bar{\rho}\nabla\cdot\frac{1}{\bar{\rho}}\boldsymbol{\mathcal{F}}' - \frac{1}{\bar{a}^2}\frac{\partial \mathcal{P}'}{\partial t} \qquad (3.63)\ \text{a,b}$$
$$f_{III} = \bar{\rho}\frac{\partial \mathbf{M}'}{\partial t}\cdot\hat{\mathbf{n}} + \hat{\mathbf{n}}\cdot[\{[\mathbf{M}]\}_1 + \{\mathbf{M}\}_2 + \{\mathbf{M}\}_3] - \boldsymbol{\mathcal{F}}'\cdot\hat{\mathbf{n}}$$

With these definitions of the functions h and f, the definitions of the four classes of problems considered here are complete, forming the basis for the analysis worked out in the remainder of these lectures. Only problems within classical acoustics can be solved easily. All others require approximations, both in modeling physical processes and in the method of solution. Modeling will be discussed in the contexts of specific applications; a few remarks help clarify the approximate method of solution described in the following section.

Remarks:

i) The classes of problems I–III defined here are described by inhomogeneous equations that even for linear stability cannot be generally solved in closed form. The chief obstacles to solution arise because the functions h and f contain not only the unknown pressure but also the velocity and temperature. For given functions $\boldsymbol{\mathcal{F}}'$ and $\mathcal{P}'$, numerical solutions could be obtained for a specified combustor and mean flow field. The results would apply only to the special case considered. To obtain some understanding of general behavior it would be necessary to consider many special cases, a tedious and expensive procedure.

ii) Therefore, we choose to work out an approximate method of solution applicable to all classes of problems. Numerical solutions, or 'simulations' then serve the important purpose of assessing the validity and accuracy of the approximate results.

iii) The approximate method of solution is based first on spatial averaging, followed by an iteration procedure involving extension of the expansion in two small parameters defined in this section. This method has been most widely used and confirmed in applications to combustion instabilities in solid propellant rockets, but it can be applied to problems arising in any type of combustor.

iv) Instabilities in solid rockets have been particularly helpful in developing the general theory for at least three reasons: 1) the mean flow field, nonuniform and generated by mass addition at the boundary, requires careful attention to processes associated with interactions between the mean flow and unsteady motions; 2) more experimental results for transient behavior have been obtained for solid rockets than for any other combustion system; and 3) although still far from being satisfactorily understood, the dynamics of burning solid propellants is better known than for any other combustion system.

v) The fluctuations of the source terms, $\mathcal{W}'$, $\boldsymbol{\mathcal{F}}'$, ... $\mathcal{S}'$ will be made explicit as required in particular applications.

4. MODAL EXPANSION AND SPATIAL AVERAGING; AN ITERATIVE METHOD OF SOLUTION

From the point of view represented in Figure 1.1, we are concerned in this section with representing the combustor dynamics. The procedure, often called 'modeling' is based on the equations of motion constructed in the preceding section and hence in principle will contain all relevant physical processes[11]. For the purposes here, all modeling of combustor dynamics and of combustion dynamics—the mechanisms and feedback in Figure 1.1—must be done in the context developed in Section 1. Thus we always have in mind the idea of wave motions somehow generated and sustained by interactions between the motions themselves and combustion processes, the latter also including certain aspects of the mean flow within the combustor.

The simplest model of the combustion dynamics is a single wave, a classical acoustic resonance as in an organ pipe, but decaying or growing due to the other processes in the chamber. In practice, the combustion processes and nonlinear gasdynamical effects inevitably lead to the presence of more than one acoustic mode. We need a relatively simple yet accurate means of treating those phenomena for problems of the sort arising in the laboratory and in practice. Modeling in this case begins with construction of a suitable method for solving the nonlinear wave equations derived in Section 3.4. In this context we may regard the analysis of the Rijke tube covered in Section 2 as a basic example of the procedure stripped of the formalism covered in this section.

The chief purpose of the analysis constructed here is, to devise methods capable of producing results useful for prediction and interpretation of unsteady motions in full-scale combustion chambers as well as for laboratory devices. That intention places serious demands on the methods used for at least two reasons:

1. processes that must be modeled are usually complicated and their theoretical representations are necessarily approximate to extents which themselves are difficult to assess; and
2. almost all input data required for quantitative evaluation of theoretical results are characterized by large uncertainties.

In this situation it seems that for practical and, as it will turn out, for theoretical purposes as well, the most useful methods will be based on some sort of spatial averaging. Direct solution of the partial differential equations, even for linear problems, is practically a hopeless task except for very special cases for simple geometries. Direct numerical simulations (DNS) or numerical solutions to the partial differential equations are not yet a real alternative for practical purposes at this time, and are usually less attractive for obtaining basic understanding. However, as we will see later, numerical solutions offer the only means for assessing the validity of approximate solutions and always can treat more complicated (realistic?) problems than we can reasonably handle with the analytical methods discussed here. In any event, one should view theory and analysis on the one hand, and numerical simulations on the other, as complementary activities.

The material on analysis and theory of combustion instabilities treated in these two lectures is based on a method of spatial averaging. The essential idea is of course not new, the method being nearly identical with similar methods used in other branches of continuum mechanics. There are a few special characteristics associated with applications to combustor that will appear in the course of the following discussion.

4.1. Application of a Green's Function for Steady Waves. The method used later to analyze nonlinear behavior has its origins in an early analysis of linear combustion instabilities in liquid rocket engines (Culick, 1961, 1963). That work was based on solution to problems of steady waves by introducing a Green's function. It is an effective strategy for this application because departures from a known soluble problem are small, due either to perturbations within the volume or at the boundary, all of order μ in the context developed in Section 3.

[11] That seems to be what some people (notably electrical engineers it seems) mean by the term 'physics-based modeling.' What would otherwise be the basis for acceptable modeling of a physical system has not been explained.

The problem to be solved is defined by equation (3.54) and its boundary conditions (3.56) derived in Section 3.4,

$$\nabla^2 p' - \frac{1}{\bar{a}^2}\frac{\partial^2 p'}{\partial t^2} = h$$
$$\hat{\mathbf{n}} \cdot \nabla p' = -f \qquad (4.1)\text{ a,b}$$

with h and f given by (3.61) a,b for linear stability. Because h and f are linear, various methods are available to build general solutions by applying the principle of superposition to elementary solutions representing steady waves. Hence we assume that the fluctuating pressure field is a steady wave system within the given chamber, having unknown spatial structure and varying harmonically in time:

$$p' = \hat{p} e^{i\bar{a}kt} \qquad (4.2)$$

where k is the complex wavenumber, also initially unknown,

$$k = \frac{1}{\bar{a}}(\omega - i\alpha) \qquad (4.3)$$

As defined here, α positive means that the wave has growing amplitude, $p' \sim e^{\alpha t}$. Of course the wave is not strictly stationary, a condition existing only if $\alpha = 0$, certainly true when $h = f = 0$, as in classical acoustics.

Even when h, f are non-zero, it is still possible that $\alpha = 0$, now defining a state of *neutral stability*. In general one must expect $\alpha \neq 0$; it is a basic assumption in all of the analysis covered in this book that α is small compared with ω, so the waves are slowly growing or decaying—they are 'almost' stationary, and their spatial structure does not change much in time. However, the results obtained are quite robust and seem often to be usable even when α/ω is not small.

The problem here is to determine the spatial distribution $\hat{p}$ and the complex wavenumber k. For steady waves we can write

$$h = \kappa \hat{h} e^{i\bar{a}kt} \;;\; f = \kappa \hat{f} e^{i\bar{a}kt}$$

where again κ is a small parameter[12] characterizing the smallness of h and f. Substitution in (4.1) a,b and dropping the common exponential time factor gives

$$\nabla^2 \hat{p} + k^2 \hat{p} = \kappa \hat{h}$$
$$\hat{\mathbf{n}} \cdot \nabla \hat{p} = -\kappa \hat{f} \qquad (4.4)\text{ a,b}$$

This is of course a well-known classical problem thoroughly discussed in many books. Many methods of solution are available for the linear problem. We use here a procedure based on introducing a Green's function discussed, for example, by Morse and Feshbach (1952, Chapter 10). This is an attractive method for several reasons, including:

1. Conversion from a differential equation, and the iterative method of solution this suggests, is an effective means for minimizing the consequences of the uncertainties inherent in problems of combustor dynamics;
2. Explicit results can be obtained for real and imaginary parts of the complex wavenumber in forms that are easily interpreted and remarkably convenient both for theoretical work and for applications;
3. The method has motivated a straightforward extension to nonlinear problems, with considerable success.

Define a Green's function satisfying the homogeneous boundary and the wave equation homogeneous except at the single point where a source is located having zero spatial extent and infinite strength such that is integral over space is finite. Thus the source is represented by a delta function $-\delta(\mathbf{r} - \mathbf{r}_0)$ and G is determined as a solution to the problem

$$\nabla^2 G(\mathbf{r}|\mathbf{r}_0) + k^2 G(\mathbf{r}|\mathbf{r}_0) = \delta(\mathbf{r} - \mathbf{r}_0)$$
$$\hat{\mathbf{n}} \cdot \nabla G(\mathbf{r}|\mathbf{r}_0) = 0 \qquad (4.5)\text{ a,b}$$

[12] Later, κ will be identified with μ introduced in Section 3.3 but it is useful in this discussion to maintain a distinction.

The notation $\mathbf{r}|\mathbf{r}_0$ as the argument of $G(\mathbf{r}|\mathbf{r}_0)$ represents the interpretation of the Green's function as the wave observed at point $\mathbf{r}$ due to a steady oscillatory point source at $\mathbf{r}_0$.

Multiply ((4.4) a,b)a by $G(\mathbf{r}|\mathbf{r}_0)$, ((4.5) a,b)a by $\hat{p}(\mathbf{r})$, subtract the results and integrate over volume (in the present case the volume of the chamber) to find

$$\begin{aligned}\iiint_V \left[G(\mathbf{r}|\mathbf{r}_0)\nabla^2\hat{p}(\mathbf{r}) - \hat{p}(\mathbf{r})\nabla^2 G\,(\mathbf{r}|\mathbf{r}_0)\right] dV + k^2 \iiint_V \left[G(\mathbf{r}|\mathbf{r}_0)\hat{p}(\mathbf{r}) - \hat{p}(\mathbf{r})G(\mathbf{r}|\mathbf{r}_0)\right] dV \\ = \kappa \iiint_V G(\mathbf{r}|\mathbf{r}_0)\hat{h}(\mathbf{r}) - \iiint \hat{p}(\mathbf{r})\delta(\mathbf{r}-\mathbf{r}_0)dV\end{aligned} \tag{4.6}$$

Because $G(\mathbf{r}|\mathbf{r}_0)$ and $\hat{p}(\mathbf{r})$ are scalar functions the second integral on the right-hand side vanishes. The first integral is rewritten using a form of Green's theorem, and the basic property of the delta function is applied to the second integral on the right-hand side:

$$\iiint_V F(\mathbf{r})\delta(\mathbf{r}-\mathbf{r}_0)dV = F(\mathbf{r}) \qquad (\mathbf{r}_1, \mathbf{r}_0 \text{ in } V) \tag{4.7}$$

Hence (4.6) becomes

$$\oiint_S [G(\mathbf{r}|\mathbf{r}_0)\nabla\hat{p}(\mathbf{r}) - p(\mathbf{r})\nabla G(\mathbf{r}|\mathbf{r}_0)]\cdot\hat{\mathbf{n}}dS = \kappa \iiint_V G(\mathbf{r}|\mathbf{r}_0)\hat{h}(\mathbf{r})dV - \hat{p}(\mathbf{r}_0)$$

where $\hat{\mathbf{n}}$ is the outward normal at the surface of the volume V in question.

Now apply the boundary conditions (4.4) a,b and (4.5) a,b and the last equation can be written in the form

$$\mathbf{p}(\hat{r}_0) = \kappa \left\{ \iiint_V G(\mathbf{r}|\mathbf{r}_0)\hat{h}(\mathbf{r})dV + \iint_S G(\mathbf{r_s}|\mathbf{r}_0)\hat{f}(\mathbf{r}_s)dS \right\} \tag{4.8}$$

Subscript $(\ )_s$ means the point $\mathbf{r}_s$ lies on the boundary surface (actually on the inside surface of the boundary). Because the operator for scalar waves is *self-adjoint* (see Morse and Feshbach 1952, Chapter 10), the Green's function possesses the property of symmetry

$$G(\mathbf{r}|\mathbf{r}_0) = G(\mathbf{r}_0|\mathbf{r}) \tag{4.9}$$

This property has the appealing physical interpretation that the wave observed at $\mathbf{r}$ due to a point source at $\mathbf{r}_0$ has the same amplitude and relative phase as for the wave observed at $\mathbf{r}_0$ when a point source is located at $\mathbf{r}$. With (4.9) we can interchange $\mathbf{r}$ and $\mathbf{r}_0$ in (4.8) to find for the steady field at position $\mathbf{r}$:

$$\hat{p}(\mathbf{r}) = \kappa \left\{ \iiint_V G(\mathbf{r}|\mathbf{r}_0)\hat{h}(\mathbf{r}_0)d\mathbf{V}_0 + \oiint_S G(\mathbf{r}|\mathbf{r}_{0s})\hat{f}(\mathbf{r}_{0s})dS \right\} \tag{4.10}$$

Equation (4.10) is not an explicit solution for the pressure field due to the source functions $\hat{h}$ and $\hat{f}$, but is rather, an integral equation because $\hat{h}$ and $\hat{f}$ in general depend on the fluctuating pressure and velocity fields themselves. However, because the sources are assumed to be small perturbations of the classical field having no sources, κ is small and $\hat{p}$ will not differ greatly from a solution to the homogeneous problem defined by $h = f = 0$. The result (4.10) represents the solution to the inhomogeneous problem; the complete solution is (4.10) plus a homogeneous solution. Advantage will be taken of the smallness of κ to find an approximate explicit solution for $\hat{p}$ by an iterative procedure discussed in Section 4.1.1.

Whatever tactic one may choose to follow, the result (4.10) is of no practical value without having a representation of $G(\mathbf{r}|\mathbf{r}_0)$. The most convenient form of $G(\mathbf{r}|\mathbf{r}_0)$ for our purpose is expansion in eigenfunctions $\psi_n(\mathbf{r})$, here the normal modes of the classical acoustics problem with no sources in the volume and homogeneous boundary conditions: $G(\mathbf{r}|\mathbf{r}_0)$ is therefore expressed as a *modal expansion,*

$$G(\mathbf{r}|\mathbf{r}_0) = \sum_{n=0}^{\infty} A_n\psi_n(\mathbf{r}) \tag{4.11}$$

where the ψ_n satisfy

$$\begin{aligned} \nabla^2\psi_n + k_n^2\psi_n &= 0 \\ \hat{\mathbf{n}}\cdot\nabla\psi_n &= 0 \end{aligned} \qquad (4.12)\ \text{a,b}$$

and the ψ_n are orthogonal functions,

$$\iiint_V \psi_m(\mathbf{r})\psi_n(\mathbf{r})dV = E_n^2\delta_{mn} \qquad (4.13)$$

Substitute (4.11) in ((4.5) a,b)a, multiply by $\psi_m(\mathbf{r})$ and integrate over the volume to find

$$\iiint_V \psi_m \sum_{n=0}^{\infty} A_n\nabla^2\psi_n dV + k^2 \iiint_V \psi_m \sum_{n=0}^{\infty} A_n\psi_n dV = \int \psi_m(\mathbf{r})\delta(\mathbf{r}-\mathbf{r}_0)dV$$

With (4.7), ((4.12) a,b) and (4.13), this equation produces the formula for A_n:

$$A_n = \frac{\psi_n(\mathbf{r}_0)}{k_n^2 - k^2} \qquad (4.14)$$

Thus the expansion (4.11) for $G(\mathbf{r}|\mathbf{r}_0)$ is

$$G(\mathbf{r}|\mathbf{r}_0) = \sum_{n=0}^{\infty} \frac{\psi_n(\mathbf{r})\psi_n(\mathbf{r}_0)}{E_n^2(k^2-k_n^2)} \qquad (4.15)$$

the modal expansion of the Green's function. Substitution of (4.15) in (4.10) leads to the formal modal expansion of the pressure field,

$$\hat{p}(\mathbf{r}) = \kappa\sum_{n=0}^{\infty} \frac{\psi_n(\mathbf{r})}{E_n^2(k^2-k_n^2)} \left\{ \iiint_V \psi_n(\mathbf{r}_0)\hat{h}(\mathbf{r}_0)dV_0 + \oiint_S \psi_n(\mathbf{r}_{0s})\hat{f}(\mathbf{r}_{0s})dS_0 \right\} \qquad (4.16)$$

Suppose that for κ tending to zero, $\hat{p}(\mathbf{r})$ approaches the unperturbed mode shape ψ_N; let the corresponding function $\hat{p}$ be denoted $\hat{p}_N$, so

$$\hat{p} \underset{\kappa\to 0}{\longrightarrow} \hat{p}_N = \psi_N \qquad (4.17)$$

Now separate the N^{th} term from the sum in (4.16) and write

$$\begin{aligned} \hat{p}(\mathbf{r}) = \psi_N(\mathbf{r})\frac{\kappa}{E_N^2(k^2-k_N^2)} &\left\{ \iiint_V \psi_N(\mathbf{r}_0)\hat{h}(\mathbf{r}_0)dV_0 + \oiint_S \psi_N(\mathbf{r}_{0s})\hat{f}(\mathbf{r}_{0s})dS_0 \right\} \\ +\kappa\sum_{n=0}^{\infty}{}' \frac{\psi_n(\mathbf{r})}{E_n^2(k^2-k_n^2)} &\left\{ \iiint_V \psi_n(\mathbf{r}_0)\hat{h}(\mathbf{r}_0)dV_0 + \oiint_S \psi_n(\mathbf{r}_{0s})\hat{f}(\mathbf{r}_{0s})dS_0 \right\} \end{aligned} \qquad (4.18)$$

where the prime in the summation sign means that the term $n = N$ is missing. This form is consistent with the requirement (4.17) only if the factor multiplying $\psi_N(\mathbf{r})$ is unity, giving the formula for the perturbed wavenumber

$$k^2 = k_N^2 + \frac{\kappa}{E_N^2} \left\{ \iiint_V \psi_N(\mathbf{r}_0)\hat{h}(\mathbf{r}_0)dV_0 + \oiint_S \psi_N(\mathbf{r}_{0s})\hat{f}(\mathbf{r}_{0s})dS_0 \right\} \qquad (4.19)$$

and (4.18) becomes

$$\hat{p}(\mathbf{r}) = \psi_N(\mathbf{r}) + \kappa\sum_{n=0}^{\infty}{}' \frac{\psi_n(\mathbf{r})}{E_n^2(k^2-k_n^2)} \left\{ \iiint_V \psi_n(\mathbf{r}_0)\hat{h}(\mathbf{r}_0)dV_0 + \oiint_S \psi_n(\mathbf{r}_{0s})\hat{f}(\mathbf{r}_{0s})dS_0 \right\} \qquad (4.20)$$

Another more direct derivation of (4.19) very useful in later analysis, may be had by first multiplying ((4.4) a,b)a by ψ_N and integrating over the volume:

$$\iiint_V \psi_N\nabla^2\hat{p}dV + k^2 \iiint_V \psi_N\hat{p}dV = \kappa \iiint_V \psi_N\hat{h}dV$$

Application of Green's theorem to the first integral gives

$$\iiint_V \hat{p}\nabla^2\psi_N dV + \oiint_S [\psi_n \nabla\hat{p} - \hat{p}\nabla\psi_n]\cdot\hat{\mathbf{n}}dS + k^2 \iiint_V \psi_n\hat{p}dV = \oiint_S \psi_N \hat{h}dV$$

after inserting $\nabla^2\psi_N = -k_N^2\psi_N$ and $\nabla\psi_N\cdot\hat{\mathbf{n}} = 0$, rearrangement gives

$$k^2 = k_N^2 + \frac{\kappa}{\iiint_V \psi_N\hat{p}dV}\left\{\iiint_V \psi_N(\mathbf{r})\hat{h}(\mathbf{r})dV + \oiint_S \psi_N(\mathbf{r}_s)\hat{f}(\mathbf{r}_s)dS\right\} \tag{4.21}$$

The integral of $\psi_N\hat{p}$ in the denominator of (4.21) can be evaluated by using (4.20) and is exactly E_n^2, providing the series in (4.20) converges. Hence (4.21) is identical to (4.19). This simple calculation has shown that (4.19) and (4.20) are consistent.

The preceding calculation contains several basic ideas behind much of the analysis used in these lectures. In summary, the original problem described by the differential equation ((4.4) a,b)a and its boundary condition ((4.4) a,b)b are converted to an integral equation, in this case (4.10), established by introducing a Green's function. This is not an explicit solution because the functions h and f generally depend on the dependent variable $\hat{p}$. However, formulation as an integral equation forms a convenient basis for approximate solution by iteration.

4.1.1. *Approximate Solution by Iteration.* To apply an iterative procedure, it is necessary first to give the Green's function $G(\mathbf{r}|\mathbf{r}_0)$ explicit form. The natural choice for problems of waves in a chamber is a series expansion in the natural modes of the chamber, a modal expansion, (4.15). For the small parameter κ tending to zero (i.e. all perturbations of the classical acoustics problem are small), a straightforward argument produces the formula (4.19) for the wavenumber and the integral equation (4.20) for $\hat{p}(\mathbf{r})$.

Equation (4.20) must be solved to give $\hat{p}$ before the wavenumber can be computed with (4.19). We should emphasize that for many practical purposes, it is really k that is required, because its imaginary part determines the linear stability of the system ($\alpha = 0$). The great advantage of this approach may be seen clearly with a simple example. Suppose $\hat{f} = 0$ and $\hat{h} = K(1+\hat{p})$ in (4.4) a,b. Then (4.20) and (4.19) become

$$\hat{p}(\mathbf{r}) = \psi_N(\mathbf{r}) + \kappa K \sum_{n=0}^{\infty}{}' \frac{\psi_n(\mathbf{r})}{E_n^2(k^2 - k_n^2)} \iiint_V \psi_n(\mathbf{r}_0)(1+\hat{p})dV_0 \tag{4.22}$$

$$k^2 = k_N^2 + \frac{\kappa K}{E_N^2}\iiint_V \psi_N(1+\hat{p})dV_0 \tag{4.23}$$

Because κ is assumed to be small, solution by successive approximation, i.e. an iterative procedure, is a logical way to proceed. The initial (zeroth) approximation to the mode shape $\hat{p}$ is (4.22) for $\kappa = 0$, $\hat{p}^{(0)} = \psi_N$. Substitution in (4.23) gives k^2 correct to first order in κ:

$$\begin{aligned}(k^2)^{(1)} &= k_N^2 + \frac{\kappa K}{E_N^2}\iiint_V \psi_N(1+\psi_N)dV_0 \\ &= k_N^2 + \kappa\frac{KI_N}{E_N^2}\end{aligned} \tag{4.24}$$

where I_N stands for the integral.

Calculation of $\hat{p}$ to first order in κ requires setting $\hat{p}$ and k^2 to their *zeroth* order values on the right-hand side of (4.22), $\hat{p}^{(0)} = \psi_N$, $(k^2)^{(0)} = k_N^2$:

$$\begin{aligned}\hat{p}^{(1)}(\mathbf{r}) &= \psi_N(\mathbf{r}) + \kappa K \sum_{n=0}^{\infty}{}' \frac{\psi_n(\mathbf{r})}{E_n^2(k_N^2 - k_n^2)} \iiint_V \psi_n(\mathbf{r}_0)(1+\psi_N(\mathbf{r}_0))dV_0 \\ &= \psi_N + \kappa\sigma_N\end{aligned}$$

Substitution of this formula for $\hat{p}$ under the integral in (4.23) then gives the second approximation $(k^2)^{(2)}$ to k^2:

$$\begin{aligned}(k^2)^{(2)} &= k_N^2 + \frac{\kappa K}{E_N^2}\iiint_V \psi_N(1+\psi_N+\kappa\sigma_N)dV_0 \\ &= (k^2)^{(1)} + \kappa^2\frac{K}{E_N^2}\iiint_V \psi_N\sigma_N dV_0\end{aligned} \tag{4.25}$$

A wonderful property of the procedure is already apparent: Calculation of the wavenumber to some order l in the small parameter requires knowing the modal functions only to order $l-1$. That is the basis for the current standard practice of computing linear stability for solid propellant rockets (the Standard Stability Prediction Program, Nickerson *et al.* 1983) using the unperturbed acoustic modes computed for the geometry in question.

The "perturbation-iteration" procedure just described is an old and widely used method to obtain solutions to nonlinear as well as linear problems. Often much attention is paid to achieving more accurate solutions by carrying the iterations to higher order in the small parameter. That is a legitimate process providing the equations themselves are valid to the order sought. In Section 3 we emphasized the importance of the expansion procedure largely for that reason. If the equations are valid, say, only to second order in the amplitude (ε), there is no need—in fact no justification—to try to find a solution to order ε^3 and higher. Similar remarks apply to the expansion in the average Mach number (μ). The procedure is fully explained in Section 4.5 for the equations derived in Section 3.4.

4.2. An Alternative Derivation of the First Order Formula. The results (4.19) and (4.21) for the complex wavenumber and mode shape can be constructively obtained in a different way. Both formulas provide means for computing the differences $k^2 - k_N^2$ and $\hat{p} - \psi_N$ between the actual (perturbed) quantities and the unperturbed quantities. It is reasonable that those results should somehow follow from comparison of the perturbed ($\kappa \neq 0$) and unperturbed ($\kappa = 0$) problems. The idea is to average the difference between the two problems weighted respectively by the other's mode shape. That is, subtract $\hat{p}$ times equation ((4.12) a,b)a from ψ_n times ((4.4) a,b)a and integrate the result over the volume of the chamber:

$$\iiint_V \left[\psi_N\nabla^2\hat{p} - \hat{p}\nabla^2\psi_N\right]dV + \iiint_V (k^2-k_N^2)\psi_n\hat{p}dV_0 = \kappa\iiint_V \psi_N\hat{h}dV$$

Now apply Green's theorem to the first integral, substitute the boundary conditions ((4.4) a,b)b and ((4.12) a,b)b and rearrange the result to find (4.21):

$$k^2 = k_N^2 + \frac{\kappa}{\iiint_V \psi_N\hat{p}dV}\left\{\iiint_V \psi_N(\mathbf{r})\hat{h}(\mathbf{r})dV + \oiint_S \psi_N(\mathbf{r}_s)\hat{f}(\mathbf{r}_s)dS\right\} \tag{4.26}$$

If k^2 is to be calculated to first order in κ, then $\hat{p}$ must be replaced by its zero order approximation $\hat{p} = \psi_N$. Because the correction to k_N^2 contains the multiplier κ, any contributions of order κ multiplying κ give terms of order κ^2. Hence to first order, (4.26) of course becomes (4.19).

This approach does not provide a recipe for computing the modal or basis functions to higher order. That does not cause difficulty here because we have the procedure given in the preceding section. We will find later that the simple derivation just given suggests a useful extension to time-dependent nonlinear problems. In that situation there is no result corresponding to (4.20) for computing the mode shapes to higher order. That deficiency is a serious obstacle to further progress, a subject of current research.

4.3. Approximate Solution for Unsteady Nonlinear Motions. The method covered in the preceding two sections, based essentially in the use of Green's functions, was the first application of modal expansions and spatial averaging to combustion instabilities (Culick 1961, 1963). In the early 1970's the procedure was extended

to treat nonlinear problems, necessarily involving time-dependence (Culick 1971, 1975). We summarize that approach here.[13]

We begin with the general problem (4.1) a,b and assume an approximation $\tilde{p}'(\mathbf{r})$ to the pressure field as a truncated expansion in a set of basis functions ψ_m,

$$\tilde{p}'(\mathbf{r},t) = \bar{p}_r \sum_{m=0}^{M} \eta_m(t)\psi_m(\mathbf{r}) \tag{4.27}$$

In this work we will always take the ψ_m to be acoustic modes defined by the geometry, the distribution of average temperature and suitable boundary conditions.[14] We would like the right-hand side of (4.27) to become more nearly equal to the actual pressure field in the combustor as more terms are included in the series, so that $\tilde{p}' \equiv p'$ in the limit:

$$\lim_{M\to\infty} \tilde{p}(\mathbf{r};t) = \lim_{M\to\infty} \sum_{m=0}^{M} \eta_m(t)\psi_m(\mathbf{r}) \tag{4.28}$$

Because the ψ_m do not satisfy the correct boundary conditions, this pointwise property certainly cannot be satisfied at the boundary. It is reasonable, however, to expect convergence in integral-squared sense; that is the integral of the square of the difference between the exact solution and (4.27) satisfies

$$\lim_{M\to\infty} \iiint \left[p'(\mathbf{r},t) - \bar{p}_r \sum_{m=0}^{M} \eta_m(t)\psi_m(\mathbf{r}) \right]^2 dV = 0 \tag{4.29}$$

We will not prove this properly, but assume its truth.

Convergence in the sense asserted by (4.29) is a common idea arising, for example, in formal treatments of Sturm-Liouville problems; see Hildebrand 1952 for a very readable discussion. The matter of convergence of approximate solutions in the present context is more complicated because one must take into account the fact that the governing equations and their solutions are expanded in the two small parameters μ and ε introduced in Section 3. We will also not discuss that problem.

The synthesis of the pressure field expressed by (4.27) does not restrict in any practical fashion the generality of the method. For definitions here we assume that the modal functions satisfy the homogeneous Neumann condition $\hat{\mathbf{n}} \cdot \nabla\psi_n = 0$, but for some applications a different boundary condition, perhaps over only part of the boundary, may serve better. Hence we will assume here that the ψ_n are eigensolutions to the problem (4.12) a,b.

We require that the approximation (4.27) to p' satisfy equation (4.1) a,b. Multiply (4.12) a,b written for ψ_N by $\tilde{p}'(\mathbf{r},t)$, subtract from (4.1) a,b written for $\tilde{p}'$ multiplied by ψ_N; and integrate the difference over the volume of the chamber to give

$$\iiint_V \left[\psi_N \nabla^2\tilde{p}' - \tilde{p}'\nabla^2\psi_N\right] dV - \iiint_V \frac{1}{\bar{a}^2}\frac{\partial^2\tilde{p}'}{\partial t^2} dV - k_N^2 \iiint_V \tilde{p}'\psi_N dV = \iiint_V \psi_N h dV$$

[13] An alternative form based on an form of Galerkin's method, extended to accommodate the sorts of problems arising in the present context, was introduced first by Zinn and his students. That procedure and the present method give identical equations before the expansion procedure is applied and further approximations are used. The applicability of that method seems to have been blunted in some cases by use of a velocity potential, thereby requiring that the unsteady field be irrotational. It seems also that the ordering procedure (in terms of the small parameters $\bar{M}_r$ and $\bar{M}'_r$) (i.e. μ and ε) has not been followed consistently, causing confusion in some derivations and conclusions. Those matters are discussed elsewhere. It seems likely that the extended form of Galerkin's method could give the same (or nearly so) results as found by the method discussed here, but the early works were not pursued further. There is no basis for comparison.

[14] The selection of boundary conditions is part of the art of applying this method. Examples covered later will clarify the point. For the present, it is helpful to think of the ψ_m as classical acoustic modes for a volume having rigid walls and the same shape as the combustion chamber in question. The ψ_m therefore do not satisfy exactly the boundary conditions actually existing in a combustor. Hence the right-hand side of (4.27) is an approximation in two respects: the series is truncated to a finite number of terms and it does not satisfy the correct boundary conditions. However, the solution carried out to the next order *does* satisfy the boundary conditions to first order. This important point is discussed in Chapter 10 of Morse and Feshbach (1952). The approximate nature of the modal expansion will be clarified as the analysis proceeds.

Apply Green's theorem to the first integral, substitute the boundary conditions (4.1) a,b and (4.12) a,b and rearrange the result to give

$$\iiint_V \frac{1}{\bar{a}^2}\frac{\partial^2 \tilde{p}'}{\partial t^2}\psi_N dV + k_N^2 \iiint_V \tilde{p}'\psi_N dV = -\left\{\iiint_V h\psi_N dV + \oiint_S f\psi_N dS\right\} \tag{4.30}$$

Now substitute the modal expansion (4.27) in the right-hand side:

$$\frac{\bar{p}_r}{\bar{a}_r^2}\sum_{m=0}^{M}\ddot{\eta}_m(t)\iiint_V \left(\frac{\bar{a}_r}{\bar{a}}\right)^2 \psi_m\psi_N dV - k_n^2\bar{p}_r\sum_{m=0}^{M}\eta_m\iiint_V \psi_m\psi_N dV = E_N^2\frac{\bar{p}_r}{\bar{a}_r^2}F_N \tag{4.31}$$

where

$$F_N = -\frac{\bar{a}_r^2}{\bar{p}_r E_N^2}\left\{\iiint_V h\psi_N dV + \oiint_S f\psi_N dS\right\} \tag{4.32}$$

and $\bar{a}_r$ is a constant reference speed of sound. The second sum reduces, due to the orthogonality of the ψ_m, to $\eta_n E_n^2$. Under the first integrals, write

$$\Delta_a = 1 - \left(\frac{\bar{a}_r}{\bar{a}}\right)^2 \tag{4.33}$$

Then the first sum in (4.31) is

$$\sum_{m=0}^{M}\ddot{\eta}_m(t)\iiint_V (1-\Delta_a)\,\psi_m\psi_N dV = E_N^2\ddot{\eta}_N - \sum_{m=0}^{M}\ddot{\eta}_m(t)\iiint_V \Delta_a\psi_m\psi_N dV \tag{4.34}$$

With these changes, equation (4.31) becomes

$$\ddot{\eta}_N + \omega_N^2\eta_N = F_N + \frac{1}{E_N^2}\sum_{m=0}^{M}\ddot{\eta}_m(t)\iiint_V \Delta_a\psi_m\psi_N dV \tag{4.35}$$

The sum on the right-hand side represents part of the effect of a non-uniform speed of sound in the chamber (if $\Delta_a \neq 0$). To simplify writing we will ignore this term until we consider special problems in later chapters. For solid rockets it is a negligible contribution. If the combustor contains flame sheets, the temperature is piecewise uniform and this term also doesn't appear, but the presence of the discontinuities generates corresponding terms arising from F_N. Thus there are useful situations in which we deal with the system of equations:

$$\ddot{\eta}_N + \omega_N^2\eta_N = F_N \tag{4.36}$$

This result, a set of coupled nonlinear equations with the forcing function F_N given by (4.34), is the basis for practically all of the analysis and theory discussed in the remainder of this book. A corresponding result is given in Appendix B for a purely one-dimensional formulation. In anticipation of later discussions, several general remarks are in order.

(i) The formulation expressed by (4.36) accommodates all relevant physical processes. In the derivation of the conservation equations in Appendix A, only inconsequential approximations were made, notably the neglect of multi-component diffusion and the representation of the reacting multi-phase medium by a single-fluid model. However, only the basic gasdynamics are known explicitly. All other processes must be modeled in suitable forms.

(ii) Despite the apparent generality of (4.36) attention must be paid to an assumption implied in the application of Green's theorem in spatial averaging. That is, the functions involved must possess certain properties of continuity within the volume of averaging. The condition is not satisfied, for example, at a flame sheet, where the velocity is discontinuous, an important exception.

(iii) The selection of functions for the modal expansion (4.27) is not unique; possible alternatives must always be considered. What works best depends on the nature of the boundary conditions. The closer the boundary is to a rigid reflecting surface, the more effective is the choice $\hat{\mathbf{n}}\cdot\nabla\psi_N = 0$, meaning that the acoustic velocity vanishes on the boundary. Because a

combustor must provide for inflow of reactants and exhaust of products, it is simply not possible that the actual enclosure be everywhere rigid and perfectly reflecting. For $\hat{\mathbf{n}} \cdot \nabla \psi_N = 0$ to be a good approximation, as it should be for the modal expansion to serve successfully as a zeroth approximation to the pressure field, the boundary must be 'nearly' reflecting. Choked inlets and outlets satisfy the condition if the Mach number at the chamber side is small (that is, the flow within the volume is consistent with the assumption $\mu \ll 1$). Also, the dynamical response of burning solid propellants is normally such that requiring $\hat{\mathbf{n}} \cdot \nabla \psi_N = 0$ is a good choice. Hence, over a broad useful range of practical conditions, defining the modal expansion functions with (4.12) a,b is a reasonable choice. Exceptions are not rare, however, and care must be exercised. For example, a Rijke tube (Section 2) will contain a heater, or a thin combustion region within the duct. Continuous functions ψ_N may not be good zeroth approximations to the actual behavior discontinuous at the heating zone; moreover, in that case $\hat{\mathbf{n}} \cdot \nabla \psi_N = 0$ at the ends is the proper choice for boundary conditions on the modal functions. More generally, if the temperature field is highly non-uniform, then the zeroth order expansion functions should take that feature into account.

(iv) An enormous advantage of the result (4.36) is its clear interpretation. A general unsteady motion in a combustor is represented by the time-evolution of a system of coupled nonlinear oscillators in one-to-one correspondence with the modes ψ_N. Although the left-hand side of (4.36) describes the motion of a linear oscillator, the forcing function F_N will in general contain terms in η_N representing linear and nonlinear damping, springiness and inertia. Consequently, as we will see, it is easy to find familiar nonlinear differential equations as special cases of (4.36). Such special results aid greatly interpretation of complicated observed behavior in terms of simpler elementary motions. Thus it is important to understand the connections between parameter defining the oscillators, the characteristics of the modes, and the definitions provided in the process of spatial averaging.

(v) Different problems are distinguished chiefly in two respects: Geometry of the combustor; and the form of the forcing function F_N. The forcing function contains the influences of gasdynamics explicitly, but all other processes must be modeled, either with theory or based on experimental results. The geometry and the boundary conditions determine the modal expansion functions ψ_N and the frequencies ω_N. For complicated geometries, as for many large solid propellant rockets and for most gas turbine combustors, computation of the ψ_N and ω_N has been a time-consuming and expensive process. That situation is gradually changing with the development of more capable software.

(vi) The relatively general context in which the oscillator equations have been derived does not exclude simpler problems which can either be treated as special cases or constructed without reference to the procedures worked out here. However, it is then often more difficult to be certain that all important processes are accounted for or properly ignored.

4.4. Application of Time-Averaging. To this point the expansion procedure based on two small parameters has been used only to derive the systems of equations describing successively more difficult classes or problems in Section 3.3.2. There are at least two additional reasons for introducing that procedure. Later we will see how an iterative method based partly on the expansion reduces those systems of equations to more readily soluble forms. In this section we apply time-averaging to convert the second-order equations (4.36) to first order equations. First, two remarks:

(i) Use of time-averaging is motivated by the experimental observation that combustion instabilities commonly show slowly varying amplitudes and phases of the modes contributing to the motions. That behavior is a consequence of the relative weakness of the disturbing processes and is therefore measured by the small parameter μ characteristic of the Mach number of the mean flow. It is essential to understand that it is not the amplitudes themselves (i.e. the parameter ε) that matters. Thus the application of time-averaging in the present context is *not* intended to treat nonlinear behavior, but is based on the weak coupling between the mean flow and the unsteady motions.

(ii) Two-time scaling is an alternative method to time-averaging. The results obtained are identical up to second order acoustics (Section 3.3.3(II) and 3.4), a conclusion not shown here but consistent with similar previous works in other fields.

According to the discussion in Section 3.3.2, we can characterize the functions h and f, and hence the forcing function F_n, as sums of terms each of which is of order μ and of zeroth or first order in ε. Thus for example, the right-hand side of (3.62) a,b has the form

$$-\mu\varepsilon\left\{\{[\mathbf{M}]\}_1+\frac{\varepsilon}{\mu}\{\mathbf{M}\}_2\right\}$$

The divergence of these terms eventually appears in h and F_n. Hence we are justified in taking F_n of order μ; to show this explicitly write (4.36) as

$$\ddot{\eta}_N+\omega_N^2\eta_N=\mu G_N \tag{4.37}$$

In any event, for μ small, the η_N differ but little from sinusoids so (without approximation) it is reasonable to express $\eta_N(t)$ in the equivalent forms

$$\eta_N(t)=r_N(t)\sin\left(\omega_N t+\phi_N(t)\right)=A_N(t)\sin\omega_N t+B_N(t)\cos\omega_N t \tag{4.38}$$

and

$$\begin{aligned} A_N(t)&=r_N\cos\phi_N\ ;\quad B_N=r_N\sin\phi_N\\ r_N&=\sqrt{A_N^2+B_N^2}\ ;\quad \phi_N=\tan^{-1}\left(\frac{A_N}{B_N}\right)\end{aligned} \tag{4.39}$$

One way to proceed follows a physical argument based on examining the time evolution of the energy of the oscillator having amplitude η_N (Culick 1976). The energy $\mathcal{E}_N$ is the sum of kinetic and potential energies,

$$\mathcal{E}_N(t)=\frac{1}{2}\dot{\eta}_N^2+\frac{1}{2}\omega_N^2\eta_N^2 \tag{4.40}$$

The time-averaged values of the energy and power input to the oscillator, due to the action of the force μG_N, are

$$\langle\mathcal{E}_N\rangle=\frac{1}{\tau}\int_t^{t+\tau}\mathcal{E}_N dt'\ ;\quad \langle\mu G_N\dot{\eta}_N\rangle=\frac{1}{\tau}\int_t^{t+\tau}\mu G_N\dot{\eta}_N dt' \tag{4.41}$$

Conservation of energy requires that the time-averaged rate of change of energy equal the time-averaged rate of work done by μG_N on the oscillator:

$$\frac{d}{dt}\langle\mathcal{E}_N\rangle=\mu\langle G_N\dot{\eta}_N\rangle \tag{4.42}$$

From (4.38), the velocity is

$$\dot{\eta}_N=\omega_N r_N\cos\left(\omega_N t+\phi_N\right)+\left[\dot{r}_N\sin\left(\omega_N t+\phi_N\right)+\dot{\phi}_N r_N\cos\left(\omega_N t+\phi_N\right)\right] \tag{4.43}$$

Following Krylov and Bogoliubov (1947) we apply the 'strong' condition that the velocity is always given by the formula for an oscillator is force-free-motion,

$$\dot{\eta}_N=\omega_N r_N\cos\left(\omega_N t+\phi_N\right) \tag{4.44}$$

Hence (4.43) is consistent with this requirement only if

$$\dot{r}_N\sin\left(\omega_N t+\phi_N\right)+\dot{\phi}_N r_N\cos\left(\omega_N t+\phi_N\right)=0 \tag{4.45}$$

Now use the definitions (4.36), (4.38), (4.39) and (4.42) to find

$$\begin{aligned}\mathcal{E}_N&=\frac{1}{2}\omega_N^2 r_N^2\\ \mu G_N\dot{\eta}_N&=\mu G_N\omega_N r_N\cos\left(\omega_N t+\phi_N\right)\end{aligned} \tag{4.46 a,b}$$

The statement "slowly varying amplitude and phase" means that the fractional changes of amplitude and phase are small in one cycle of the oscillation and during the interval of averaging τ if τ is at least equal to the period of the fundamental mode:

$$\frac{\tau}{r_N}\frac{dr_N}{dt} \ll 1\ ; \quad \frac{\tau}{2\pi}\frac{d\phi_N}{dt} \ll 1 \tag{4.47}$$

These inequalities imply that r_N and ϕ_N may be treated as constants during the averaging carried out in (4.41). To see this, imagine that r_N for example, is expanded in Taylor series for some time t_1 in the interval τ, $t < t_1 < t+\tau$:

$$r_N(t) = r_N(t_1) + (t - t_1)\left(\frac{dr_N}{dt}\right)_{t_1} + \cdots$$

For r_N slowly varying, $\dot{r}_N$ doesn't vary much during a period and may be assigned some average value. The increment $t - t_1$ has maximum value τ; so the second term is negligible according to the first of (4.41). Therefore $r_N(t) \approx r_N(t_1)$ for any t_1 in the interval of averaging and the assertion is proved.

Substitution of (4.46) a,b in (4.42) then gives

$$\omega_N r_N \frac{dr_N}{dt} = \mu\frac{r_N}{\tau}\int_t^{t+\tau} G_N \cos(\omega_N t' + \phi_N)dt'$$

and

$$\frac{dr_N}{dt} = \mu\frac{1}{\omega_N\tau}\int_t^{t+\tau} G_N \cos(\omega_N t' + \phi_N)dt' \tag{4.48}$$

The corresponding equation for the phase $\phi_N(t)$ is found by substituting (4.38) and (4.39) in (4.45) to give

$$r_N\frac{d\phi_N}{dt} = -\frac{\mu}{\omega_N}G_N \sin(\omega_N t + \phi_N) \tag{4.49}$$

Now time average this equation over the interval τ, the left-hand side is approximately constant for theorem give above, and the equation for $\phi_N(t)$ is

$$r_N\frac{d\phi_N}{dt} = -\mu\frac{1}{\omega_N\tau}\int_t^{t+\tau} G_N \sin(\omega_N t' + \phi_N)dt' \tag{4.50}$$

With the relations (4.39), equations (4.48) and (4.50) can be converted to equations for A_N and B_N:

$$\begin{aligned}\frac{dA_N}{dt} &= \frac{\mu}{\omega_N\tau}\int_t^{t+\tau} G_N \cos\omega_N t'dt' \\ \frac{dB_N}{dt} &= -\frac{\mu}{\omega_N t}\int_t^{t+\tau} G_N \sin\omega_N t'dt'\end{aligned} \tag{4.51 a,b}$$

Whichever pair one chooses to use, (4.48) and (4.50) or (4.51) a,b, the general formal problem of solving a system of coupled second order equations (4.37) for the oscillators, has been converted to the simpler approximate formal problem of solving a system of coupled first order equations. The essential basis for that conversion is the removal of the fast oscillatory behavior with the definition (4.38), a transformation made possible because the changes of amplitudes and phases take place on a much slower (i.e. longer) time scale than do the oscillations. The presence and role of two time scales is more evident in the following alternative derivation:

From the second equality of (4.38), we find the velocity

$$\dot{\eta}_N = \omega_N\left[A_N\cos\omega_N t - B_N\sin\omega_N t\right] + \left[\dot{A_N}\sin\omega_N t + \dot{B_N}\cos\omega_N t\right]$$

Now enforce the condition corresponding to (4.45),

$$\dot{A_N}\sin\omega_N t + \dot{B_N}\cos\omega_N t = 0 \tag{4.52}$$

and the velocity is

$$\dot{\eta}_N = \omega_N\left[A_N\cos\omega_N t - B_N\sin\omega_N t\right] \tag{4.53}$$

Substitution in (4.37) gives

$$\omega_N \left[\dot{A_N}\cos\omega_N t - \dot{B_N}\sin\omega_N t\right] + \omega_N^2\left[-A_N\sin\omega_N t - B_N\cos\omega_N t\right] + \omega_N^2\left[A_N\sin\omega_N t + B_N\cos\omega_N t\right] = \mu G_N$$

and

$$\dot{A_N}\cos\omega_N t - \dot{B_N}\sin\omega_N t = \frac{\mu}{\omega_N}G_N$$

Multiply by $\cos\omega_N t$ and substitute (4.52) for $\dot{B}_N\cos\omega_N t$ to give

$$\dot{A_N}\cos^2\omega_N t - \sin\omega_N t\left[-\dot{A_N}\sin\omega_N t\right] = \frac{\mu}{\omega_N}G_N\cos\omega_N t$$

so

$$\frac{dA_N}{dt} = \frac{\mu}{\omega_N}G_N\cos\omega_N t \tag{4.54}$$

Similarly,

$$\frac{dB_N}{dt} = -\frac{\mu}{\omega_N}G_N\sin\omega_N t \tag{4.55}$$

We now introduce two time-scales, τ_f the first scale, of the order of the period of the fundamental oscillation (in fact, we might as well set $\tau_f = 2\pi/\omega_1$); and τ_s, the slow scale characterizing transient changes of the amplitudes and phases of the oscillations. Two corresponding dimensionless time variables can be defined, $t_f = t/\tau_f$ and $t_s = t/\tau_s$. Thus we consider the amplitudes and phases to be functions of the slow variable t_s while the forcing functions G_N depend on both t_f and to because they depend on the η_N, $(i = 1, 2, \cdots)$

$$\eta_N = A_N(t_s)\sin\left(2\pi\frac{\omega_N}{\omega}t_f\right) + B_N(t_s)\cos\left(2\pi\frac{\omega_N}{\omega_1}t_f\right)$$

In terms of the dimensionless time variables,

$$\frac{1}{\tau_s}\frac{dA_N}{dt_s} = \frac{\mu}{\omega_N}G_N\cos\omega_N t$$

and averaging over the fast variable we have

$$\frac{1}{\tau_s}\int_{t_f}^{t_f+\tau_f}\frac{1}{\tau_s}\frac{dA_N}{dt'_s}dt'_f = \frac{\mu}{\omega_N}\frac{1}{\tau_f}\int_{t_f}^{t+\tau_f}G_N\cos\left(2\pi\frac{\omega_N}{\omega_1}t'_f\right)dt'_f$$

On the left-hand side, dA_N/dt'_s is assume to be sensibly constant in the interval τ_f and we have

$$\frac{1}{\tau_s}\frac{dA_N}{dt'_s} = \frac{\mu}{\omega_N\tau_f}\int_{t_f}^{t+\tau_f}G_N\left(t'_f, t'_s\right)\cos\left(2\pi\frac{\omega_N}{\omega_1}t'_f\right)dt'_f \tag{4.56}$$

Those parts of G_N depending on t'_s are taken also to be constant and if we now rewrite this equation in terms of dimensional variables, we recover (4.51)a with $\tau = \tau_f = 2\pi/\omega$. Similar calculations will produce again (4.51)b. Note that due to the nonlinear coupling, the amplitude and phases of all modes normally change on roughly the same scale as that for the fundamental mode; thus the single interval of averaging works for all modes.

In Section 7.2 we will use a continuation method to assess the ranges of parameters and other conditions for which the first order equations give accurate results when compared with solutions to the complete oscillator equations. In the development of the theoretical matters described in this book, the sets of first order equations have been central. They remain extremely useful both for theoretical work and for applications.

4.5. The Procedure for Iterative Solution. The oscillator equations (4.33) and (4.34) are not yet in a form that can be readily solved because the functions F_N, defined by (4.30) contain not only p' but also the dependent variables ρ', T' and $\mathbf{u}'$ in the functions h and f. With the two-parameter expansion as the basis, the iteration procedure provides a means for expressing F_N in terms of p' only. Thus eventually the oscillator equations become a system soluble for the modal amplitudes $\eta_N(t)$. There are of course approximations required, but magnitudes of their effects can always be estimated in terms of the parameters ε and μ. To appreciate how the procedure is constructed, it is helpful always to keep in mind the correspondence between the smallness of ε and μ, and the distortions they represent of the unperturbed classical acoustic field.

There are two chief types of distortions or perturbations: Those represented by ε, arising as nonlinear effects of finite amplitudes,[15] classified generally as energy transfer between modes; and those measured by μ, consequences of interactions, hence energy transfer, between the steady and unsteady fields. Each of those types of perturbations may be identified within the volume in question and at the boundary. Quite generally, then, we must take into account perturbations of the classical acoustic field, associated with three kinds of energy transfer: linear transfer between the mean and fluctuating motions; nonlinear transfer between modes, or mode coupling, independent of the average flow field; and nonlinear energy transfer between the mean flow and fluctuating fields. The way in which we view and accommodate those perturbations determines our choice of basis functions ψ_N used in the modal expansion (4.27).

4.5.1. *Linear Energy Transfer Between the Mean and Fluctuating Motions.* Any combustor designed for steady, or at most slowly varying conditions on the acoustic time scale, must have provision for supplying reactants and exhausting products. There must therefore be average flow within the volume and through openings in the enclosing boundary. If the reactants are liquid or gaseous, then openings exist for both inflow and outflow. In combustors for solid propellants, flow enters at the boundary but there are not openings for that purpose.

(A) Volumetric Interactions

The general equations of motion in principle contain all interactions between the mean and fluctuating motions within the volume. Many are shown explicitly as the bracketted terms $[\bar{\mathbf{M}}]$, $\{\bar{\mathbf{M}}\}$, $[\rho_1]$, $\{p_1\}$, $\cdots$ defined in Section (3.3). Those terms in the forms given there account for interactions of the mean flow velocity with the acoustic field and have long served that purpose well in investigations of combustion instabilities. Additional consideration are required to treat interactions associated with entropy and vorticity waves, including turbulence and noise, a subject covered in Section (7.4).

Special effects also arise when the average temperature field is nonuniform; the last term in (4.33) represents one consequence of nonuniform average temperature but others are contained in the formula given for h, equation (3.55). Nonuniformities of temperature cause nonuniformities in the speed of sound which may be regarded as nonuniformities in the index of refraction for acoustic waves. Thus in the general context of wave motions, phenomena such as refraction and diffraction must arise. However, the analysis covered here for wave systems slowly varying on the acoustic time scale, obscures wave phenomena of that sort; they have rarely been addressed explicitly in the field of combustion instabilities and then only in connection with very special problems. However, the consequences of refraction and diffraction are contained implicitly in distortions of the structure of the steady waves.

It is extremely important that large differences in the average speed of sound be accounted for as accurately as possible. That is best done by including them in the functions used in the modal expansion. Formally that amounts to including all terms in h representing linear interactions between the acoustic and mean fields, in the equations for the ψ_m. That is, such large perturbations are better not included in the procedure best suited for dealing with small perturbations. In practice, the only example of this tactic have been concerned with flows in ducts containing a compact zone of heating thin relative to the acoustic wavelength. The modal functions are then formed in piecewise fashion, the usual wave equation being solved separately for the two regions characterized by different uniform temperatures upstream and downstream of the zone of heating treated as a surface of discontinuity. Then the functions are joined with suitable matching conditions.

For the most part, therefore, energy transfer between the acoustic field and the mean flow within the volume of a combustor is due to interactions with the mean velocity, characterized by the parameter μ. The analysis is strictly limited to perturbations linear in the Mach number of the mean flow (see the footnote in the preceding page).

(B) Boundary Conditions

The situation in respect to processes at the boundary is considerably more complicated and in fact cannot be placed in a firm basis without detailed examination of ancillary problems. Only two possibilities have so far been

[15] Recall that in this work, nonlinear behavior is measured in terms of the amplitude ε of the unsteady motions. It is intrinsic to their derivation (Section 3) that the governing equations are linear in μ, i.e. in the Mach number of the mean flow.

of practical interest: physical openings in the boundary of the combustor; and a burning surface. Conditions to be set on the acoustic field at an opening depend on the flow field through and outside the boundary. In classical acoustics with no flow, an opening into an atmosphere held at constant pressure is almost perfectly reflecting, with the fluctuating pressure nearly zero in the plane of the opening. A perfectly reflecting rigid wall causes the fluctuating velocity to vanish there. Thus in those two limits, the boundary conditions to 0^{th} order on the pressure field are respectively $p' = 0$ and $\hat{\mathbf{n}} \cdot \nabla p' = 0$.

Subsonic flow through an orifice presents a boundary condition to acoustic waves closer to the case of no flow, $p' \approx 0$, than to a rigid wall. On the other hand, if the inlet flow is choked upstream close[16] to the orifice, or the outlet flow exhausts through a choked nozzle, the boundary condition is closer to the for a rigid wall, $\hat{\mathbf{n}} \cdot \nabla p' \approx 0$. That is the case for propulsion systems, with the possible exception of the primary combustion chamber in a gas turbine. The actual boundary conditions are more complicated but for linear behavior can be represented by impedance or admittance functions defined for steady waves. For the more common case of choked flows, that boundary condition is expressed as

$$\hat{\mathbf{n}} \cdot \hat{\mathbf{u}}\left(\mathbf{r}_s, w\right) = A_s\left(\mathbf{r}_s, w\right) \hat{p}\left(\mathbf{r}_s, w\right) = \mu a_s\left(\mathbf{r}_s, w\right) \hat{p}\left(\mathbf{r}_s, w\right) \tag{4.57}$$

where $A_s = \mu a_s$ is the dimensional admittance function shown here to be proportional to the Mach number of the average flow. (Tsien 1952; Crocco and Cheng 1956; Culick 1961, 1963) Generally, A_s is a complex function,

$$A_s = |A_s| e^{i\phi_A} = \mu |a_s| e^{i\phi_A} \tag{4.58}$$

The representation (4.57) is based on the idea that when exposed to an oscillatory fluctuation of pressure, a physical surface responds in first approximation such that its velocity normal to itself is proportional to the impressed pressure, possibly with a phase or time delay. That idea is extended in the present context to describe fluctuations of flow at a fictious surface forming part of the boundary enclosing the combustor volume, or at the downstream edge of the combustion zone at a burning surface. Thus we have a simple and direct way of making explicit the first term in the definition (3.57) of the boundary function f for steady waves:

$$\begin{aligned} \bar{\rho} \frac{\partial \mathbf{M}'}{\partial t} \cdot \hat{\mathbf{n}} = \bar{\rho}\bar{a} \frac{\partial \mathbf{u}'}{\partial t} \cdot \hat{\mathbf{n}} &= \bar{\rho}\bar{a} \frac{\partial}{\partial t} \left[\hat{\mathbf{n}} \cdot \hat{\mathbf{u}}\left(\mathbf{r}_s, w\right) e^{i\bar{a}kt}\right] \\ &= \mu \bar{\rho}\bar{a} a_s\left(\mathbf{r}_s, t\right) i\bar{a}k \hat{p}\left(\mathbf{r}_s, w\right) e^{i\bar{a}kt} \\ &= \mu \bar{\rho}\bar{a}^2 k \left(i|a_s| e^{i\phi_a}\right) \hat{p}\left(\mathbf{r}_s, w\right) e^{i\bar{a}kt} \end{aligned} \tag{4.59}$$

An equivalent form is

$$\bar{\rho} \frac{\partial \mathbf{M}'}{\partial t} \cdot \hat{n} = \mu \bar{\rho}\bar{a}^2 k \left\{-Im(a_s) + i\, Re(a_s)\right\} \hat{p}\left(\mathbf{r}_s, w\right) e^{i\bar{a}kt} \tag{4.60}$$

Although the admittance function is defined for steady waves initially, (4.49) can be converted to a form approximately applicable to problems having arbitrary dependence on time. The time derivative of some function φ for steady waves, so we can make the correspondence

$$\frac{\partial \varphi}{\partial t} \longleftrightarrow i\bar{a}k \frac{\partial \varphi}{\partial t}$$

Hence we write (4.49) as

$$\bar{\rho} \frac{\partial \mathbf{M}'}{\partial t} \cdot \hat{\mathbf{n}} = \mu \bar{\rho}\bar{a} \left[\bar{a}k\, Im\left\{a_s\right\} p' + \, Re\left\{a_s\right\} \frac{\partial p'}{\partial t}\right] \tag{4.61}$$

This form of a boundary condition will be useful in later applications.

The chief point here is that for choked inlet and exhaust flows, the function f in the boundary condition $\hat{\mathbf{n}} \cdot \nabla p' = -f$ is of order μ. That is, perturbations from the condition defining a rigid impermeable wall are all proportional to the magnitude of the Mach number of the mean flow. Corresponding reasoning applies to the less important case of subsonic flow exhausting into surroundings held at constant pressure.[17] Now we set the

[16] 'Close' means within a short distance relative to the wavelength of the dominant oscillation.

[17] Less important for practical applications. However there are many laboratory devices operating at close to atmospheric pressure and exhausting into the atmosphere for which the condition treated here is appropriate.

boundary condition by using (3.51) evaluated at the boundary; for linear steady waves we have

$$p' = \frac{1}{\bar{a}k}\left[\gamma\bar{p}\nabla\cdot\mathbf{M}_1' + \mu\{[p]_1\} - \frac{1}{\varepsilon}\mathcal{P}'\right]_{\mathbf{r}=\mathbf{r}_s} \tag{4.62}$$

Again we may define an admittance function to eliminate $\nabla\cdot\mathbf{M}_1'$ in favor of the local pressure fluctuation. We leave the calculation to special applications.

We conclude that for linear problems, perturbations of the classical acoustics problem due to energy transfer between the mean and unsteady fields are represented to order μ, both within the volume and at the boundary. This result is of course consistent with the order to which the differential equations are valid within the approximation used here (see a remark following equation (3.39). For that reason, we cannot in any event carry terms of higher order in μ unless the governing equations used here are re-derived.

As an example to illustrate some implications of the preceding remarks, consider the case of flow through a uniform duct of length L, supplied through choked valves and exhausting through a choked nozzle. Suppose that by some means, for example by installing a speaker, oscillations can be excited and sustained in the duct. If there were no flow and rigid plates were placed at both ends ($z = 0, L$), classical 'organ pipe' acoustic modes would be found experimentally, having frequencies $\omega_N = n(\bar{a}/L)$. The velocity and pressure distributions for these steady axial modes are proportional to $\sin k_N x$ and $\cos k_N x$ respectively. Suppose we set, for example,

$$p'(z,t) = \hat{p}_0 \cos k_N z \cos\omega_N t \tag{4.63}$$

where $\omega_N = \bar{a}k_N$. The unperturbed acoustic momentum equation,

$$\bar{\rho}\frac{\partial\mathbf{u}'}{\partial t} = -\nabla p'$$

is satisfied with (4.52) if $\mathbf{u}'$ has only the axial component,

$$u'(z,t) = \frac{\hat{p}_0}{\bar{\rho}\bar{a}}\sin k_N z \sin\omega_N t \tag{4.64}$$

The velocity field has nodes ($u' = 0$) at the ends and the pressure field has anti-nodes, reaching maximum amplitude $\hat{p}_0$ when $t = 0,\ 2\pi/\omega_N,\ 4\pi/\omega_N,\ \cdots$. Now suppose that average flow is introduced and that the cross-sectional areas available for the flow upstream and downstream are small fractions of the cross-sectional area of the duct. Then the average Mach numbers at $z = 0,\ L$ are small ($\mu \ll 1$). Hence the distortions of the classical organ pipe modes are small. In particular, the modes of the velocity field are slightly displaced by the same amounts downstream of their unperturbed positions at $x = 0,\ L$. Thus the wavelength and frequency of the modes are unchanged and the unperturbed mode shapes are close approximations to the actual shapes with the flow, as sketched in Figure 4.1.

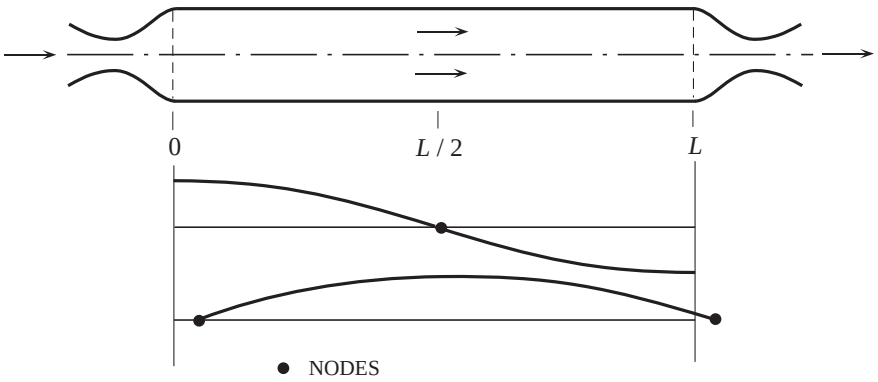

FIGURE 4.1. Fundamental Longitudinal Mode, Velocity Mode Shape: – – – – Classical (no flow); —— Duct with flow choked upstream and downstream

If the Mach numbers at the entrance ($z = 0$) and at the exit ($z = L$) are not small, then the nodes of the velocity wave are displaced by larger amounts, but the wavelength, and hence the frequency, suffer only small changes. This behavior suggests what is true quite generally in practice, that the processes in a combustion

chamber have relatively small effects in the frequencies of the normal modes. Consequently, as we will emphasize repeatedly, comparison of observed frequencies with those predicted is not a useful basis for assessing the correctness of the theory in question.

4.5.2. *Energy Transfer Between Modes; Nonlinear Mode Coupling.* If the functions ψ_N used in the modal expansion are those computed according to classical acoustics, then in general linear coupling between modes will appear in the right-hand sides of the systems (4.33) and (4.34). When the mean flow field is nonuniform, interactions between the mean and fluctuating fields will cause linear mode coupling proportional to the average Mach number. Formally such contributions are included among those discussed in the preceding section, i.e. they are of order μ.

In principle, linear coupling between modes can be formally eliminated by transformation to a new set of modal expansion functions by diagonalizing the matrix of coefficients (Culick 1997). There may be some applications for which the linear coupling should be explicitly treated, but here we assume that either linear coupling is absent on physical grounds or has been eliminated by suitable transformation.

Hence energy transfer between modes is of order ε^2 or higher and is necessarily nonlinear; calculations in the next section show that we can write the system (4.34) schematically in the form

$$\ddot{\eta}_N + \omega_N^2 \eta_N = -\mu \left(D_N \dot{\eta}_N + E_N \eta_N \right) + F_N^{NL} \tag{4.65}$$

The function F_N^{NL} contains all nonlinear processes. According to its development in Section 3 consists of a sum of groups of terms of order ε, ε^2, $\cdots$, $\mu\varepsilon$, $\mu\varepsilon^2$, $\cdots$. In general, F_N cannot be represented by a diagonal matrix: Nonlinear coupling of the modes always exists and, among other consequences, is an important process in the evolution of linear unstable motions into stable limit cycles.

4.5.3. *Zeroth and First Order Solutions to the Oscillator Equation.* We defer to a later section analysis including nonlinear energy transfer of order $\mu\varepsilon$, and we assume that the average temperature is approximately uniform, so the last term of (4.33) is negligible. The problem comes down to solving (4.34) for the $\eta_N(t)$,

$$\ddot{\eta}_N + \omega_N^2 \eta_N = F_N \tag{4.66}$$

with

$$F_N = -\frac{\bar{a}_r^2}{\bar{p}_r E_N^2} \left\{ \iiint_v h \psi_N dV + \oiint_S f \psi_N dS \right\} \tag{4.67}$$

and h and f are given by (3.55) and (3.57):

$$\begin{aligned} h = & -\bar{\rho} \left[\nabla \cdot \left(\bar{\mathbf{M}} \cdot \nabla \mathbf{M}' + \mathbf{M}' \cdot \nabla \bar{\mathbf{M}} \right) - \frac{1}{\bar{a}^2} \frac{\partial}{\partial t} \left(\bar{\mathbf{M}} \cdot \nabla p' + \gamma p' \nabla \cdot \bar{\mathbf{M}} \right) \right] \\ & - \left\{ \bar{\rho} \nabla \cdot \left(\mathbf{M}' \cdot \nabla \mathbf{M}' + \frac{\rho'}{\bar{\rho}} \frac{\partial \bar{\mathbf{M}}'}{\partial t} \right) - \frac{1}{\bar{a}^2} \frac{\partial}{\partial t} \left(\mathbf{M} \cdot \nabla p' + \gamma p' \nabla \cdot \mathbf{M} \right) \right\} \\ & + \left[\frac{1}{\bar{\rho}} \nabla \cdot \left(\frac{1}{\bar{\rho}} \boldsymbol{\mathfrak{F}}' \right) - \frac{1}{\bar{a}^2} \frac{\partial \boldsymbol{\mathfrak{P}}'}{\partial t} \right] + \left\{ \frac{1}{\bar{p}} \nabla \cdot \left(\frac{1}{\bar{\rho}} \boldsymbol{\mathfrak{F}}' \right) - \frac{1}{\bar{a}^2} \frac{\partial \boldsymbol{\mathfrak{P}}'}{\partial t} \right\} \end{aligned} \tag{4.68}$$

$$f = \bar{\rho} \frac{\partial \mathbf{M}'}{\partial t} \cdot \hat{\mathbf{n}} + \hat{\mathbf{n}} \cdot \left[\bar{\rho} \mathbf{M}' \cdot \nabla \bar{\mathbf{M}} + \bar{\mathbf{M}} \cdot \nabla \mathbf{M}' \right] + \hat{\mathbf{n}} \cdot \left\{ \bar{\rho} \mathbf{M}' \cdot \nabla \mathbf{M}' + \rho' \frac{\partial \mathbf{M}'}{\partial t} \right\} + \left[\boldsymbol{\mathfrak{F}}' \right] \cdot \hat{\mathbf{n}} + \left\{ \boldsymbol{\mathfrak{F}}' \right\} \cdot \hat{\mathbf{n}} \tag{4.69}$$

Recall that the left-hand side of (4.55) follows upon inserting in the linear wave operator the modal expansion (4.27) for p';

$$p' = \bar{p}_r \sum_{m=1}^{M} \eta_m(t) \psi_m(\mathbf{r}) \tag{4.70}$$

The iterative procedure is a way of expressing the driving forces F_N in terms of the amplitudes η_m, so (4.55) becomes a system of equations for the amplitudes. As we have explained earlier (Section 3.3) we use ε as a

measure of the size of the pressure disturbance and write always

$$p' = \varepsilon p_1(\mathbf{r}_1, t) \tag{4.71}$$

However, we must allow the other dependent variables vary with ε in a more complicated manner; it is reasonable at this point to assume dependence as a power series in ε:

$$\begin{aligned} \mathbf{M}' &= \varepsilon \mathbf{M}_1 + \varepsilon^2 \mathbf{M}_2 + \cdots \\ T' &= \varepsilon T_1 + \varepsilon^2 T_2 + \cdots \end{aligned} \tag{4.72}$$

and so forth. All components of the fluctuations, p_1, $\mathbf{M}_1$, $\mathbf{M}_2$, $\cdots$, T_1, T_2, $\cdots$ become distorted by the mean flow. That possibility is taken into account by writing

$$\begin{aligned} p' =& \varepsilon p_1 = \varepsilon \left[p_{10} + \mu p_{11} + \mu^2 p_{12} + \cdots \right] \\ \mathbf{M}' =& \varepsilon \mathbf{M}_1 + \varepsilon^2 \mathbf{M}_2 + \cdots = \varepsilon \left[\mathbf{M}'_{10} + \mu \mathbf{M}_{11} + \cdots \right] \\ & + \varepsilon^2 \left[\mathbf{M}'_{20} + \mu \mathbf{M}_{21} + \cdots \right] \\ T =& \varepsilon T_1 + \varepsilon^2 T_2 + \cdots = \varepsilon \left[T_{10} + \mu T_{11} + \cdots \right] \\ & + \varepsilon^2 \left[T_{20} + \mu T_{21} + \cdots \right] \end{aligned} \tag{4.73}$$

It is apparent that the number of functions to be determined rapidly gets out of hand as more terms are retained in the series expansion. However to the order we choose to investigate here, that difficulty doesn't appear, for the following reason. Examine a typical terms in h say the first in each of the brackets:

$$\begin{aligned} h &= -\bar{\rho} \left[\nabla \cdot \left(\bar{\mathbf{M}}_1 \cdot \nabla \mathbf{M}' \right) + \cdots \right] - \left\{ \bar{\rho} \nabla \cdot \left(\mathbf{M}' \cdot \nabla \mathbf{M}' \right) + \cdots \right\} + \cdots \\ &= -\mu \bar{\rho} \nabla \cdot \left[\bar{\mathbf{M}}_1 \cdot \nabla \left(\varepsilon \mathbf{M}'_1 + \varepsilon^2 \mathbf{M}'_2 + \cdots \right) + \cdots \right] - \bar{\rho} \left\{ \nabla \cdot \left(\varepsilon \mathbf{M}'_1 + \varepsilon^2 \mathbf{M}'_2 + \cdots \right) \cdot \nabla \left(\varepsilon \mathbf{M}'_1 + \varepsilon^2 \mathbf{M}'_2 + \cdots \right) + \cdots \right\} + \cdots \end{aligned}$$

Now substitute (4.62) to give

$$\begin{aligned} h =& -\mu \bar{\rho} \nabla \cdot \left[\bar{\mathbf{M}}_1 \cdot \nabla \left(\varepsilon \mathbf{M}'_{10} + \varepsilon \mu \mathbf{M}'_{11} + \cdots + \varepsilon^2 \mathbf{M}'_{20} + \varepsilon^2 \mu \mathbf{M}'_{21} + \cdots \right) + \cdots \right] = \\ & - \bar{\rho} \nabla \cdot \left\{ \left(\varepsilon \mathbf{M}_{10} + \varepsilon \mu \mathbf{M}'_{11} + \cdots \right) \cdot \nabla \left(\varepsilon \mathbf{M}'_{10} + \varepsilon \mu \mathbf{M}'_{11} + \cdots \right) + \cdots \right\} + \cdots \end{aligned}$$

Multiplying the various brackets and showing explicitly only those terms to be retained, we find

$$h = -\mu \varepsilon \bar{\rho} \nabla \cdot \left[\bar{\mathbf{M}}_1 \cdot \nabla \mathbf{M}'_{10} + \cdots \right] - \bar{\rho} \nabla \cdot \left\{ \varepsilon^2 \mathbf{M}_{10} \cdot \nabla \mathbf{M}_{10} + \cdots \right\} + \cdots$$

This procedure leads eventually to the forms for h and f with only terms of order $\mu\varepsilon$ and ε^2:

$$\begin{aligned} h =& -\mu\varepsilon \left[\bar{\rho} \nabla \cdot \left(\bar{\mathbf{M}}_1 \cdot \nabla \mathbf{M}_{10} + \mathbf{M}_{10} \cdot \nabla \bar{\mathbf{M}}_1 \right) - \frac{1}{\bar{a}^2} \frac{\partial}{\partial t} \left(\bar{\mathbf{M}}_1 \cdot \nabla p_{10} + \gamma p_{10} \nabla \cdot \bar{\mathbf{M}}_1 \right) \right] \\ & - \varepsilon^2 \left\{ \bar{\rho} \nabla \cdot \left(\mathbf{M}_{10} \cdot \nabla \mathbf{M}_{10} + \frac{\rho_{10}}{\bar{\rho}} \frac{\partial \mathbf{M}_{10}}{\partial t} \right) - \frac{1}{\bar{a}^2} \frac{\partial}{\partial t} \left(\mathbf{M}_{10} \cdot \nabla p_{10} + \gamma p_{10} \nabla \cdot \mathbf{M}_{10} \right) \right\} \\ & + \mu\varepsilon \left[\frac{1}{\bar{\rho}} \nabla \cdot \left(\frac{1}{\bar{\rho}} \boldsymbol{\mathcal{F}}' \right) - \frac{1}{\bar{a}^2} \frac{\partial \boldsymbol{\mathcal{P}}'}{\partial t} \right] + \varepsilon^2 \left\{ \frac{1}{\bar{\rho}} \nabla \cdot \left(\frac{1}{\bar{\rho}} \boldsymbol{\mathcal{F}}' \right) - \frac{1}{\bar{a}^2} \frac{\partial \boldsymbol{\mathcal{P}}'}{\partial t} \right\}_{\varepsilon^2} \end{aligned} \tag{4.74}$$

$$\begin{aligned} f =& \bar{\rho} \left[\frac{\partial \mathbf{M}'}{\partial t} \cdot \hat{\mathbf{n}} \right]_{\mu\varepsilon} + \bar{\rho} \left\{ \frac{\partial \mathbf{M}'}{\partial t} \cdot \hat{\mathbf{n}} \right\}_{\varepsilon^2} + \mu\varepsilon \bar{\rho} \hat{\mathbf{n}} \cdot \left[\mathbf{M}_{10} \cdot \nabla \bar{\mathbf{M}}_1 + \bar{\mathbf{M}}_1 \cdot \nabla \mathbf{M}_{10} \right] \\ & + \varepsilon^2 \bar{\rho} \hat{\mathbf{n}} \cdot \left\{ \mathbf{M}_{10} \cdot \nabla \mathbf{M}_{10} \right\} + \mu\varepsilon \left[\boldsymbol{\mathcal{F}}' \cdot \hat{\mathbf{n}} \right]_{\mu\varepsilon} + \varepsilon^2 \left\{ \boldsymbol{\mathcal{F}}' \cdot \hat{\mathbf{n}} \right\}_{\varepsilon^2} \end{aligned} \tag{4.75}$$

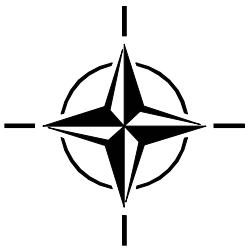

5. SOME FUNDAMENTALS OF ACOUSTICS

According to the experiences related in Section 1, combustion instabilities may be regarded as unsteady motions closely approximated as classical acoustical motions with perturbations due ultimately to combustion processes. That view, initially an emprical conclusion, motivated the general form of the analytical framework constructed in Section 4. Relatively little knowledge of classical acoustics is required to understand and apply that construction formally.

However, interpretation of the details of observed behavior, and effective use of the theory to develop accurate representations of actual motions in combustors require firm understanding of the fundamentals of acoustics. The purpose of this section is to provide a condensed summary of the basic parts of the subject most relevant to the main subject of this book. We therefore ignore those processes distinguishing combustion chambers from other acoustical systems. Except for brief discussion of nonlinear gas dynamics, we restrict attention to the Problem O defined in Sections 3.3.3 and 3.4.

5.1. The Linearized Equations of Motion; The Velocity Potential. We will be concerned here with unsteady motions in a pure non-reacting gas at rest. The governing equations are 3.40 for Problem O, Classical Acoustics, leading to the corresponding wave equation and its boundary condition, equations 3.52 with h_0 and f_0 given by 3.55 for constant average density $\bar{\rho}$ and written with dimensional variables:

$$\nabla^2 p' - \frac{1}{\bar{a}^2}\frac{\partial^2 p'}{\partial t^2} = \nabla\cdot\boldsymbol{\mathcal{F}}' - \frac{1}{\bar{a}^2}\frac{\partial \mathcal{P}'}{\partial t}$$
$$\hat{\mathbf{n}}\cdot\nabla p' = -\bar{\rho}\frac{\partial \mathbf{u}'}{\partial t}\cdot\hat{\mathbf{n}} - \boldsymbol{\mathcal{F}}'\cdot\hat{\mathbf{n}} \qquad (5.1)\ \text{a,b}$$

In the absence of condensed material, the definitions (A.18) and (A.20) of the unperturbed functions $\boldsymbol{\mathcal{F}}$ and $\mathcal{P}$ are:

$$\boldsymbol{\mathcal{F}} = \nabla\cdot\overleftrightarrow{\boldsymbol{\tau}}_v + \mathbf{m}_e - \mathbf{u}w_e \qquad (5.2)$$

$$\mathcal{P} = \frac{R}{C_v}\left[\overleftrightarrow{\boldsymbol{\tau}}_v\cdot\nabla\cdot\mathbf{u} - \nabla\cdot\mathbf{q} - Q_e\right] + RTw_e \qquad (5.3)$$

where

$\overleftrightarrow{\boldsymbol{\tau}}_v$: viscous stress tensor (force/area)

$\mathbf{q}$: rate of conductive heat transfer (energy/area-s)

$\mathbf{m}_e$: rate of momentum addition by external sources (mass-velocity/volume-s)

w_e : rate of mass addition by external sources (mass/volume-s)

Q_e : rate of energy addition by external sources (energy/volume-s)

Thus the function $\boldsymbol{\mathcal{F}}$ contains all processes causing changes of momentum of the gas, except for that due to internal pressure differences; and $\mathcal{P}$ represents all sources of energy addition. The linearized forms of the source terms will be constructed as required for specific problems. For most of this section we will treat only problems for which h_0 and f_0 vanish, giving the simplest equations for classical acoustics,

$$\nabla^2 p' - \frac{1}{\bar{a}^2}\frac{\partial^2 p'}{\partial t^2} = 0$$
$$\hat{\mathbf{n}}\cdot\nabla p' = 0 \qquad (5.4)\ \text{a,b}$$

With no sources in the volume or on the boundary, motions exist only for initial value problems in which the pressure and its time derivative are specified at some initial time, t_0.

In this case, the wave equation is used to describe freely propagating waves following an initial disturbance or, when the boundary condition (5.13)b is enforced, the normal modes for a volume enclosed by a rigid boundary. The condition $\hat{\mathbf{n}}\cdot\nabla p' = 0$ means that the velocity normal to the boundary is zero, because the acoustic velocity is computed from the acoustic momentum (3.40)b written in dimensional form with $\boldsymbol{\mathcal{F}} = 0$:

$$\bar{\rho}\frac{\partial \mathbf{u}'}{\partial t} = -\nabla p' \qquad (5.5)$$

so

$$\hat{\mathbf{n}} \cdot \nabla p' = \bar{\rho} \frac{\partial \mathbf{u}'}{\partial t}$$

from which

$$\frac{\partial}{\partial t} (\hat{\mathbf{n}} \cdot \mathbf{u}') = -\frac{1}{\bar{\rho}} \hat{\mathbf{n}} \cdot \nabla p' = 0 \tag{5.6}$$

Hence $\hat{\mathbf{n}} \cdot \mathbf{u}' = 0$ always

We have just derived the equations for classical acoustics by specializing the general equations of unsteady motion. It is also useful to arrive at the same conclusion in a slightly different way, beginning with the equations for inviscid motion in a homogeneous medium:

$$\textit{Conservation of Mass}: \qquad \frac{\partial \rho}{\partial t} + \nabla \cdot (\rho \mathbf{u}) = 0 \tag{5.7}$$

$$\textit{Conservation of Momentum}: \qquad \rho \frac{\partial \mathbf{u}}{\partial t} + \rho \mathbf{u} \cdot \nabla \mathbf{u} + \nabla p = 0 \tag{5.8}$$

$$\textit{Conservation of Energy}: \qquad \rho \frac{\partial}{\partial t} \left(e + \frac{1}{2} u^2 \right) + \rho \mathbf{u} \cdot \nabla \left(e + \frac{1}{2} u^2 \right) + \nabla \cdot (p \mathbf{u}) = 0 \tag{5.9}$$

$$\textit{Equation of State}: \qquad p = \rho R T \tag{5.10}$$

Remove the kinetic energy from the energy equation by subtracting $\mathbf{u}\cdot$ (momentum equation) to give

$$\rho \frac{De}{Dt} + p \nabla \cdot \mathbf{u} = 0 \tag{5.11}$$

where $\frac{D}{Dt} = \frac{\partial(\quad)}{\partial t} + \mathbf{u} \cdot \nabla(\quad)$. Because all irreversible processes have been ignored the entropy of a fluid element remains constant, $\frac{Ds}{Dt} = 0$, a result that follows directly by substituting the mass and energy equations in the thermodynamic definition of the entropy of an element:

$$\rho \frac{Ds}{Dt} = \rho \frac{De}{Dt} - \frac{p}{\rho} \frac{D\rho}{Dt} = -p \nabla \cdot \mathbf{u} + \frac{p}{\rho} (\rho \nabla \cdot \mathbf{u}) = 0 \tag{5.12}$$

Taking the density to be a function of pressure and entropy, we can write for an isentropic process

$$d\rho = \left(\frac{\partial \rho}{\partial s} \right)_p ds + \left(\frac{\partial \rho}{\partial p} \right)_s dp = \left(\frac{\partial \rho}{\partial p} \right)_s dp = \frac{1}{a^2} dp \tag{5.13}$$

where

$$a^2 = \left(\frac{\partial \rho}{\partial p} \right)_s \tag{5.14}$$

will turn out to be the speed of propagation of small disturbances, the 'speed of sound'. With this definition, we can rewrite the continuity equation (5.7) for the pressure:

$$\frac{\partial p}{\partial t} + \rho a^2 \nabla \cdot \mathbf{u} + \mathbf{u} \cdot \nabla p = 0 \tag{5.15}$$

This result is quite general: in particular, its derivation did not involve using the special characteristics of a perfect gas.

Alternatively, we may derive this equation for the special case of a perfect gas for which $de = C_v(T) dT$ and the equation of state is (5.10). Add T times (5.7) to C_v^{-1} times (5.11) with $de = C_v dT$; then use (5.10) to find

$$\frac{\partial p}{\partial t} + \left(1 + \frac{R}{C_V} \right) p \nabla \cdot \mathbf{u} + \mathbf{u} \cdot \nabla p = 0 \tag{5.16}$$

But $R = C_p - C_v$, so $R/C_v = \gamma - 1$ for a perfect gas. Comparison of (5.14) and (5.15) gives the formula for the speed of sound in a perfect gas:

$$a^2 = \sqrt{\frac{\gamma p}{\rho}} = \sqrt{\gamma R T} \tag{5.17}$$

For an isentropic process of a perfect gas, equation (5.13) can be integrated,

$$d\rho = a^2 dp = \frac{\rho}{\gamma p} dp$$

which gives

$$p = p_0 \left(\frac{\rho}{\rho_0} \right)^{\gamma} \tag{5.18}$$

where ρ_0, p_0 are constant reference values.

We may now eliminate the density from the momentum equation (5.8) to find

$$\frac{\partial \mathbf{u}}{\partial t} + \mathbf{u} \cdot \nabla \mathbf{u} + \frac{1}{\rho_0} \left(\frac{p_0}{p} \right)^{1/2} \nabla p = 0 \tag{5.19}$$

Finally, we obtain the wave equation for the pressure by differentiating (5.16) with respect to time and substituting (5.19) and $a^2 = \gamma p/\rho$:

$$\frac{\partial^2 p}{\partial t^2} - a_0^2 \frac{p}{p_0} \nabla \cdot \left[\frac{\nabla p}{(p/p_0)^{1/\gamma}} \right] = \gamma p \nabla \cdot (\mathbf{u} \cdot \nabla \mathbf{u}) - \gamma \frac{\partial p}{\partial t} \nabla \cdot \mathbf{u} - \frac{\partial}{\partial t} (\mathbf{u} \cdot \nabla p) \tag{5.20}$$

The boundary condition is defined by taking the component of (5.19) normal to the boundary:

$$\hat{\mathbf{n}} \cdot \nabla p = - \left(\frac{p}{p_0} \right)^{1/2} \rho_0 \left[\hat{\mathbf{n}} \cdot \frac{\partial \mathbf{u}}{\partial t} + \hat{\mathbf{n}} \cdot \nabla (\mathbf{u} \cdot \nabla \mathbf{u}) \right] \tag{5.21}$$

Equation (5.20) and its boundary condition are easily linearized by assuming that the gas is at rest and that the fluctuations are all of the same order. To second order in the fluctuations we find

$$\begin{aligned} \frac{\partial^2 p'}{\partial t^2} - a_0^2 \nabla^2 p' = & \left\{ p_0 \nabla \cdot (\mathbf{u}' \cdot \nabla \mathbf{u}') - \gamma \frac{\partial p'}{\partial t} \nabla \cdot \mathbf{u}' - \frac{\partial}{\partial t} (\mathbf{u}' \cdot \nabla p') \right\} \\ & + \rho_0 \left\{ (\gamma - 1) \left(\frac{p'}{p_0} \right) \nabla^2 \left(\frac{p'}{p_0} \right) - \left(\nabla \frac{p'}{p_0} \right)^2 \right\} \end{aligned} \tag{5.22}$$

$$\hat{\mathbf{n}} \cdot \nabla p' = -\rho_0 \frac{\partial \mathbf{u}'}{\partial t} \cdot \hat{\mathbf{n}} - \rho_0 \left\{ \frac{1}{\gamma} \left(\frac{p'}{p_0} \right) \frac{\partial \mathbf{u}'}{\partial t} \cdot \hat{\mathbf{n}} + \hat{\mathbf{n}} \cdot (\mathbf{u}' \cdot \nabla \mathbf{u}') \right\} \tag{5.23}$$

Equations (5.4) a,b are recovered when the second order terms are neglected.

5.1.1. *The Velocity Potential.* It is often convenient to introduce scalar and vector potentials Φ and $\mathbf{A}$ from which the velocity is found by differentiation:

$$\mathbf{u} = -\nabla \Phi + \nabla \times \mathbf{A} \tag{5.24}$$

With this representation, the dilation and curl (rotation) of the velocity field are separated:

$$\nabla \cdot \mathbf{u}' = -\nabla^2 \Phi \; ; \quad \nabla \times \mathbf{u}' = \nabla \times \nabla \times \mathbf{A} \tag{5.24}$$

In general, both potentials are required if the mean velocity is non-zero or sources are present in the flow. The boundary conditions may also induce non-zero rotational flow. Here only the scalar potential is required for small amplitude motions because in that limit, the classical acoustic momentum is (5.5); taking the curl with uniform average density gives

$$\bar{\rho} \frac{\partial}{\partial t} (\nabla \times \mathbf{u}') = -\nabla \times (\nabla p') = 0$$

Hence if $\nabla \times \mathbf{u}' = 0$ initially, it remains so and we can take $\mathbf{A} = 0$.

The acoustic equations for momentum, 3.40 and 3.40 in dimensional variables are

$$\begin{aligned} \frac{\partial \mathbf{u}'}{\partial t} + \frac{1}{\bar{\rho}} \nabla p' = 0 \\ \frac{\partial p'}{\partial t} + \gamma \bar{\rho} \nabla \cdot \mathbf{u}' = 0 \end{aligned} \tag{5.25 a,b}$$

Differentiate the first with respect to time and insert the second to give the wave equation for the velocity fluctuation,

$$\frac{\partial^2 \mathbf{u}'}{\partial^2} - \bar{a}^2 \nabla^2 \mathbf{u} = 0 \tag{5.26}$$

Now substitute $\mathbf{u}' = -\nabla\Phi$ to give

$$\nabla \left[\frac{\partial^2 \Phi}{\partial t^2} - \bar{a}^2 \nabla^2 \Phi \right] = 0$$

which is satisfied if the terms in brackets are a function of time only, so

$$\frac{\partial^2 \Phi}{\partial t^2} - \bar{a}^2 \nabla^2 \Phi = f(t) \tag{5.27}$$

The right-hand side represents a source field for the potential, uniform over all space. We may absorb $f(t)$ by defining a new potential $\Phi_1 = \Phi + \int^t dt' \int^{t'} f(t_1) dt_1$ and relabel $\Phi_1 \rightarrow \Phi$ to find[18] the wave equation for Φ:

$$\frac{\partial^2 \Phi}{\partial t^2} - \bar{a}^2 \nabla^2 \Phi = 0 \tag{5.28}$$

When the velocity potential is used, the acoustic velocity is calculated with (5.24) and $\mathbf{A} = 0$

$$\mathbf{u}' = -\nabla\Phi \tag{5.29}$$

The acoustic pressure is found by setting $\mathbf{u}' = -\nabla\Phi$ in the momentum equation (5.25) a,b, giving

$$\nabla \left(-\frac{\partial \Phi}{\partial t} + \frac{1}{\bar{\rho}} p' \right) = 0$$

This solution is satisfied if the terms in parentheses are a function of t only, $g(t)$, so

$$p' = \bar{\rho} \left(\frac{\partial \Phi}{\partial t} + g(t) \right) \tag{5.30}$$

As above, we may define a new potential $\Phi(t) + \int^t g(t')dt' = \Phi_1(t)$ and hence absorb $g(t)$ so we may redefine $\Phi_1 \rightarrow \Phi$ and

$$p' = \bar{\rho} \frac{\partial \Phi}{\partial t} \tag{5.31}$$

The conditions under which the acoustic field can be completely described by a velocity potential alone are precise and, so far as problems involving combustion are concerned, very restrictive. Any analysis or theory based on the velocity potential alone must also include demonstration that the vector potential can be ignored, i.e. set equal to a constant or zero. In general, the presence of a non-uniform mean flow field and various kinds of sources in the problems we are concerned with in this work, require that the velocity field be derived from both scalar and vector potentials. Use of the unsteady pressure as the primary flow variable provides a simpler approach for many purposes, but, as we will find later, apparently possesses unavoidable fundamental limitations.

5.2. Energy and Intensity Associated with Acoustic Waves. In this section we establish definitions of energy density and the intensity—i.e. the flow of energy—for classical acoustic waves. The definitions are only approximate under the more complicated conditions existing in a combustor but the general ideas remain.

Following Landau and Lifschitz (1959) we return to the basic energy equation (5.9) for inviscid flow. The idea is to establish a connection between the rate of change of something (the energy) within a volume and the flow of something (the intensity) through the closed boundary of that volume. Integrate the energy equation over a volume fixed in space; and apply Gauss' theorem to the terms on the right-hand side:

$$\begin{aligned} \frac{\partial}{\partial t} \int \rho \left(e + \frac{u^2}{2} \right) dV &= - \int \nabla \cdot \left[\rho \mathbf{u} \left(e + \frac{u^2}{2} \right) \right] dV - \int \nabla \cdot (\rho \mathbf{u})\, dV \\ &= - \oiint \left(e + \frac{u^2}{2} \right) \rho \mathbf{u} \cdot d\mathbf{S} - \oiint \rho \mathbf{u} \cdot d\mathbf{S} \end{aligned}$$

[18] Alternatively, one can reason that when the velocity is found by taking the gradient of $\Phi + \iint f$, the term in f contributes nothing and hence can be simply dropped. The desired solution is unaffected by setting $f = 0$.

This relation must be written to second order in the isentropic fluctuations; for example,

$$\rho e = \bar{\rho}\bar{e} + \rho' \left[\frac{\partial}{\partial \rho}(\rho e)\right]_{\bar{\rho}} + \frac{1}{2}\rho'^2 \left[\frac{\partial^2(\rho e)}{\partial \rho^2}\right]_{\bar{\rho}\bar{e}} + \ldots$$

$$= \bar{\rho}\bar{e} + \rho'\bar{k} + \frac{1}{2}\frac{\rho'^2}{\bar{\rho}\bar{a}^2} + \ldots$$

Eventually the result is

$$\frac{\partial}{\partial t}\int \mathcal{E} dV = -\oiint \mathcal{E}\mathbf{u}\cdot d\mathbf{S} - \oiint p'\mathbf{u}'\cdot d\mathbf{S} \tag{5.32}$$

where

$$\mathcal{E} = \frac{1}{2}\frac{p'^2}{\bar{\rho}\bar{a}^2} + \frac{1}{2}\bar{\rho}u'^2 \tag{5.33}$$

is the acoustic energy per unit volume and $p'\mathbf{u}'$ is the **intensity**, the flux of acoustic energy through an area normal to the direction of propagation (energy/area-S).

The first term on the right-hand side of (5.32) is third order in the fluctuations and must be dropped. Hence we have the important result interpreted in Figure 5.1.

$$\frac{\partial \mathcal{E}}{\partial t} + \nabla\cdot(p'\mathbf{u}') = 0$$

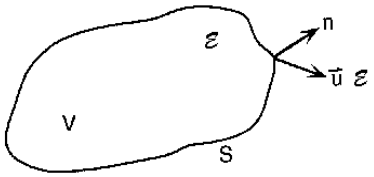

FIGURE 5.1. Acoustic Energy and Intensity

Table 5.1 summarizes the basic properties of plane sinusoidal waves. Brackets $\langle\ \ \rangle$ denote time averages over some interval τ

$$\langle(\ \ )\rangle = \frac{1}{\tau}\int_T^{t+\tau}(\ \ )dt' \tag{5.34}$$

5.3. The Growth or Decay Constant. In practice, due to natural dissipative processes, freely propagating waves and oscillations in a chamber will decay in space and time if there is no external source or energy. If there is an internal source of energy, waves may be unstable, having amplitudes increasing in time. The basic measure of the growth or decay of waves is the constant appearing in the exponent describing the sinusoidal spatial and temporal dependence of small amplitude waves, the definitions (5.62). For 'standing' or 'stationary' waves in a chamber, the wavelength, and hence wavenumber, is real and constant, but the frequency is complex:

$$\omega \to \omega + i\alpha \tag{5.35}$$

and the variables of the motion have the behavior in time

$$e^{-i(\omega+i\alpha)t} \equiv e^{-i\omega t}e^{\alpha t} \tag{5.36}$$

For this definition (5.34), $\alpha < 0$ means that the waves decay.

Normally in practice, $\left|\frac{\alpha}{\omega}\right| \ll 1$, implying that the fractional change of amplitude is small in one cycle of the oscillation. Thus when time averaging is carried out over one or a few cycles, $e^{\alpha t}$ may be taken as roughly constant, and the average energy density computed with (5.32) and (5.33), is

$$\langle\mathcal{E}\rangle = e^{2\alpha t}\frac{1}{4}\left[\frac{|\hat{p}|^2}{\bar{\rho}\bar{a}^2} + \bar{\rho}|\hat{u}|^2\right] \tag{5.37}$$

TABLE 5.1.

Results for Rightward and Leftward Traveling Sinusoidal Waves

Wave to Right	**Wave to Left**
$p'_+ = \hat{p}_+ e^{-i(\omega t - kx)}$	$p'_- = \hat{p}_- e^{-i(\omega t + kx)}$
$u'_+ = \hat{p}_+ e^{-i(\omega t - kx)}$	$u'_- = \hat{u}_- e^{-i(\omega t + kx)}$
$\hat{u}_+ = \frac{\hat{p}_+}{\rho_0 a_0}$	$\hat{u}_- = -\frac{\hat{p}_-}{\rho_0 a_0}$
$\varepsilon_+ = \frac{p'^2_+}{\rho_0 a_0}$	$\varepsilon_- = \frac{p'^2_-}{\rho_0 a_0}$
$l_+ = p'_+ u'_+ = \frac{p'^2_+}{\rho_0 a_0}$	$l_- = p'_- u'_- = -\frac{p'^2_-}{\rho_0 a_0^2}$
$\langle (\quad) \rangle = \frac{1}{\tau}\int_t^{t+\tau} (\quad) dt'$	
$\langle p'^2_+ \rangle = \frac{1}{2}\hat{p}^2_+$	$\langle p'^2_- \rangle = \frac{1}{2}\hat{p}^2_-$
$\langle \varepsilon_+ \rangle = \frac{\hat{p}^2_+}{2\rho_0 a_0^2}$	$\langle \varepsilon_- \rangle = \frac{\hat{p}^2_-}{2\rho_0 a_0^2}$
$\langle l_+ \rangle = \frac{\hat{p}^2_+}{2\rho_0 a_0}$	$\langle l_- \rangle = \frac{p^2_-}{2\rho_0 a_0}$
More generally: $p' = \hat{p} e^{i(\omega t + \varphi)}$;	$\bar{u}' = \hat{\mathbf{u}} e^{i(\omega t + \varphi)}$
$\langle \varepsilon \rangle = \frac{1}{4}\left[\frac{\lvert\hat{p}\rvert^2}{\rho_0 a_0^2} + \rho_0 \lvert\hat{u}\rvert^2\right] = \frac{1}{4}(p' p'^* + \rho_0 \mathbf{u}' \cdot \mathbf{u}'^*)$	
$\langle l \rangle = \frac{1}{2}\lvert\hat{p}\rvert\lvert\hat{\mathbf{u}}\rvert \cos(\varphi - \psi) = \frac{1}{4}(p'^* \mathbf{u}' + p' \mathbf{u}'^*)$	

where $(\quad)^*$ denotes complex conjugate.

Hence we have the important interpretations which serve as the basis for measuring values of α:

$$\alpha = \frac{1}{|\hat{p}|}\frac{d|\hat{p}|}{dt}$$
$$\alpha = \frac{1}{2\langle \mathcal{E} \rangle}\frac{d\langle \mathcal{E} \rangle}{dt} \qquad (5.38)\ \text{a,b}$$

The sign of α is a matter of definition and has no fundamental significance. If the time dependence is taken to be $e^{i(\omega + i\alpha)t}$ then $\alpha < 0$ means that waves are amplified.

The formulas (5.39) define local values of the growth constant. It is often more meaningful to know the value for the entire volume of the system in question, found by using $\int \langle \mathcal{E} \rangle dV$ rather than $\langle \mathcal{E} \rangle$:

$$\alpha = \frac{1}{2\int \langle \mathcal{E} \rangle dV}\frac{d}{dt}\int \langle \mathcal{E} \rangle dV \qquad (5.39)$$

5.4. Boundary Conditions: Reflections from a Surface. In the absence of other sources, the linearized boundary condition on the pressure at a surface is the first term of (5.1 b), here in dimensional form:

$$\hat{\mathbf{n}} \cdot \nabla p' = -\bar{\rho}\frac{\partial \mathbf{u}'}{\partial t} \cdot \hat{\mathbf{n}} \qquad (5.40)$$

The acoustic surface impedance z_a is defined by

$$\mathbf{u}' \cdot \hat{\mathbf{n}} = \frac{1}{z_a} p' \tag{5.41}$$

and the acoustic surface admittance y_a is the reciprocal of the admittance:

$$y_a = \frac{1}{z_a} \tag{5.42}$$

Then for harmonic motions, $p' = \hat{p} e^{-i\omega t}$, we can rewrite (5.40) as

$$\hat{\mathbf{n}} \cdot \nabla p' = -i \frac{\bar{\rho}\omega}{z_a} p' = -i \bar{\rho} \omega y_a p' \tag{5.43}$$

The units of impedance are (pressure/velocity) $\equiv$ (density $\times$ velocity). Hence for the medium, the product $\bar{\rho}\bar{a}$ is called the characteristic impedance, having value 42 g/cm^2-s. at standard conditions. Dimensionless forms are defined as:

$$\begin{aligned} &\text{acoustic impedance ratio:} \quad \zeta_a = \frac{z_a}{\bar{\rho}\bar{a}} \\ &\text{acoustic admittance ratio:} \quad \eta_a = \frac{1}{\zeta_a} \end{aligned} \tag{5.44}$$

In general, impedance functions are complex; the real and imaginary parts are called:

$$\begin{aligned} Re(z_a): &\quad \text{acoustic resistance} \\ Im(z_a): &\quad \text{acoustic reactance} \end{aligned} \tag{5.45}$$

From (5.41) and (5.42), the surface admittance is

$$y_a = \frac{\mathbf{u} \cdot \hat{\mathbf{n}}}{p'}$$

and the dimensionless surface admittance ratio is

$$\eta_a = \bar{\rho}\bar{a} y_a = \frac{\bar{\rho}\bar{a}^2}{\bar{p}} \frac{\bar{\mathbf{M}}' \cdot \hat{\mathbf{n}}}{p'/\bar{p}} = \gamma \frac{M_n'}{p'/\bar{p}} \tag{5.46}$$

where M_n' is the fluctuation of the Mach number normal to the surface.

If the surface is impermeable, the velocity at the surface is the velocity of the surface itself. However, if the surface is permeable, or, as for a burning propellant, mass departs the surface, then the impedance and admittance functions are defined in terms of the local velocity fluctuations presented[19] to the acoustic field, no matter what their origin.

Quite generally then, the admittance function represents the physical response of processes at the surface. It is of course an assumption that in response to an impressed pressure fluctuation, the fluctuation of velocity normal to the surface is proportional to the pressure change. Alternative definitions of quantities representing the acoustic boundary condition at a surface will arise when we consider special situations.

5.4.1. *Reflections of Plane Waves at a Surface.* Confinement of waves in a chamber to form modes necessarily involves reflections at the boundary surfaces. In solid propellant rockets the processes causing reflection are complicated, being responsible not only for confining the waves but also are the dominant means for transferring energy to the oscillating field in the chamber. Even at inert surfaces, more than the simple process of reflection is involved. Viscous stresses and heat conduction in the region adjacent to a surface cause dissipation of energy, discussed in Section 5.6.

Here we assume that all activity at the surface can be represented by a complex impedance or admittance function. The calculation follows that discussed by Morse and Ingard (1968). We consider reflection of a planar wave, Figure 5.2, allowing for the possibility of unequal angles of incidence and reflection, and for simplicity we

[19] For burning propellants, care must be taken with definition of the surface at which the boundary condition is imposed. Usually the velocity at the 'edge' of the combustion zone in the gas phase is the most convenient choice. Thus the admittance presented to the acoustic field is not that at the burning surface itself.

assume that there is no transmitted wave. The incident wave travels in the direction defined by the unit vector $\hat{\mathbf{k}}_i$ and the wavenumber vector is

$$\mathbf{k} = \frac{2\pi}{\lambda}\hat{\mathbf{k}} \tag{5.47}$$

We can represent the acoustic pressure and velocity in this plane wave by

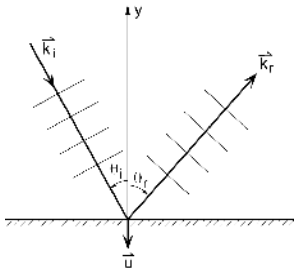

FIGURE 5.2. Reflection of a Plane Wave. Plane waves propagating in direction $\mathbf{k} = \frac{2\pi}{\lambda}\hat{\mathbf{k}}$

$$\begin{aligned} p'(\mathbf{r};t) &= g_i(\mathbf{k}_i \cdot \mathbf{r} - \omega t) \\ \mathbf{u}'(\mathbf{r};t) &= \frac{\hat{k}_r}{\bar{\rho}\bar{a}} g_i(\mathbf{k}_i \cdot \mathbf{r} - \omega t) \end{aligned} \tag{5.48 a,b}$$

Similar formulas hold for the reflected wave with $\mathbf{k}_i$ replaced by $\mathbf{k}_r$ lying in the direction defined by the unit vector $\hat{\mathbf{k}}_r$. The representations are therefore:

Incident Wave			**Reflected Wave**		
p'_i	$=$	$u_i(\xi_i)$	p'_r	$=$	$g_r(\xi_r)$
$\mathbf{u}'_i$	$=$	$\hat{\mathbf{k}}_i \frac{1}{\bar{\rho}\bar{a}} g_i(\xi_i)$	$\mathbf{u}'_r$	$=$	$\hat{\mathbf{k}}_r \frac{1}{\bar{\rho}\bar{a}} g_r(\xi_r)$
ξ_i	$=$	$\mathbf{k}_i \cdot \mathbf{r} - \omega t$	ξ_r	$=$	$\mathbf{k}_r \cdot \mathbf{r} - \omega t$
	$=$	$k(x\sin\theta_i - y\cos\theta_i) - \omega t$		$=$	$k(x\sin\theta_r - y\cos\theta_r) - \omega t$

Because the frequency is the same for the incident and reflected waves, so are the magnitudes of the wavenumbers:

$$|\mathbf{k}_i| = \frac{\omega}{\bar{a}} = |\mathbf{k}_r| \tag{5.49}$$

Reflection is assumed to occur at $y = 0$. By definition of z_a, the surface impedance, with the normal velocity outward from the surface equal to $u_y = \mathbf{u} \cdot \hat{\mathbf{j}} = -\mathbf{u} \cdot \hat{\mathbf{n}}$ where $\hat{\mathbf{n}}$ is the unit outward normal vector:

$$z_a = \left(\frac{p'}{u'_y}\right)_{y=0} = \bar{\rho}\bar{a}\frac{g_i(kx\sin\theta_i - \omega_t) + g_r(kx\sin\theta_r - \omega_t)}{\cos\theta_i g_i(kx\sin\theta_i - \omega_t) - \cos\theta_r g_r(kx\sin\theta_r - \omega_t)} \tag{5.50}$$

In general z_a is variable along the surface. Suppose that in fact z_a is constant, independent of x. That can be true if

$$\begin{aligned} \theta_i &= \theta_r = \theta \\ g_r(\xi) &= \beta g_i(\xi) \end{aligned} \tag{5.51}$$

Then (5.50) becomes

$$z_a \cos\theta = \bar{\rho}\bar{a}\frac{1+\beta}{1-\beta} \tag{5.52}$$

and the complex reflection coefficient β is related to the surface impedance by

$$\beta = \frac{z_a \cos\theta - \bar{\rho}\bar{a}}{z_a \cos\theta + \bar{\rho}\bar{a}} \tag{5.53}$$

This result is special because no transmitted wave has been accounted for. For example, if $z_a = \bar{\rho}\bar{a}$—perfect impedance matching exists at the interface—(5.52) gives $\beta = 0$ when $\theta = 0$, so there is no reflected wave. That is true in one sense because in physical terms $z_a = \bar{\rho}\bar{a}$ means that the same gas exists in both sides of the interface. Thus we are simply describing wave propagation in a continuous medium. On the other hand, the physical picture treated here accommodates no transmitted wave, which means that when there is no reflection, processes must exist at the interface providing perfect absorption.

Now suppose $\theta \neq 0$ but $z_a = \bar{\rho}\bar{a}$. Then (5.52) gives β non-zero, i.e. partial absorption and some of the incident wave is reflected.

5.5. Wave Propagation in Tubes; Normal Modes. The simplest form of combustor is a straight tube, having generally non-uniform cross-section and not necessarily axisymmetric. Although the changes of cross-section may be abrupt—even discontinuous—experience has shown that good results may be obtained by assuming that the velocity fluctuations are uniform at every section and parallel to the axis: the flow is treated as one-dimensional. The governing equations are given in Appendix B, equations (B.2)–(B.4) with no sources:

$$\textit{Conservation of Mass}: \qquad \frac{\partial \rho'}{\partial t} + \frac{\partial}{\partial x}(\bar{\rho}u'S_c) = 0 \tag{5.54}$$

$$\textit{Conservation of Momentum}: \qquad \bar{\rho}\frac{\partial u'}{\partial t} + \frac{\partial p'}{\partial x} = 0 \tag{5.55}$$

$$\textit{Conservation of Energy}: \qquad \bar{\rho}C_v\frac{\partial T'}{\partial t} + \bar{p}\frac{1}{S_c}\frac{\partial}{\partial x}(u'S_c) = 0 \tag{5.56}$$

The wave equation for the pressure is:

$$\frac{1}{S_c}\frac{\partial}{\partial x}\left(S_c\frac{\partial p'}{\partial x}\right) - \frac{1}{\bar{a}^2}\frac{\partial^2 p'}{\partial t^2} = 0 \tag{5.57}$$

5.5.1. *Waves in Tubes.*

(a) Normal Modes for a Tube Closed at Both Ends

Results for a tube closed at both ends not only contain many ideas basic to general oscillations in chambers, but also are widely useful for practical applications. For a tube closed by rigid walls, the boundary conditions at the ends are that the velocity must vanish. The momentum equation (5.54) then states that acceleration and therefore the pressure gradient must vanish at the ends for all time:

$$\frac{\partial p'}{\partial x} = 0 \qquad x = 0, L; \quad \text{all } t \tag{5.58}$$

General linear motions within the tube can be constructed as superpositions of *normal modes* defined in general by two properties:

(i) sinusoidal variations in time

(ii) the motion at any point bears always a fixed phase relation with that at any other point in the volume

Those conditions imply here that the pressure can be expressed as

$$p'(x;t) = \hat{p}(x)e^{-i\bar{a}kt} \tag{5.59}$$

where k is the complex wavenumber, related in general to the complex frequency by the formula

$$\bar{a}k = \omega + i\alpha \tag{5.60}$$

Because there are no dissipative processes in this problem, $\alpha = 0$ so the wavenumber is real. Substitution of (5.59) in (5.57) with S independent of x gives

$$\frac{d^2\hat{p}}{dx^2} + k^2\hat{p} = 0 \tag{5.61}$$

A solution to (5.61) satisfying (5.58) at $x = 0$ is $\hat{p} = A\cos kx$. To satisfy the condition at $x = L$, $\cos kL = 0$. Then k can assume only certain values k_l, called *characteristic* or *eigen* values:[20]

$$k_l = l\frac{\pi}{L} \qquad (l = 0, 1, 2, \cdots) \tag{5.62}$$

Corresponding to each k_l is a *characteristic function,* or *eigenfunction,*

$$\frac{\hat{p}_l}{\bar{p}_0} = A_l \cos(k_l x) \tag{5.63}$$

For the problems we treat in this book, the motions represented by the k_l, $\hat{p}_l$, and $\hat{u}_l$ are usually called *normal modes,* $\bar{a}k_l = \omega_l$ being the *normal* or *modal frequency,* and $\hat{p}_l$, $\hat{u}_l$ are the *mode shapes* of pressure and velocity. All of these terms are used for two- and three-dimensional motions as well.

A normal mode is characterized by its frequency and the spatial distributions, or 'shapes' of all dependent variables. The mode shape for the velocity is derived from the mode shape (5.63) by integrating the acoustic momentum equation (5.55) written for $\hat{u}_l$:

$$-i\bar{a}k_l\hat{u}_l = -\frac{1}{\bar{\rho}}\frac{d\hat{p}_l}{dx} = \frac{k_l}{\bar{\rho}}\bar{p}_l A_l \sin k_l x$$

Thus

$$\hat{u}_l = i\frac{\bar{p}_l}{\bar{\rho}\bar{a}}A_l \sin k_l x \tag{5.64}$$

or, written as the Mach number of the mode,

$$\hat{M}_l = i\frac{1}{\gamma}A_l \sin k_l x \tag{5.65}$$

(b) Normal Modes for a Tube Open at Both Ends

In this case, the pressure is assumed fixed at the ends, for example because the tube is immersed in a large reservoir having constant pressure, and $p' = 0$. For isentropic motions, $\frac{\rho'}{\bar{\rho}} = \frac{1}{\gamma}\frac{p'}{\bar{p}}$ so $\rho' = \frac{1}{\bar{a}^2}p'$ and the continuity equation (5.54) is

$$\frac{\partial p'}{\partial t} + \frac{\bar{a}^2}{\bar{\rho}}\frac{\partial u'}{\partial x} = 0 \tag{5.66}$$

Hence if p' is fixed, the velocity gradient must vanish at the ends. Set $p' = Ae^{-i\bar{a}kt}\sin kx$ and substitute in (5.66)

$$i\frac{\bar{a}}{\bar{p}}kAe^{-i\bar{a}kt}\sin kx = -\frac{\bar{a}^2}{\bar{\rho}}\frac{\partial u'}{\partial x}$$

[20] Only for $l \geq 1$ do we find wave modes. For $l = 0$, a qualitatively different mode exists for which the pressure is uniform in the volume but pulsates at a frequency well below that for the fundamental wave mode. The velocity is practically zero and the oscillator is sustained by some sort of external action. A prosaic example is the low frequency sound one can create by blowing across the narrow opening at the neck of a bottle. In this case the mode is called the *Helmholtz mode* and the bottle is behaving as a *Helmholtz resonator.*

The left-hand side vanishes (and hence $\partial u'/\partial x = 0$) at $x = 0$ for any k, but at $x = L$, we must have $\sin k_l L = 0$. Hence $k_l = (2l+1)\frac{\pi}{L}$ and the normal mode shape and frequency are

$$\frac{\hat{p}_l}{\bar{p}} = A_l \sin(k_l x) \quad ; \qquad k_l = l\frac{\pi}{L} \quad (l = 1, 2, \cdots) \tag{5.67}$$

and the mode shape for the velocity is

$$\frac{\hat{u}_l}{\bar{a}} = \hat{M}_l = i\frac{1}{\gamma} A_l \cos k_l x \tag{5.68}$$

(c) Normal Modes for a Tube Closed at One End and Open at the Other

Reasoning similar to the above leads in this case to the normal modes when the tube is closed at $x = 0$:

$$\frac{\hat{p}_l}{\bar{p}} = A_l \cos(k_l x) \quad ; \qquad \left(k_l = (2l+1)\frac{\pi}{2L}\right) \quad (l = 1, 2, \cdots)$$
$$\frac{\hat{u}_l}{a} = -i\frac{1}{\gamma} A_l \sin(k_l x)$$

5.5.2. *Normal Modes for Tubes Having Discontinuities of Cross-Sectional Area.* Combustors having discontinuous area distributions are commonly used in solid propellant rockets and in various laboratory devices. Consider the example sketched in Figure 5.3. The boundary conditions at the ends are:

$$\begin{aligned} x = 0: \qquad & \frac{d\hat{p}}{dx} = 0 \\ x = \beta L: \qquad & \hat{p} = 0 \end{aligned} \tag{5.69 a,b}$$

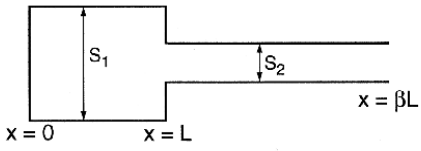

FIGURE 5.3. A Uniform Tube Having a Single Discontinuity.

Possible solutions in the regions to the left and right of the discontinuity are:

$$\begin{aligned} \frac{\hat{p}}{\bar{p}} &= A\cos kx \qquad (0 \le x \le L) \\ \frac{\hat{p}}{\bar{p}} &= B\sin k(\beta L - x) \qquad (L < x \le \beta L) \end{aligned} \tag{5.70 a,b}$$

Note that $k = \omega/\bar{a}$ is the same throughout the tube because the motion occurs everywhere at the same frequency.

Completing the problem comes down to determining the conditions for matching the solutions. Two are required:

(i) continuity of pressure:

$$\lim_{\varepsilon \to 0} [\hat{p}(L - \varepsilon) - \hat{p}(L + \varepsilon)] = 0$$

which gives

$$A\cos kL = B\sin(\beta - 1)kL \tag{5.71}$$

(ii) continuity of acoustic mass flow:

Integrate the wave equation (for harmonic motions) across the discontinuity,

$$\int_{L-\varepsilon}^{L+\varepsilon} \left[\frac{d}{dx}(S_c \frac{d\hat{p}}{dx} + k^2 S_c \hat{p} \right] dx = 0$$

Because $\hat{p}$ is continuous, this relation becomes

$$\lim_{\varepsilon \to 0} \left[\left(S_c \frac{d\hat{p}}{dx} \right)_{L+\varepsilon} - \left(\frac{d\hat{p}}{dx} \right)_{L-\varepsilon} \right] = 0$$

Thus, with $\bar{\rho}$ constant and $\frac{d\hat{p}}{dx} \sim \hat{u}$:

$$(\bar{\rho} S_c \hat{u})_{L+\varepsilon} - (\bar{\rho} S_c \hat{u})_{L-\varepsilon} \tag{5.72}$$

After substituting the waveforms (5.70) a,b, and using (5.71) we find the transcendental equation for the modal wavenumbers:

$$\frac{S_1}{S_2} \tan k_l L = \cot k_l (\beta - 1) L \tag{5.73}$$

This method of solving a problem with discontinuities is only approximate: a practical question is: how large are the errors? To gain some idea of the errors incurred, tests at ambient temperature ('cold flow tests') were carried out by Mathis, Derr and Culick (1973) for the geometry of a T-burner used for measuring the combustion response of burning solid propellants. Results are shown in Figure 5.4. The measured values of both the frequencies and the mode shapes are surprisingly well-predicted by this theory. The principal reason is that the influence of a discontinuity is confined to a relatively small region near the change of area, but the characteristics of the normal modes depend on the motion in the entire volume.

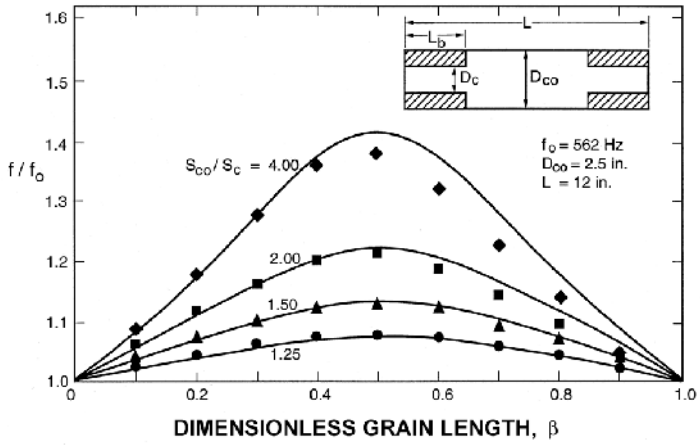

FIGURE 5.4. Comparison of Experimental and Theoretical Results for Normal Frequencies in a T-Burner (Ambient Temperature)

5.6. Normal Acoustic Modes and Frequencies for a Chamber. We now consider a volume of any shape enclosed by a rigid boundary and containing a uniform gas at rest. Unsteady small amplitude motions therefore satisfy the linear wave equation (5.4) a,b and its boundary condition ((5.4) a,b)b requiring that the velocity normal to the boundary vanish at all times. By this definition given in Section 5.5.1, normal modes are solutions to this problem which oscillate sinusoidally in time and have fixed phase relations throughout the volume. We assume the form[21] $p' = \psi e^{-i\bar{a}kt}$. The formal problem is to find ψ satisfying the scalar wave equation, also called the Helmholtz wave equation, with vanishing normal gradient at the surface:

$$\begin{aligned} \nabla^2 \psi + k^2 \psi &= 0 \\ \hat{n} \cdot \nabla \psi &= 0 \end{aligned} \tag{5.74 a,b}$$

[21] Consistent with the general character of this problem, we replace $\hat{p}$ by ψ, introducing a common notation for normal modes. The velocity potential Φ satisfies the same pair of equations, a result reflected by equation (5.31) which for sinusoidal motions means that p' and Φ are proportional: $p' = i\bar{a}k\bar{\rho}\Phi$.

There are many well-written books covering this problem and its solution, for example Hildebrand (1952), Morse and Feshbach (1952), and Morse and Ingard (1968). The simplest approach is based on the method of separation of variables, applicable for closed form solutions in thirteen coordinate systems; see, e.g., Morse and Feshbach (1952). In practical applications to combustors, only rectangular and circular cylindrical chambers are important.

5.6.1. *Normal Modes for Rectangular Chambers.* The wave equation in Cartesian coordinates is

$$\frac{\partial^2\psi}{\partial x^2}+\frac{\partial^2\psi}{\partial y^2}+\frac{\partial^2\psi}{\partial z^2}+k^2\psi=0$$

and $\hat{n}\cdot\nabla\psi$ must vanish on the six flat surfaces each perpendicular to a coordinated axis, Figure 5.5. Applying the method of separation of variables leads to a solution having the form

$$\psi = A\cos(k_x x)\cos(k_y y)\cos(k_z z) \tag{5.75}$$

and

$$k^2 = k_x^2 + k_y^2 + k_z^2 \tag{5.76}$$

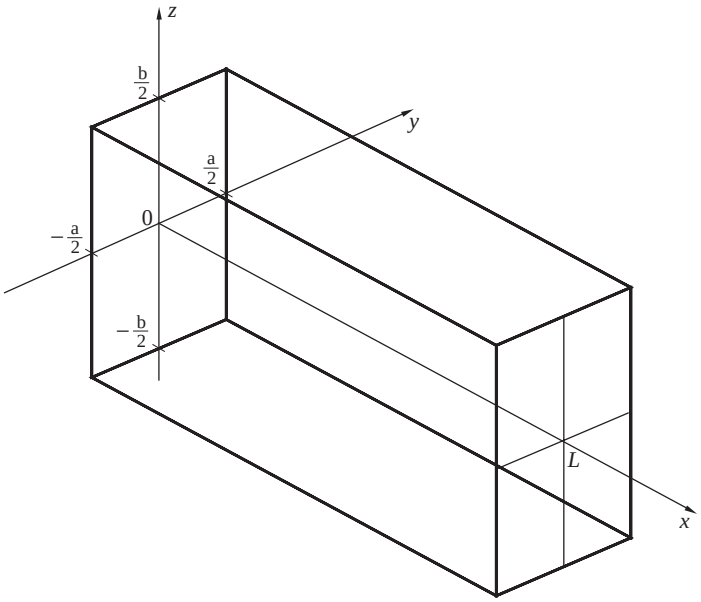

FIGURE 5.5. Rectangular Chamber

The boundary conditions must be satisfied:

$$\begin{aligned}
\frac{\partial\psi}{\partial x}&=0 \qquad && x=0,L\\
\frac{\partial\psi}{\partial y}&=0 && y=-\frac{a}{2},\frac{a}{2}\\
\frac{\partial\psi}{\partial z}&=0 && z=-\frac{b}{2},\frac{b}{2}
\end{aligned} \tag{5.77 a,b,c}$$

Reasoning similar to that given in Section 5.5.1 leads to the values of the wavenumbers

$$\begin{aligned}
k_x &= l\frac{\pi}{L}\\
k_y &= m\frac{\pi}{b}\\
k_z &= n\frac{\pi}{c}
\end{aligned} \tag{5.78 a,b,c}$$

and the mode shapes are

$$\psi_{lmn} = A_{lmn} \cos\left(l\frac{\pi}{L}x\right) \cos m\frac{\pi}{a}\left(y+\frac{a}{2}\right) \cos n\frac{\pi}{b}\left(z+\frac{b}{2}\right) \tag{5.79}$$

The distributions of pressure therefore have the same form in all directions; of course the components (5.78) a,b,c can assume any of the allowed values, and the frequency is given by (5.76), $\omega = \bar{a}k$.

5.6.2. *Normal Modes for a Circular Cylindrical Chamber.* Let x be the polar axis (Figure 5.6) and the wave equation in circular cylindrical coordinates is

$$\frac{1}{r}\frac{\partial}{\partial r}\left(r\frac{\partial\psi}{\partial r}\right) + \frac{1}{r^2}\frac{\partial^2\psi}{\partial\theta^2} + \frac{\partial^2\psi}{\partial x^2} + k^2\psi = 0 \tag{5.80}$$

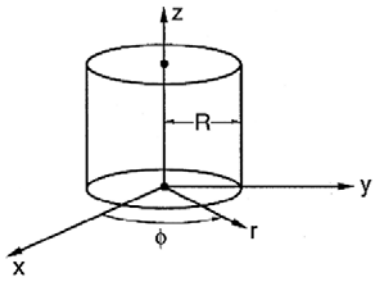

FIGURE 5.6. Circular Cylindrical Coordinates

The boundary condition requires that $\hat{n}\cdot\nabla\psi$ vanish at the ends and on the lateral boundary:

$$\begin{aligned} \frac{\partial\psi}{\partial x} &= 0 \qquad & x = 0, L \\ \frac{\partial\psi}{\partial r} &= 0 \qquad & r = R \end{aligned} \tag{5.81}$$

Application of the method of separation of variables leads to a solution of the form

$$\psi(r,x,\theta;t) = A\left\{\begin{matrix}\cos n\theta \\ \sin n\theta\end{matrix}\right\} \cos k_l z J_m\left(\kappa_{mn}\frac{r}{R}\right) \tag{5.82}$$

To satisfy the boundary conditions, the values of k_l are integral multiples of π/L as above and the κ_{mn} are the roots of the derivative of the Bessel function:

$$\frac{dJ_m(\kappa_{mn})}{dr} = 0 \tag{5.83}$$

Figure 5.7 shows the lowest six modes in the transverse planes, and the identifying values of n and m. More extended results are given in standard texts and collections of special functions.

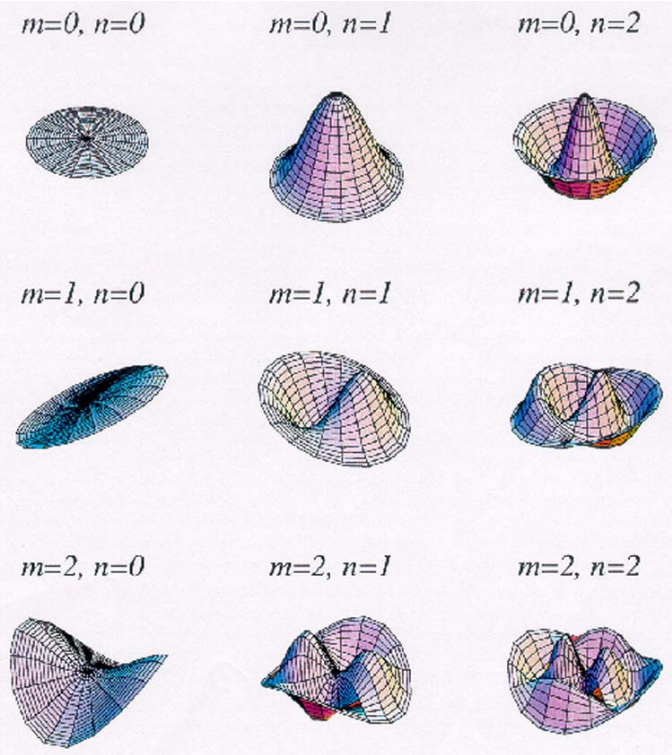

FIGURE 5.7. The First Six Transverse Modes in a Circular Cylinder

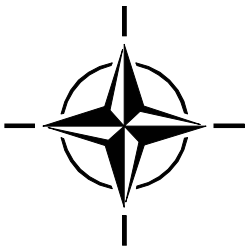

6. LINEAR STABILITY OF COMBUSTOR DYNAMICS

All problems of unsteady motion in combustion systems can be divided into the two classes: linearized and nonlinear. From the earliest discoveries of their transient behavior until the late 1950s 'combustion instabilities' implied small amplitude unsteady (and unwanted) motions growing out of a condition of linear instability. Even with the expanding awareness that the nonlinear properties must be understood as well, the linear behavior remains an essential part of understanding all aspects of combustion instabilities, including the consequences of nonlinear processes.

The literature of linear combustion instabilities contains many papers dealing with special problems. There seems often to be a tendency to regard the results as somehow disconnected. However, apparent differences arise chiefly from the differences in the processes accounted for and in the choices of models for those processes. So long as the problems are dominated by oscillating behavior in combustors, probably most, if not practically all of the results can be obtained in equivalent forms by suitable applications of the methods explained here. That statement is not as outrageous as it may seem, following as it does from the generality of the expansion procedures and the method of averaging covered in Section 4.

6.1. Solution for the Problem of Linear Stability. By 'solution' we mean here formulas for calculating the amplitudes $\eta_n(t)$ of modes retained in the expansion for the pressure field, $p'(\mathbf{r},t) = \bar{p}\Sigma\eta_n(t)\psi_n(\mathbf{r})$. The amplitudes satisfy the oscillator wave equations (4.36)

$$\frac{d^2\eta_n}{dt^2} + \omega_n^2\eta_n = F_n + F_n^c \tag{6.1}$$

where F_n^c stands for the generalized 'force' associated with the exercise of control; and F_n is the spatial average of that part (sometimes called the 'projection' on the basis function ψ_n) of the internal processes affecting the motion of the n^{th} oscillator, given by (4.32):

$$F_n = -\frac{\bar{a}^2}{\bar{p}E_n^2}\left\{\int h\psi_n dV + \oiint f\psi_n dS\right\} \tag{6.2}$$

Here we ignore F_n^c because we are concerned only with the internal behavior of the system. In general, the F_n contain contributions associated with the motions of oscillators other than the n^{th}—i.e. the modes are coupled. For analysis of linear stability we are justified in ignoring that coupling, for reasons given by Culick (1997). Each F_n is therefore a linear function of the amplitude and velocity of the oscillator, having the form

$$F_n = F_n^\eta\eta_n + F_n^{\dot\eta}\frac{d\eta_n}{dt} \tag{6.3}$$

where the F_n^η and $F_n^{\dot\eta}$ are constants, depending only on the mode.

With these assumptions, the oscillator equations (6.1) are the uncoupled set

$$\frac{d^2\eta_n}{dt^2} - F_n^{\dot\eta}\frac{d\eta_n}{dt} + \left(\omega_n^2 - F_n^\eta\right)\eta_n = 0 \tag{6.4}$$

Because the equations are uncoupled, the normal modes ψ_n for the corresponding classical acoustic problem are also the normal modes for the linear problem of combustor dynamics. The general problem of determining linear stability has therefore come down to the problem of determining the stability of the normal modes. In the usual fashion we assume sinusoidal time dependence with complex frequency:

$$\eta_n(t) = \hat{\eta}_n e^{i\Omega t} \tag{6.5}$$

Equation ((5.4) a,b) gives the quadratic equation for Ω_n:

$$\Omega^2 - iF_n^{\dot\eta}\Omega + \left(\omega_n^2 - F_n^\eta\right) = 0 \tag{6.6}$$

with solution

$$\Omega = i\frac{1}{2}F_n^{\dot\eta} + \omega_n\sqrt{1 - \frac{1}{\omega_n^2}\left[F_n^\eta + \frac{1}{4}\left(F_n^{\dot\eta}\right)^2\right]} \tag{6.7}$$

where we take the (+) sign on the radical to give a positive real frequency. Hence the amplitudes are

$$\eta_n(t) = e^{\frac{1}{2}F_n^{\dot\eta}t}e^{-i\omega_n\sqrt{1-\zeta_n^2}t} \tag{6.8}$$

and

$$\zeta_n = \frac{1}{\omega_n}\sqrt{F_n^{\eta} + \frac{1}{4}\left(F_n^{\dot\eta}\right)^2} \tag{6.9}$$

The n^{th} mode is stable of

$$F_n^{\dot\eta} < 0 \tag{6.10}$$

That is, the coefficient of $\dot\eta_n$ in the expression for F_n must be positive for the n^{th} mode to be stable.

Now according to the methods of Fourier analysis, an arbitrary disturbance at some initial time (say $t = 0$) in the chamber can be synthesized of the normal modes. The time-evolution of the disturbance is therefore determined by the $\eta_n(t)$. In particular, an arbitrary disturbance in a combustor is stable if (and only if) all of the normal modes are stable and we arrive at the general result for the linear stability of a combustor:

(i) Write the linearized function for the force acting on the n^{th} oscillator (spatially averaged acoustic mode) in the form

$$F_n = F_n^{\eta}\eta_n + F_n^{\dot\eta}\frac{d\eta_n}{dt}$$

(ii) Then any initial disturbance in a combustor is stable if and only if all the $F_n^{\dot\eta}$ are negative:

$$\text{Linear Stability} \iff F_n^{\dot\eta} < 0 \quad (\text{all } n)$$

The preceding calculation and its conclusion, illustrate further a point first made in Section 3. We have found a means of computing the linear stability of a combustor without knowing the linear motions themselves. The complex frequency (6.7) is in fact the frequency for the actual linear modes including the influences of all the processes accounted for. But calculation of the F_n^{η} and $F_n^{\dot\eta}$ with the formula (6.2) requires knowledge only of the unperturbed normal modes—their frequencies ω_n and shapes $\psi_n(\mathbf{r})$. The formal statement of this property is that the eigenvalues (Ω_n) to any order in the relevant expansion parameter (here $\bar M_r := \mu$) can be computed knowing the eigenfunctions (ψ_n) only to one less order. The eigenvalues Ω_n are here given to first order in the Mach number of the average flow but only the unperturbed classical eigenfunctions ψ_n are required. This is the basic characteristic of the expansion procedures with spatial averaging that makes the method devised here so useful in practice.

6.2. An Alternative Calculation of Linear Stability. An equivalent calculation of the result for linear stability makes direct use of the formula for the wavenumber. Write

$$\eta_n = \hat\eta_n e^{-i\bar a k t} \quad ; \qquad F_n = \hat F_n e^{-i\bar a k t}$$

and substitute in (6.1) with F_n^c ignored to find

$$(\bar a k)^2 = (\bar a k_n)^2 + \frac{1}{\hat\eta_n}\left(\hat F_n^{(r)} + i\hat F_n^{(i)}\right) \tag{6.11}$$

With $\bar a k = \omega + i\alpha$, this formula is

$$\omega^2 + i(2\alpha\omega) - \alpha^2 = \omega_n^2 + \frac{1}{\hat\eta_n}\left(\hat F_n^{(r)} + i\hat F_n^{(i)}\right)$$

where $(\quad)^{(r)}$ and $(\quad)^{(i)}$ stand for real and imaginary parts. Because α and $\hat F_n$ are of first order in the expansion parameter and terms of higher order must be dropped[22], we ignore α^2 with respect to ω^2. Then the real and imaginary parts of the last equation give

$$\omega^2 = \omega_n^2 + \frac{1}{\hat\eta_n}\hat F_n^{(r)}$$

$$\alpha = -\frac{1}{2\omega_n}\hat F_n^{(i)}$$

[22]Recall the remarks in Section 4.

where ω has been set equal to ω_n in the right-hand sides to ensure that higher order terms are not retained. Now take the square root of the first equation and again drop higher order terms to find

$$\omega = \omega_n - \frac{1}{2\omega_n}\frac{\hat{F}_n^{(r)}}{\hat{\eta}_n}$$
$$\alpha = -\frac{1}{2\omega_n}\frac{\hat{F}_n^{(i)}}{\hat{\eta}_n} \qquad (6.12)\ \text{a,b}$$

The system is unstable if $\hat{F}_n^{(i)}$ is negative. This condition is essentially a generalized form of Rayleigh's criteria discussed further in Section 6.4.

After higher order terms are dropped from (6.7), the real and imaginary parts of ω are

$$\omega = \omega_n - \frac{1}{2\omega_n}F_n^{\eta}$$
$$\alpha = \frac{1}{2}F_n^{\dot{\eta}} \qquad (6.14)\ \text{a,b}$$

Comparison of (6.12) a,b and 5.14 gives the connections between the two representations of the forcing function[23]:

$$F_n^{\eta} = \frac{\hat{F}_n^{(r)}}{\hat{\eta}_n}$$
$$F_n^{\dot{\eta}} = -\frac{1}{\omega_n}\frac{\hat{F}_n^{(i)}}{\hat{\eta}_n} \qquad (6.15)\ \text{a,b}$$

Generally F_n will contain several processes, each of which will depend linearly on η_n and $\frac{d\eta_n}{dt}$ and appears additively in F_n. Hence formulas corresponding to (6.15) a,b apply to each of the individual processes. They are often useful, if only for checking correctness, in detailed calculations.

6.3. An Example: Linear Stability with Distributed Sources of Heat and Motion of the Boundary. As a first approximation to problems of combustion instabilities it is useful to ignore all processes involving interactions between the unsteady and steady fields, and focus attention on the two generic causes of instabilities: time-dependent energy addition and motions of the boundary. With suitable interpretation the second may represent the influence of unsteady combustion of a solid propellant. Then in dimensional variables the linearized pressure and momentum equations ((3.46) a-e)d and ((3.46) a-e)b, and the boundary condition (3.57) on the pressure fluctuations are

$$\frac{\partial p'}{\partial t} + \gamma\bar{p}\nabla\cdot\mathbf{u}' = \frac{R}{C_v}\dot{Q}' \qquad (6.12)$$

$$\bar{\rho}\frac{\partial u'}{\partial t} + \nabla p' = 0 \qquad (6.13)$$

$$\hat{\mathbf{n}}\cdot\nabla p' = -\bar{\rho}\frac{\partial \mathbf{u}'}{\partial t}\cdot\hat{\mathbf{n}} \qquad (6.14)$$

Now form the wave equation as in Section 3.4, so the problem is governed by the two equations

$$\nabla^2 p' - \frac{1}{\bar{a}^2}\frac{\partial^2 p'}{\partial t^2} = h$$
$$\hat{\mathbf{n}}\cdot\nabla p' = -f \qquad (6.19)\ \text{a,b}$$

where

$$h = -\frac{1}{\bar{a}^2}\frac{R}{C_v}\frac{\partial \dot{Q}'}{\partial t}$$
$$f = -\bar{\rho}\frac{\partial \mathbf{u}'}{\partial t}\cdot\hat{\mathbf{n}} \qquad (6.20)\ \text{a,b}$$

[23]The $(-)$ sign in (6.15) a,b arises from the $(-)$ sign in the exponential time dependence.

The expansion procedure and application of spatial averaging leads to the explicit oscillator equations (4.36):

$$\frac{d^2\eta_n}{dt^2} + \omega_n^2\eta_n = -\frac{\bar{a}^2}{\bar{p}E_n^2}\left\{\int\left[-\frac{1}{\bar{a}^2}\frac{R}{C_v}\frac{\partial\dot{Q}'}{\partial t}\right]\psi_n dV + \iint\left[-\bar{\rho}\frac{\partial \mathbf{u}'}{\partial t}\cdot\hat{\mathbf{n}}\right]\psi_n dS\right\} \tag{6.21}$$

FIGURE 6.1. A Tube with Distributed Heat Addition and an Oscillating Piston to Drive Waves

As a simple example, consider the one-dimensional problem of waves excited in a tube fitted with a piston, Figure 6.1, and with distributed heat addition provided by an electrically heated coil. Only longitudinal modes are accounted for, and

$$\psi_n = \cos(k_n x) \quad , \qquad k_n = n\frac{\pi}{L} \quad , \qquad E_n^2 = \frac{1}{2}S_c L \tag{6.21}$$

where $S_c = \pi R^2$ is the cross-section area of the tube. We ignore any average motion in the tube, and suppose that the average thermodynamic properties are maintained constant and uniform by suitable steady heat losses through the walls of the tube. The heat addition and motion of the piston are sinusoidal, having phases ϕ_Q and ϕ_n with respect to pressure oscillations:

$$\begin{aligned} \dot{Q}' &= \left|\hat{\dot{Q}}(x)\right| e^{-i(\bar{a}kt-\phi_Q)} \\ \mathbf{u}_p'\cdot\hat{\mathbf{n}} &= |\hat{u}_p|\, e^{-i(\bar{a}kt-\phi_p)} \end{aligned} \tag{6.22 a,b}$$

Hence for use in h and f:

$$\begin{aligned} \frac{\partial\dot{Q}'}{\partial t} &= -i\bar{a}k\left|\hat{\dot{Q}}(x)\right| e^{-i(\bar{a}kt-\phi_Q)} \\ \frac{\partial}{\partial t}\left(\mathbf{u}_p'\cdot\hat{\mathbf{n}}\right) &= -i\bar{a}k\,|\hat{u}_p|\, e^{-i(\bar{a}kt-\phi_u)} \end{aligned} \tag{6.23 a,b}$$

With $\eta_n = \hat{\eta}_n e^{i\bar{a}kt}$, substitution in the oscillator equations (6.21) leads to

$$\begin{aligned} \left[-(\bar{a}k)^2 + \omega_n^2\right]\hat{\eta}_n = -\frac{\bar{a}^2}{\bar{p}E_n^2}\Bigg\{&-\frac{1}{\bar{a}^2}\frac{R}{C_v}(-i\bar{a}k)\int\cos(k_n x)\left|\hat{\dot{Q}}(x)\right| e^{i\phi_Q}dV \\ &+i\bar{\rho}\bar{a}k\oiint\cos(k_n x)|\hat{u}_p|e^{i\phi_u}\Bigg\} \end{aligned}$$

After some rearrangement, and setting $\bar{a}k = \omega - i\alpha$, we find

$$\begin{aligned} (\omega+i\alpha)^2 = \omega_n^2 - i(\omega+i\alpha)\frac{\bar{a}^2}{\bar{p}(\frac{1}{2}S_c L)}\Bigg\{&\frac{1}{\bar{a}^2}\frac{R}{C_v}S_c\int_0^L\cos(k_n x)\frac{\left|\hat{\dot{Q}}(x)\right|}{\hat{\eta}_n}e^{i\phi_Q}dx \\ &-\bar{\rho}S_c\frac{|\hat{u}_p|}{\hat{\eta}_n}e^{i\phi_p}\Bigg\} \end{aligned}$$

Because $|\hat{\dot{Q}}|$ and $|\hat{u}_p|$ are small perturbations we can write this equation to first order in small quantities:

$$\omega^2 - i(2\alpha\omega) = \omega_n^2 - i\omega_n\frac{2}{\bar{p}L}\frac{R}{C_v}\int_0^L\left[\cos(k_n x)\frac{\left|\hat{\dot{Q}}(x)\right|}{\hat{\eta}_n}e^{i\phi_p}dx + i\omega_n\frac{2\gamma}{L}\frac{|\hat{u}_p|}{\hat{\eta}_n}e^{i\phi_u}\right]dx$$

Take the real and imaginary parts to find

$$\omega^2 = \omega_n^2 + \frac{2\omega_n}{\bar{p}L}\left(\frac{R}{C_v}\right)\int_0^L \left[\cos(k_n x)\frac{\left|\hat{\dot{Q}}(x)\right|}{\hat{\eta}_n}\sin\phi_Q dx - \frac{2\gamma\omega_n}{L}\frac{|\hat{u}_p|}{\hat{\eta}_n}\sin\phi_u\right]dx$$
$$\alpha = \frac{1}{\bar{p}L}\frac{R}{C_v}\int_0^L \left[\cos(k_n x)\frac{\left|\hat{\dot{Q}}(x)\right|}{\hat{\eta}_n}\cos\phi_Q dx - \frac{\gamma}{L}\frac{|\hat{u}_p|}{\hat{\eta}_n}\cos\phi_u\right]dx \qquad (6.24)\ \text{a,b}$$

Internal feedback, and hence a condition for instability, exists of either or both $|\hat{\dot{Q}}|$ and $|\hat{u}_p|$ depend on the fluctuating pressure (or velocity). For example, set

$$|\hat{\dot{Q}}| = q_0\hat{\eta}_n\psi_n = q_0\hat{\eta}_n\cos k_n x$$
$$|\hat{u}_p| = u_0\hat{\eta}_n \qquad (6.25)\ \text{a,b}$$

and (6.24) a,b becomes

$$\omega^2 = \omega_n^2 + 2\omega_n\left(Aq_0\sin\phi_q - Bu_0\sin\phi_u\right)$$

where

$$A = \frac{1}{2\bar{p}}\frac{R}{C_v} \quad ; \qquad B = \frac{\gamma}{L} \qquad (6.26)$$

To first order in small quantities we find the results for the frequency and decay or growth constant:

$$\omega = \omega_n + Aq_0\sin\phi_Q - Bu_0\sin\phi_u$$
$$\alpha = Aq_0\cos\phi_Q - Bu_0\cos\phi_u \qquad (6.27)\ \text{a,b}$$

Remarks:

(i) the n^{th} mode is unstable if $Aq_0\cos\phi_Q > Bu_0\cos\phi_u$

(ii) the first term in α is an example of Rayleigh's criterion discussed in Section 6.3:

a) if $0 \le \phi_u \le \frac{\pi}{2}$ then a necessary condition for instability is $0 \le \phi_Q \le \frac{\pi}{2}$.

b) instability of the n^{th} mode is encouraged if $|\hat{\dot{Q}}(x)|\cos k_n x$ is larger, i.e. if the heat addition is greater where the mode shape of the pressure.

It is important also to notice that due to the spatial averaging, one cannot distinguish the ultimate effects of volumetric and surface processes. There is an equivalence of the influences of the various processes, their importance in respect to position within the chamber being dominated by their location with respect to the mode shapes. That characteristic has far-reaching consequences.

6.4. Rayleigh's Criterion and Linear Stability. As part of his research on the excitation of acoustic waves by heat addition in chambers, Lord Rayleigh (1878, 1945) formulated the following explanation for the production of tones in a Rijke tube:

> "If heat be periodically communicated to, and abstracted from, a mass of air vibrating (for example) in a cylinder bounded by a piston, the effect produced will depend upon the phase of the vibration at which the transfer of heat takes place. If heat be given to the air at the moment of greatest condensation, or be taken from it at the moment of greatest rarefaction, the vibration is encouraged. On the other hand, if heat be given at the moment of greatest rarefaction, or abstracted at the moment of greatest condensation, the vibration is discouraged."

That paragraph has become probably the most widely cited explanation for the presence of combustion instabilities generally. For easy reference, the explanation has long been referred to as "Rayleigh's Criterion."

It is important to realize that Rayleigh addressed only the conditions under which unsteady heat addition 'encourages' oscillations, i.e. is a destablilizing influence. Other processes, stabilizing or destabilizing are neither

excluded nor included, and there is certainly no implication that satisfaction of the criterion is either a necessary or a sufficient condition for instability to exist. Several published examples exist of quantitative realizations of the criterion (Putnam 1971; Chu 1956; Zinn 1986; Culick 1987, 1992). The purpose of this section is to establish a generalized form of Rayleigh's Criterion by using the analysis based on spatial averaging.

The main idea is that a positive change of the time-averaged energy of a modal oscillator in a cycle of oscillation is exactly equivalent to the principle of linear instability, that the growth constant should be positive for a motion to be unstable. To establish the connection we use the oscillator equations,

$$\frac{d^2\eta_n}{dt^2} + \omega_n^2\eta_n = F_n \tag{6.27}$$

The instantaneous energy[24] of the n^{th} oscillator is

$$\mathcal{E}_n = \frac{1}{2}\left(\dot{\eta}_n^2 + \omega_n^2\eta_n^2\right) \tag{6.28}$$

and the change of energy in one cycle is the integral over one period of the rate at which work is done by the force F_n:

$$\Delta\mathcal{E}_n = \int_t^{t+\tau_n} F_n(t')\dot{\eta}_n(t')dt' \tag{6.29}$$

Under the integral, F_n and $\dot{\eta}_n$ must be real quantities: here we use the real parts of both functions,

$$\begin{aligned} \eta_n &= \hat{\eta}_n e^{-i\bar{a}kt} = |\hat{\eta}_n|e^{-i\bar{a}kt} \\ F_n &= \hat{F}_n e^{-i\bar{a}kt} = |\hat{F}_n|e^{-i(\bar{a}kt+\phi_F)} = |\hat{F}_n|\left(\cos\phi_F - i\sin\phi_F\right)e^{-i\bar{a}kt} \end{aligned} \tag{6.31 a,b}$$

We measure all phases with respect to the pressure, so $\hat{\eta}_n$ is real and, being the maximum amplitude, is positive. Substitution in the oscillator equations gives

$$k^2 = \frac{1}{\bar{a}^2}\left(\omega_n^2 - \frac{\hat{F}_n}{\hat{\eta}_n}\right)$$

of which the real and imaginary parts are to first order in small quantities:

$$\begin{aligned} \omega^2 &= \omega_n^2 - Re\left(\frac{\hat{F}_n}{\hat{\eta}_n}\right) = \omega_n^2 - \left|\frac{\hat{F}_n}{\hat{\eta}_n}\right|\cos\phi_F \\ \alpha_n &= \frac{1}{2\omega_n} Im\left(\frac{\hat{F}_n}{\hat{\eta}_n}\right) = \frac{-1}{2\omega_n}\left|\frac{\hat{F}_n}{\hat{\eta}_n}\right|\sin\phi_F \end{aligned} \tag{6.32)a,b}$$

Also for use in (6.29) we have

$$\dot{\eta}_n = i\bar{a}k|\hat{\eta}_n|e^{-i\bar{a}kt} = \bar{a}k|\hat{\eta}_n|e^{-i\left(\bar{a}kt+\frac{\pi}{2}\right)} \approx \omega_n|\hat{\eta}_n|e^{-i\left(\omega_n t+\frac{\pi}{2}\right)}$$

so

$$Re(\dot{\eta}_n) = \omega_n|\hat{\eta}_n|\cos\left(\omega_n t + \frac{\pi}{2}\right) = -\omega_n|\hat{\eta}_n|\sin\omega_n t \tag{6.33}$$

The real part of F_n is

$$Re(F_n) = |\hat{F}_n|\cos\left(\omega_n t + \phi_F\right) = |\hat{F}_n|\left\{\cos\omega_n t\cos\phi_F - \sin\omega_n t\sin\phi_F\right\} \tag{6.34}$$

Hence the right-hand side of (6.29) is

$$\begin{aligned} \Delta\mathcal{E}_n = \int_t^{t+\tau_n} Re(F_n)Re(\eta_n)dt' &= \omega|\hat{F}_n|\int_t^{t+\tau_n}\left\{\sin^2\omega_n t'\sin\phi_F - \frac{1}{2}\sin 2\omega_n t'\cos\phi_F\right\}dt' \\ &= \omega|\hat{F}_n||\hat{\eta}_n|\frac{\tau_n}{2}\sin\phi_F \end{aligned}$$

Substitution of (6.32)a,b leads to the formula

$$\Delta\mathcal{E}_n = 2\pi\alpha_n\omega_n|\hat{\eta}_n|^2 \tag{6.35}$$

which establishes the desired connection between Rayleigh's criterion and linear stability:

[24] $\mathcal{E}_n$ is not the energy of the n^{th} acoustic mode, which is given by the integral of (5.33) over the volume of the chamber.

Remarks:

(i) Positive α_n (the system is linearly unstable) implies that the average energy of the oscillator increases, and vice-versa.
(ii) Rayleigh's original criterion is equivalent to the principle of linear instability **if** only heat exchange is accounted for and is **neither** a necessary **nor** a sufficient condition for existence of a combustion instability.
(iii) The extended form (6.35) of Rayleigh's criterion is exactly equivalent to the principle of linear instability.

Putnam (1971) has made the widest use of Rayleigh's Criterion in practical situations. His book and papers give many examples of applying the Criterion as an aid to making changes of design to avoid oscillations generated by heat release, particularly in power generating and heating systems.

In the past fifteen years many groups have been making direct observations on laboratory systems to check the validity of the Criterion's implications. The key step is based on the assumption that radiation by certain intermediate species in hydrocarbon reactions (CH and OH are the most common indentifiers) can be interpreted as a measure of the rate of chemical reactions taking place and hence of the rate at which energy is released. Simultaneous measurement we made of the spatial distribution of radiation in a system, and of the pressure oscillations, the results then allow at least a qualitative assessment of the extent to which the oscillations are being driven by the energy released in the combustion field, or whether other mechanisms may be active.

It seems that the first report of that sort of effort appeared in a Ph.D. thesis (Sterling, 1987; Sterling and Zukoski, 1991). Figure 6.2 is a sketch of the dump combustor used as the test device, and Figure 6.3 shows the main result.

FIGURE 6.2. The Caltech Dump Combustor (Sterling 1985)

6.5. Explicit Formulas For Linear Stability. The term 'stability of motions' has several interpretations for flows in combustion chambers, including:

(i) the stability of laminar average flow when viscous and inertial properties of the medium dominate, leading to turbulence, a field of distributed vorticity if the steady flow is unstable;
(ii) the stability of shear layers, commonly producing large scale vortex motions when a shear layer is unstable;
(iii) the stability of laminar flame fronts, responsible for one source of turbulent combustion when fronts are unstable;
(iv) the stability of small disturbances which, when the compressibility and inertia of the medium dominate, can develop into acoustic waves.

In terms of the modes of motion mentioned in Section 3.1 and discussed further in Section 3.3, the phenomena (i)–(iii) are classified as waves of vorticity and the fourth comprises acoustic waves. Here we are concerned only with the stability of acoustic waves. The results are very general, accommodating all relevant processes and applicable, in principle, to any combustion chamber. Eventually the obstacles to successful applications are associated almost entirely with problems of modeling. In the first instance, the formal results given here establish explicitly what modeling is required.

6.5.1. *Linear Stability in Three Dimensions.* The formulas (6.14) a,b are general, restricted only by the approximations used in formulating the analytical framework. Hence the problem of obtaining results specific to any given problem comes down to finding explicit forms for F_n^η and $F_n^{\dot\eta}$, i.e. evaluating the integrals defining F_n,

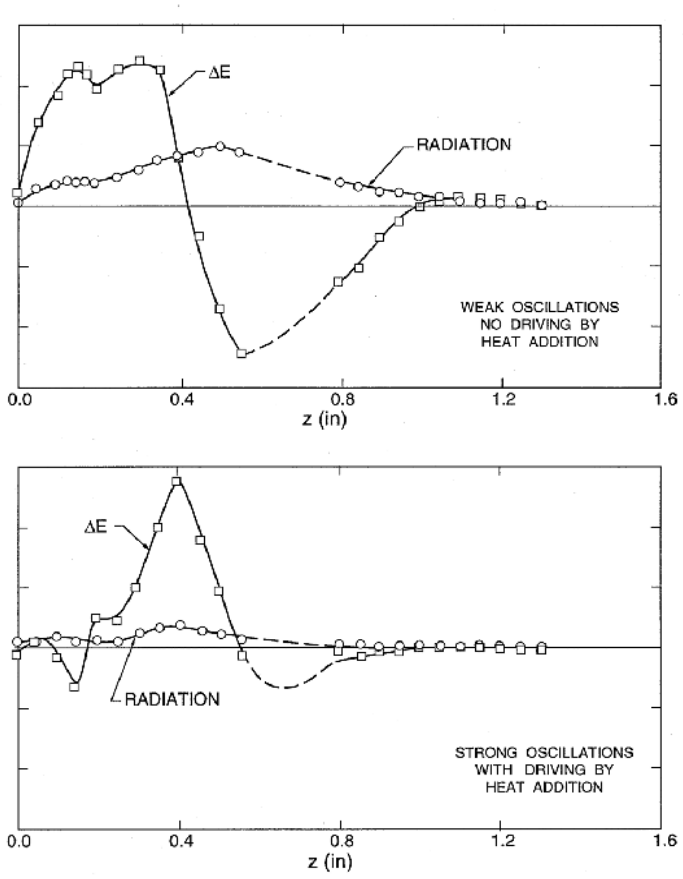

FIGURE 6.3. Experimental Confirmation of Rayleigh's Criteria (Sterling and Zukoski, 1991)

equation (6.2). The functions h and f are given by (4.72) and (4.73) to second order in the fluctuations. Here we need only the linear parts, terms of order $\mu\varepsilon$. With μ and ε absorbed in the definitions of the variables, we have

$$h = -\bar{\rho}\nabla\cdot\left(\bar{\mathbf{M}}\cdot\nabla\mathbf{M}' + \mathbf{M}'\cdot\nabla\bar{\mathbf{M}}\right) - \frac{1}{\bar{a}^2}\frac{\partial}{\partial t}\left(\bar{\mathbf{M}}\cdot\nabla p' + \gamma p'\nabla\cdot\bar{\mathbf{M}}\right) + \left[\frac{1}{\bar{\rho}}\nabla\cdot\left(\frac{1}{\bar{\rho}}\mathcal{F}'\right) - \frac{1}{\bar{a}^2}\frac{\partial P'}{\partial t}\right]_{\mu\varepsilon} \tag{6.36}$$

$$f = \bar{\rho}\left[\frac{\partial\mathbf{M}'}{\partial t}\cdot\hat{n}\right]_{\mu\varepsilon} + \bar{\rho}\hat{n}\cdot\left(\bar{\mathbf{M}}\cdot\nabla\mathbf{M}' + \mathbf{M}'\cdot\nabla\bar{\mathbf{M}}\right) + \left[\hat{n}\cdot\mathcal{F}'\right]_{\mu\varepsilon} \tag{6.37}$$

where the subscript $\mu\varepsilon$ means that the quantity in expanded to include only terms of first order in the mean flow and the fluctuations, i.e. terms $O(\bar{M}_r M_r')$.

Substitution of (6.36) and (6.37) and some rearrangement leads to the result

$$\begin{aligned}\int \hat{h}\psi_n dV + \oiint f\psi_n dS = {} & \bar{\rho}k_n^2\int\left(\bar{\mathbf{M}}\cdot\hat{\mathbf{M}}\right)\psi_n dV \\ & - \bar{\rho}\int\left(\hat{\mathbf{M}}\times\nabla\times\bar{\mathbf{M}}\right)\cdot\nabla\psi_n dV \\ & + i\frac{k_n}{\bar{a}}\int\psi_n\left[\bar{\mathbf{M}}\cdot\nabla\hat{p} + \gamma\hat{p}\nabla\cdot\bar{\mathbf{M}}\right]dV \\ & - i\frac{k_n}{\bar{a}}\int\psi_n\hat{\mathcal{P}}dV - \int\hat{\mathcal{F}}\cdot\nabla\psi_n dV \\ & + \bar{p}\bar{a}k_n\oiint\psi_n\hat{\mathbf{M}}\cdot\hat{n}dS\end{aligned} \tag{6.38}$$

Note that we have removed the exponential time factor for linear harmonic motions and (6.38) contains the amplitudes of fluctuations, denoted by ($\hat{}$). Two remarks are important:

(i) the mean flow field may be rotational ($\nabla\times\bar{\mathbf{M}} \neq 0$) and sources are accommodated ($\nabla\cdot\bar{\mathbf{M}} \neq 0$).
(ii) owing to the ordinary procedure discussed in Section 3, the substitutions of classical acoustic mode shapes are required in the right-hand side:

$$\hat{p} = \bar{p}\hat{\eta}_n\psi_n \; ; \quad \hat{M} = \frac{i}{\gamma k_n^2}\hat{\dot{\eta}}_n\nabla\psi_n \tag{6.39}$$

where $\hat{\dot{\eta}}_n = i\bar{a}k_n\eta_n$.

Eventually the complex wavenumber, (6.11), is

$$\begin{aligned} k^2 = k_n^2 + \frac{\bar{a}^2}{\bar{p}E_n^2}\Bigg\{ & i\bar{p}\bar{a}k_n \oiint\left(\frac{\hat{\mathbf{M}}}{\hat{\eta}_{\mathbf{n}}} + \frac{1}{\gamma}\bar{\mathbf{M}}\gamma_n\right)\cdot\hat{n}\gamma_n dS \\ & + i(\gamma-1)\frac{k_n}{\bar{a}}\bar{p}\int(\nabla\cdot\bar{\mathbf{M}})\,\psi_n^2 dV - i\frac{k_n}{\bar{a}}\int\frac{\hat{\mathcal{P}}}{\hat{\eta}_n}\psi_n dV \\ & - \int\frac{\hat{\mathcal{F}}}{\hat{\eta}_n}\cdot\nabla\psi_n dV\Bigg\} \end{aligned} \tag{6.40}$$

It is important to understand that in the result unsteady gasdynamics (acoustics) and interactions between the acoustics and the mean flow are accounted for 'exactly' to $O(\bar{M}_r)$.

The real and imaginary parts of (6.40), written symbolically as equations (6.12) a,b and (6.14) a,b are sums of contributions from the various processes accounted for. For example, the formula for the growth constant appears in the form

$$\alpha = (\alpha)_{combustion} + (\alpha)_{mean\ flow/acoustics} + (\alpha)_{nozzle} + \cdots$$

Similar results can be derived for the case when the one-dimensional approximation is used. The required basis for the calculations is given by Culick (1998). The results for the frequency and growth constant are:

$$\begin{aligned} \omega = \omega_n + \frac{\bar{a}^2}{2\omega_\ell\bar{p}E_\ell^2}\Bigg\{ & -\bar{p}\bar{a}k_\ell\left[\left(\frac{\hat{u}^{(i)}}{\hat{\eta}_\ell}\psi\right)S_c\right]_0^L \\ & + \bar{p}\bar{a}k_\ell\int_0^L\frac{1}{S_c}\int\left(\frac{\hat{u}_b^{(i)}}{\hat{\eta}_\ell}\right)dq\psi_\ell S_c dz\Bigg\} + \text{ volumetric contributions (combustion)} \end{aligned} \tag{6.41}$$

$$\begin{aligned} \alpha = -\frac{\bar{a}^2}{2\omega_\ell\bar{p}E_\ell^2}\Bigg\{ & \bar{p}\bar{a}k_\ell\left[\left(\frac{\hat{u}^{(i)}}{\hat{\eta}_\ell}\psi_\ell + \frac{1}{\gamma}\bar{u}\gamma_\ell^2\right)S_c\right]_0^L \\ & - \bar{p}\bar{a}k_\ell\int_0^L\frac{1}{S_c}\int\left(\frac{\hat{u}_b^{(i)}}{\hat{\eta}_\ell} + \frac{1}{\gamma}\bar{u}_b\psi_\ell\right)dq\psi_\ell S_c dz \\ & + \frac{k_\ell\bar{p}^L}{\bar{a}}\int_0^L\frac{1}{k_\ell^2}\left(\frac{d\psi_\ell}{dz}\right)^2\frac{1}{S_c}\int\bar{u}_b dq S_c dz\Bigg\} + \text{ volumetric contributions (combustion)} \end{aligned} \tag{6.42}$$

Two remarks on interpretation

(i) the first two terms in the formula for α represent the dynamical response of the enclosing surface and the net effect of linear interactions between the acoustic field and the mean flow.
(ii) the last term represents a dissipative process commonly called 'flow turning' due to inelastic acceleration of the incoming flow, initially normal to the surface, to the local axial velocity parallel to the surface. This process generates unsteady vorticity at the surface; the result shown here does not capture the entire contribution. See Flandro (1995) and Mulhotra (2001).

These results for linear stability have been applied extensively to problems of combustion instabilities in solid propellant rockets. Their validity has long been confirmed. However, their accuracy depends entirely on the accuracy of modeling processes rather than the gasdynamics shown explicitly in (6.40)–(6.42).

Due to the large uncertainties associated with modeling some processes, it is difficult—in fact impossible at this time—to make an entirely satisfactory comparison between theoretical results and measurements. Hence the best way to check theory is to compare results obtained here with results of numerical simulations, all for the same problem. Even this procedure is imperfect because different approximations must be made in the two approaches—it is impossible to solve the 'same' problem numerically and with the analysis given here.

Results of an example for a solid propellant rocket are shown in Figures 6.4–6.6. The calculations were carried out for nonlinear behavior. Figure 6.4 shows the development of the unstable motion into a stable limit cycle and Figure 6.5 is a comparison of the spectra of the waveforms in the limit cycle. The approximate analysis can be carried out only for a finite number of modes. As a consequence, although the frequencies are accurately predicted, the amplitudes have greater errors for the higher modes. Figure 6.6 shows one effect of truncating the modal expansion. For this example the effect is not large—the two-mode approximation seems quite adequate. That is not always true, a matter discussed in the following Section.

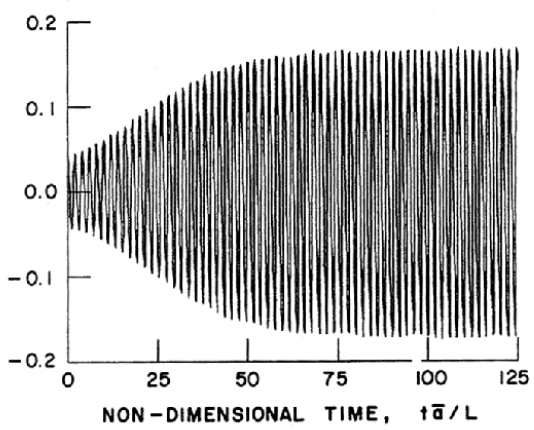

(a) Approximate Analysis

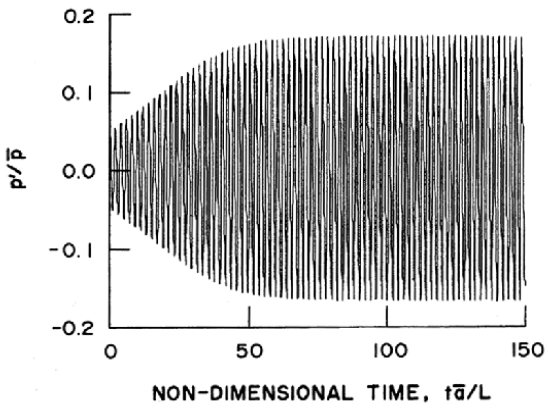

(b) Numerical Simulation

FIGURE 6.4. Growth of Unstable Motions According to (a) the Approximate Analysis; and (b) a Numerical Simulation

Frequencies and amplitudes of acoustic pressures

	Frequency, Hz					Amplitude, $\lvert p'/\bar{p} \rvert$				
Mode	1	2	3	4	5	1	2	3	4	5
Numerical	926	1824	2698	3595	4491	0.151	0.042	0.0234	0.0203	——
Approximate	895	1785	2683	3571	4449	0.151	0.0478	0.0280	0.0153	0.0188

(a)

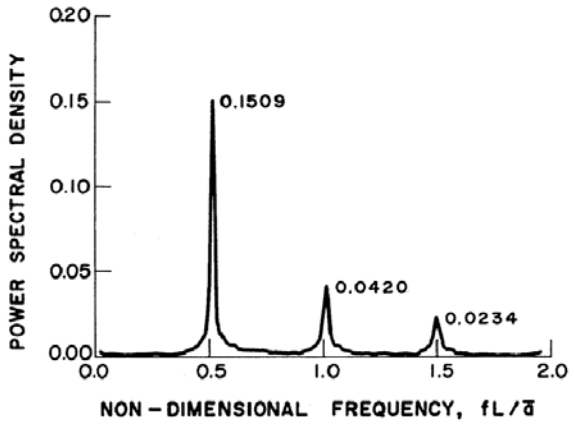

(b)

FIGURE 6.5. Comparison of the Spectra for the Waveforms in Figure 6.4

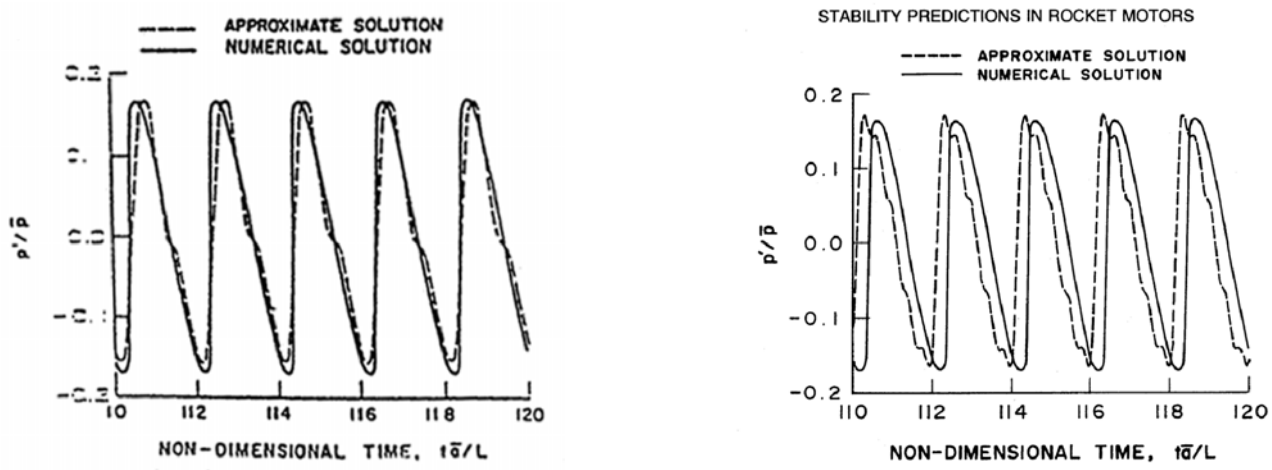

FIGURE 6.6. Effect of Truncation in the Waveforms

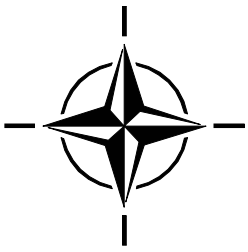

7. NONLINEAR BEHAVIOR

It is linear behavior, especially linear stability, that is most easily understood and therefore has dominated discussions of combustion instabilities. Almost no attention has been paid to nonlinear behavior in works on control of combustion instabilities. One justification for that deficiency has been the view that if control of the oscillations works properly, it should stop the growth before the amplitude reaches a large value. There are several reasons why that reasoning is flawed:

- if the growth rates are unusually large the control system may not have a sufficiently large bandwidth to be effective;
- because combustion systems are intrinsically nonlinear design of a control system based only on linear behavior may produce a control system far from optimal;
- linear control demands actuation at the frequency of the oscillation to be controlled, while nonlinear control of particular types are effective at lower frequencies; an example is described in Section 7.
- observed nonlinear behavior contains much information about properties of the system in question and in the interests of understanding should not be ignored.

Existing examples of controlling combustion instabilities have almost totally ignored issues of nonlinear behavior. In no demonstration, either in the laboratory or full-scale, have the amplitudes of the oscillations been predicted or interpreted either before or after control has been exercised. Hence nothing has been learned about why the initially unstable motions reach the amplitudes they did, or, why the control system affected them in the observed way. In fact few attempts exist to determine quantitatively the stability of motions. Hence the subject of controlling the dynamics of combustion systems has largely been a matter of exercising the principles of control with little attention paid to the characteristics of the systems ('plants') being controlled. It seems that following this strategy is likely not the most fruitful way of achieving meaningful progress. Especially, this is not a sound approach to developing the basis for designing control systems. The current state of the art is that feedback control is designed and applied in *ad hoc* fashion for systems already built and exhibiting instabilities.

A central concern of a controls designer is construction of a 'reduced order' model of the system. What that really means in the present context is the need to convert the partial differential equations of conservation developed in Section 3, to a finite system of ordinary differential equations. The analysis developed in Section 3 and 4 accomplishes exactly that purpose. It is not the only approach possible (e.g. proper orthogonal decomposition has been examined briefly) but the method of modal expansion and spatial averaging has many favorable properties and has been proven to work well.

The main purposes of this section are to quote a few results displaying some aspects of the nonlinear behavior arising from gasdynamics; and to illustrate some consequences of truncating the modal expansion, that is, what might be the consequences of reducing the order of the model. Another important issue we will examine briefly is the application of time-averaging. As the calculations in Section 4 showed, the great advantage of time-averaging is that it replaces N second order oscillator equation by $2N$ first order equations. That transformation enormously reduces the cost of obtaining solutions, aids theoretical work, and provides a simplified representation for application of feedback control. But as for truncation, the question arises: How accurate are the results and what are the limits of the validity of time-averaging?

Only the nonlinearities due to gasdynamics are treated in this section. The results must be viewed with that caveat, particularly because the forms of the nonlinearities are very special, if only because the dominant coupling acts to cause energy to flow from low to high frequency waves, the tendency which produces the familiar steepening of compressive disturbances into shock waves.

7.1. The Two-Mode Approximation. This is the simplest class of problems for which nonlinear mode coupling is accommodated. Each mode is characterized by two constants: α (energy gain or loss) and θ (frequency shift). The energy gain or loss may be nonlinear—that is, α could in principle depend on amplitude—but here both α and θ are taken to be constant, characterizing entirely the linear processes. As a result of several works

in the past few years, the two mode approximation is quite well understood (Awad and Culick, 1986; Paparizos and Culick, 1989; Yang and Culick 1990; Jahnke and Culick, 1994; Culick, 1994).

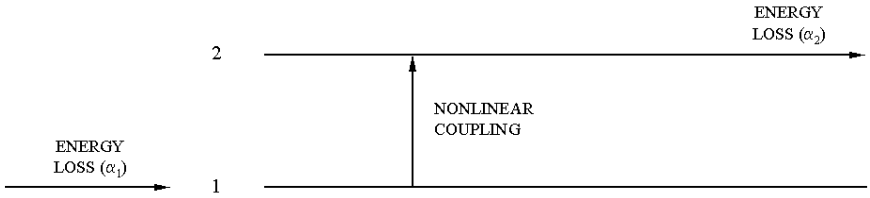

FIGURE 7.1. Energy Flow in the Two Mode Approximation

Only gasdynamic nonlinearities to second order are accounted for here. Their special form allows the convenient closed form solutions to the time-averaged equations, first found by Awad (1983). The results provide much basic understanding which is applicable to more complicated nonlinear problems. For example, contrary to one's expectation based on the behavior of shock waves, nonlinear behavior in the present context need not involve large amplitudes, and the pressure oscillation may appear to be a clean sinusoid, free of significant harmonic content. The basic reason is that here the two-mode system both gains and loses energy; each interaction with the environment is necessary. In the absence of the nonlinear modal coupling, or some other linear process, limit cycles cannot exist. Moreover, both stable and unstable limit cycles exist.

Truncation of the modal expansion to two modes introduces errors because the flow of energy to higher modes is blocked. The amplitude of the highest mode is therefore greater than the correct value in order to provide the higher linear rate of energy loss required to sustain a limit cycle. The example in Section 6.5.1 shows this effect.

It's an interesting feature of the two-mode approximation that nonlinear instability to stable limit cycles seems not to exist. Although no rigorous proof exists, experience with many examples has shown that conclusion to be quite generally true if only the acoustic (gasdynamics) nonlinearities are accounted for. 'Triggering' or pulsing to stable limit cycles does occur for special forms of nonlinear energy gain from the environment (i.e. extinction from the mean flow or supply from combustion processes).

If we ignore linear mode coupling and account for acoustic nonlinearities to second order, the oscillator equations can be put in the form

$$\frac{d^2\eta_n}{dt^2} + \omega_n^2\eta_n = \alpha_n\dot{\eta}_n + \theta_n\eta_n - \sum_{i=1}^{\infty}\sum_{j=1}^{\infty}\{A_{nij}\dot{\eta}_i\dot{\eta}_j + B_{nij}\eta_i\eta_j\} + F_n^{NL} \tag{7.1}$$

where F_n^{NL} represents other nonlinear contributions. The coefficients A_{nij}, B_{nij} are defined as integrals involving the basis functions ψ_{nij}. Hence their values are fixed primarily by the geometry of the chamber in question. See Culick (1976) for additional details of the derivation of (7.1). It is extremely important that the nonlinear gasdynamic terms involve no cross-products $\dot{\eta}_i\eta_j$ and also (not obvious here) no 'self-coupling', terms proportional to $\dot{\eta}_n^2$ or η_n^2. Those properties are the formal reasons that nonlinear instabilities do not exist if only these nonlinearities are included.

Equation (7.1) simplify considerably for longitudinal modes. Due to orthogonality and special properties of the $\cos k_n z$, the double sum becomes a single sum and (7.1) can be put in the form:

$$\begin{aligned}\frac{d^2\eta_n}{dt^2} + \omega_n^2\eta_n = \alpha_n\dot{\eta}_n + \theta_n\eta_n &- \sum_{i=1}^{\infty}\left[C_{ni}^{(1)}\dot{\eta}_i\dot{\eta}_{n-i} + D_{ni}^{(1)}\eta_i\eta_{n-i}\right] \\ &- \sum_{i=1}^{\infty}\left[C_{ni}^{(2)}\dot{\eta}_i\dot{\eta}_{n+i} + D_{ni}^{(2)}\eta_i\eta_{n+i}\right] + F_n^{NL}\end{aligned} \tag{7.2}$$

The time-averaged forms of (7.2) are

$$\frac{dA_n}{dt} = \alpha_n A_n + \theta_n B_n + \frac{n\beta}{2}\sum^{i}[A_i(A_{n-i} - A_{i-n} - A_{i+n}) - B_i(B_{n-i} - B_{i-n} - B_{i+n})]$$
$$\frac{dB_n}{dt} = -\theta_n A_n + \alpha_n B_n + \frac{n\beta}{2}\sum^{i}[A_i(B_{n-i} - B_{i-n} - B_{i+n}) - B_i(A_{n-i} - A_{i-n} - A_{i+n})] \quad (7.3)\ \text{a,b}$$

where as in Section 3, $\eta_n = A_n \cos\omega_n t + B_n \sin\omega_n t$. For longitudinal modes, the frequencies are all integral multiples of the fundamental, a property that is crucial to the forms of (7.3) a,b. For example, for transverse modes in a cylindrical chamber, the nonlinear terms contain factors representing modulation.

For two modes, the four first order equations are

$$\frac{dA_1}{dt} = \alpha_1 A_1 + \theta_1 B_1 - \beta(A_1 A_2 - B_1 B_2)$$
$$\frac{dB_1}{dt} = \alpha_1 B_1 + \theta_1 A_1 - \beta(B_1 A_2 - A_1 B_2)$$
$$\frac{dA_2}{dt} = \alpha_2 A_2 + \theta_2 B_2 - \beta(A_1^2 - B_1^2) \quad (7.4)\ \text{a,b,c,d}$$
$$\frac{dB_2}{dt} = \alpha_2 B_2 + \theta_2 A_2 - 2\beta B_1 A_1$$

The great advantage of this system of equations is that some useful exact results can be found. One way to find them is to change independent variables to the amplitude and phases (Γ_n, ϕ_n) of the two modes by writing

$$\eta_1(t) = \Gamma_1(t)\sin(\omega_1 t + \phi_1)$$
$$\eta_2(t) = \Gamma_2(t)\sin(2\omega_1 t + \phi_2)$$

where $\Gamma_n = \sqrt{A_n^2 + B_n^2}$. The governing equations for Γ_1, Γ_2 and the effective relative phase $\psi = 2\phi_1 - \phi_2$ are

$$\frac{d\Gamma_1}{dt} = \alpha_1\Gamma_1 - \beta\Gamma_1\Gamma_2\cos\psi$$
$$\frac{d\Gamma_2}{dt} = \alpha_2\Gamma_2 - \beta\Gamma_1^2\cos\psi \quad (7.5)\ \text{a,b,c}$$
$$\frac{d\psi}{dt} = (\theta_1 - 2\theta_1) + \beta(2\Gamma_1 - \frac{\Gamma_1^2}{2}\sin\psi$$

where

$$\beta = \frac{\theta_2 - 2\theta_1}{2\alpha_1\alpha_2} \quad (7.6)$$

The problem of linear stability is solved directly:

$$\alpha_1, \alpha_2 < 0 \iff \text{small amplitude motions are stable} \quad (7.7)$$

Nonlinear behavior in general poses two basic questions:

(i) What are the conditions for existence of limit cycles?
(ii) What are the conditions that the limit cycles are stable?

Stability of a limit cycle of course is a matter entirely separate from the linear stability of small amplitude motions. We are concerned here with a system executing a steady limit cycle. If the limit cycle in stable, then if slightly disturbed, the motion will eventually return to its initial form

(a) Existence of Limit Cycles

In this time-averaged formulation, existence of limit cycles corresponds to existence of stationary or equilibrium points of the system (7.5) a,b,c:

$$\frac{d\Gamma}{dt} = \frac{d\Gamma_2}{dt} = \frac{d\psi}{dt} = 0 \iff \text{transcendental algebraic equations}$$

The solutions are

$$\Gamma_{10} = \frac{1}{K}\sqrt{-\alpha_1\alpha_2(1+\beta^2)}$$
$$\Gamma_{20} = \frac{1}{K}\sqrt{\alpha_1^2(1+\beta^2)} \qquad (7.8)\ \text{a,b,c}$$
$$\psi_o = \tan^{-1}(-\beta)$$

where

$$K = \frac{\gamma+1}{2\gamma}\omega_1 \qquad (7.9)$$

For Γ_{10} to be real, $-\alpha_1\alpha_2$ must be positive, implying that the constants α_1, α_2 must have opposite signs. The physical interpretation is that if the first mode is unstable, for example, $\alpha > 0$, then the second mode must be stable ($\alpha_2 < 0$): the rate of energy flow into the first mode must equal the rate of loss from the second mode in order that the amplitudes be constant in time. The transfer rate upwards due to coupling must have the same value. Similar reasoning explains the care when the second grade is unstable, requiring that the first mode to be stable.

(b) Stability of Limit Cycles

To determine the stability of the limit cycles, the variables are written as $\Gamma_i = \Gamma_{i0} + \Gamma_i'$, $\psi = \psi_o + \psi'$ and substituted in the governing equations (7.5) a,b,c. The linearized equations for the disturbances are then solved for characteristic value λ in the assumed forms $\Gamma_i' = \Gamma_{i0}' e^{\lambda t}, \cdots$. For stability, an initial disturbance must decay. Applying that requirement produces regions of stability in the plane of the parameters $\beta_o = (\theta_2 - 2\theta_1)^2/(\alpha_2 + 2\alpha_1)^2$ and α_2/α_1, shown in Figure 7.2

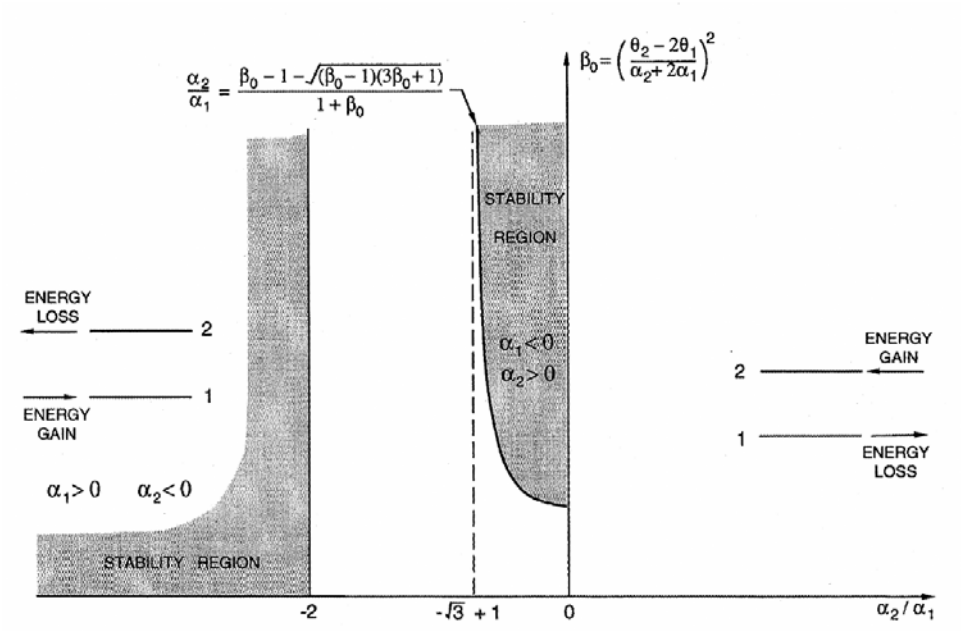

FIGURE 7.2. Regions of Stability for Two Modes, Time-Averaged Equations

There is presently no basis for understanding why stable limit cycles occur only for the special ranges of parameters shown in Figure 7.2. Moreover, it is impossible at this stage to understand the extent to which the shapes of the regions of stability depend on the use of time-averaged equations and on truncation to two modes. It is important for both practical and theoretical reasons to assess and quantify as far as possible the consequences of time-averaging and truncation. Considerable progress has been made in that direction by using a continuation method to solve the systems of oscillator equations. Some results are discussed in the following section.

Here it is useful to examine several special cases. Figure 7.3 shows that if the parameters are chosen so that the operating point lies with the range for stable limit cycles and the first mode is unstable, truncation may have relatively small effects. On the other hand, if the limit cycle is unstable within the two-mode approximation with an unstable first mode, it may become stable (with the same values of $\alpha_1, \alpha_2, \theta_1, \theta_2$) if more stable modes are accounted for.

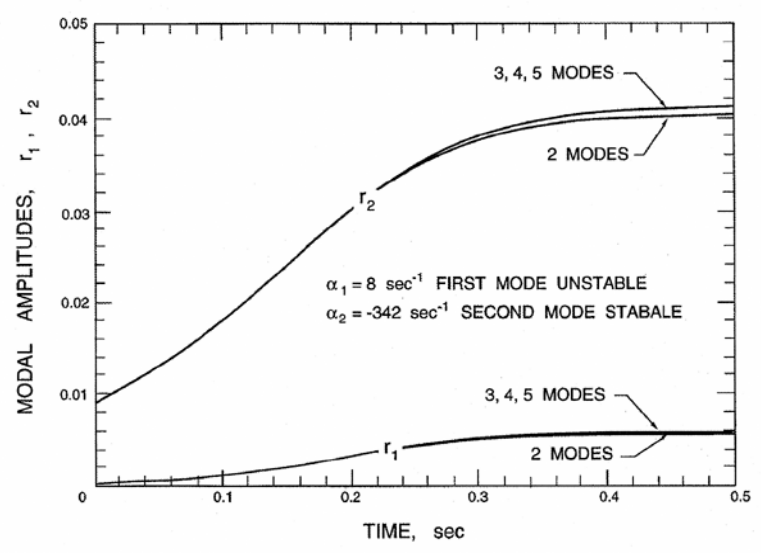

FIGURE 7.3. Effects of Truncation for a Stable Limit Cycle/First Mode Unstable

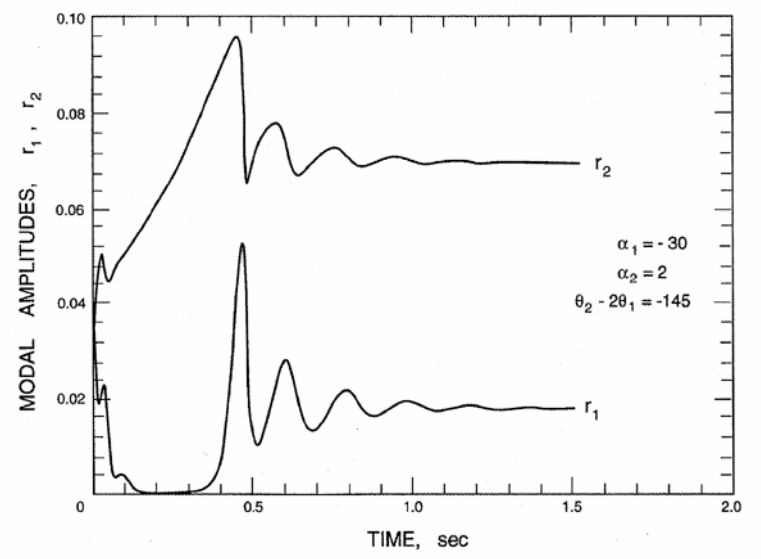

FIGURE 7.4. Development of a Stable Limit Cycle when the Second Mode is Unstable

Figure 7.4 is interesting for a quite different reason. In this case the second mode is unstable, and the motion evolves to a stable limit cycle. However, unlike the example in Figure 7.3, the amplitudes do not grow smoothly and monotonically to their values in the limit cycle. Their erratic behavior is due to the fact that with the second mode unstable, energy must flow from high frequency to low frequency. That is contrary to the direction of flow imposed naturally by the fluid mechanics (of the steepening of a compressive disturbance into a shock wave). The conflict between the natural action of the nonlinear coupling on the one hand and the flow of energy imposed by

energy exchange with the environment causes the amplitudes of the two modes to wander during the transient phase before finally reaching their ultimate values.

7.2. Application of a Continuation Method. Much of the work during the past decade at Caltech on chamber dynamics has been directed to understanding the extent to which nonlinear behavior can be explained on the basis of nonlinear gasdynamics. The reasoning is that first we know the model of gasdynamics—the Navier-Stokes equations for compressible flow—so we can do accurate analysis; and second, those features that cannot be explained must be due to other causes so, by elimination we have some guidelines for what we should seek in other processes. Experience has shown that 'other processes' is this context most probably means combustion.

To carry out this program with numerical simulations—after all, few exact results exist—would be a formidable task because of the number of characteristic parameters. The parameter space comprises those defining the geometry of a chamber and two parameters (α_n, θ_n) characterizing linear behavior of each mode. The effect required to search the parameter space is much reduced by applying a continuation method. The procedure is an efficient system means of locating values of parameters for which the dynamical behavior suffers a qualitative change, i.e. bifurcation points. The simplest—almost trivial—example is the Hopf bifurcation point which arises when for a stable system one of the values α_n changes from a negative to a positive value; the system becomes linearly unstable and under suitable conditions the motion develops into a stable limit cycle. In fact, linear instability is not always such a simple matter. We have found cases with special sorts of nonlinear processes that a Hopf bifurcation may occur when the critical value of the critical α_n is non-zero.

The essential idea of a continuation method applied to limit cycles is illustrated in Figure 7.5 where the variables of the motion are $x(t)$ and μ is the parameter in question, the bifurcation parameter. A continuation method is a computational (numerical) scheme for following, in this case, the changes of a period solution—a limit cycle—as the values of one or more parameters are changed. A picture like Figure 7.5 is impossible to draw for more than three coordinates so the conventional display of information is a bifurcation diagram in which the amplitude of one variable in the limit cycle is plotted versus the parameters varied as the continuation method is applied. Figure 7.5 shows two examples, a Hopf bifurcation, also called a *supercritical bifurcation* and a *subcritical bifurcation* with a turning point. Those are the two types of bifurcation most common in the present context.

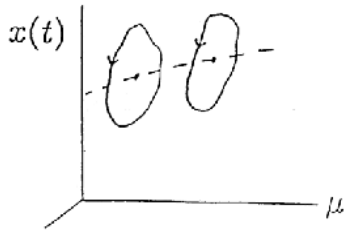

FIGURE 7.5. Schematic Illustration of the Continuation Method Applied to Limit Cycles

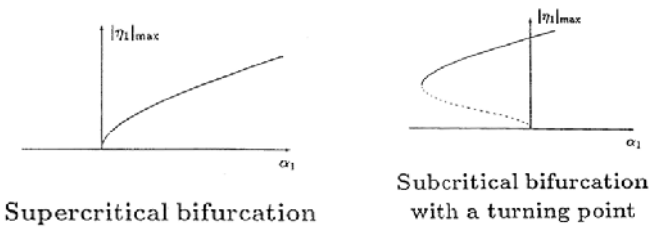

FIGURE 7.6. Two Examples of Bifurcation

Thus a bifurcation diagram is a locus of equilibrium point traced as the bifurcation parameter is changed. As a practical matter, application of a continuation method is more systematic and cheaper to use than use of numerical simulations. We have successfully used a continuation method (Doedel *et al.* 1991a,b; Doedel *et al.* 1997) to investigate four classes of problems:

(i) consequences of time-averaging
(ii) consequences of truncating the modal expansion
(iii) influences of the linear parameters (α_n, θ_n) on nonlinear behavior
(iv) pulsed instabilities: the conditions for existence of stable limit cycles in a linearly stable system.

The problems (i) and (ii) are central to the matter of constructing reduced-order models. Hence it is important to emphasize that in our view, application of the continuation method to investigate the consequences of time-averaging and truncation is part of the procedure for establishing the validity of reduced order models within the framework of analysis based on modal expansion and spatial averaging.

The continuation method is a powerful means for investigating many nonlinear problems in the classic listed above. For more extensive discussions see Jahnke and Culick (1994); Burnley (1996); Burnley and Culick (1996); and Ananthkrishnan and Culick (2002). As an illustration we quote here some results for limit cycles for systems of longitudinal modes when only the gasdynamical nonlinearities are accounted for. We are interested in the consequences of truncation with time-averaging.

In Section 7.1 we cited a few results for the limiting case of two modes described by the four equations found with time-averaging. Figure 7.3 shows the special example of as effect of truncating the series expansion for the time-averaged system: increasing the number of modes apparently widens the region of stability. In fact, use of the continuation method has established the result that the existence for region of stability for limit cycles with two modes is due to truncation. When the first mode is unstable, stable limit cycles exist for all values of α, if more than two modes are taken into account. That is true even if the original oscillator equations are used.

Figure 7.7 shows that if time-averaging is not used, there is a turning point in the bifurcation diagram. If

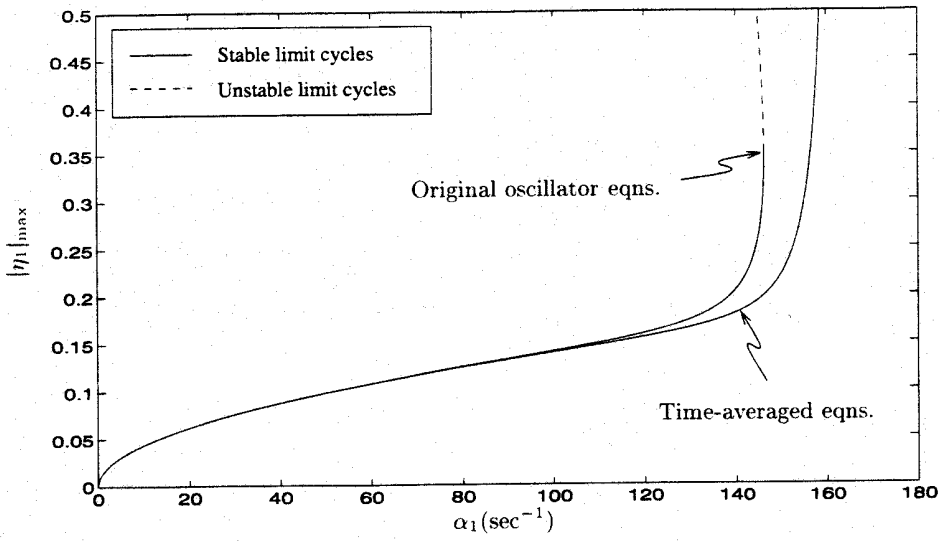

FIGURE 7.7. Effect of Time-Averaging for Two Modes

more than two modes are accounted for, the boundary of stability persists for the time-averaged equations but does not appear if more than two modes are included. Figure 7.8 is the result for the time-averaged equations and Figure 7.9 shows the case of 4 modes computed for the full oscillator equations.

It seems true that if the system is only slightly unstable, then the system of time-averaged equations for two-longitudinal modes is a good approximate model for investigating nonlinear behavior. However, if one is generally interested in producing reduced order models, the effects of truncation and time-averaging should be investigated. Applying a continuation method seems to be the best approach for doing so.

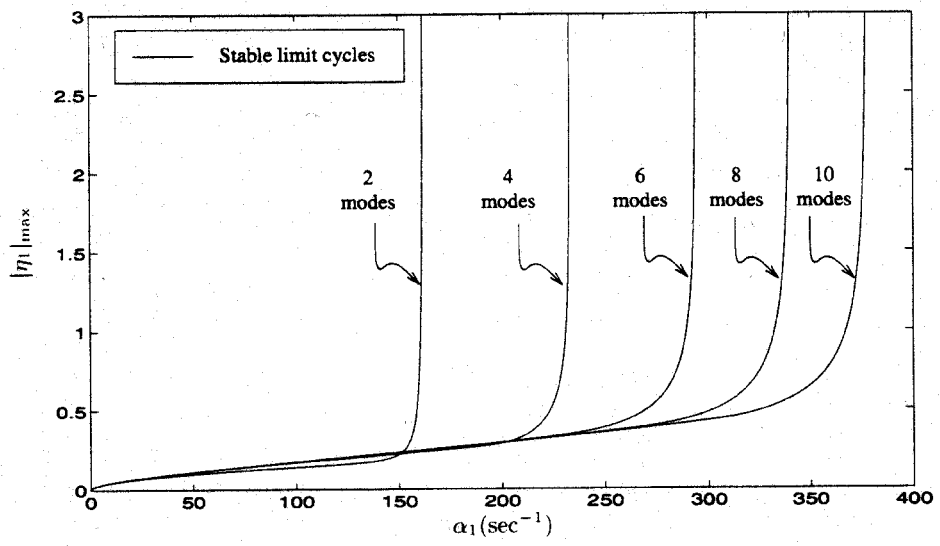

FIGURE 7.8. Stability Boundaries by Truncation of the Time-Averaged Equations

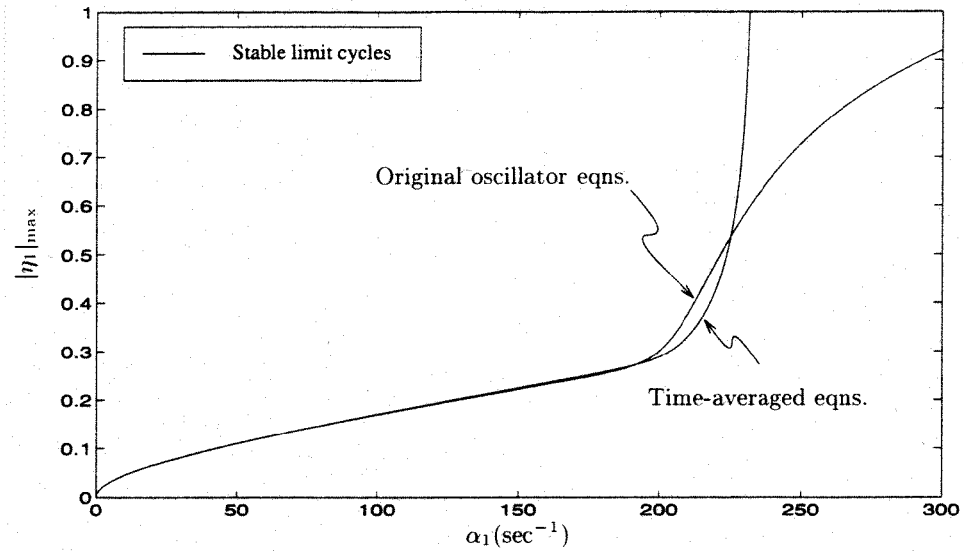

FIGURE 7.9. Maximum Amplitude of η_1 in The Limit Cycle: Four Modes, Comparison of Results for the Full Oscillator and the Time-Averaged Equations

7.3. Hysteresis and Control of Combustion Instabilities. The existence of hysteresis in the dynamical behavior of combustions is both an interesting phenomenon to investigation and a characteristic that has potentially important practical consequences. It seems that the first evidence for hysteresis in combustors was found by Russian researchers concerned with instabilities in liquid rockets (Natanzon *et al* 1993; Natanzon 1999). In that case, Natanzon and his co-workers proposed bifurcation of *steady states* of combustion, and the associated hysteresis, as a possible explanation for the random occurrences of combustion instabilities. The Russian workers were in a special situation affording them the opportunity to make such observations. The large Russian boosters were designed to use many (up to thirty-three) liquid rocket engines in a single stage. Hence large numbers of nominally identical engines were manufactured and tested for operational use. Sufficient data were obtained that statistical analysis of the behavior could be carried out. Hence a basis existed for identifying random behavior. The idea is the following.

In a liquid rocket many zones of recirculation are created at the injector where jets of liquid fuel and/or oxidizer enter the chamber. As an approximation, one may regard a recirculation zone as a chemical reactor whose behavior is known to be well-characterized by the temperature of the incoming gases entrained from the environment, and the average temperature within the zone. A fairly simple calculation based on consideration of energy and mass flows leads to the results sketched in Figure 7.10. The upper and lower branches of the

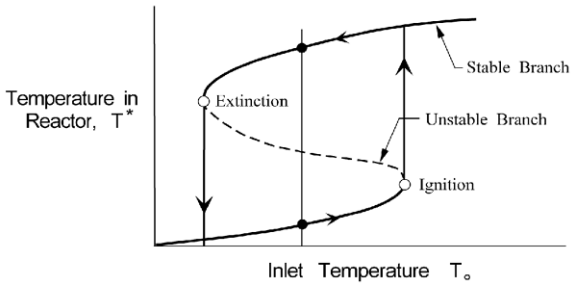

FIGURE 7.10. Hysteresis Loop for a Recirculated Zone Idealized as a Simple Chemical Reactor

hysteresis loop represent different branches of stable combustion. Those states have different influences on the state of combustion in the chamber. It was Natanzon's assertion that the state associated with the lower branch in Figure 7.10 (the cold recirculation zone) is more unstable and prone to lead to combustion instabilities. Which branch is reached depends on the history of the engine, starting from ignition or some other sort of abrupt transient. The final state of a recirculation zone therefore depends on random 'accidents' of history. Therefore random occurences or combustion instabilities may be observed. Figure 7.11 is a sketch of a possible recirculation zone and adjacent flow of a fuel or oxidizer jet, this model has been used as the basis for numerical calculations supporting Natanzon's proposal.

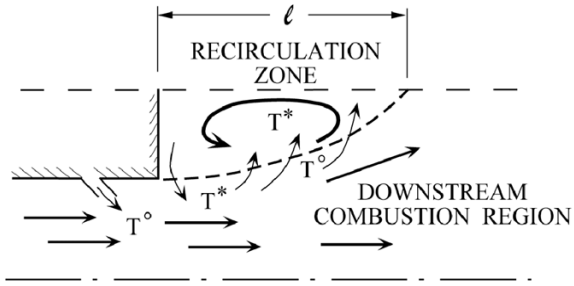

FIGURE 7.11. Sketch of a Recirculation Zone formed by a Jet of Fuel or Oxidizer

In the mid-1980's research with a dump combustor at Caltech revealed the presence of a different kind of hysteresis of dynamical states of combustion (Smith, 1985; Sterling, 1987). The combustor has been described in Section 1, Figure 1.3; Figure 6.2 shows the inlet region and the recirculation zone at the dump plane during steady combustion. The combustor showed combustion instabilities in the neighborhood of the stability boundary defined in the plane of flow rate and equivalence ratio. Figure 7.12(a). Figure 7.12(b) shows the hysteresis loop, observed as dependence of the level if pressure oscillation on equivalent ratio with the total flow rate held constant. This sort of behavior has been observed also in other dump combustors (J. Cohen, UTRC; and G. Richards, METC) as well as as in a flame-driven Rijke tube (Seywert, 2001) and in an electrically driven Rijke tube (Matveev, 2002).

More recent works (Knoop *et al.* 1996; Isella *et al.* 1996) have established the physical nature of the hysteresis in this case and have shown how active control can be used to extend the range of steady operation into the hysteretic region. High speed films have confirmed that the upper branch of the loop is associated with shedding of large vortices which, causing periodic combustion of entrained reactants sustain high amplitude pressure oscillations. The lower branch is associated with relatively quiet combustion in a shear layer shed from the lip at the inlet.

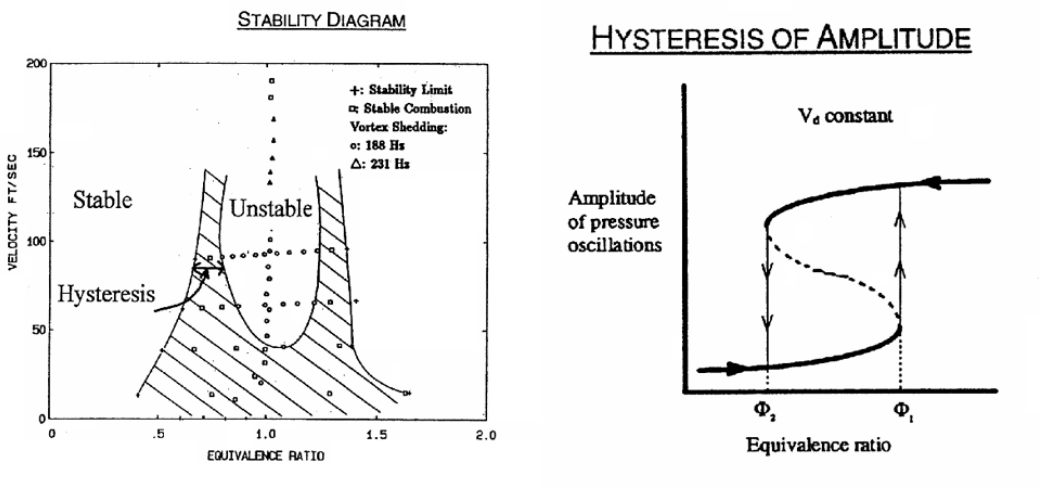

(a) (b)

FIGURE 7.12. (a) Stability Boundary and (b) an Idealized Hysteresis Loop for the Caltech Dump Combustor

Familiar considerations of dynamical behavior suggest that it should be possible to achieve pulsed transitions between the two branches of stable dynamical states. Those processes were demonstrated by Knoop *et al* and Isella *et al* by injecting pulses of fuel at the inlet plane. Single pulses of fuel always cause transition from the upper to the lower branch. Thus with suitable sensing and actuation it is possible always to maintain the low level of oscillations (effectively 'noise') within the zone where hysteresis exists.

This is a form of nonlinear control. Although it has been demonstrated only for the range of equivalence ratio covering the zone of hysteresis, it is an important demonstration of active control at a frequency far less than the frequency of the oscillations. That is a significant characteristic because if the reduced bandwidth required of the control system, particularly the actuation.

7.4. Representing Noise in Analysis of Combustor Dynamics. Even a small laboratory combustor radiates considerable noise, generated by turbulent motions (often called 'combustion noise') within the chamber. See, for example, the spectrum reproduced earlier as Figure 1.4. The scaling laws are not known, but it is obvious to any bystander that a full-scale combustor of any sort is noisy indeed. Presently it is not well understood how important noise is to the behavior of combustion instabilities or to the application of feedback control. The purpose of this section is to introduce a means for investigating those matters within the framework developed in Sections 3 and 4.

There are three sorts of problems that will arise:

(i) formal construction of noise (stochastic) sources in the framework of spatially averaged equations for unsteady motions in a combustor;
(ii) modelling the noise sources;
(iii) solving the stochastic differential equations.

The first step, as explained in Section 3.1, is to apply the principle of splitting small disturbances into the three basic modes of propagation: acoustic waves, vorticity waves, and entropy waves. All of the discussion so far in these lectures has been devoted to the acoustic field. Noise is associated with the random motions comprising mainly vorticity but also entropy (or temperature) waves in a combustion chamber. Our concern in the present context is directed chiefly to interactions of those motions with the acoustic field. The formal representation will be relatively simple and intuitively persuasive, but modelling the details remains to be accomplished. Numerical results require assumptions that cannot be justified *a priori*.

Following the principle of splitting, we write the flow variables as sums of the three contributions, one each corresponding to the three modes of motion:

$$\begin{aligned} p' &= p'_a + p'_\Omega + p'_s \\ \mathbf{\Omega}' &= \mathbf{\Omega}'_a + \mathbf{\Omega}'_\Omega + \mathbf{\Omega}'_s \\ s' &= s'_a + s'_\Omega + s'_s \\ \mathbf{u}' &= \mathbf{u}'_a + \mathbf{u}'_\Omega + \mathbf{u}'_s \end{aligned} \qquad (7.10)\ \text{a,b,c,d}$$

Subscripts $(\ )_a$, $(\ )_\Omega$, $(\ )_s$ denote acoustic, vortical and entropic contributions. Once again, the ordering procedure explained in Sections 3 and 4 allows us to derive meaningful results by considering only the first order components. Hence we assume that only the acoustic waves contain pressure fluctuation; only the waves of vorticity contain vorticity fluctuations; and only the entropy waves have fluctuations of entropy. The velocity field possesses contributions from all three modes.

The idea then is to substitute the assumed general forms of the variables and substitute in the primitive equations of motion expanded to third order in the fluctuations. Then form the nonlinear equation for the pressure and apply spatial averaging. This procedure was first reported by Culick *et al.* (1992) but in revised and corrected form by Burnley (1996) and Burnley and Culick (1999). Eventually one finds the oscillator equations,

$$\ddot{\eta}_n + \omega_n^2 \eta_n = F_n$$

by now F_n contains stochastic sources. The 'general' form of F_n is

$$-\frac{\bar{p}E_n^2}{\bar{a}^2}F_n = \bar{\rho}I_1 + \frac{1}{\bar{a}^2}I_2 + \bar{\rho}I_3 + \frac{1}{\bar{a}^2}I_4 + \bar{\rho}I_5$$
$$+ \oiint \left[\rho\frac{\partial \mathbf{u}'}{\partial t}\cdot\hat{u} + \bar{\rho}\frac{\partial \mathbf{u}'}{\partial t}\right]\cdot\hat{\mathbf{n}}\psi_n dS - \int \mathbf{\mathcal{F}'}\cdot\nabla\psi_n dV + \frac{1}{\bar{a}^2}\int \frac{\partial P'}{\partial t}\psi_n dV$$

where

$$I_1 = \int [\bar{\mathbf{u}}\cdot\nabla\mathbf{u}' + \mathbf{u}'\cdot\nabla\bar{\mathbf{u}}]\cdot\nabla\psi_n dV$$

and similar definitions for the remaining integrals I_1. See the references for details.

Then the unsteady velocity field is split according to (7.10) a,b,c,d. Eventually re-arrangement and application of the assumptions discussed above leads to the result

$$\begin{aligned} \ddot{\eta}_n + \omega_n^2\eta_n = 2\alpha_n\dot{\eta}_n + 2\omega_n\theta_n\eta_n - \sum_{i=1}^{\infty}\sum_{i=1}^{\infty}[A_{nij}\dot{\eta}_i\dot{\eta}_j + B_{nij}\eta_i\eta_j] \\ + \sum[\xi_{ni}^v\dot{\eta}_i + \xi_{ni}\eta_i] + \Xi_n + \left(F_n^{NL}\right)_{other} \end{aligned} \qquad (7.11)$$

where the ξ_{ni}^v, ξ_{ni} and Ξ_n are stochastic sources defined as integrals over the vortical and entropic fluctuations of the velocity. See the references cited above for details.

No modeling based on experimental, theoretical or phenomenological grounds has been accomplished. Explicit results have been obtained by approximating the stochastic sources as white noise processes having properties chosen to be realistic, i.e. the results seem to be reasonably consistent with available measurements of actual behavior.

Two types of stochastic influences arise in (7.11):

(i) Ξ_{ni}, Ξ_{ni}^v represent stochastic influences on the 'spring' or natural frequency of the n^{th} mode and on the damping or growth rate. These are formally referred to as 'multiplicative noise sources' because they appear as factors multiplying the dependent variables, the displacement and velocity of the n^{th} oscillator.

(ii) Ξ_n represents a stochastic driving source causing excitation of the n^{th} oscillator even in the absence of driving by combustion processes; the Ξ_n are formally called 'additive noise sources'.

It is evident from the form of (7.11) that the random character of the stochastic sources will appear as random fluctuations imposed on the amplitudes $\eta_n(t)$ of the acoustic modes; exactly the sort of behavior found experimentally. Thus, Fourier synthesis of the pressure field, the modal expansion, continues to serve as a good approximate representation of the deterministic results can be obtained by retaining only a small number of terms.

Results were obtained first for the simplest, case of two modes, with noise sources only in the fundamental mode. Nonlinear gasdynamic coupling transfer stochastic behavior to the second mode. Computations have been carried out with a Monte-Carlo method to give probability density functions, with the equations written in the Stratonovich form of stochastic differential equations (Burnley, 1996). Figure 7.13 shows the pressure trace and spectrum for a simulation in which the first mode is unstable.

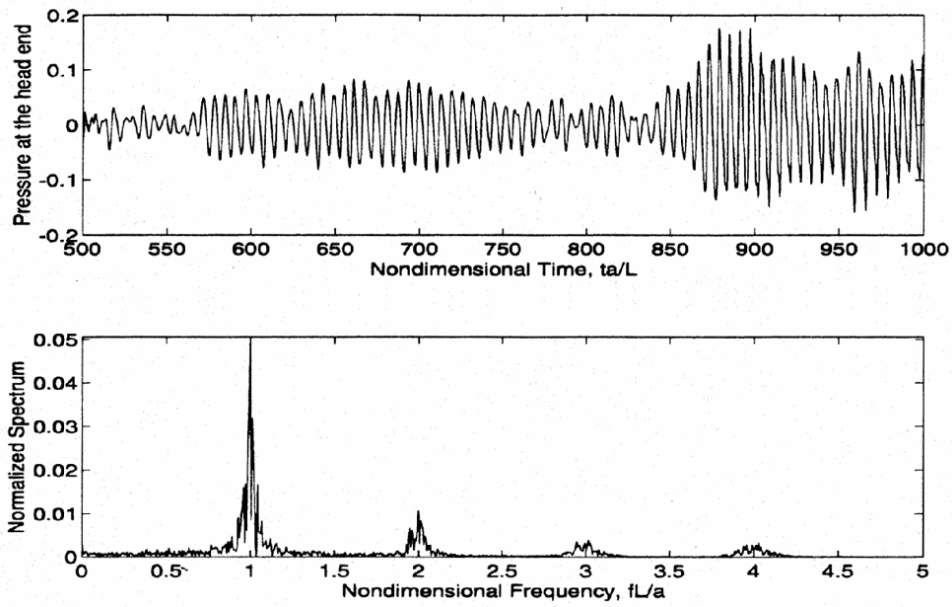

FIGURE 7.13. Pressure Trace and Spectrum for a Simulation with Noise; Four Modes Included, First Mode Unstable

This method of accounted for noise in a combustor seems to be very promising. However modeling the noise sources is in a primitive state, and comparisons of results with experimental observations can only be done qualitatively.

7.5. System Identification for Combustor Dynamics with Noise. Use of system identification in the field of combustor dynamics seems to have been developed first by Russian groups as part of their development of liquid rocket engines, beginning perhaps as early as the 1950's but certainly in the 1960's (Agarkov *et al.* 1993).

In several papers during the 1980's, Hessler (1979, 1980, 1982) and Duer and Hessler (1984), and more recently Hessler and Glick (1998) have asserted that the oscillations observed as combustion instabilities in solid rocket motors are *driven* rather than *self-excited.* The sources of the driving—i.e. the 'mechanisms'—are supposed to be either vortex shedding or noise. Hessler and co-workers conclude that the properties of the noise measured in a stable chamber can be used as the basis for infusing properties of the primary mechanism causing instabilities when they arise or more correctly, such data will provide quantitative information about the static stability margins—how close the dominant acoustic modes are to becoming unstable.

The basic idea is sound. When the mechanisms are interpreted as driving forces independent of the acoustic field, and they are assumed to be broad-band, then the acoustic modes are excited to amplitudes related directly to the amount of damping (α_n). Hence the idea is to process noisy records in such a fashion as to extract the values of the linear parameters (α_n, θ_n). The proposed method can be tested using the oscillator equations with some sources derived in the preceding section.

Seywert and Culick (1999) have reported results of some numerical simulations carried out to check the idea just described. In particular, the main purpose was to determine the accuracy with which the experimental method would give the linear parameters. The procedure is straightforward. To be definite and to keep the computations within practical bounds, we consider a system of four modes, each containing noise sources which, as explained in Section 7.4, are assumed to be white noise. The amplitudes of the noise (rms values) are selected so that random amplitude fluctuations in the pressure spectrum have values in the ranges experimentally observed (Seywert and Culick).

Three types of problems arise, associated with the three types of noise sources: additive noise, Ξ_n; and two kinds of multiplicative noise, ξ_n^v which affects mainly the growth and decay rates, and ξ_n which causes random variations of the frequency. In all cases we are concerned here with discovering the ways in which noise affects the result of system identification. The idea is to select values of the α_n, θ_n and carry out numerical simulations. The data are then processed to give values of the α_n, θ_n which now have mean values and some uncertainties due to the presence of the noise. The questions to be answered are: How close are the mean values to the time values used as inputs? and How large are the uncertainties? These are important practical matters. If the method is effective, then data from hot firings of full-scale combustors could be used to infer the linear parameters characterizing the dynamics represented by several modes. Those parameters identify the poles of the response function of the chamber. Hence a relatively straightforward process would give the information required to proceed with designing a linear control system (see Section 2.5).

Actually there are two ways to get the information: process pressure records naturally occurring; or process the pressure record following an pulse. The method of pulsing has long been used as means of assessing the stability margin of liquid rockets (Harrje and Reardon, 1972). Both methods have been used for a stable system of four longitudinal modes having the parameters given in the table; the fundamental frequency is 900 s^{-1}. Figure 7.14 shows a simulated pressure trace and Figure 7.15 shows its power spectrum and construction using Berg's method.[25]

mode	1	2	3	4
$\alpha_n(s^{-1})$	-50	-375	-584	-889
$\theta_n(s^{-1})$	12.9	46.8	-29	-131

TABLE 7.1. Values of the Linear Parameters

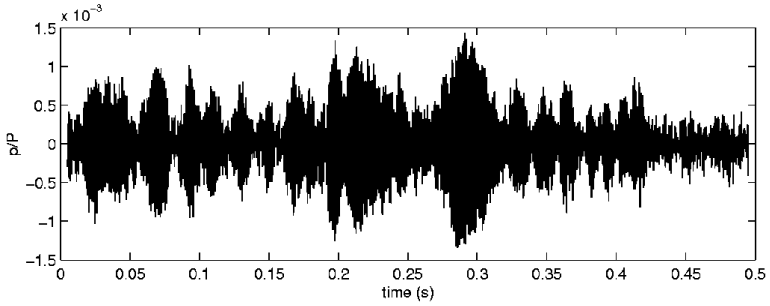

FIGURE 7.14. Simulated Pressure Trace with Noise; All Modes Stable

[25]Berg's method is a standard method of signal processing, widely available. We have used the software included in the Signal Processing Toolbox, and extension of MATLAB.

In Figure 7.17, a simulated response to a pulse is fitted by the superposition of four modes:

$$\frac{p'}{\bar{p}} = \sum_{i=1}^{4} A_i e^{\alpha_i t} \cos(\omega_i t + \phi_i)$$

The parameters A_i, α_i, ω_i, ϕ_i are fitted using a least squares method.

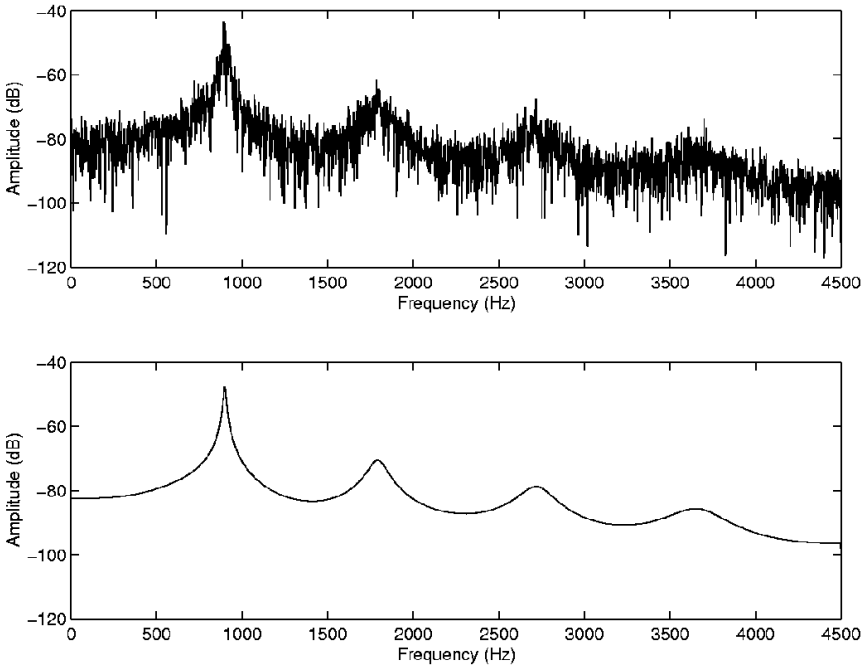

FIGURE 7.15. Application of Berg's Method: Power Spectrum of the Pressure Trace in Figure 7.14 and its Reconstruction

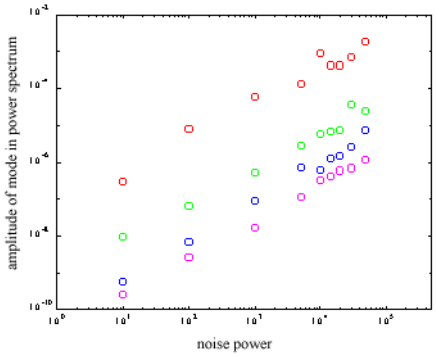

FIGURE 7.16. Dependence of the Peak Amplitudes of the Power Spectra for Four Modes, on Noise Power

Without good data for the noise in an actual combustor and no model, we assume white noise sources. Their amplitudes are chosen so that the average (rms) values of the simulated pressure records are reasonable Table 7.2 shows the relation between the rms value of the system response $(p'/\bar{p})$ and the noise power of Ξ. The 'noisepower' cannot be measured, being the height of the power spectral density of the noise. Figure 7.16 gives a more detailed picture, showing how the amplitudes of the spectra of the four modes increase with noise power.

We use the noise power as a parameter. Figure 7.18 shows an example of the sort of results one finds for multiplicative noise in the modal damping ($\xi_n^v \neq 0$; $\xi_n = 0$; $\Xi_n = 0$). The corresponding results of using the pulse method are given in Figure 7.19.

Noise Power of Ξ_n	rms Values of $p'/\bar{p}$
10^1	.005%
10^3	.05%
10^5	.5%

TABLE 7.2. Relation Between the Noise Power of Ξ_n and the rms Value of the Simulated Pressure Fluctuation

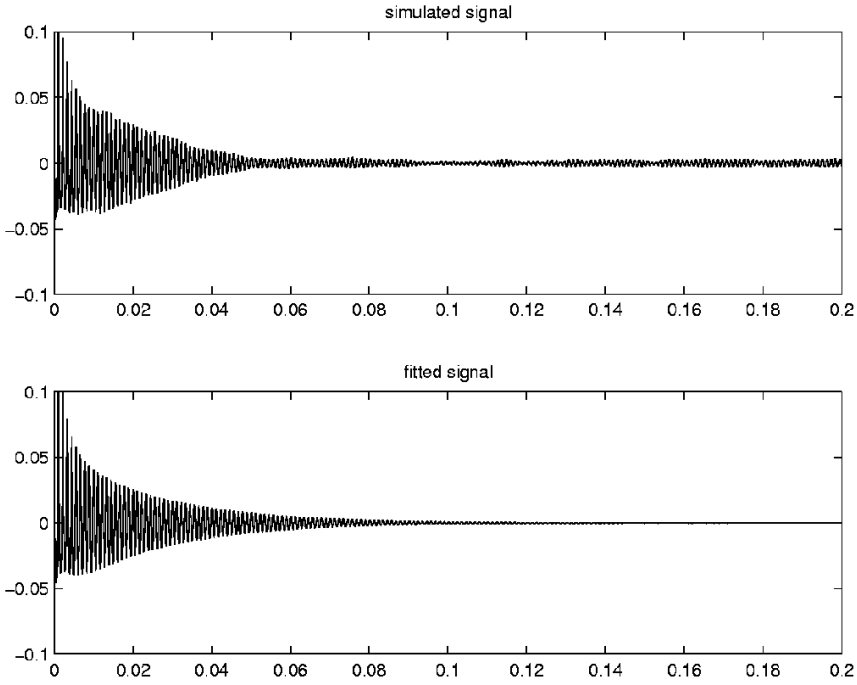

FIGURE 7.17. Reconstructed Pressure Trace for the Transient Response Excited by a 10% Pulse

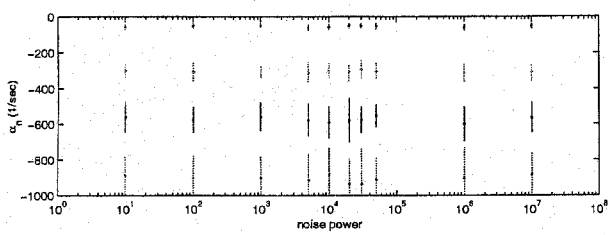

Noise	α_1	α_2	α_3	α_4
10^1	-57±14	-301±31	-560±84	-886±98
10^2	-51±13	-307±52	-576±75	-903±126
10^3	-47±11	-307±38	-558±78	-901±117
10^4	-56±16	-300±51	-591±88	-883±150
10^5	-59±18	-310±53	-598±95	-914±128
10^6	-53±15	-310±46	-564±84	-905±172
10^7	-59±19	-313±44	-591±83	-887±124
correct	-50	-325	-584	-889

FIGURE 7.18. Values of Decay Rates (Modal Attenuation) Found with Berg's Method with Multiplicative (ξ_n) Noise

We conclude from these results that substantial errors may accompany system identification in the presence of realistic (we believe) noise. How significant the errors are depends the particular application at hand and in how small the stability margins are. For a weakly stable system, values of the margins determined in this way are suspect because of the finite uncertainties. The results would therefore not be useful as a basis for representing the combustor's response function.

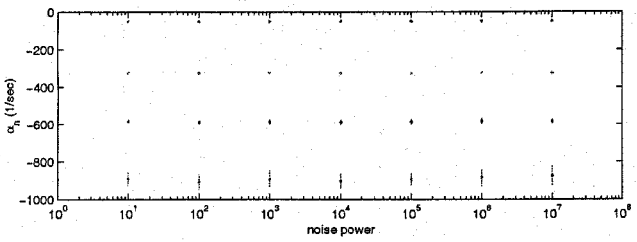

Noise	α_1	α_2	α_3	α_4
10^1	-50±2	-323±6	-584±9	-889±35
10^2	-50±2	-325±5	-589±8	-908±36
10^3	-50±2	-322±4	-587±10	-891±44
10^4	-50±3	-326±5	-589±8	-902±37
10^5	-49±3	-326±4	-586±12	-895±35
10^6	-50±2	-324±4	-582±15	-886±43
10^7	-49±3	-327±4	-583±11	-877±51
correct	-50	-325	-584	-889

FIGURE 7.19. Values of Decay Rates (Modal Attenuation) Found with the Method of Pulsing

It should be clear from the nature of the methods described here that the system must be stable (i.e. all modes must be stable) for this application. For example, if data (simulated) for a limit cycle are processed in this fashion, the inferred values of α_n, θ_n have no apparent connection with the correct values.

8. PASSIVE CONTROL OF COMBUSTION INSTABILITIES

Given the irrefutable observational evidence that combustion instabilities will almost inevitably occur during development of new motors, the problem of treating them becomes crucially important. The goal must be to eliminate undesirable oscillation, but as a practical matter it may well be satisfactory to reduce their amplitudes to acceptable levels. The manufacturer and the customer must then be confident that the amplitudes will not grow unexpectedly at some later time.

Figure 1.6 suggests the intentions or goals of introducing passive control:

(i) Increase the losses of acoustic energy so they exceed the gains in the frequency range where the instability occurs;

(ii) Reduce the gains of acoustic energy below the losses; or

(iii) Shift the natural frequencies of the chamber modes so that none lie within the range of frequencies where the gains of acoustic energy exceed the losses.

The chief ways of achieving these goals in practice are:

(i) Increase the losses of acoustic energy:
- modify the geometry including possibly, the shape of the nozzle entry section
- add resonators, baffles or 'resonant rods'
- introduce stability additives

(ii) Reduce the gains of acoustic energy:
- eliminate geometrical causes of vortex shedding
- change the composition of the propellant—notably the size distribution of oxidizer particles
- introduce stability additives

(iii) Shift the natural frequencies of the chamber
- change the geometry of the chamber

Of the various possibilities, the most commonly used now are changes of geometry, and introduction of stability additives.

Generally there are three reasons to revise the internal design: eliminate possible causes of vortex shedding; shift the frequencies of the normal modes; and increase the gains, or reduce the losses of acoustic energy. The last tactic rests on understanding the contributions to the growth/decay constant, as well as the way in which the shape of the grain changes with time during a firing. The results shown in Figure 8.1 illustrate the point.

It is particularly important to know as well as possible the relative importance of pressure and velocity coupling. That understanding requires knowing the acoustic mode shapes—easily acquired (or estimated if necessary)—and, more importantly, the response functions of the propellant for pressure and velocity coupling. We have emphasized in Section 2 that at the present time data for the pressure coupled response can be obtained only with difficulty and considerable uncertainty. There is no method for routinely determining the velocity coupled response.

The problem of relating changes of composition of a propellant to changes of its combustion dynamics remains essentially unsolved. Experience has provided some guidelines (influences of AP particle size distribution is perhaps the best example) but what is available has largely to do with the effects of quite significant changes of composition on the pressure-coupled response. The consequences of small changes of composition (which may be inadvertant and within manufacturing specifications) are simply not understood. The inability to obtain accurate experimental results is a serious obstacle to improving this situation.

To good approximation, the dynamics of velocity coupling are not understood. Qualitative ideas are available (see Section 2) but—again due to the lack of a good test method—the true mechanisms cannot be determined

and it is impossible to collect quantitative information. This remains, in the author's opinion, the most significant and difficult outstanding problem in this field.

In practice, much reliance has been placed on small changes of propellant composition, the use of 'stability additives.' Following the early use of resonance rods to provide stability in small motors, the favorable effects of stability additives were first investigated in the 1950s and 1960s (Summerfield 1960; Waesche 1999; Price 1971; Evans and Smith 1978). Much of the experience rests in proprietary company files, possibly under the heading "fairy dust."

Stability additives seem to have two main consequences: they may change the propellant response function (pressure or velocity coupling or both); and they certainly affect the properties of condensed combustion products that act to attenuate acoustic oscillations. As many as 80 different additives have been studied, but only a very small number have been widely used. The most common are aluminum oxide and zirconium oxide. Changing the properties of the primary metallic aluminum in the propellant may have substantial favorable consquences.

Changes in the response function may be due both to physical and chemical processes. What actually happens cannot be established unambiguously. In this situation, the collaboration of experimental tests (however crude); observation of the behavior of sub- and full-scale motors; spectulation; and theory, is extremely important. The continued elaboration of analyses of the sort discussed briefly in Section 2 is basic to this process, including calculation of linear and nonlinear dynamical behavior in motors.

For motors containing aluminum, the most significant damping process is the viscous interaction between condensed material and the surrounding gases under oscillatory conditions. The amount of attenuation is proportional to the amount of condensed material present but especially depends on the particle size distribution. Figure 8.1 shows the results of calculations of the attenuation. The main and extremely important point is that for a given frequency and particle loading (mass of particles per unit mass of gas/particle mixture) the maximum attenuation is strongly dependent on particle size. Hence in practice, means are sought to alter the combustion of the propellant and aluminum to generate particles of condensed aluminum oxide having size suitable for greastest damping of the instability at hand. In recent years this has been possibly the most widely used (or at least contemplated) strategy to treat instabilities in motors operating with metallized propellants and has often been successful. The strategy is of course less relevant to smokeless and low smoke systems. Hence the search for 'fairy dust.'

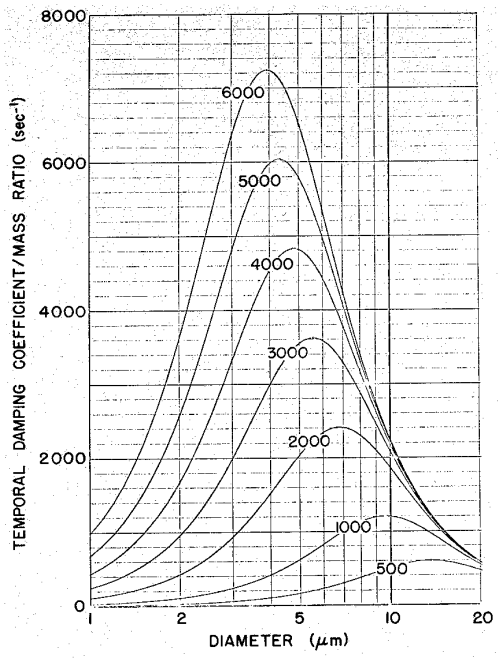

FIGURE 8.1. Attenuation of Acoustic Waves by Particles Suspended in a Gas.

A. EQUATIONS OF MOTION

Combustion systems commonly contain condensed phases: liquid fuel or oxidizer and combustion products including soot and condensed metal oxides. Hence the equations of motion must account for two or three phases and at least one species in each. For investigating the dynamics of combustors, it is entirely adequate to represent each phase as its mass average over all member species. It is unnecessary to distinguish liquid and solid material and we assume a single species in the condensed phase, devoted by subscript $(\ )_l$. For some applications it is appropriate to extend the representation slightly to accommodate distributions of particle sizes, not included in this appendix. There is some advantage to treating the gas phase as a multi-component reacting mixture. As the primitive conservation equations we therefore begin with the following set:

A.1. General Equations of Motion. Conservation of Species

$$\frac{\partial \rho_i}{\partial t} + \nabla \cdot (\rho_i \mathbf{u}_i) = w_i + w_i^{(l)} + w_{ei} \tag{A.1}$$

Global Conservation of Mass, Gas Phase

$$\frac{\partial \rho_g}{\partial t} + \nabla \cdot (\rho_g \mathbf{u}_g) = w_g^{(l)} + w_{eg} \tag{A.2}$$

Global Conservation of Mass, Condensed Phase[26]

$$\frac{\partial \rho_l}{\partial t} + \nabla \cdot (\rho_l \mathbf{u}_l) = -w_g^{(l)} + w_{el} \tag{A.3}$$

Global Conservation of Momentum

$$\frac{\partial}{\partial t}\left(\sum^{i} \rho_i \mathbf{u}_i + \rho_l \mathbf{u}_l\right) + \nabla \cdot \left(\sum \rho_i \mathbf{u}_i \mathbf{u}_i + \rho_l \mathbf{u}_l\right) + \nabla p = \nabla \cdot \overleftrightarrow{\boldsymbol{\tau}}_v + \mathbf{m}_{eg} + \mathbf{m}_{el} \tag{A.4}$$

Global Conservation of Energy

$$\frac{\partial}{\partial t}\left(\sum \rho_i e_{oi} + \rho_l e_{ol}\right) + \nabla \cdot \left(\sum \rho_i \mathbf{u}_i e_{oi} + \rho_l \mathbf{u}_l e_{ol}\right) + \nabla \cdot \left(\sum p_i \mathbf{u}_i\right) = \nabla \cdot \left(\overleftrightarrow{\boldsymbol{\tau}}_v \cdot \mathbf{u}_g\right) - \nabla \cdot \mathbf{q} + Q_e \tag{A.5}$$

Equation of State, Gas Phase

$$p = \rho_g R_g T_g \tag{A.6}$$

For simplification, the above equations already contain some terms involving mass averaging over the species comprising the gas phase, namely the viscous tensor $\overleftrightarrow{\boldsymbol{\tau}}_v$; the vector $\mathbf{q}$ representing heat conduction; and the equation, of state (A.6). For more complete derivations of the equations for multicomponent mixtures, see for example Chapman and Cowling (1958); Hirschfelder, Curtis and Bird (19); Truesdell and Toupin (1960); and Williams (1985). Superscript $(\ )^{(l)}$ means that the liquid phase is the source and subscript $(\ )_e$ denotes an external source. It follows from repeated use of the Gibbs-Dalton law for mixtures of perfect gases that p is the sum of partial pressures, ρ_g is the sum of the densities and R is the mass average of the individual gas species, so for the gas phase we have

$$\begin{aligned} p &= \sum p_i \\ \rho_g &= \sum \rho_i \\ R_g &= \frac{1}{\rho_g} \sum \rho_i R_i \end{aligned} \tag{A.7 a,b,c}$$

[26] Note that ρ_l represents the mass of condensed material per unit volume of chamber, *not* the density of the material itself.

Subscript $(\ )_i$ identifies the i^{th} gaseous species; and in all cases except T_g, $(\ )_g$ means a mass average over all gas species as, for example,

$$\mathbf{u}_g = \frac{1}{\rho_g}\sum \rho_i \mathbf{u}_i = \sum Y_i \mathbf{u}_i \tag{A.8}$$

where $Y_i = \rho_i/\rho_g$ is the mass concentration of the i^{th} species.

Writing equations (A.1)–(A.5) explicitly with sums over species allows proper accounting of the influencesof diffusion, and leads to the formula for energy released by chemical reactions written in the conventional fashion. Thus the basis for subsequently modeling is rigorously set. For analysis of unsteady motins in combustors it is perfectly adequate to reduce the general description for a multicomponent mixture to a model representing a single fluid having the mass-averaged properties of the actual mixture. Details of the procedure may be found elsewhere (Culick 1999). Only the results are germane here. The set of equations forming the basis for the theory and analysis we discuss in these lectures is:

$$\frac{D\rho}{Dt} = -\rho\nabla\cdot\mathbf{u} + \mathcal{W} \tag{A.9}$$

$$\rho\frac{D\mathbf{u}}{Dt} = -\nabla p + \boldsymbol{\mathcal{F}} \tag{A.10}$$

$$\rho\mathbf{C}_v\frac{DT}{Dt} = -p\nabla\cdot\mathbf{u} + \mathcal{Q} \tag{A.11}$$

$$\frac{Dp}{Dt} = -\boldsymbol{\gamma}p\nabla\cdot\mathbf{u} + \mathcal{P} \tag{A.12}$$

$$\frac{Ds}{Dt} = \frac{1}{T}\mathcal{S} \tag{A.13}$$

$$p = \mathbf{R}\rho T \tag{A.14}$$

For completeness we have also included the equation (A.13) for the entropy, obtained in familiar fashion by applying the combined. First and Second Laws of Thermodynamics to an element of fluid. That is, the relation $de = Tds - pdv$ can be written

$$\begin{aligned}\frac{Ds}{Dt} &= \frac{1}{T}\left(\frac{De}{Dt} + p\frac{Dv}{Dt}\right)\\ &= \frac{1}{T}\left(\mathbf{C}_v\frac{DT}{Dt} + p\frac{Dv}{Dt}\right)\end{aligned} \tag{A.15}$$

Substitution of (A.9) and (A.11) gives (A.13) with the source

$$\mathcal{S} = \mathcal{Q} - \frac{p}{\rho^2}\mathcal{W} \tag{A.16}$$

It is important to realize that this formulation contains all relevant physical processes, including those representing the actions of external influences associated, for example, with active control of combustor dynamics.

The source functions in (A.9)–(A.13) are

$$\mathcal{W} = w_e - \nabla\cdot(\rho_l\delta\mathbf{u}) \tag{A.17}$$

$$\boldsymbol{\mathcal{F}} = \nabla\cdot\overleftrightarrow{\boldsymbol{\tau}}_v + \mathbf{m}_e + \mathbf{m}_D - \boldsymbol{\sigma}_e - \delta\mathbf{u}_l w_g^{(l)} + \mathbf{F}_l + \delta\mathbf{F}_l \tag{A.18}$$

$$\begin{aligned}\mathcal{Q} = {}& \overleftrightarrow{\boldsymbol{\tau}}_v\cdot\nabla\cdot\mathbf{u} - \nabla\cdot\mathbf{q} + Q^w + Q_e - (e_{og}w_{og} + e_{ol}w_l) + \chi_D + \sum h_i\nabla\cdot(\rho_g\mathbf{V}_i Y_i)\\ & - \mathbf{u}\cdot(\mathbf{m} - \boldsymbol{\sigma}_e) + (\mathbf{u}\cdot\delta\mathbf{u})\,w_g^{(l)} + \delta Q_l + \delta\mathbf{u}\cdot\mathbf{F}_l - \mathbf{u}\cdot(\boldsymbol{\mathcal{F}} - \mathbf{F}_l)\end{aligned} \tag{A.19}$$

$$\mathcal{P} = \frac{\mathbf{R}}{\mathbf{C}_v}\mathcal{Q} + \mathbf{R}T\left[\mathcal{W} - \nabla\cdot(\rho_l\delta\mathbf{u})\right] \tag{A.20}$$

$$\mathcal{S} = \mathcal{Q} - \frac{p}{\rho^2}\mathcal{W} \tag{A.21}$$

The quantities $\delta(\quad)$ represent differences between values for the gas and condensed phases. For example, $\delta T = T_l - T_g$ in the difference in temperature between the temperature T_l of the condensed phase and that, T_g, of the gas phase.

A.2. Expansions in Mean and Fluctuating Variables. Following the steps suggested in Section 3.3 to produce equations (3.23)–(3.28) will give the expressions for the brackets defined there to simplify the appearance of the equations:

$$\{[\rho]\}_1 = \bar{\mathbf{M}}\cdot\nabla\rho' + \rho'\nabla\cdot\bar{\mathbf{M}} + \mathbf{M}'\cdot\nabla\bar{\rho} \tag{A.22}$$

$$\{\rho\}_2 = \nabla\cdot(\rho'\mathbf{M}') \tag{A.23}$$

$$\{[M]\}_1 = \bar{\rho}(\bar{\mathbf{M}}\cdot\nabla\mathbf{M}' + \mathbf{M}'\cdot\nabla\bar{\mathbf{M}} + \rho'\frac{\bar{D}\bar{\mathbf{M}}}{Dt} \tag{A.24}$$

$$\{M\}_2 = \rho'\frac{\partial\mathbf{M}'}{\partial t} + \bar{\rho}\mathbf{M}'\cdot\nabla\mathbf{M}' + \rho'\left(\bar{\mathbf{M}}\cdot\nabla\mathbf{M}' + \mathbf{M}'\cdot\nabla\bar{\mathbf{M}}\right) \tag{A.25}$$

$$\{M\}_3 = \rho'\mathbf{M}'\cdot\nabla\mathbf{M}' \tag{A.26}$$

$$\{[T]\}_1 = \bar{\rho}C_v\left(\bar{\mathbf{M}}\cdot\nabla T' + \mathbf{M}'\cdot\nabla\bar{T}\right) + C_v\rho'\frac{\bar{D}\bar{T}}{Dt} + p'\cdot\nabla\bar{\mathbf{M}} \tag{A.27}$$

$$\{T\}_2 = C_v\rho'\frac{\partial T'}{\partial t} + C_v\rho'\left(\bar{\mathbf{M}}\cdot\nabla T' + \mathbf{M}'\cdot\nabla\bar{T}\right) + C_v\bar{\rho}\mathbf{M}'\cdot\nabla T' + p'\nabla\cdot\mathbf{M}' \tag{A.28}$$

$$\{T\}_3 = C_v\rho'\mathbf{M}'\cdot\nabla T' \tag{A.29}$$

$$\{[p]\}_1 = \bar{\mathbf{M}}\cdot\nabla p' + \mathbf{M}'\cdot\nabla\bar{p} + \gamma p'\nabla\cdot\bar{\mathbf{M}} \tag{A.30}$$

$$\{p\}_2 = \mathbf{M}'\cdot\nabla p' + \gamma p'\nabla\cdot\mathbf{M}' \tag{A.31}$$

$$\{[s]\}_1 = \bar{\rho}\bar{T}\bar{\mathbf{M}}\cdot\nabla s' + \rho'\bar{T}\frac{\bar{D}\bar{s}}{Dt} + \bar{\rho}\left(\bar{T}\mathbf{M}' + T'\bar{\mathbf{M}}\right)\cdot\nabla\bar{s} \tag{A.32}$$

$$\{s\}_2 = \rho'\bar{T}\frac{\bar{D}s'}{Dt} + \rho'T'\frac{\bar{D}\bar{s}}{Dt} + \left(\rho'\bar{T} + \bar{\rho}T'\right)\mathbf{M}'\cdot\nabla\bar{s} + \bar{\rho}T'\frac{\partial s'}{\partial t} \tag{A.33}$$

$$\{s\}_3 = \left(\bar{\rho}T' + \rho'\bar{T}\right)\mathbf{M}'\cdot\nabla s' + \rho'T'\left(\mathbf{M}'\cdot\nabla\bar{s} + \bar{\mathbf{M}}\cdot\nabla s'\right) \tag{A.34}$$

$$\{s\}_4 = \rho'T'\mathbf{M}'\cdot\nabla s' \tag{A.35}$$

The subscript $\{\quad\}_n$ on the curly brackets means that the contained quantities are written to order n in the fluctuations of flow variables. Similarly, the square brackets indicate that the terms are of first order in the Mach number of the mean flow. Higher order square brackets are not required, as explained in Section 3.3.1.

B. THE EQUATIONS FOR ONE-DIMENSIONAL UNSTEADY MOTIONS

These are many problems for which the flow may be approximated as one-dimensional. Even when the approximation may not seem as accurate as we might like, it is always a good beginning. The desired results are usually obtained without real effect and often are inspiringly close to the truth. An elementary example is computation of the normal modes for a straight tube having discontinuities, Section 5.5.2. Here we are concerned with situations in which influences at the lateral boundary must be accounted for. The formulation of the general problem is then essentially the counterpart of the constitution of the one-dimensional equations for steady flow in ducts thoroughly discussed by Shapiro (1953).

Accounting for changes of area in the one-dimensional approximation is a straightforward matter; following the rules applied to derivations appearing in the three-dimensional equations:

$$\begin{aligned} \mathbf{u}\cdot\nabla(\quad) &\rightarrow u\frac{\partial}{\partial x}(\quad) \\ \nabla\cdot(\quad) &\rightarrow \frac{1}{S_c}\frac{\partial}{\partial x}S_c(\quad) \\ \nabla^2(\quad) &= \frac{1}{S_c}\frac{\partial}{\partial x}S_c\frac{\partial(\quad)}{\partial x} \end{aligned} \tag{B.1}$$

where the axis of the duct lies along the x-direction and $S_c(x)$ is the distribution of the cross-section area.

More interesting are consequences of processes at the lateral boundary, particularly when there is flow through the surface. The most important applications arise in solid propellant rockets when burning propellant forms all or part of the lateral surface. Inflow of mass momentum and energy must be accounted for (Culick 1971, 1973; Culick and Yang 1992). The equations have the same form as the three-dimensional equations derived in Appendix A, equations (A.9)–(A.13) but the rule (B.1) applied and only the velocity component u along axis of the duct taken to be non-zero:

Conservation of Mass

$$\frac{D\rho}{dt} = -\rho\frac{1}{S_c}\frac{\partial}{\partial x}(S_c u) + \mathcal{W}_1 + \mathcal{W}_{1s} \tag{B.2}$$

Conservation of Momentum

$$\rho\frac{Du}{Dt} = -\frac{\partial p}{\partial x} + \mathcal{F}_1 + \mathcal{F}_{1s} \tag{B.3}$$

Conservation of Energy

$$\rho C_v\frac{DT}{Dt} = -p\frac{1}{S_c}\frac{\partial}{\partial x}(S_c u) + \mathcal{Q}_1 + \mathcal{Q}_{1s} \tag{B.4}$$

Equation for the Pressure

$$\frac{Dp}{Dt} = -\gamma p\frac{1}{S_c}\frac{\partial}{\partial x}(S_c u) + \mathcal{P}_1 + \mathcal{P}_{1s} \tag{B.5}$$

Equation for the Entropy

$$\frac{Ds}{Dt} = \frac{1}{T}(\mathcal{S}_1 + \mathcal{S}_{1s}) \tag{B.6}$$

where

$$\frac{D}{Dt} = \frac{\partial}{\partial t} + u\frac{\partial}{\partial x} \tag{B.7}$$

The source terms $\mathcal{W}_1$, $\mathcal{F}_1$, $\mathcal{Q}_1$, $\mathcal{P}_1$ and $\mathcal{S}_1$ are the one-dimensional forms of (A.17)–(A.21) written for the axial component of velocity only and with the rules (B.1) applied. In addition, sources of mass, momentum and energy associated with flow through the lateral boundary are represented by the symbols with subscript $(\quad)_s$ (Culick 1973, Culick and Yang 1995):

$$\mathcal{W}_{1s} = \frac{1}{S_c}\int m_s dq = \frac{1}{S_c}\int \left[m_s^g + m_s^l\right] dq \tag{B.8}$$

$$\mathcal{F}_{1s} = \frac{1}{S_c}\int \left[(u_s - u)m_s^g + (u_{ls} - u_l)m_s^l\right] dq \tag{B.9}$$

$$\mathcal{Q}_{1s} = \frac{1}{S_c}\int \left[(h_{0s} - e_0)m_s^g + (e_{l0s} - u_{l0})m_s^l + C_v T m_s^g\right] dq \tag{B.10}$$

$$\mathcal{P}_{1s} = \frac{R}{C_v}Q_{s1} \tag{B.11}$$

$$\mathcal{S}_{1s} = \frac{1}{p}Q_{1s} = \frac{p}{\rho}\mathcal{W}_{1s} \tag{B.12}$$

Superscripts $(\quad)^{(g)}$ and $(\quad)^{(l)}$ refer respectively to the gas and liquid phases and subscript $(\quad)_s$ denotes values at the surface. The mass fluxes at the surface, $m_s^{(g)}$ and $m_s^{(l)}$ are of course computed as values normal to the boundary and are positive for inward flow. Here q stands for the parameter of the local section normal to the axis.

B.1. Equations for Unsteady One-Dimensional Motions. Forming the equations for the fluctuating motions within the one-dimensional approximation is done in exactly the same way as for the general equations, Appendix A. We need only apply the rules (B.1) and add to the inhomogeneous functions h and f the contributions from processes at the boundary. As for the general three-dimensional equations, we defer writing the fluctuations $\mathcal{W}_1'$, $\mathcal{F}_1'$, $\cdots$ until we consider specific problems.

The procedure introduced in Section 3.3.3 for forming the systems of equations for a hierarchy of problems applies equally to one-dimensional motions. As above, the equations are obtained from the three-dimensional equations by applying the rules (B.1): the results can be constructed when needed. However, the contributions from processes at the lateral boundary are special. Written to first order in the fluctuations and the Mach number of the mean flow; the dimensional forms of (B.8)–(B.12) are:

$$\mathcal{W}_{1s}' = \frac{1}{S_c}\int \left(m_s^2\right)' dq \tag{B.13}$$

$$\begin{aligned}\mathcal{F}_{1s}' = {} & \frac{1}{S_c}\left(\bar{u}_s - \bar{u}\right)\int \left(m_s^g\right)' dq + \frac{1}{S_c}\left(\bar{u}_{ls} - \bar{u}\right)\int \left(m_s^l\right)' dq \\ & + \frac{1}{S_c}\left(u_s' - u'\right)\int \bar{m}_s^g dq + \frac{1}{S_c}\left(u_{ls}' - u_l'\right)\int \bar{m}_s^l dq\end{aligned} \tag{B.14}$$

$$\begin{aligned}\mathcal{Q}_{1s}' = {} & \frac{1}{S_c}\left(\bar{h}_{0s} - e_0\right)\int \left(m_s^g\right)' dq + \frac{1}{S_c} + \left(\bar{e}_{l0s} - \bar{e}_{l0}\right)\int \left(m_s^l\right)' dq + C_v\bar{T}\int \left(m_s^g\right)' dq \\ & + \frac{1}{S_c}\left(h_{0s}' - e_0'\right)\int \bar{m}_s^{g'} dq + \frac{1}{S_c} + \left(e_{l0s}' - e_{l0}'\right)\int \bar{m}_s^l + C_v T\int \left(m_s^g\right)' dq\end{aligned} \tag{B.15}$$

$$\mathcal{P}_{1s}' = \frac{R}{C_v}Q_{1s}' \tag{B.16}$$

$$\mathcal{S}_{1s}' = \frac{1}{p}Q_{1s}' - \frac{p}{\rho}\mathcal{W}_{1s}' \tag{B.17}$$

REFERENCES

Aaron, K. and Culick, F.E.C. (1984).

Akiba, R. and Tanno, M. (1959) "Low Frequency Instability in Solid Propellant Rocket Motors," *Proceedings of the 1st Symposium (International) on Rockets and Astronautics,* Tokyo, pp. 74–82.

Ananthkrishnan, N. and Culick, F.E.C. (2002) "Modeling and Dynamics of Nonlinear Acoustic Waves in a Combustion Chamber," 38^{th} AIAA/ASME/SAE/ASEE Joint Propulsion Conference & Exhibit, 7–10 Jul 2002, Indianapolis, Indiana, AIAA-2002-3592.

Anil Kumar, K.R. and Lakshmisha, K.N. (2000) "Nonlinear Intrinsic Instability of Solid Propellant Combustion Including Gas-Phase Thermal Inertia," *Comb. Sci. and Tech.,* Vol. 158, pp. 135–166.

Anil Kumar, K.R. and Lakshmisha, K.N. (2002) "Dynamic Combustion of Solid Propellants: Effects of Unsteady Condensed Phase Degradation Layer," *J. Prop and Power,* Vol. 15, No. 2, pp. 312–321.

Avalon, G., Casalis, G. and Grifford, J. (1998) "Flow Instabilities and Acoustic Resonance of Channels with Wall Injection," AIAA Paper No. 98–3218.

Avalon, G., Ugurtas, B. Grisch, F. and Bresson, F. (2000) "Numerical Computations and Visualization Tests of the Flow Inside a Cold Gas Simulation with Characterization of a Parietal Vortex Shedding," AIAA-2000-3387.

Awad, E. and Culick, F.E.C. (1986) "On the Existence and Stability of Limit Cycles for Longitudinal Acoustic Modes in a Combustion Chamber," *Combustion Science and Technology*, Vol. 46, pp. 195–222.

Awad, E. (1983) "Nonlinear Acoustic Instabilities in Combustion Chambers," Ph.D. Thesis, California Institute of Technology.

Barrére, M. and Bernard, J.J. (1962) "Combustion Instability of Solid Propellant with Time Delay Distribution," *8th Symposium (International) on Combustion,* William and Wilkins, pp. 886–894.

Baum, J.D. and Levine, J.N. (1982) "Numerical Techniques for Solving Nonlinear Instability Problems in Solid Rocket Motors," *AIAA Journal,* Vol. 20, No. 7, pp. 955–961.

Baum, J.D. and Levine, J.N. and Lovine, R.L. (1988) "Pulsed Instability in Rocket Motors: Comparison Between Predictions and Experiments," *Journal of Propulsion and Power,* Vol. 4, No. 4, pp. 308–316.

Beckstead, M.W., Ryan, N.W. and Baer, A.D. (1966) "Non-Acoustic Instability of Composite Propellant Combustion," *AIAA J.,* Vol. 4, No. 9, pp. 1622–1628.

Beckstead, M.W (1967) "Low Frequency Instability: A Comparison of Theory and Experiment," Paper 67-13, The Combustion Institute.

Beckstead, M.W. and Boggs, T.L. (1967) "The Effect of Oxidizer Particle Size on Non-acoustic Instability," *Fourth ICRPG Combustion Conference,* Stanford Research Institute.

Beckstead, M.W. and Culick, F.E.C. (1967) "A Comparison of Analysis and Experiment for the Response Function of a Burning Surface," *Fourth ICRPG Combustion Conference,* Stanford Research Institute; also Rept. NWCTP 4531, May 1968, U.S. Naval Weapons Center.

Beckstead, M.W. and Price, E.W. (1967) "Nonacoustic Combustion Instability," *AIAA J.,* Vol. 5, No. 11, pp. 1989–1996.

Beckstead, M.W., Mathes, H.B., Price, E.W. and Culick, F.E.C. (1969) "Combustion Instability of Solid Propellants," *12th Symposium (International) on Combustion,* pp. 203–211.

Beckstead, M.W. and Culick, F.E.C. (1971) "A Comparison of Analysis and Experiment for Solid Propellant Combustion Instability," *AIAA Journal,* Vol. 9, No. 1, pp. 147–154.

Beckstead, M.W., Derr, R.L. and Price, C.F. (1972) "A Model of Composite Solid Propellant Combustion Based on Multiple Flames," *AIAA Journal,* Vol. 8, pp. 2200–2207.

Beckstead, M.W., Richards, R.S. and Brewster, B.S. (1987) "Distributed Combustion Effects of Particle Damping," *AIAA J.,* Vol. 22, No. 3, pp. 383–387.

Beckstead, M.W. (1980) "Model for Double-Base Combustion," *AIAA J.,* Vol. 18, No. 8, pp. 980–985.

Beckstead, M.W. (1991) "A Review of Soviet Combustion and Combustion Instability Work on Solid Propellants," 28^{th} JANNAF Combustion Meeting, San Antonio, Texas.

Beckstead, M.W. and Erikson, W.W. (1996) "Solid Monopropellant Oscillatory Combustion Instabilities," Proceedings of the 2^{nd} International Conference on Combustion Conversion and Environmental Problems of Energetic Materails, St. Petersburg, Russia.

Beddini, R.A. (1998) "The Role of Turbulence Interactions in Solid Propellant Combustion Instability," 34^{th} AIAA/ASME/SAE/ASEE Joint Propulsion Conference, July 1998, AIAA Paper No. 98-3703.

Beddini, R.A. and Lee, Y. (1998) "The Treshold Condition of Propellant Velocity Response and its Relation to Local Turbulence Transition," 35^{th} JANNAF Combustion Meeting.

Bird, J.F., et al, (1960) "Effect of Solid Propellant Compressiblity on Combustion Instability," *J. Chem. Phys.,* Vol. 32, pp. 1423–1429.

Biron, D., Hébrard, P., Pauzin, S., and Laverdant, A. (1986) "Etude du couplage acoustique – instabilities aerodynamiques sur une acoustique," École Centrale de Lyon, Proceedings edited by Springer-Verlag.

Blomshield, F. and Mathes, H.B. (1993) "Pressure Oscillations in Post-Challenger Space Shuttle Redesigned Solid Rocket Motors," *J. Propulsion and Power*, Vol. 9, No. 2, pp. 217–221.

Brewster, Q. and Son, S.F. (1995) "Quasi-Steady Combustion Modeling of Homogeneous Solid Propellants," *Comb. and Flame,* Vol. 103, pp. 11–26.

Brewster, Q., Ward, M.J. and Son, S.F. (2000) "Simplified Combustion Modeling of Double Base Propellant: Gas Phase Chain Reaction vs. Thermal Decomposition," *Comb. Sci. and Tech.,* Vol. 159, pp. 1–30.

Brooks, K.P. and Beckstead, M.W. (1995) "The Dynamics of Aluminum Combustion," *J. Prop. and Power,* Vol. 11, No. 4, pp. 769–780.

Brown, R.S., Muzzy, R.J. and Steinle, M.E. (1967) "Effect of Surface Reactions on Acoustic Response of Solid Propellants," *AIAA J.,* Vol. 5, No. 9, p. 1718.

Brown, R.S., Dunlap, R., young, S.W. and Waugh, R.C. (1981) "Vortex Shedding as a Source of Acoustic Energy in Segmented Solid Rockets," *J. Spacecraft and Rockets*, Vol. 18, No. 4, pp. 312–319.

Brownlee, W.G. (1964) "Nonlinear Axial Combustion Instability in Solid Rocket Propellant Rocket Motors," *AIAA Journal,* Vol. 2, No. 2, pp. 275–284.

Burnley, V. (1996) "Nonlinear Combusiton Instabilities and Stochastic Sources," Ph.D. Thesis, Aeronautics, California Institute of Technology.

Burnley, V.S. and Culick, F.E.C. (1996) "Influence of Random Excitations on Acoustic Instabilities in Combustion Chambers," *AIAA Journal*, 38(8), 1403–1410.

Burnley, V.S. and Culick, F.E.C. (1997) "Comment on 'Triggering of Longitudinal Combustion Instabilities in Rocket Motors: Nonlinear Combustion Response'," *Journal of Propulsion and Power*, 16(1), 164–165.

Caltech MURI (2002) "Investigation of Novel Energetic Materials to Stabilize Rocket Motors," Final Report, ONR Contract No. N00014-95-1-1338, 1 October 1995 – 30 September 2001.

Cantrell, R.H., Hart, R.W. and McClure, F.T. (1964) "Linear Acoustic Gains and Losses in Solid Propellant Rocket Motors," *AIAA J.,* Vol. 2, No. 6, pp. 1100–1105.

Cantrell, R.H., McClure, F.T. and Hart, R.W. (1965) "Effects of Thermal Radiation on the Acoustic Response Function of Solid Propellants," *AIAA J.,* Vol. 3, No. 3, pp. 418–426.

Cantrell, R.H. and Hart, R.W. (1966) "Interaction Between Sound and Flow in Acoustic Cavities: Mass, Momentum, and Energy Transfer," *J. Acoust. Soc. Of America,* Vol. 36, pp. 697–706.

Cauty, F. (1999) "Solid-Propellant Combustion Response Function from Direct Measurement Methods: ONERA Experience," *J. Prop. and Power,* Vol. 15, No. 6, pp. 837–843.

Cardiff, E.H., Pinkham, J.D. and Micci, M.M. (1999) "Magnetic Flowmeter Measurement of a Pressure-Coupled Response of a Plateau Solid Propellant," *J. Prop. Power,* Vol. 15, No. 6, pp. 844–848.

Cheng, S.-I. (1954) "High Frequency Combustion Instability in Solid Propellant Rockets," *Jet Propulsion,* Pt. I, pp. 27–32, Pt. II, pp. 102–109.

Cheng, S.-I. (1955) "On 'Unstable Burning of Solid Propellants'," *Jet Propulsion,* Vol. 25, pp. 79–80.

Cheng, S.-I. (1959) "Combustion Instability in Solid Rockets Using Propellants with Suspended Metallic Powders," *1st Symposium (International) on Rockets and Astronautics,* Tokyo, pp. 62–70.

Cheng, S.-I. (1960) "Combustion Instability in Solid Rockets Using Propellants with Reactive Additives," *ARS Progress in Astronautics and Rocketry: Solid Propellant Rocket Research,* Vol. 1, edited by M. Summerfield, Academic Press, pp. 393–422.

Cheng, S.-I. (1962) "Unstable Combustion in Solid-Propellant Rocket Motors," *8th Symposium (International) on Combustion,* Williams and Wilkins, pp. 81–96.

Chu, B.-T. (1956) "Energy Transfer to Small Disturbances in a Viscous Heat Conductive Medium," Department of Aeronautics, Johns Hopkins University (no identifying number).

Chu, B.-T. and Kovasznay, L.S.G. (1957) "Non-linear Interactions in a Viscous Heat Conducting Compressible Gas," *J. Fluid Mech.*, Vol. 3, No. 5, pp. 494–512.

Clavin, P. and Lazini, D. (1992) "Theoretical Analysis of Oscillatory Burning of Homogeneous Solid Propellant Including Non-Steady Gas Phase Effects," *Comb. Sci. and Tech.,* Vol. 83, pp. 1–32.

Coates, R.L., Cohen, N.S. and Harvill, L.P. (1967) "An Interpretation of L* Combustion Instability in Terms of Acoustic Instability Theory," *AIAA J.,* Vol. 5, No. 5, pp. 1097–2004.

Cohen, N.S. and Strand, L.D. (1982) "An Improved Model for the Combustion of AP Composite Propellants," *AIAA Journal,* Vol. 20, No. 12, pp. 1739–1746.

Cohen, N.S. and Strand, L.D. (1985) "Combustion Response to Compositional Fluctuations," *AIAA Journal,* Vol. 23, No. 5, pp. 760–767.

Cohen, N.S. and Strand, L.D. (1985) "Effect of AP Particle Size on Combustion Response to Crossflow," *AIAA Journal,* Vol. 23, No. 5, pp. 776–780.

Cohen, N.S., Shusser, M., Culick, F.E.C. and Beddini, R.A., (1999) "Combustion Modeling of AP Composite Propellants for Stability Analysis," 36th JANNAF Combustion Meeting.

Cozzi, F., DeLuca, L.T. and Novozhilov, B.V. (1999) "Linear Stability and Pressure-Driven Response Function of Solid Propellants with Phase Transition," *J. Prop and Power,* Vol. 15, No. 6, pp. 806–875.

Crocco, L. and Cheng, S.-I. (1956) *Theory of Combustion Instability in Liquid-Propellant Rockets*, AGARDograph No. 8, Butterworths Scientific Publications, London.

Crocco, L., Grey, J. and Harrje, D.T. (1960) "Theory of Liquid Propellant Rocket Combustion Instability and Its Experimental Verification," *ARS J,* Vol. 30, No. 2, pp. 159–168.

Crocco, L. (1964) "Theoretical Studies on Liquid Propellant Rocket Instability," *10th Symposium (International) on Combustion,* The Combustion Institute, Pittsburgh, PA, pp. 1101–1128.

Culick F.E.C. (1961) "High Frequency Pressure Oscillations in Liquid Rockets," Sc.D. Thesis, M.I.T. Department of Aeronautics and Astronautics.

Culick F.E.C. (1963) "High Frequency Oscillations in Liquid-Propellant Rockets," *AIAA Journal,* Vol. 1, No. 5, pp. 1097–1104.

Culick, F.E.C. (1966) "Acoustic Oscillations in Solid Propellant Rocket Chambers," *Astronautica Acta,* Vol. 12, pp. 113–126.

Culick, F.E.C. (1967) "Calculation of the Admittance Function for a Burning Surface," *Astronautics Acta,* Vol. 13, No. 3, pp. 221–238.

Culick, F.E.C. (1967) "A Review of Calculations of the Admittance Function for a Burning Surface," *Combustion of Solid Propellants and Low Frequency Combustion Instability,* NOTS TP 4244, Naval Weapons Center, China Lake, CA, Appendix A.

Culick, F.E.C. (1968) "A Review of Calculations for Unsteady Burning of a Solid Propellant," *AIAA Journal,* Vol. 6, No. 12, pp. 2241–2255.

Culick, F.E.C. (1969) "An Elementary Calculation of the Combustion of a Solid Propellant," *Astronautics Acta,*.

Culick, F.E.C. (1969) "Some Problems in the Unsteady Burning of Solid Propellants," Naval Weapons Center Report NWC TP 4668.

Culick, F.E.C. and Dehovitz, G.L. (1969) "An Elementary Calculation for the Burning Rate of Composite Solid Propellants," *Comb. Sci. and Tech.,* Vol. 1, pp. 193–204.

Culick, F.E.C. (1970) "Stability of Longitudinal Oscillations with Pressure and Velocity Coupling in a Solid Propellant Rocket," *Comb. Sci. and Tech.,* Vol 2, No. 4, pp. 179–201.

Culick, F.E.C. (1971) "Nonlinear Growth and Limiting Amplitude of Acoustic Oscillations in Combustion Chambers," *Combustion Science and Technology,* Vol. 3, pp. 1–16.

Culick, F.E.C. (1976) "Nonlinear Behavior of Acoustic Waves in Combustion Chambers," Parts I and II, *Acta Astronautica,* Vol. 3, pp. 714–757.

Culick, F.E.C. and Magiawala, K. (1979) "Excitation of Acoustic Modes in a Chamber by Vortex Shedding," *J. Sound and Vibration*, Vol. 64, No. 3, pp. 455–457.

Culick, F.E.C. (1980) "Report of the JANNAF Workshop on Pressure Oscillations in Ramjets," 17^{th} JANNAF Combustion Meeting.

Culick, F.E.C. and Rogers, T. (1980) "Modeling Pressure Oscillations in Ramjets," 16^{th} AIAA/SAE/ASME Joint Propulsion Conference, Hartford, Connecticut, AIAA Paper 80-1192.

Culick, F.E.C. (1987) "A Note on Rayleigh's Criterion," *Combustion Science and Technology*, Vol. 56, pp. 159–166.

Culick, F.E.C. (1988) "Combustion Instabilities in Liquid-Fueled Propulsion Systems—An Overview," AGARD 72B Specialists' Meeting of the Propulsion and Energetics Panel AGARD CP 450.

Culick, F.E.C., Paparizos, L., Sterling, J. and Burnley, V.S. (1992) "Combustion Noise and Combustion Instabilities in Propulsion Systems," *Proceedings of the AGARD Conference on Combat Aircraft Noise*, AGARD CP512.

Culick, F.E.C. (1992) "Combustion Instabilities and Rayleigh's Criterion," *Modern Research Topics in Aerospace Propulsion*, (In honor of Corrado Casci), pp. 135–151.

Culick, F.E.C. and Yang, V. (1992) "Prediction of the Stability of Unsteady Motions in Solid Propellant Rocket Motors," *Nonsteady Burning and Combustion Stability of Solid Propellants,* edited by L. DeLuca, E.W. Price and M. Summerfield, Vol. 143, *Progress in Astronautics and Aeronautics,* AIAA, Washington, pp. 719–780.

Culick, F.E.C. (1994) "Some Recent Results for Nonlinear Acoustics in Combustion Chambers," *AIAA Journal*, Vol. 32, No. 1, pp. 146–169.

Culick, F.E.C. and Yang, V. (1995) "Overview of Combustion Instabilities in Liquid-Propellant Rocket Engines," First International Symposium on Liquid Rocket Engine Combustion Instability, The Pennsylvania State University, AIAA Progress Series, Vol. 169.

Culick, F.E.C. (1997) "A Note on Ordering Perturbations and the Insignificance of Linear Coupling in Combustion Instabilities," *Combustion Science and Technology*, Vol. 126, pp. 359–379.

Culick, F.E.C. Isella, G. and Seywert, C. (1998) "Influences of Combustion Dynamics on Linear and Nonlinear Unsteady Motions in Solid Propellant Rockets," AIAA-98-3704.

Culick, F.E.C. (1999) "Combustor Dynamics: Fundamentals, Acoustics and Control," A Short Course of Lectures.

Culick, F.E.C. (2002) "A Short Course of Lectures on Combustion Dynamics: Fundamentals, Acoustics and Control," accesible on the website http://www.its.caltech.edu/∼culick.

DeLuca, L. (1990) "A Critical Review of Solid Rocket Propellant Transient Flame Models," *Pure and Applied Chem.,* Vol. 63, pp. 825–.

DeLuca, L. and Galfetti, L. (1991) "Combustion Modeling and Stability of Double-Based Propellants," *Modern Research Topics in Aerospace Propulsion,* Springer-Verlag, N.Y., pp. 109–134.

DeLuca, L. (1992) "Theory of Nonsteady Burning and Combustion Stability of Solid Propellants by Flame Models," *Combustion Stability of Solid-Propellant,* edited by L. DeLuca, E.W. Price and M. Summerfield, *Progress in Astronautics and Aeronautics,* Vol. 143, AIAA, Washington, pp. 519–600.

DeLuca, L., DiSilvestro, R. and Cozzi, F. (1995) "Intrinsic Combustion Instability of Solid Energetic Materials," *J. Prop and Power,* Vol. 11, No. 4, pp. 804–875.

Denison, M.R. and Baum, E. (1961) "A Simplified Model of Unstable Burning in Solid Propellants," *ARS Journal,* Vol. 31, No. 8, pp. 278–285.

Dickinson, L.A. (1962) "Command Initiation of Finite Wave Combustion Instabilities in Solid Propellant Rocket Engines," *ARS Journal*, April (pp. 643–644).

Dickinson, L.A. and Jackson, F. (1963) "Combustion in Solid Propellant Rocket Engines," Fifth AGARD Colloquium, High Temperature Phenomena.

Doedel, E.J., Champneys, A.R., Fairgrieve, T.F., Kuznetsov, Y.A., Sandstede, B., Wang, X. (1997) "AUTO 97: Continuation and Bifurcation Software for Ordinary Differential Equations," Concordia University, Montreal, Canada.

Doedel, E.J., Keller, H.B., Kernevez, J.P. (1991a) "Numerical Analysis and Control of Bifurcation Problems, (I) Bifurcation in Finite Dimensions," *International Journal of Bifurcation and Chaos*, Vol. 1, No. 3, pp. 493–520.

Doedel, E.J., Keller, H.B., Kernevez, J.P. (1991b) "Numerical Analysis and Control of Bifurcation Problems, (II) Bifurcation in Infinite Dimensions," *International Journal of Bifurcation and Chaos*, Vol. 1, No. 4, pp. 745–772.

Dotson, K.W., Koshigoe, S. and Pace, K.K. (1995) "Vortex Driven Pressure Oscillations in the Titan IV Solid Rocket Motor Upgrade," AIAA Paper No. 95-2732.

Duer, J. and Hessler, R. (1984) "Forced Oscillation Theory and Applications," 20^{th} AIAA/ASME/SAE/ASEE Joint Propulsion Conference, AIAA Paper No. 84-1356.

Dunlap, R. and Brown, R.S. (1981) "Exploratory Experiments on Acoustic Oscillations Driven by Periodic Vortex Shedding," *AIAA J.*, Vol. 19, No. 3, pp. 408–409.

Dunlap, R., Blackner, A.M., Waugh, R.C., Brown, R.S. and Willoughby, P.G. (1990) "Internal Flow Field Studies in a Simulated Cylindrical Port Rocket Chamber," *J. Prop. and Power,* Vol. 6, No. 6, pp. 690–704.

Dupays, J. and Vuillot, F. (1998) "Propagation of an Acoustic Wave in a Two-Phase Reactive Medium," AIAA Paper No. 98-3696.

Ernst, R.C. (1976) "A Combustion Model for Low Frequency Instability in Turbofan Augmentors," 12^{th} AIAA/SAE Propulsion Conference, AIAA Paper No. 76-680.

Evans, G.I. and Smith, P.K. (1978) "The Suppression of Combustion Instability in Smokeless Solid Propellant Rocket Motors," AIAA Paper 78-1568, *14^{th} AIAA/SAE Joint Propulsion Conference.* Also see Paper #27, *AGARD Conference Proceedings* No. 259, *Solid Rocket Motor Technology*, National Technical Information Service (NTIS), Springfield, VA, July 1979.

Flandro, G.A. and Jacobs, H.R. (1974) "Vortex-Generated Sound in Cavities," AIAA Paper No. 73-1014, published in *Aeroacoustics: Jet and Combustion Noise*, AIAA Series *Progress in Astronautics and Aeronautics.* Vol. 37, pp. 521–533.

Flandro, G.A. (1986) "Vortex Driving Mechanism in Oscillatory Rocket Flows," *J. Propulsion and Power*, Vol. 2, No. 3, pp. 206–214.

Flandro, G.A. (1995) "Effects of Vorticity on Rocket Combustion Instability," *J. Propulsion and Power* Vol. 11, No. 4, pp. 607–625.

Friedly, J.C. and Petersen, E.E. (1966) "Influence of Combustion Parameters on Instability in Solid Propellant Motors," *AIAA J.,* Vol. 4, Pt. I: "Development of Model and Linear Analysis," pp. 1604–1609; Pt. II: "Nonlinear Analysis," pp. 1932–1937.

Geckler, E.D. (1955) "Unsolved Problems in Solid Propellant Combustion," *5^{th} Symposium (International) on Combustion,* Reinhold, pp. 29–40.

Gostintsev, Yu.A., Pokhil, P.F. and Sukhanov, L.A. (1970) "Complete System of Equations for Nonsteady Processes at Propellant Burning in Semi-Closed Volume," *Dokl. AN SSSR,* Vol. 195, No. 1, pp. 137–140.

Grad, H. (1949) "Resonance Burning in Rocket Motors," *Communications on Pure Applied Mathematics,* Vol. 2, pp. 79–102.

Green, L., Jr. (1958) "Some Properties of Solid Propellant Burning," *Jet Propulsion,* Vol. 28, pp. 386–392.

Gusachenko, L.K., Zarko, V.E. and Rychkov, A.D. (1999) "Effect of Melting on Dynamic Combustion Behavior of Energetic Materials," *J. Prop. and Power,* Vol. 15, No. 6, pp. 876–822.

Hart, R.W. and McClure, F.T. (1959) "Combustion Instability: Acoustic Interaction with a Burning Propellant Surface," *J. Chem. Phys.,* Vol. 30, pp. 1501–1514.

Hart, R.W. and Cantrell, R.H. (1963) "Amplification and Attenuation of Sound by Burning Propellants," *AIAA J.,* Vol. 1, No. 2, pp. 398–404.

Hart, R.W. and McClure, F.T. (1965) "Theory of Acoustic Instability in Solid-Propellant Rocket Combustion," *10^{th} (International) Symposium on Combustion,* The Combustion Institute, Pittsburgh, PA, pp. 1047–1065.

Hart, R.W., Farrell, R.A. and Cantrell, R.H. (1966) "Theoretical Study of a Solid Propellant Having a Heterogeneous Surface Reaction. I-Acoustic Response, Low and Intermediate Frequencies," *Comb. and Flame,* Vol. 10, pp. 367–380.

Hessler, R. (1979) "Studies of Motor Instability Problems," 16^{th} JANNAF Combustion Sub-Committee Meeting.

Hessler, R. (1980) "Prediction of Finite Pressure Oscillations in Stable Rocket Motors," 17^{th} JANNAF Combustion Sub-Committee Meeting.

Hessler, R. (1982) "Forced Oscillation Prediction," 19^{th} JANNAF Combustion Sub-Committee Meeting.

Hessler, R. and Glick, R. (1998) "Application of Maximum Entropy Method to Passively Extract Motor Stability Information," Workshop 'Measurement of Thermophysical and Ballistic Properties of Energetic Material', Politecnico di Milano, Milan, Italy.

Hildebrand, F.B. (1952) *Methods of Applied Mathematics*, Prentice-Hall, Inc., New York.

Horton, M.D. (1961) "One-Dimensional Solid Propellant Oscillatory Burner," *ARS Journal,* Vol. 31, pp. 1596–1597.

Horton, M.D. (1962) "Acoustic Admittance of a Burning Solid Propellant Surface," *ARS Journal,* Vol. 32, No. 4, pp. 644–645.

Horton, M.D. and Price, E.W. (1963) "Dynamic Characteristics of Solid Propellant Combustion," *Ninth Symposium (International) on Combustion,* Academic Press, N.Y., pp. 303–310.

Horton, M.D. and Rice, D.W. (1964) "The Effect of Compositional Variables upon Oscillatory Combustion of Solid Rocket Propellants," *Comb. and Flame,* Vol. 8, pp. 21–28.

Ibiricu, M.W. and Williams, F.A. (1975) "Influence of Externally Applied Thermal Radiation on the Burning Rates of Homogeneous Solid Propellants," *Combustion and Flame,* Vol. 24, pp. 185–198.

Isella, G., Seywert, C., Culick, F.E.C. and Zukoski, E.E. (1996) "A Further Note on Active Control of Combustion Instabilities Based on Hysteresis," *Combustion Science and Technology*, Vol. 126, pp. 381–388.

Isella, G. and Culick, F.E.C. (2000) "Modeling Propellant Dynamics and Their Effects on the Global Dynamics of a Combustion Chamber," (in preparation).

Isella, G. and Culick F.E.C. (2000) "Modeling the Combustion Response Function with Surface and Gas Phase Dynamics," 38^{th} AIAA Aerospace Sciences Meeting, AIAA-2000-0310.

Isella, G.C. (2001) "Modeling and Simulation of Combustion Chambers and Propellant Dynamics and Issues in Active Control of Combustion Instabilities," Ph.D. Thesis, California Institute of Technology.

Istratov, A.G. and Librovich, V.B. (1964) "On the Stability of Propellant Combustion," *Zh. Prikl. Mekh. I Tekh. Fiz.,* No. 5, pp. 38–43.

Jahnke, C. and Culick, F.E.C. (1994) "An Application of Dynamical Systems Theory to Nonlinear Combustion Instabilities," *Journal of Propulsion and Power*, Vol. 10, No. 4, pp. 508–517.

King, M.K. (1979) "Erosive Burning of Composite Solid Propellants: Experimental and Modeling Studies," *J. Spacecraft and Rockets,* Vol. 16, No. 3, pp. 154–162.

King, M.K. (1980) "Composite Propellant Modeling," AIAA Paper No. 80-1124.

Knoop, P., Culick, F.E.C. and Zukoski, E.E. (1996) "Extension of the Stability of Motions in a Combustion Chamber by Nonlinear Active Control Based on Hysteresis," *Combustion Science and Technology*, Vol. 123, pp. 363–376.

Kochevets, S. Buckmaster, J. and Jackson, T.L. (2000) "Random Propellant Packs and the Flames They Support," AIAA-2000-3461.

Krier, H. et al. (1968) "Entropy Waves Produced in Oscillatory Combustion of Solid Propellants," *Third ICRPG/AIAA Solid Propulsion Conference,* Atlantic City, NJ.

Krier, H., T'ien, J.S., Sirignano, W.A. and Summerfield, M. (1968) "Non-Steady Burning Phenomena of Solid Propellants: Theory and Experiment," *AIAA J.,* Vol. 6, No. 2, pp. 278–285.

Krylov, N. and Bogoliubov, N. (1947) *Introduction to Nonlinear Mechanics*, Princeton University Press.

Kumar, R.N. (1973) "Condensed Phase Details in the in the Time-Independent Combustion of AP/Composite Propellants," *Comb. Sci. and Tech.,* Vol. 8, No. 2, pp. 133–148.

Kumar, R.N. and Culick, F.E.C. (1977) "Role of Condensed Phase Details in the Oscillatory Combustion of Composite Propellants," *Comb. Sci. and Tech.,* Vol. 15, No. 2, pp. 179–199.

Kuo, K.K., Gore, J.P. and Summerfield, M. (1984) "Transient Burning of Solid Propellants," *Fundamentals of Solid-Propellant Combustion,* edited by K.K. Kuo and M. Summerfield, *Progress in Astronautics and Aeronautics,* Vol. 90, AIAA, New York, pp. 599–659.

Landau, L.D. and Lifschitz, E.M. (1959) *Fluid Mechanics*, Addison-Wesley Publishing Co.

LeBreton, P., Guéry, J.-F., Vuillot, F., and Prévost, M. (1999) "Recent Advances in the Prediction of SRM Thrust Oscillations," *Premier Colloque Européen sur la Technologie des Lanceurs-Vibrations des Lanceurs*, Toulouse, France.

Lengellé, G. (1970) "Thermal Degradation Kinetics and Surface Pyrolyses of Vinyl Polymers," *AIAA J.,* Vol. 8, No. 11, pp. 1989–1996.

Lengellé, G., Kuentzmann, P. and Rendolet, C. (1974) "Response of a Solid Propellant to Pressure Oscillations," AIAA Paper No. 74-1209.

Levine, J.N. and Baum, J.D. (1983) "Modeling of Nonlinear Combustion Instability in Solid Propellant Rocket Motor," *19th Symposium (International) on Combustion,* pp. 769–776.

Levine, J.N. and Baum, J.D. (1983) "A Numerical Study of Nonlinear Instability Phenomena in Solid Rockets," *AIAA J.,* Vol. 21, No. 4 (pp. 557–564).

Levine, J.N. and Culick, F.E.C. (1972) "Numerical Analysis of Nonlinear Longitudinal Combustion Instability in Metalized Solid-Propellant Rocket Motors, Vol. 1 Analysis and Results," Ultrasystems, Inc., Report prepared for the Air Force Rocket Propulsion Laboratory, AFRPL TR–72–88.

Levine, J.N. and Culick, F.E.C. (1974) "Nonlinear Analysis of Solid Rocket Combustion Instability," Ultrasystems, Inc., Report prepared for the Air Force Rocket Propulsion Laboratory, AFRPL TR–74–45.

Lewis Laboratory Staff (1954) "Summary of Preliminary Investigations into the Characteristics of Combustion Screech in Ducted Burners," NACA-TR-1384.

Lord Rayleigh (1878) "The Explanation of Certain Acoustic Phenomena," *Royal Institution Proceedings*, VIII, pp. 536–542.

Lord Rayleigh (1945) *Theory of Sound*, Vol. 2, Dover, New York, Section 322g, pp. 232–234.

Louwers, J. and Gadiot, G.M.H.J.L. (1999) "Model for Nonlinear Transient Burning of Hydrazine Nitroformate," *J. Propulsion and Power,* Vol. 15, No. 6, pp. 778–782.

Lovine, R. L., Dudley, D. P., and Waugh, R. C. (1983) "Standardized Stability Prediction Method for Solid Rocket Motors," Vol. I, II and III. Aerojet Solid Propulsion Company. Report prepared for the Air Force Rocket Propulsion Laboratory, AFRPL-TR-76-32.

Lupuglazoff, N. and Vuillot, F. (1996) "Parietal Vortex-Shedding as a Cause of Instability for Long Solid Propellant Motors," AIAA Paper No. 96-0761.

Lupuglazoff, N. and Vuillot, F. (1998) "Numerical Simulations of Parietal Vortex Shedding Phenomena in a Cold Flow Set-Up," AIAA Paper No. 98-3220.

McClure, F.T., Hart, R.W. and Bird, J.F. (1960) "Acoustic Resonance in Solid Propellant Rockets," *J. Appl. Phys.,* Vol. 31, pp. 884–896.

McClure, F.T., Bird, J.F. and Hart, R.W. (1962) "Erosion Mechanism for Non-linear Instability in the Axial Modes of Solid Propellant Rocket Motors," *ARS J.,* Vol. 32, No. 3, pp. 374–378.

McManus, K., Poinsot, T. and Candel, S. (1993) "A Review of Active Control of Combustion Instabilities," *Progress in Energy and Combustion Science*, 19(1): 1–29.

Magiawala, K. and Culick, F. E. C. (1979) "Measurements of Energy Exchange Between Acoustic Fields and Non-Uniform Steady Fields," *Journal of Sound and Vibration*, Vol. 75, pp. 503–512.

Majdalani, J. (1999) "Vortical and Acoustic Mode Coupling Inside a Two-Dimensional Cavity with Transpiring Walls," *J. Acoust. Soc. of Amer.,* Vol. 106, No. 1, pp. 46–56.

Majdalani, J., Flandro, G.A. and Roh, T.-S. (2000) "Convergence of Two Analytical Flow Field Models Predicting a Destabilizing Agent in Rocket Combustion," *J. Prop. and Power,* Vol. 16, No. 3, pp. 492–497.

Malhotra, S. (2002) "On Combustion Instability," Ph.D. Thesis in preparation, California Institute of Technology.

Marble, F.E. and Rogers, D.E. (1956) "A Mechanism of High-Frequency Oscillation in Ramjet Combustors and Afterburners," *Jet Propulsion.*

Marble, F.E. and Wooten, D.C. (1970) "Sound Attenuation in a Condensing Vapor," *The Physics of Fluids*, Vol. 13, No. 12, pp. 2657–2664.

Marxman, G.A. and Wooldridge, C.E. (1968) "Effects of Surface Reactions on the Solid Propellant Response Function," *AIAA J.,* Vol. 6, No. 3, pp. 468–471.

Marxman, G.A. and Wooldridge, C.E. (1971) "Finite-Amplitude Axial Instability in Solid-Rocket Combustion," *12th Symposium (International) on Combustion,* pp. 115–127.

Mason, D.R., Folkman, S.L. and Behring, M.A. (1979) "Thrust Oscillations of the Space Shuttle Solid Rocket Boosters Motor During Static Tests," AIAA Paper No. 79-1138.

Mathes, B., Derr, R.L. and Culick, F.E.C. (1973).

Mathes, H.B. (1980) "Assesment of Chamber Pressure Oscialltions in the Shuttle Solid Rocket Booster Motors," AIAA Paper No. 80-1091.

Minch, M.M. and Kuo, K.K. (1995) "Characterization and Stability Behavior of Solid Propellants,"

Moore, F.K. and Maslen, S.H. (1954) "Transverse Oscillations in a Cylindrical Combustion Chamber," NACA-TN-3152.

Morse, P.M. (1936) *Vibration and Sound*, McGraw-Hill Book Co., New York.

Morse, P.M. and Feshbach, H. (1952) *Methods of Theoretical Physics*, McGraw-Hill Book Company.

Morse, P. and Ingard, L. (1968) *Theoretical Acoustics*, McGraw-Hill Book Co., New York.

Nachbar, W. and Green, L., Jr. (1959) "Analysis of a Simplified Model of Solid Propellant Resonant Burning," *J. Aerospace Sci.,* ol. 26, No. 8, pp. 518–526.

Nachbar, W. and Green, L., Jr. (1960) "Closure," *ARS J.,* Vol. 30, No. 6, pp. 576–577.

Natanzon, M.S. and Menshikova, O.M. (1992) "Bifurcation of Steady Combustion Regimes and Their Influence on the Onset of High-Frequency Oscillations in Combustion Chambers," *Physics of Combustion and Explosion*, Vol. 23, No. 4, pp. 10–18.

Natanzon, M. (1999) *Unsteady Combustion in Liquid Rocket Engines*, Electronic translation from the Russian edition (1984) with a revised Chapter 8 on Bifurcations; translation editor F.E.C. Culick.

Nickerson, G. R., Culick, F.E.C., and Dang, L.G. (1983) "Standard Stability Prediction Method for Solid Rocket Motors, Axial Mode Computer Program, User's Manual," Software and Engineering Associates (SEA), Inc. Report prepared for the Air Force Rocket Propulsion Laboratory, AFRPL-TR-83-01.

Nomoto, H. and Culick, F.E.C. (1982) "An Experimental Investigation of Pure Tone Generation by Vortex Shedding in a Duct," *J. Sound and Vibration*, Vol. 84, No. 2, pp. 247–252.

Novikov, S.S. and Ryazantzev, Yu.S. (1964) "On the Stability of Propellant Combustion," *Zh. Prikl. Mekh. I Tekh. Fiz.,* No. 1, pp. 57–61.

Novozhilov, B.V. (1965) "Burning of a Powder Under Harmonically Varying Pressures," *J. Appl. Mech. and Tech. Phys.,* Vol. 6, No. 6, pp. 141–144.

Novozhilov, B.V. (1965) "Condition of Stability of Steady-State Propellant Burning," *Zh. Prikl. Mekh. Tekh. Fiz.,* No. 4, pp. 157–160.

Novozhilov, B.V. (1965) "Propellant Burning at Harmonically Varying Pressure," *Zh. Prikl. Mekh. i Tekh. Fiz.,* No. 6, pp. 141–144.

Novozhilov, B.V. (1965) "Stability Criterion for Steady-State Burning of Powders," *J. Appl. Mech. and Tech. Phys.,* Vol. 6, No. 4, pp. 157–160.

Novozhilov, B.V. (1966) "Nonlinear Oscillations of Propellant Burning Rate," *Zhurnal Prikladnoi Mekhaniki I Tekhnicheskoi Fiziki,* No. 5, pp. 31–41.

Novozhilov, B.V. (1968) "Theory of Nonsteady Burning of Homogeneous Propellants," *Fizika Goreniya I Vzryva,* Vol. 4, No. 4, pp. 482–493.

Novozhilov, B.V. (1970) "Equation for Nonsteady Propellant Burning Rate," *Zh. Prikl. Mekh. i Tekh. Fiz.,* No. 4, pp. 73–78.

Novozhilov, B.V. (1973) "Nonstationary Combustion of Solid Rocket Fuels," Nauka, Moscow, Translation AFSC FTD-MD-24-317-74.

Novozhilov, B.V. (1992) "Second Harmonic Nonlinear Resonance in Propellant Combustion," *24th Symposium (International) on Combustion,* The Combustion Institute, Pittsburgh, PA, pp. 1939–1945.

Novozhilov, B.V. (1992) "Theory of Nonsteady Burning and Combustion Stability of Solid Propellants by the Zel'dovich-Novozhilov Method," *Nonsteady Burning and Combustion Stability of Solid Propellants,* DeLuca, L., Price, E.W. and Summerfield, M. (Editors), AIAA Progress Series, Vol. 14-3, pp. 601–641.

Novozhilov, B.V. (1993) "Acoustic Admittance of the Surface of Burning Condensed Matter," *Sov. J. Chem. Physics,* Vol. 10, No. 11, pp. 2363–2384.

Novozhilov, B.V., Kohno, M. Maruizumi, H., Shimada, T. (1996) "Solid Propellant Burning Rate Response Function of Higher Order," The Institute of Space and Astronautical Science, Report No. 661, Kanagawa, Japan.

Ofelein, J.C. and Yang, V. (1993) "Comprehensive Review of Liquid-Propellant Combustion Instabilities in F-1 Engines," *Journal of Propulsion and Power*, Vol. 9, pp. 637–677.

Paparizos, L. and Culick, F.E.C. (1989) "The Two-Mode Approximation to Nonlinear Acoustics in Combustion Chambers. I. Exact Solutions for Second Order Acoustics," *Combustion Science and Technology*, Vol. 65(1–3), pp. 39–66.

Perry, E.W. (1970) "Investigation of the T-Burner and its Role in Combustion Instability Studies," Ph.D. Thesis, California Institute of Technology.

Price, E.W. (1960) "Combustion Instability in Solid Propellant Rockets," *ARS J.,* Vol. 30, No. 6, pp. 574–576.

Price, E.W. (1965) "Experimental Solid Rocket Instability," *10^{th} (International) Symposium on Combustion,* The Combustion Institute, Pittsburgh, PA, pp. 1067–1082.

Price, E.W. (1971) "Comments on Role of Aluminum in Suppressing Instability in Solid Propellant Rocket Motors," *AIAA J.*, Vol. 9, pp. 987–990.

Price, C.F., Boggs, T. and Derr, R.L. (1979) "The Steady-State Behavior of Ammonium Perchlorate and HMX," AIAA Paper No. 79-0164.

Putnam, A.A. (1971) *Combustion Driven Oscillations in Industry,* Elsevier, New York.

Raun, R.L. and Beckstead, M.W. (1993) "A Numerical Model for Temperature Gradient Effects on Rijke Burner Oscillations," *Combustion and Flame,* Vol. 94, No. 1/2, pp. 1–24.

Raun, R.L., Beckstead, M.W., Finlinson, J.C. and Brooks, K.P. (1993) "A Review of Rijke Tubes, Rijke Burners and Related Devices," *Prog. in Comb. Energy and Science,* Vol. 19, No. 4, pp. 313–364.

Roberts, A.K. and Brownlee, W.G. (1971) "Nonlinear Longitudinal Combustion Instability: Influence of Propellant Combustion," *AIAA Journal,* Vol. 9, No. 1, pp. 140–147.

Schultz, R., Green, L., Jr. and Penner, S. (1958) "Studies of the Decomposition Mechanism, Erosive Burning, Sonance and Resonance for Solid Composite Propellants," *3rd AGARD Colloquium on Combustion and Propulsion,* Pergamon Press, pp. 367–420.

Sehgal, R. and Strand, L. (1964) "A Theory of Low Frequency Combustion Instability in Solid Rocket Motors," *AIAA J.,* pp. 696–702.

Seywert, C. (2001) "Combustion Instabilities: Issues in Modeling and Control," Ph.D. Thesis, California Institute of Technology.

Seywert, C. and Culick, F.E.C. (1999) "Some Influences of Noise on Combustion Instabilities and Combustor Dynamics," 36^{th} JANNAF Combustion Conference.

Shapiro, A. (1953) *The Dynamics and Thermodynamics of Compressible Fluid Flow,* Ronald Press, N.Y.

Shusser, M., Cohen, N.S. and Culick, F.E.C. (2000) "Combustion Response of AP Composite Propellants," 37^{th} JANNAF Combustion Meeting, submitted to *AIAA J. Prop. and Power.*

Shusser, M., Culick, F.E.C. and Cohen, N.S. (2000) "Combustion Response of Ammonium Perchlorate," 36^{th} AIAA/ASME/SAE/ASEE Joint Propulsion Meeting, AIAA-2000-3694, accepted for publication in *AIAA Journal,* 2001.

Shusser M., Cohen N.S. (2001) "Effect of Variable Thermal Properties of the Solid Phase on Composite Solid Propellant Combustion," Caltech Internal Document CI01-04, submitted to *Astronautica Acta,* 2001.

Shusser, M. and Culick, F.E.C. (2001) "Analytical Solution for Composite Solid Propellant Response Function," 37^{th} AIAA Joint Propulsion Conference, Caltech Internal Document CI01-02, submitted to *AIAA Journal* 2001.

Shusser, M., Culick, F.E.C. and Cohen, N.S., (2001) "Pressure Exponent of a Composite Solid Propellant," Caltech Internal Document CI01-03, submitted to *AIAA Journal,* 2001.

Smith, A.F. (1960) "A Theory of Oscillatory Burning of Solid Propellants Assuming a Constant Surface Temperature," *ARS Progress in Astronautics and Rocketry: Solid Propellant Rocket Research,* Vol. I, edited by M. Summerfield, Academic Press, pp. 375–391.

Smith, D.A. and Zukoski, E.E. (1985) "Combustion Instability Sustained by Unsteady Vortex Combustion," 21^{st} AIAA/SAE/ASME/ASEE Joint Propulsion Conference, AIAA Paper No. 85-1248.

Smith, D.A. (1985) "An Experimental Study of Acoustically Excited, Vortex Driven Combustion Instability Within a Rearward Facing Step Combustor," Ph.D. Thesis, California Institute of Technology.

Smith, R.P. and Sprenger, D.F. (1954) "Combustion Instability in Solid Propellant Rockets," 4^{th} *Symposium (International) on Combustion,* Williams and Wilkins, pp. 893–906.

Sterling, J.D. (1987) "Longitudinal Mode Combustion Instabilities in Air Breathing Engines," Ph.D. Thesis, California Institute of Technology.

Sterling, J.D. (1993) "Nonlinear Analysis and Modelling of Combustion Instabilities in a Laboratory Combustor," *Combustion Science and Technology*, Vol. 89, pp. 167–179.

Sterling, J.D. and Zukoski, E.E. (1991) "Nonlinear Dynamics of Laboratory Combustor Pressure Oscillations," *Combustion Science and Technology*, Vol. 77, pp. 225–238.

Summerfield, M. (1951) "A Theory of Unstable Propulsion in Liquid-Propellant Rocket Systems," *Am. Rocket Soc. J.*, Vol. 21, No. 5, pp. 108–114.

Summerfield, M., editor (1960) *Solid Propellant Rocket Research*, Vol. 1 of the ARS (AIAA) Progress Series in Astronautics and Rocketry, Academic Press, New York.

Summerfield, M., Caveny, L.H. Battista, R.A., Kubota, N., Gostintsev, Yu.A., and Isoda, H. (1971) "Theory of Dynamic Extinguishment of Solid Propellants with Special Reference to Nonsteady Heat Feedback Law," *J. of Spacecraft and Rockets,* Vol. 8, No. 3, pp. 251–258.

Tennekes, H. and Lumley, J.L. (1972) *A First Course in Turbulence*, M.I.T. Press.

T'ien, J.S. (1972) "Oscillatory Burning of Solid Propellants Including Gas Phase Time Lag," *Comb. Sci, and Tech.,* Vol. 5, pp. 47–54.

Traineau, J.C., Prévost, M., Vuillot, F., LeBreton, P., Cuny, J., Preioni, N. and Bec, R. (1997) "A Sub-Scale Test Program to Assess the Vortex Shedding Driven Instabilities in Segmented Solid Rocket Motors," AIAA Paper No. 97-3247.

Truesdell, C. and Toupin, R. (1960) "The Classical Field Theories," *Handbuch des Physik*, Vol. III/1, Springer-Verlag, Berlin.

Tsien, H.S. (1952) "The Transfer Functions of Rocket Nozzles," *J. Am. Rocket Soc.*, Vol. 22, pp. 139–143.

Ugurtas, B., Avalon, G., Lupuglazoff, N. and Vuillot, F. (1999) "Numerical Computations of Hydrodynamic Instabilities Inside Channels with Wall Injection," AIAA Paper No. 99-2505.

Ugurtas, B., Avalon, G., Lupuglazoff, N., Vuillot, F. and Casalis, G. (2000) "Stability and Acoustic Resonance of Internal Flows Generated by Side Injection," *J. Propulsion and Power*.

UIUC MURI (2002) "Pressure-Coupled Response Function Measurements by Various Techniques for MURI Propellants," Final Report UILU-ENG-2002-4003, ONR Contract No. N00014-95-1-1339, September 1997 – September 2001.

Vuillot, F., Traineau, J.C., Prévost, M. and Lupoglazoff, N. (1993) "Experimental Validation of Stability Assesment Methods for Segmented Rocket Motors," AIAA Paper No. 93-1883.

Vuillot, F. (1995) "Vortex Shedding Phenomena in Solid Rocket Motors," *J. Propulsion and Power*, Vol. 11, No. 4, pp. 626–639.

Waesche, R.H.W., Wenograd, J. and Summerfield, M. (1961) "Research on Solid Propellant Combustion Instability," Aeronautical Engineering Rept. 564b, Princeton University.

Waesche, R.H.W., Wenograd, J. and Summerfield, M. (1961) "Entropy Wave Observations in Oscillatory Combustion of Solid Propellants: A Progress Report," Paper No. 64-154, AIAA.

Waesche, R.H.W. and Summerfield, M. (1961) "Solid Propellant Combustion Instability: Oscillatory Burning of Solid Rocket Propellants," Aerospace and Mechanical Sciences Rept. 751, Princeton University.

Waesche, R.H.W. (1999) "Mechanisms and Methods of Suppression of Oscillatory Burning by Metallic Additives," *AIAA J. Prop. & Power*, Vol. 15, Nov–Dec. 1999, pp. 919–922. Also see 35^{th} *JANNAF Combustion Meeting*, CPIA Pub. 680, Dec. 1998.

Ward, M.J., Son, S.F. and Brewster, M.Q. (1998) *Comb. and Flame,* Vol. 114, pp. 556–568.

Williams, F.A. (1962) "Response of a Burning Solid to Small Amplitude Pressure Oscillations," *Journal of Applied Physics,* Vol. 33, p. 3153.

Williams, F.A. (1973) "Quasi-Steady Flow Theory in Unsteady Burning of a Homogeneous Solid Propellant," *AIAA J.,* Vol. 11, No. 9, pp. 1328–1330.

Williams, F.A. (1985) *Combustion Theory,* Benjamin/Cummings, Menlo Park, CA.

Wood, W.A. (1963) "Oscillatory Burning of Solid Composite Propellants," 9^{th} *Symposium (International) on Combustion,* Academic Press, pp. 335–344.

Wooten, D.C. (1966) "The Attenuation and Dispersion Sound in a Condensing Medium," Part I of Ph.d. Thesis, California Institute of Technology.

Yang, V. and Culick, F.E.C. (1990) "On the Existence and Stability of Limit Cycles for Transverse Acoustic Oscillations in a Cylindrical Combustion Chamber I: Standing Modes," *Combustion Science and Technology*, Vol. 72, pp. 37–65.

Zabrowski, M.A. and Brewster, M.Q. (1996) "Theory of Unsteady Combustion of Solids: Investigation of Quasi-Steady Assumption," *J. Prop and Power,* Vol. 12, No. 3, pp. 564–573.

Zak, T. (1993) "An Investigation of the Reacting Vortex Structure Associated with Pulsed Combustion," Ph.D. Thesis, California Institute of Technology.

Zel'dovich, Ya. B. (1942) "On the Combustion Theory of Powder and Explosives," *J. Exp. and Theor. Phys.,* Vol. 12, No. 11, pp. 493–510.

Zel'dovich, Ya. B. (1942) "On the Theory of the Combustion of Powders and Explosives," *Zh. Eksp. Teor. Fiz.,* Vol. 12, No. 11–12, pp. 498–524.

Zel'dovich, Ya. B., Leipunskii, O.I. and Librovich, V.B. (1975) "Theory of Nonsteady Propellant Burning," Nauka, Moscow.

Zetterstrom, K.-A. and Sjöblom, B. (1985) "An Experimental Study of Side Dump Ramjet Combustors," *International Symposium on Airbreathing Engines*, Paper 85-7024.

Zinn, B.T. (1986) "Pulsating Combustion," in *Advanced Combustion Methods*, A.J. Weinberg (Ed.), Academic Press, London.

Zinn, B.T. and Lores, M.E. (1972) "Application of the Galerkin Method in the Solution of Nonlinear and Axial Combustion Instability Problems in Liquid Rockets" *Comb. Sci. and Tech.,* Vol. 4, No. 6, pp. 269.

Zinn, B.T. and Powell, E.A. (1970a) "Application of the Galerkin Method in the Solution of Combustion Instability Problems," *Proceedings of the 19th International Astronautical Congress*, Vol. 3, pp. 59–73.

Zinn, B.T. and Powell, E.A. (1970b) "Nonlinear Combustion Instability in Liquid-Propellant Rocket Engines," *Thirteenth Symposium (International) on Combustion.*

ATTACHMENT — AIAA-2002-3592

N. Ananthkrishnan, Shardul Deo, F.E.C. Culick

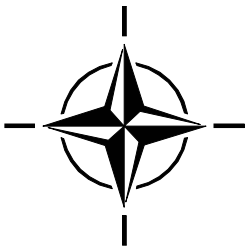

Modeling and Dynamics of Nonlinear Acoustic Waves in a Combustion Chamber

N. Ananthkrishnan* and Shardul Deo†
Indian Institute of Technology (Bombay), Mumbai 400076, India
and
Fred E.C. Culick‡
California Institute of Technology, Pasadena, CA 91125

Abstract

Future combustors designed for better efficiency and lower pollutant emission are expected to operate closer to their stability boundary, thereby increasing the risk of encountering combustion instability. Onset of combustion instability leads to limit cycle oscillations in the acoustical fluctuations that can often reach amplitudes large enough to cause severe damage. Active control strategies are, therefore, being considered to prevent combustion instabilities, but their development requires nonlinear models that can faithfully capture the combustor system dynamics. A framework for the approximate analysis of the nonlinear acoustics in a combustion chamber exists, which includes all relevant linear contributions and also second order gasdynamic nonlinearities. Nonlinear combustion effects in the form of pressure and velocity coupling models have also been incorporated into the analysis with the aim of capturing the phenomenon of triggered instability, where the acoustical fluctuations are linearly stable to small perturbations, but show a limit cycle behavior for larger perturbations. However, several questions such as those relating to 1) modal truncation of the equations for the acoustic dynamics, 2) absence of triggered limit cycles in the formulation with only second order gasdynamic nonlinearities, and 3) the form of the velocity coupling function, including the need for a threshold character, have not been satisfactorily resolved. In this paper, we address some of these questions on modeling and dynamics of acoustic waves in combustion chambers, using the approximate analysis, that have remained unanswered over the years.

1. Introduction

Combustion chambers operating under conditions that favor high efficiency and low pollutant emission are prone to suffer from combustion instabilities. These instabilities arise due to a coupling between the unsteady fluid motion and the combustion processes in the chamber. This interaction can be thought of as analogous to a positive feedback mechanism where fluctuations in the flow properties and in the combustion heat release drive each other in a regenerative manner. Amplitude dependent nonlinearities then cut in to limit the growth in the fluctuations. Thus, to an observer external to the chamber, combustion instabilities appear as self-excited limit cycle oscillations in the flow variables. It was shown by Chu and Kovasznay [**1**] that the fluctuations could be represented by a combination of acoustic, vortical, and entropic waves propagating in the combustion chamber. Traditionally, the term combustion instability has been used to refer to instabilities in the acoustical fluctuations. These acoustic oscillations can often reach amplitudes large enough to cause severe damage, and sometimes even complete failure. As a result, considerable effort has been made in the past to predict the onset of acoustic instabilities in combustion chambers. Solid propellant rocket motors have been known to exhibit two qualitatively different kinds of behavior at onset of combustion instability: 1) linear instability, where the acoustical fluctuations, in response to a small perturbation, build up to a limit cycle, and 2) nonlinear instability, where the acoustical fluctuations show a stable, damped response for small perturbations, but show a limit cycle response to larger perturbations. Nonlinear instability of this nature has been called pulsed or triggered instability [**2, 3**]. Both linear and nonlinear (triggered) instability have been observed in recent experiments on a gas turbine combustor as well [**4**].

Much of the early work on combustion instability dealt with the question of linear stability, assuming that the acoustic oscillations could be described in terms of the classical acoustic modes of the combustion chamber. The linear combustion instability problem appears to have been satisfactorily addressed, though work continues on the effects of the vorticity and entropy waves in the combustion chamber on the stability of the acoustic oscillations [**5, 6**]. It was, however, recognized early on that the dynamics of acoustic waves in combustion chambers was essentially nonlinear, and that it was necessary to be able to understand and model the nonlinear behavior of

*Assistant Professor, Department of Aerospace Engineering, Senior Member AIAA, akn@aero.iitb.ac.in
†Undergraduate Student, Department of Aerospace Engineering, deo@aero.iitb.ac.in
‡Richard L. and Dorothy M. Hayman Professor of Mechanical Engineering and Professor of Jet Propulsion, Fellow AIAA, fecfly@caltech.edu

these acoustic waves. The subject of nonlinear acoustics in combustion chambers began to be addressed by several researchers in the 1960's and 1970's. Most of these developments have been reviewed by Culick [**7, 8**], and are, therefore, not repeated here. The work by Culick [**9, 10**] during this period provided a general framework for the analysis of the nonlinear dynamics and stability of acoustic waves in combustion chambers. Under this framework, the partial differential equations of fluid conservation were approximated by a spatial averaging procedure to a set of ordinary differential equations for the amplitudes of the acoustic modes. The approximations in the analysis, and the derivation of the equations for the acoustic modes, have been described on several occasions [**7, 8**]. The equations for the modal amplitudes form a set of coupled, nonlinear differential equations that account for all relevant linear processes and include contributions from nonlinear gasdynamics to second order. On truncating the equations to a finite number of modes, the modal equations could be solved for the time evolution of the acoustic oscillations.

Culick and Yang [**11**] reported a numerically computed solution for the acoustic oscillations with a five-mode truncation of the approximate equations that was found to compare reasonably with a more exact numerical solution [**11**]. Conditions for the existence and stability of the limit cycle oscillations, and the qualitative dependence of the limit cycles on the system parameters, for the case of two longitudinal acoustic modes, were reported by Awad and Culick [**12**], and by Paparizos and Culick [**13**]. However, none of these studies were able to demonstrate triggered instability. It was felt, but not conclusively established, that the approximate analysis with nonlinear, second order gasdynamics alone was not capable of showing triggered instability. Extensions of the formulation to include third order gasdynamic nonlinearities and higher order interactions between the mean flow and the acoustics were equally unsuccessful in capturing triggered instability [**14**] in contrast to earlier results reported by Zinn [**15**]. The difference between the two conclusions remains unexplained. Nonlinear combustion models then remained the most attractive candidate to represent triggered instability within the framework of the approximate analysis. Unsteady combustion in solid propellant rockets had already been described in terms of pressure and velocity coupling models [**16**]. Numerical studies by Levine and Baum [**17**] with an ad hoc velocity coupling model showed that triggered instabilities could indeed be found when nonlinear combustion processes were accounted for. However, the form of the velocity coupling function was purely empirical and it was difficult to judge its validity or uniqueness. Also, it was not easy to arrive at qualitative conclusions regarding the conditions for onset of triggered instability from numerical simulations alone.

A significant step forward in the investigations came with the introduction of the methods of modern dynamical systems theory by Jahnke and Culick [**18**] to the analysis of nonlinear combustion instabilities. By using a continuation algorithm, it became possible to systematically and efficiently compute all steady state and limit cycle solutions over a range of parameter values. Stability of each steady state and limit cycle solution could be numerically established, and points of onset of instability could be identified with bifurcations. The qualitative behavior of the acoustic waves at onset of combustion instability then depends on the type of bifurcation, and on the nature of the limit cycles that emerge at the bifurcation point. This information is usually represented in the form of a plot of steady state values (peak amplitude in case of a limit cycle) against a suitable parameter in a bifurcation diagram. For longitudinal acoustic modes in a combustion chamber of uniform cross section, Jahnke and Culick [**18**] showed that results from a two-mode approximation were qualitatively dissimilar to those from a four- or six-mode approximation. However, they could draw no conclusion about the number of acoustic modes that need to be retained in their analysis, nor did their computations with second order gasdynamics alone display triggered limit cycles. Culick et al [**19**] extended the work in [**18**] by including the nonlinear combustion model of Levine and Baum [**17**] in addition to the second order gasdynamic nonlinearities. They confirmed that the nonlinear velocity coupling term in the Levine-Baum model did induce triggered limit cycles. However, their results with and without time-averaging showed significant discrepancies. Their studies also suggested that a four-mode approximation could satisfactorily capture the qualitative dynamics for the case of a first mode instability. Experiments by Ma et al [**20**] have suggested that the velocity coupling function has a threshold nature, i.e., there is a threshold value of the acoustic velocity below which the effects of nonlinear combustion are not felt. In a recent paper, using a four-mode truncation and an ad hoc threshold velocity coupling model, Burnley and Culick [**21**] have computed a bifurcation diagram which shows triggered limit cycles. Additional results are available in the thesis by Burnley [**22**].

Despite the impressive progress over the last three decades in modeling the nonlinear dynamics of acoustic waves in combustion chambers, many questions yet remain unanswered. For example, first of all, there is still no convincing argument for how many modes need to be retained in a truncated model of the coupled oscillator equations in order to predict the qualitative dynamics of the acoustic modes correctly. Secondly, though widely believed, it has never been definitely established that the approximate analysis with second order gasdynamics alone could not show triggered instability. Thirdly, the form of the velocity coupling function and, in particular, the need for a threshold character, has not been satisfactorily explained. These and such other questions have gained significance in the light of recent focus on active control of combustion instabilities [**23, 24**]. Rather than restrict operation to safe, stable regions at the cost of decreased performance, future combustors seeking higher performance will be operated closer to their stability boundary, thereby increasing the risk of encountering combustion instability. Active control strategies promise to provide a feasible solution to the problem of preventing instability in these combustors, but they are expected to depend heavily on nonlinear models that can successfully capture the qualitative features of the combustion system dynamics. The approximate formulation developed by Culick and his co-workers appears to provide a suitable framework for the development of active control laws for combustion instability, but there is a need to address questions such as those listed above before the Culick framework can be confidently applied to devise active combustion control strategies. Recent developments [**25, 26, 27**] in the use of bifurcation theory for the modeling of large-amplitude limit cycle oscillations have made it possible to seek answers to some questions on the qualitative dynamics of the acoustic waves at onset of combustion instability.

In the remainder of this paper, we first closely examine the coupled oscillator equations for the acoustic modal amplitudes. A careful study of the energy transfer between the acoustic modes provides a clue to the number of modes that need to be retained for a qualitatively correct analysis of the limit cycles at onset of combustion instability. The minimum order of the modal truncation for the first and second mode instability cases is determined, thereby resolving a longstanding issue in the modeling of acoustic waves in combustion chambers. Following this, two known mechanisms for triggered instability in coupled oscillator systems are briefly reviewed. With this knowledge, we then explain the lack of triggered limit cycles in the approximate formulation containing only second order gasdynamic nonlinearities. This is a result that, though widely believed in the past, has been theoretically established here for the first time. Finally, nonlinear combustion mechanisms for triggering are studied. Observations by Culick et al [**19**] that nonlinear pressure coupling does not lead to triggering are now explained. Velocity coupling models used in the past are evaluated and are found to display non-physical dynamical behavior. The need for a threshold velocity coupling function is critically examined and a new form of the velocity coupling function is derived that naturally shows a threshold character. The approach at all times is from the viewpoint of the qualitative theory of dynamical systems. However, numerical results are provided to illustrate the conclusions arrived at from the theory.

2. Coupled Oscillator Equations

The nonlinear dynamics of acoustic waves in a combustion chamber has been modeled by Culick [**10**] as a set of coupled second order oscillators, one for each acoustic mode. For the case of a combustion chamber of uniform cross section as considered in [**18, 19**], the modal natural frequencies can be assumed to be integral multiples of the primary acoustic mode frequency. Then, the coupled oscillator equations, with time non-dimensionalized by the primary mode frequency, can be written as follows:

$$\begin{aligned} \ddot{\eta}_n - 2\hat{\alpha}_n\dot{\eta}_n + n(n-2\hat{\theta}_n)\eta_n = \quad & -\sum_{i=1}^{n-1}\left(\hat{C}_{ni}^{(1)}\dot{\eta}_i\dot{\eta}_{n-i} + \hat{D}_{ni}^{(1)}\eta_i\eta_{n-i}\right) \\ & -\sum_{i=1}^{\infty}\left(\hat{C}_{ni}^{(2)}\dot{\eta}_i\dot{\eta}_{n+i} + \hat{D}_{ni}^{(2)}\eta_i\eta_{n+i}\right) \end{aligned} \tag{2.1}$$

where η_n is the amplitude of the n^{th} acoustic mode. Equation (2.1) includes linear contributions from combustion processes, gas-particle interactions, boundary conditions, and interactions between the steady and unsteady flow fields. Additionally, Eq. (2.1) also includes contributions from nonlinear gasdynamics to second order as given by the quadratic terms on the right hand side, where the coefficients $\hat{C}, \hat{D}$ are as follows:

$$\hat{C}_{ni}^{(1)} = \frac{-1}{2\gamma i(n-i)}[n^2 + i(n-i)(\gamma-1)]$$

$$\hat{C}^{(2)}_{ni} = \frac{1}{\gamma i(n+i)}[n^2 - i(n+i)(\gamma-1)]$$
$$\hat{D}^{(1)}_{ni} = \frac{\gamma-1}{4\gamma}[n^2 - 2i(n-i)]$$
$$\hat{D}^{(2)}_{ni} = \frac{\gamma-1}{2\gamma}[n^2 + 2i(n+i)]$$

The parameters $\hat{\alpha}_n$ and $\hat{\theta}_n$ in Eq. (2.1) are defined as

$$\hat{\alpha}_n = \alpha_n/\omega_1, \quad \hat{\theta}_n = \theta_n/\omega_1$$

where ω_1 is the natural frequency of the first acoustic mode. For a cylindrical chamber of $L/D = 11.8$, the first mode frequency, ω_1, is 5654.86 rad/s, and typical values for the linear growth rates, α_n, and frequency shifts, θ_n, are as given in Table 1. It can be seen from Table 1 that the modes are generally lightly damped and have only small frequency shifts, which means that the shifted modal frequencies remain appoximately integral multiples of the shifted primary mode frequency. It may also be noticed that the oscillators in Eq. (2.1) are linearly uncoupled, but are coupled through the nonlinear gasdynamic terms. In particular, it will be seen later that the quadratic terms on the right hand side of Eq. (2.1) with coefficients $\hat{C}^{(1)}$ and $\hat{D}^{(1)}$ ensure that the set of oscillators is resonantly coupled. For a set of resonantly coupled, lightly damped, nonlinear oscillators as in Eq. (2.1), it is not immediately obvious as to which modes affect the stability of a particular mode. Therefore, the question of how many higher order modes need to be retained for a correct solution of the n^{th} mode instability problem is not easy to answer. Previous numerical results [**18, 19**] suggest that when too few modes are retained in an analysis, the qualitative predictions of the nonlinear dynamic behavior at instability may be incorrect. At the same time, inclusion of higher order modes beyond a point does not seem to have a significant influence on the quantitative accuracy. Both these observations are not surprising, but 'How few (modes) is too few?' is a question that has not received a satisfactory answer to date.

Table 1. Data for parameters α_n and θ_n.

Mode	1	2	3	4	5	6
α_n, 1/s	Free	−324.8	−583.6	−889.4	−1262.7	−1500.0
θ_n, rad/s	12.9	46.8	−29.3	−131.0	−280.0	−300.0

2.1. Energy Transfer. Looking at Eq. (2.1), it is clear that in the absence of the second order gasdynamic terms on the right hand side, the individual modes behave as uncoupled linear oscillators. The coupling, and hence the energy transfer, between the modes is entirely due to the nonlinear gasdynamics. The influence of the nonlinear terms in the energy transfer process is presented in a concise form in Table 2 for the first eight modes. Each entry in the second column of Table 2 represents a pair of nonlinear gasdynamic terms that transfer energy to a particular mode from a lower numbered mode, i.e., energy transfer up the mode numbers from lower to higher modes. The third column, on the other hand, lists the terms that cause reverse energy transfer, i.e., from higher mode numbers to the lower ones. For instance, in the row for mode number 2, a term '13' implies that the second mode is excited by terms of the form $\eta_1\eta_3$ and $\dot{\eta}_1\dot{\eta}_3$. The term '13' represents a reverse transfer of energy from the third mode to the second mode. It can be seen that terms with $\hat{C}^{(1)}$ and $\hat{D}^{(1)}$ as coefficients appear in the second column of Table 2, while the third column consists of terms with $\hat{C}^{(2)}$ and $\hat{D}^{(2)}$ as coefficients.

Table 2. Inter-modal energy transfers.

Mode number	Energy transfer up the modes	Reverse energy transfer
1		**12**, 23, 34, 45, 56, 67, 78
2	11	13, **24**, 35, 46, 57, 68
3	12, 21	14, 25, **36**, 47, 58
4	13, 22, 31	15, 26, 37, **48**
5	14, 23, 32, 41	16, 27, 38
6	15, 24, 33, 42, 51	17, 28
7	16, 25, 34, 43, 52, 61	18
8	17, 26, 35, 44, 53, 62, 71	

A look down the second column of Table 2 shows that every term in the energy transfer up the modes acts as a near-resonant excitation. For instance, consider the first mode to be oscillating at its (shifted) natural frequency ω_1^s, and recall that the (shifted) natural frequencies of the higher modes are approximately integral multiples of that of the first mode. Then, the terms '11' will excite the second mode at exactly $2\omega_1^s$, which is approximately equal to its (shifted) natural frequency. Likewise, terms like '12' and '21' will excite the third mode at a frequency $3\omega_1^s$, which will nearly resonate with its (shifted) natural frequency, and so on. Hence, the modes in Eq. (2.1) represent a set of resonantly coupled oscillators. In contrast, the reverse energy transfer terms in the third column of Table 2 typically excite the modes at frequencies much higher than their resonant frequency, and hence contribute little to the overall modal amplitudes, except for the terms in boldface. The boldface terms represent parametric excitations which can alter the dynamics of the modes, in contrast to the other terms which act as external forcings that can merely contribute to the modal amplitude at a particular frequency. When the boldfaced terms are taken to the left hand side of the respective oscillator equation in Eq. (2.1), they can be seen to alter the frequency and damping of the modes, and thus, they can change the qualitative dynamical behavior. This can be clearly seen, for example, by writing the dynamical equation for the first mode with the parametric excitations moved to the left hand side as follows:

$$\ddot{\eta}_1 + [-2\hat{\alpha}_1 + \hat{C}_{11}^{(2)}\dot{\eta}_2]\dot{\eta}_1 + [(1 - 2\hat{\theta}_1) + \hat{D}_{11}^{(2)}\eta_2]\eta_1 = \ [other\ RHS\ terms] \tag{2.2}$$

The term involving $\hat{C}_{11}^{(2)}$ represents a reverse transfer of energy from the second to the first mode that could potentially destabilize the first mode. The effect of the other boldface terms in Table 2 can be similarly interpreted as a change in the damping and frequency of the oscillator equation in which they appear.

2.2. Modal Truncation. We are now in a position to answer the question of how many modes need to be retained in an analysis to obtain qualitatively correct results for an n^{th} mode instability. Consider the case where the first mode goes linearly unstable and begins oscillating at a frequency Ω (which may be slightly different from its shifted natural frequency ω_1^s due to nonlinear effects). Energy is then transferred to the second mode, which is resonantly excited by the terms '11' and set into oscillation at a frequency of 2Ω. A part of the energy from the second mode is reverse transferred to the first mode due to the boldfaced '12' terms in Table 2. Thus, the dynamics of the first mode is nonlinearly coupled to that of the second mode, and it is necessary to consider the first and second mode oscillators coupled together. However, since the parametric excitation terms '12' can significantly alter the dynamics of the first mode, it is important that they are correctly represented. When the third and higher modes are neglected, the second mode cannot transfer energy up the mode numbers as per the terms in the second column of Table 2. Instead, it is forced to reverse transfer part of this energy to the first mode, due to which the parametric excitations are larger than they ought to be, and the resulting dynamics may show large-amplitude limit cycles that are spurious. Such spurious limit cycles were observed, but could not be explained, in the two-mode continuation results of Jahnke and Culick [**18**], and, previously, in the two-mode analytical results reported by Awad and Culick [**12**], and by Paparizos and Culick [**13**]. Hence, the modal truncation should be such that all significant energy transfers up the modes are accommodated. This requires that all modes that directly receive energy from modes 1 and 2, individually or collectively, should be represented in the truncated set of equations. It is seen from Table 2 that direct energy transfer from modes 1 and 2 to the higher modes occurs through the terms '12' and '21' to the third mode, and through the term '22' to the fourth mode. All other energy transfers to the higher modes are indirect in the sense that they require the participation of the first/second mode and another higher mode. Thus, in a first mode instability, the third and fourth modes play an important role as energy sinks and must be included in the modal truncation, even though their direct influence on the dynamics of the first mode is not significant. In summary, the truncated set of equations for correct qualitative analysis of a first mode instability should contain at least four modes — the unstable mode (mode 1), the coupled modes (mode 2), and the energy sinks (modes 3 and 4). This argument can be easily extended to determine the minimum order of the modal truncation for analysis of an n^{th} mode instability. For example, in case of a second mode instability, it can be shown that the modal truncation must retain at least the first eight modes.

Continuation results for first and second mode instability have been reported in [**18, 19, 22**], where upto sixteen modes have been retained. Examination of these results confirms that computations for first mode instability with a modal truncation that did not retain at least four modes were qualitatively incorrect. Similarly, second mode instability computations that retained fewer than eight modes are seen to be qualitatively inconsistent. In the

following sections of this paper, we shall examine the first mode instability problem with a four-mode truncation. In particular, we shall be interested in conditions under which triggered limit cycles occur.

3. Triggered Limit Cycles

The set of coupled acoustic oscillators in Eq. (2.1) can be seen to have an equilibrium state where each $\eta_n = 0$, i.e., none of the acoustic modes are excited. Since the oscillators are all linearly decoupled, the linear damping coefficient for each mode, $\hat{\alpha}_n$, determines whether or not that particular mode is linearly stable. When each $\hat{\alpha}_n$ is negative, then the equilibrium state of the set of acoustic oscillators is linearly stable. In that case, small perturbations from the equilibrium state damp out with time, and the system of oscillators tends to return to its equilibrium state. Combustion instability occurs when one of the modes gets undamped, i.e., the corresponding $\hat{\alpha}_n$ changes sign from negative to positive. For positive $\hat{\alpha}_n$, the equilibrium state is linearly unstable, and small perturbations in the acoustic mode amplitudes initially grow with time. Nonlinear effects then become important and the modal amplitudes eventually settle down to a periodic oscillation called a limit cycle. Thus, given a model for the nonlinear dynamics of the acoustic waves, such as that in Eq. (2.1), one needs to predict the amplitude and frequency of the limit cycle oscillations at onset of combustion instability. This is easily done by using a continuation and bifurcation software such as AUTO97 [**28**]. Consider the first mode instability problem with a four-mode truncation of the set of oscillators in Eq. (2.1), where the only nonlinear terms are due to second order gasdynamics. Equilibrium states and limit cycles for this case have been computed for varying values of first mode damping parameter $\hat{\alpha}_1$ using the data in Table 1. Results are obtained for the amplitudes of the first four modes and, in case of limit cycles, also the time period of the oscillation. Of these, the first mode amplitude is plotted in Fig. 1 (plots for the other modal amplitudes are qualitatively similar) over a range of values of the parameter $\hat{\alpha}_1$. Figure 1 shows that the zero-amplitude equilibrium is linearly stable for $\hat{\alpha}_1 < 0$ and becomes unstable for $\hat{\alpha}_1 > 0$, with onset of instability occuring at $\hat{\alpha}_1 = 0$. Stable limit cycles emerge at the critical point $\hat{\alpha}_1 = 0$, which is called a supercritical Hopf bifurcation point. For any negative value of $\hat{\alpha}_1$, the only stable solution is the zero-amplitude equilibrium, and the acoustic waves tend to damp out, no matter how large the initial perturbation. Thus, the coupled oscillator model with second order gasdynamics alone shows only linear instability.

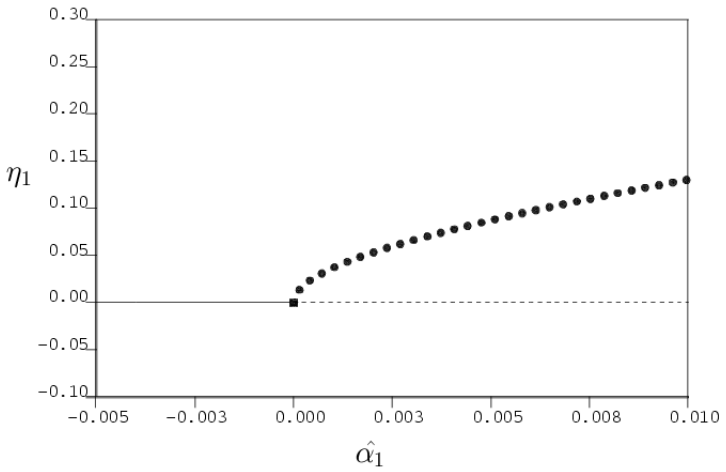

FIGURE 1. Stable limit cycles at a supercritical Hopf bifurcation for a first mode instability with second order gasdynamics alone (full line — stable equilibrium, dashed line — unstable equilibrium, filled circle — stable limit cycle, filled square — Hopf bifurcation).

Solid propellant rockets, as discussed earlier, have been known to show both linear and nonlinear or triggered instability. Examples of triggered instability are shown in the schematic bifurcation diagrams in Fig. 2, where x is a variable and μ is a parameter. In each of the diagrams in Fig. 2, there is a range of values of the parameter μ for which a stable equilibrium state co-exists with a stable limit cycle. For any parameter value in this range, small perturbations in x from the equilibrium state will tend to decay with time, but for larger perturbations,

the system may show stable limit cycle oscillations. That is, though the equilibrium state is linearly stable, the system could be pulsed or triggered into limit cycle behavior. These stable limit cycles are called triggered limit cycles. The triggered limit cycles in Fig. 2 are qualitatively different from the stable limit cycles in Fig. 1 in two respects: 1) Triggered limit cycles in Fig. 2 exist to the left of the Hopf bifurcation point that signifies onset of (linear) combustion instability, whereas the stable limit cycles in Fig. 1 occur only for parameter values to the right of the Hopf bifurcation. 2) Moving along the parameter axis from left to right, the triggered limit cycles in Fig. 2 begin abruptly with a finite non-zero amplitude at a fold bifurcation, as against the stable limit cycles in Fig. 1 whose amplitude starts from zero at the Hopf bifurcation point. Triggered limit cycles are, therefore, also called large-amplitude limit cycles in the literature [**25, 26, 27**]. The onset of triggered limit cycles at a fold bifurcation can be considered to be a nonlinear combustion instability phenomenon. Thus, with increasing values of the parameter μ, the systems in Fig. 2 first show a nonlinear combustion instability at a fold bifurcation, and then a linear combustion instability at a Hopf bifurcation.

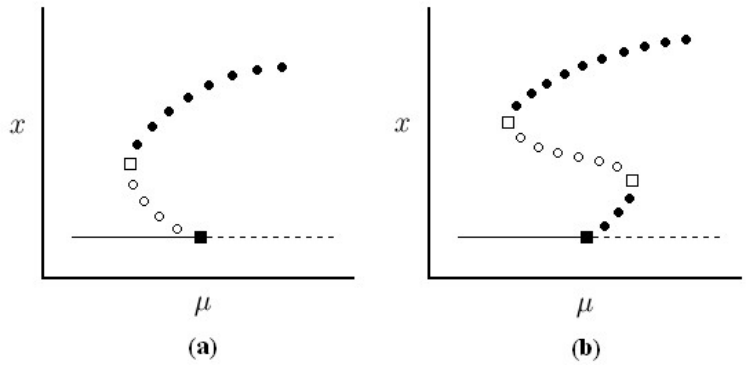

FIGURE 2. Triggered limit cycles at (a) subcritical Hopf bifurcation, and (b) supercritical Hopf bifurcation (full line — stable equilibrium, dashed line — unstable equilibrium, filled circle — stable limit cycle, empty circle — unstable limit cycle, filled square — Hopf bifurcation, empty square — fold bifurcation).

Triggered limit cycles can be a disquieting phenomenon due to the sudden increase in the amplitudes of the acoustic modes. Moreover, the phenomenon is worrisome because triggered instability could occur even when linearly stable operating conditions have been ensured. Hence, there is a need to develop models that can faithfully capture the qualitative dynamics of triggered limit cycles in combustion chambers. Unfortunately, the coupled acoustic oscillator model in Eq. (2.1), from past experience and as seen in Fig. 1, does not seem to accommodate triggered limit cycles, but this has never been definitely established. We can now explain the lack of triggered limit cycles in the oscillator model of Eq. (2.1) by comparing the influence of the second order gasdynamic nonlinearities with nonlinear terms that are known to cause triggering in coupled oscillator systems. There are two known mechanisms for generation of triggered limit cycles in systems of resonantly coupled oscillators.

1. Nonlinear damping terms of the form $|f(\eta_n)|\dot{\eta}_n$ or $|f(\dot{\eta}_n)|\dot{\eta}_n$ have been shown to produce triggered limit cycles with either subcritical or supercritical Hopf bifurcations, as sketched in Fig. 2 [**26**].
2. Parametric excitation terms of the form $c\dot{\eta}_{2n}\dot{\eta}_n$ or $c\eta_{2n}\dot{\eta}_n$ are also known to be able to create a subcritical Hopf bifurcation and triggered limit cycles, as pictured in Fig. 2(a), depending on the sign of the coefficient c, i.e., $c < 0$ for triggering, and $c > 0$ for non-triggering [**27**].

Examining the nonlinear terms in the equation for the first acoustic mode, which is reproduced below from Eq. (2.2),

$$\ddot{\eta}_1 + [-2\hat{\alpha}_1 + \hat{C}_{11}^{(2)}\dot{\eta}_2]\dot{\eta}_1 + [(1 - 2\hat{\theta}_1) + \hat{D}_{11}^{(2)}\eta_2]\eta_1 = \ [other\ RHS\ terms] \tag{3.3}$$

it can be observed that there are no nonlinear damping terms, but the second order gasdynamic term $\hat{C}_{11}^{(2)}\dot{\eta}_2\dot{\eta}_1$ does indeed act as a parametric excitation of the desired form as listed in 2. above. (The other parametric excitation term $\hat{D}_{11}^{(2)}\eta_2\eta_1$ is clearly not of the desired form.) However, on using the expressions following Eq. (2.1), the

coefficient $\hat{C}_{11}^{(2)}$ can be evaluated to be

$$\hat{C}_{11}^{(2)} = (3-2\gamma)/2\gamma$$

which is usually positive, where γ is the ratio of specific heats. The term $\hat{C}_{11}^{(2)}\dot{\eta}_2\dot{\eta}_1$, thus, turns out to be a parametric excitation of the non-triggering type. It follows that second order gasdynamic nonlinearities, as they exist, are incapable of inducing triggered limit cycles. As an academic exercise, one may choose an arbitrary non-physical value of γ that makes the coefficient $\hat{C}_{11}^{(2)}$ negative; then, triggered limit cycles can indeed be observed [**29**]. In summary, triggered limit cycles observed in solid propellant rockets cannot be explained by modeling the second order gasdynamic nonlinearities alone.

The most promising source for the triggering mechanism then appears to be nonlinear combustion. The approximate formulation of Eq. (2.1) already accounts for contributions from linear combustion processes. Nonlinear combustion phenomena can be included in the coupled oscillator system of Eq. (2.1) by introducing additional terms F_n^{nc} representing pressure and velocity coupling effects. The modal equations for the set of coupled oscillators then appear as

$$\begin{aligned}\ddot{\eta}_n - 2\hat{\alpha}_n\dot{\eta}_n + n(n-2\hat{\theta}_n)\eta_n = \quad & -\sum_{i=1}^{n-1}\left(\hat{C}_{ni}^{(1)}\dot{\eta}_i\dot{\eta}_{n-i} + \hat{D}_{ni}^{(1)}\eta_i\eta_{n-i}\right) \\ & -\sum_{i=1}^{\infty}\left(\hat{C}_{ni}^{(2)}\dot{\eta}_i\dot{\eta}_{n+i} + \hat{D}_{ni}^{(2)}\eta_i\eta_{n+i}\right) + F_n^{nc} \end{aligned} \tag{3.4}$$

where η_n is again the amplitude of the n^{th} acoustic mode. Culick et al [**19**] and Burnley [**22**] considered the nonlinear pressure coupling terms in the Levine-Baum model as a possible candidate for the creation of triggered limit cycles. They observed that the nonlinear pressure coupling terms did indeed cause triggering, but the required values of the coefficients of these terms turned out to be unrealistically large. Their observations can now be explained by noting that the nonlinear pressure coupling terms in the Levine-Baum model are in fact second order parametric excitation terms with a negative coefficient (see Eq. (33) of Culick et al [**19**]), and, hence, of the type that can cause triggering. Then, for a first mode instability problem with second order gasdynamics and nonlinear pressure coupling, the parametric excitation terms in the equation for the first acoustic mode appear as $(\hat{C}_{11}^{(2)} + C_1^{pc})\dot{\eta}_2\dot{\eta}_1$, where C_1^{pc} is the coefficient of the pressure coupling term. Now, the combined coefficient $(\hat{C}_{11}^{(2)} + C_1^{pc})$ is required to be negative for triggering to occur, and although C_1^{pc} is known to be negative, it clearly needs to be large enough to overcome the positive value due to $\hat{C}_{11}^{(2)}$. Unfortunately, for reasonable values of C_1^{pc}, the combined coefficient is still positive, and, as a result, the nonlinear pressure coupling model does not lead to triggering. This leaves us to consider velocity coupling models as a possible candidate to explain the occurrence of triggered instability.

4. Velocity Coupling Models

Levine and Baum [**17**] suggested a velocity coupling function of the form $F_n^{nc} = f(\dot{\eta}_n)\dot{\eta}_n$, with $f(\dot{\eta}_n) = C_n^{vc}|\dot{\eta}_n|$, to model the nonlinear combustion response to an acoustic velocity parallel to the burning surface. The equation for the first acoustic mode, with second order gasdynamics and the Levine-Baum velocity coupling model, is then of the form

$$\ddot{\eta}_1 + [-2\hat{\alpha}_1 + \hat{C}_{11}^{(2)}\dot{\eta}_2 + C_1^{vc}|\dot{\eta}_1|]\dot{\eta}_1 + [(1-2\hat{\theta}_1) + \hat{D}_{11}^{(2)}\eta_2]\eta_1 = \ [other\ RHS\ terms] \tag{4.5}$$

The velocity coupling function in Eq. (4.5) represents a nonlinear damping mechanism, and can, therefore, be expected to create triggered limit cycles at onset of first mode combustion instability. This is confirmed by computing equilibrium points and limit cycles for a four-mode truncation of the coupled oscillator system Eq. (3.4) for the data in Table 1. The velocity coupling function in the equation for the first acoustic mode is taken as shown in Eq. (4.5) with $C_1^{vc} = 0.2$. Results for the first mode amplitude are plotted in Fig. 3 for varying values of the parameter $\hat{\alpha}_1$. Triggered limit cycles are clearly seen in Fig. 3 at a subcritical Hopf bifurcation, similar to that sketched in the schematic bifurcation diagram of Fig. 2(a). Thus, the Levine-Baum velocity coupling model along with the second order gasdynamic nonlinearities is adequate to capture triggered limit cycles in solid propellant combustion systems. However, from a qualitative point of view, the dynamics represented by the bifurcation diagram in Fig. 3 is not entirely satisfactory. This is because the stable triggered limit cycles terminate at some positive value of $\hat{\alpha}_1$ beyond which there are no stable equilibrium or limit cycle solutions. This implies that,

where there are no stable solutions, the slightest perturbation will cause the modal amplitudes to eventually grow to infinity. Such dynamical behavior is clearly non-physical and must be eliminated.

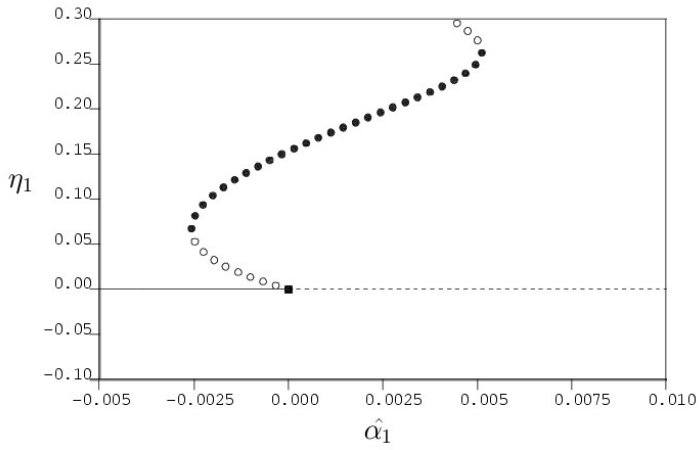

FIGURE 3. Triggered limit cycles at a subcritical Hopf bifurcation for a first mode instability with second order gasdynamics and the Levine-Baum velocity coupling function (full line — stable equilibrium, dashed line — unstable equilibrium, filled circle — stable limit cycle, empty circle — unstable limit cycle, filled square — Hopf bifurcation).

Levine and Baum [**17**] also suggested that threshold effects that had been observed experimentally be incorporated in the velocity coupling function. Burnley and Culick [**21**] modified the Levine-Baum velocity coupling function by introducing a dead zone to obtain an ad hoc velocity coupling function with a threshold, as follows:

$$\begin{aligned} f(\dot{\eta}_1) &= 0, & |\dot{\eta}_1| < |\dot{\eta}_1^t| \\ f(\dot{\eta}_1) &= C_1^{vc}|\dot{\eta}_1 - \dot{\eta}_1^t|, & |\dot{\eta}_1| \geq |\dot{\eta}_1^t| \end{aligned} \tag{4.6}$$

where $\dot{\eta}_1^t$ is the threshold value of $\dot{\eta}_1$. Computation of equilibrium and limit cycle solutions is carried out as before, but with the Burnley-Culick velocity coupling function in Eq. (4.6) instead of the Levine-Baum model. The parameter C_1^{vc} in Eq. (4.6) is retained unchanged, i.e., $C_1^{vc} = 0.2$, and a threshold value of $\dot{\eta}_1^t = 0.02$ is chosen. A plot of the first mode amplitude for this case with varying values of the parameter $\hat{\alpha}_1$ is shown in Fig. 4, where triggered limit cycles of the form sketched in Fig. 2(b) may be observed at a supercritical Hopf bifurcation. However, it is known that functions $f(\dot{\eta}_1)$ that are approximately quadratic in shape, e.g., the Levine-Baum function, show triggered limit cycles of the subcritical type, while those that are approximately quartic (fourth-order), like the Burnley-Culick function, show triggered limit cycles of the supercritical type [**26**]. It is not difficult to come up with velocity coupling models with no threshold, but with an approximately quartic function $f(\dot{\eta}_1)$, that also produce triggered limit cycles of the supercritical type as in Fig. 4 [**30**]. Thus, the change from subcritical triggering in Fig. 3 to supercritical triggering in Fig. 4 cannot be attributed to the threshold effect in the Burnley-Culick velocity coupling function. Besides, the non-physical dynamical behavior seen over a range of positive values of $\hat{\alpha}_1$ in Fig. 3 persists in Fig. 4 as well.

To resolve this issue, we go back to the bifurcation diagram of Fig. 3 and the Levine-Baum velocity coupling model. It is clear that the qualitative dynamics of triggered limit cycles at onset of first mode combustion instability at the subcritical Hopf bifurcation is adequately captured in Fig. 3. This means that the form of the Levine-Baum velocity coupling function is appropriate for small $\dot{\eta}_1$, i.e., near the region of onset of instability. The non-physical dynamics in Fig. 3 occurs for larger values of η_1 and $\dot{\eta}_1$, which implies that the form of the Levine-Baum velocity coupling model requires to be corrected for large $\dot{\eta}_1$, without affecting its shape in the neighborhood of $\dot{\eta}_1 = 0$. The lowest order correction term to the Levine-Baum function which meets these requirements is a quadratic term with value zero at $\dot{\eta}_1 = 0$, slope zero at $\dot{\eta}_1 = 0$, and a magnitude that subtracts from the value of the function for large $\dot{\eta}_1$. The new velocity coupling function, with such a quadratic term included, can be expressed as

$$f(\dot{\eta}_1) = C_1^{vc}|\dot{\eta}_1| - D_1^{vc}|\dot{\eta}_1|^2 \tag{4.7}$$

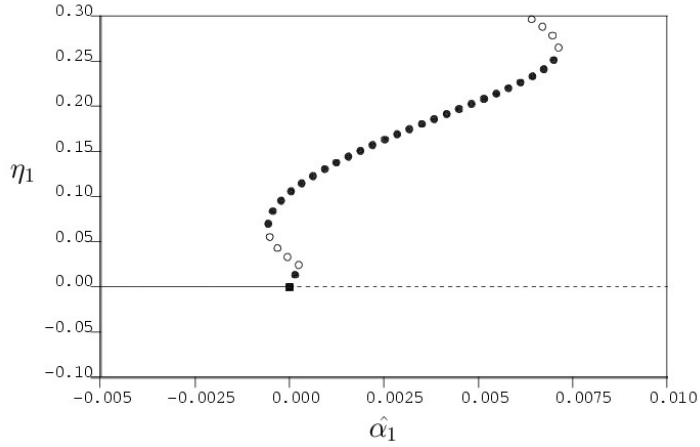

FIGURE 4. Triggered limit cycles at a supercritical Hopf bifurcation for a first mode instability with second order gasdynamics and the Burnley-Culick threshold velocity coupling function (full line — stable equilibrium, dashed line — unstable equilibrium, filled circle — stable limit cycle, empty circle — unstable limit cycle, filled square — Hopf bifurcation).

For a particular choice of the coefficients, $C_1^{vc} = 0.2$ and $D_1^{vc} = 0.8$, the shape of the new velocity coupling function appears as plotted in Fig. 5. Surprisingly, the nonlinear function in Fig. 5 naturally shows a threshold character, but one that is quite different from the Burnley-Culick function. Computations are now carried out for equilibrium solutions and limit cycle amplitudes under identical conditions as was done for Fig. 3, but with the new velocity coupling function in Eq. (4.7) instead of the Levine-Baum model. Results for the first mode amplitude with varying parameter $\hat{\alpha}_1$ are shown in Fig. 6. As expected, the subcritical Hopf bifurcation in Fig. 6 is identical to that in Fig. 3, and the qualitative dynamics of the triggered limit cycles in the vicinity of the Hopf bifurcation point, i.e., for small η_1 and $\dot{\eta}_1$, remains unchanged. However, the stable limit cycles persist for all positive values of the parameter $\hat{\alpha}_1$, and the non-physical dynamical behavior in Fig. 3 is, therefore, eliminated in Fig. 6. Thus, the new velocity coupling function in Fig. 5 provides a satisfactory picture of the qualitative dynamics of the triggered limit cycles created at onset of combustion instability. In addition, the new velocity coupling function that is derived from dynamical considerations naturally satisfies the physical requirement of having a threshold character.

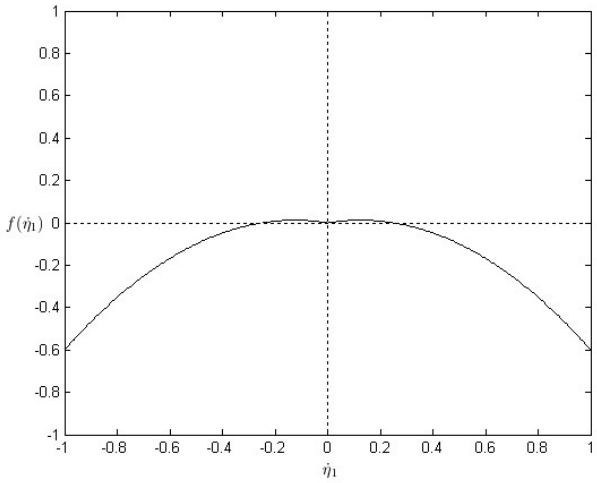

FIGURE 5. The form of the velocity coupling function obtained by correcting the Levine-Baum function with a suitable quadratic term.

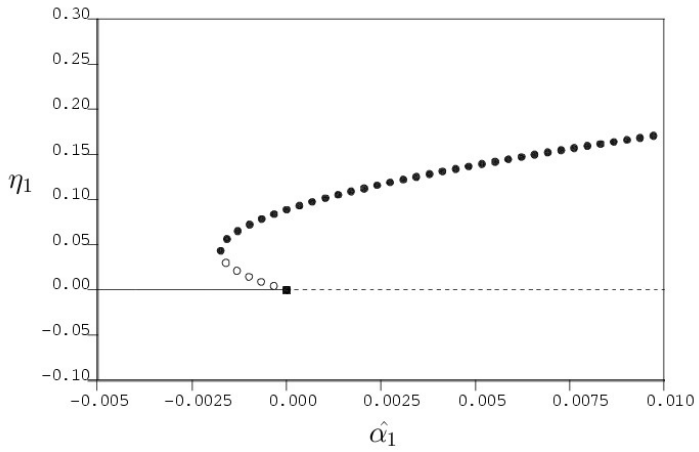

FIGURE 6. Triggered limit cycles at a subcritical Hopf bifurcation for a first mode instability with second order gasdynamics and the threshold velocity coupling function in Fig. 5 (full line — stable equilibrium, dashed line — unstable equilibrium, filled circle — stable limit cycle, empty circle — unstable limit cycle, filled square — Hopf bifurcation).

5. Conclusions

Several questions regarding the modeling and dynamics of acoustic waves in combustion chambers have been addressed in this paper using the approximate analysis originally developed by Culick. First among these is the question of modal truncation, i.e., how many modes need to be retained in a truncated model of the coupled oscillator equations in order to predict the qualitative dynamics of the acoustic waves correctly. Previous studies of first and second mode instabilities arbitrarily chose to retain between two and sixteen modes. We have now shown that a first mode instability requires a minimum of four modes in the modal truncation, while for a second mode instability, one needs to retain at least the first eight modes. Secondly, it has been widely believed from previous studies that the approximate analysis with only second order gasdynamic nonlinearities could not show triggered limit cycles. This has now been theoretically established by recognizing that second order gasdynamics does not contribute either nonlinear damping or parametric excitation terms in the form required to cause triggered limit cycles. Finally, nonlinear combustion mechanisms for triggering based on pressure and velocity coupling models have been studied. Results from a previous study which suggested that pressure coupling does not lead to triggering have now been explained. Velocity coupling models have been shown to induce triggered instability due to a nonlinear damping mechanism. Velocity coupling models used in the past have been examined, and a new velocity coupling function has been derived that captures the qualitative dynamics at onset of triggered instability. Interestingly, our velocity coupling function naturally shows a threshold nature unlike previous velocity coupling models that had an artificially imposed threshold character.

6. Acknowledgments

This work was supported in part by the California Institute of Technology; partly by the Caltech Multidisciplinary University Research Initiative under Grant No. N00014-95-1-1338 (Dr. Judah Goldwasser, Program Manager); partly by the Department of Energy Advanced Gas Turbine Systems Research (AGTSR) Program under Subcontract No. 98-02-SR072 (Dr. Larry Golan, Program Manager); and partly by the Air Force Office of Scientific Research (AFOSR) under Grant No. F49620-99-1-0118 (Dr. Mitat Birkan, Program Manager).

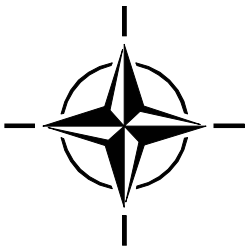

Bibliography

[1] Chu, B.-T., and Kovasznay, L.S.G., "Nonlinear Interactions in a Viscous Heat-Conducting Compressible Gas," *Journal of Fluid Mechanics*, Vol. 3, No. 5, 1957, pp. 494-512.
[2] Baum, J.D., Levine, J.N., and Lovine, R.L., "Pulse Triggered Nonlinear Combustion Instability in Solid Rocket Motors," *AIAA Journal*, Vol. 22, No. 10, 1984, pp. 1413-1419.
[3] Baum, J.D., Levine, J.N., and Lovine, R.L., "Pulsed Instability in Rocket Motors: A Comparision Between Predictions and Experiments," *Journal of Propulsion and Power*, Vol. 4, No. 4, 1988, pp. 308-316.
[4] Lieuwen, T.C,, "Experimental Investigation of Limit Cycle Oscillations in an Unstable Gas Turbine Combustor," *Journal of Propulsion and Power*, Vol. 18, No. 1, 2002, pp. 61-67.
[5] Flandro, G.A., "Effects of Vorticity on Rocket Combustion Stability," *Journal of Propulsion and Power*, Vol. 11, No. 4, 1995, pp. 607-625.
[6] Garcia-Schafer, J.E., and Linan, A., "Longitudinal Acoustic Instabilities in Slender Solid Propellant Rockets: Linear Analysis," *Journal of Fluid Mechanics*, Vol. 437, 2001, pp. 229-254.
[7] Culick, F.E.C., "Some Recent Results for Nonlinear Acoustics in Combustion Chambers," *AIAA Journal*, Vol. 32, No. 1, 1994, pp. 146-169.
[8] Culick, F.E.C., "Combustion Instabilities in Propulsion Systems," *Unsteady Combustion*, F.E.C. Culick et al (eds.), Kluwer Academic Publishers, Netherlands, 1996, pp. 173-241.
[9] Culick, F.E.C., "Nonlinear Growth and Limiting Amplitude of Acoustic Oscillators in Combustion Chambers," *Combustion Science and Technology*, Vol. 3, No. 1, 1971, pp. 1-16.
[10] Culick, F.E.C., "Nonlinear Behavior of Acoustic Waves in Combustion Chambers, Parts I and II," *Acta Astronautica*, Vol. 3, 1976, pp. 714-757.
[11] Culick, F.E.C., and Yang, V., "Prediction of the Stability of Unsteady Motions in Solid Propellant Rocket Motors," *Nonsteady Burning and Combustion Stability of Solid Propellants*, L. de Luca, E.W. Price, and M. Summerfield (eds.), AIAA, Washington, 1992.
[12] Awad, E., and Culick, F.E.C., "On the Existence and Stability of Limit Cycles for Longitudinal Acoustic Modes in a Combustion Chamber," *Combustion Science and Technology*, Vol. 46, No. 6, 1986, pp. 195-222.
[13] Paparizos, L.G., and Culick, F.E.C., "The Two-Mode Approximation to Nonlinear Acoustics in Combustion Chambers, I. Exact Solution for Second Order Acoustics," *Combustion Science and Technology*, Vol 65, 1989, pp. 39-65.
[14] Yang, V., Kim, S.I., and Culick, F.E.C., "Triggering of Longitudinal Pressure Oscillations in Combustion Chambers, I: Nonlinear Gasdynamics," *Combustion Science and Technology*, Vol. 72, No. 5, 1990, pp. 183-214.
[15] Zinn, B.T., "A Theoretical Study of Nonlinear Combustion Instability in Liquid Propellant Rocket Engines," *AIAA Journal*, Vol. 6, No. 10, 1968, pp. 1966-1972.
[16] Culick, F.E.C., "Stability of Longitudinal Oscillations with Pressure and Velocity Coupling in a Solid Propellant Rocket," *Combustion Science and Technology*, Vol. 2, No. 4, 1970, pp. 179-201.
[17] Levine, J.N., and Baum, J.D., "A Numerical Study of Nonlinear Instability Phenomena in Solid Rocket Motors," *AIAA Journal*, Vol. 21, No. 4, 1983, pp. 557-564.
[18] Jahnke, C.C., and Culick, F.E.C., "Application of Dynamical Systems Theory to Nonlinear Combustion Instabilities," *Journal of Propulsion and Power*, Vol. 10, No. 4, 1994, pp. 508-517.
[19] Culick, F.E.C., Burnley, V., and Swenson, G., "Pulsed Instabilities in Solid Propellant Rockets," *Journal of Propulsion and Power*, Vol. 11, No. 4, 1995, pp. 657-665.
[20] Ma, Y., van Moorhem, W.K., and Shorthill, R.W., "Experimental Investigation of Velocity Coupling in Combustion Instability," *Journal of Propulsion and Power*, Vol. 7, No. 5, 1991, pp. 692-699.
[21] Burnley, V.S., and Culick, F.E.C., "Influence of Random Excitations on Acoustic Instabilities in Combustion Chambers," *AIAA Journal*, Vol. 38, No. 8, 2000, pp. 1403-1410.
[22] Burnley, V.S., "Nonlinear Combustion Instabilities and Stochastic Sources," Ph. D. Thesis, California Inst. of Technology, Pasadena, CA, 1996.
[23] Poinsot, T., Bourienne, F., Candel, S.H., and Esposito, E., "Suppression of Combustion Instabilities by Active Control," *Journal of Propulsion and Power*, Vol. 5, No. 1, 1989, pp. 14-20.
[24] McManus, K.R., Poinsot, T., and Candel, S.M., "A Review of Active Control of Combustion Instabilities," *Progress in Energy and Combustion Science*, Vol. 19, 1993, pp. 1-29.
[25] Ananthkrishnan, N., and Sudhakar, K., "Characterization of Periodic Motions in Aircraft Lateral Dynamics," *Journal of Guidance, Control, and Dynamics*, Vol. 19, No. 3, 1996, pp. 680-685.
[26] Ananthkrishnan, N., Sudhakar, K., Sudershan, S., and Agarwal, A., "Application of Secondary Bifurcations to Large Amplitude Limit Cycles in Mechanical Systems," *Journal of Sound and Vibration*, Vol. 215, No. 1, 1998, pp. 183-188.

[27] Ananthkrishnan, N., Sudershan, S., Sudhakar, K., and Verma, A., "Large Amplitude Limit Cycles in Resonantly Coupled Oscillators," *Journal of Sound and Vibration*, Vol. 231, No. 5, 2000, pp. 1377-1382.

[28] Doedel, E.J., Wang, X.J., Fairgrieve, T.F., Champneys, A.R., Kuznetsov, Y.A., and Sandstede, B., "AUTO97: Continuation and Bifurcation Software for Ordinary Differential Equations (with HomCont)," California Inst. of Technology, Pasadena, CA, 1998.

[29] Ananthkrishnan, N., "Qualitative Dynamics of Nonlinear Acoustic Waves in a Combustion Chamber, I: Modal Truncation and Triggering," Guggenheim Jet Propulsion Center Documents on Active Control of Combustion Instabilities, CI 00-03, California Inst. of Technology, Pasadena, CA, 2000.

[30] Ananthkrishnan, N., "Qualitative Dynamics of Nonlinear Acoustic Waves in a Combustion Chamber, III: Velocity Coupling Models," Guggenheim Jet Propulsion Center Documents on Active Control of Combustion Instabilities, CI 01-01, California Inst. of Technology, Pasadena, CA, 2001.